Removal of nanoparticles by flotation processes

Ming Zhang

Université Fédérale

Toulouse Midi-Pyrénées

THÈSE

En vue de l'obtention du

DOCTORAT DE L'UNIVERSITÉ DE TOULOUSE

Délivré par :

Institut National des Sciences Appliquées de Toulouse (INSA de Toulouse)

Présentée et soutenue par :
ZHANG Ming
le lundi 26 janvier 2015

Titre :

ELIMINATION DE NANOPARTICULES PAR DES PROCEDES DE FLOTTATION

École doctorale et discipline ou spécialité :
ED MEGEP : Génie des procédés et de l'Environnement

Unité de recherche :
LABORATOIRE D'INGENIERIE DES SYSTEMES BIOLOGIQUES ET DES PROCEDES

Directeur/trice(s) de Thèse :

Pr. GUIRAUD Pascal

Jury :

Pr. CHAUDRET Bruno	INSA Toulouse	Président
Dr. BENEVENTI Davide	INP Grenoble	Rapporteur
Dr. DUVAL Hervé	Ecole Centre Paris	Rapporteur
Pr. BOUYER Denis	Université Montpellier 2	Examinateur
Dr. TROMPETTE Jean-Luc	INP Toulouse	Examinateur
Pr. WANG Dongsheng	CAS, Beijing	Examinateur
Dr. TOURBIN Mallorie	INP Toulouse	Examinateur
Pr. GUIRAUD Pascal	INSA Toulouse	Directeur de thèse

Acknowledgements

I am extremely grateful to my supervisor Professor Pascal GUIRAUD for his guidance, devotion, and continual support throughout my study in France. His mentorship, motivation and friendship guided me during this research to achieve our objectives. His serious attitude and broad vision of scientific research will always impact me in my future work. His optimism and enthusiasm for life also give me much positive influence in life. I would like to express my gratitude for his full trust of my competence and kind consideration to me even during the period when I was stuck in the work or I suffered some difficulties in life.

Thank you so much all the colleagues in LISBP: without your kind help, this work could not be finished. Thank Lucie VIALARET with whom I started the work in the lab, and it is such a pleasure to work with you. Thanks a lot José MOREAU, without your help, it would be impossible to conduct the flotation trials, the essential part of my work. Thank you Nathalie CLERGERIE and Aurore DIDI, your kind help in analytical techniques really facilitated my experiments. Thank you Marie-Line de Solan Bethmale in LGC and Florence LERAY in BIO 1 of LISBP for the ICP-AES and ICP-MS measurements that were pretty significant to evaluate the flotation treating efficiency in my research. Thank Dr. Jian WEI and Dr. Chengcheng LI. Our discussion about the Ph.D. study helped me to broaden my mind of study. I would also like to give my sincere thanks to all other colleagues in our team and the lab.

I sincerely thank Prof. Bruno CHAUDRET, the president of thesis' jury, and also extend my sincere gratitude to the reviewers of my dissertation, Dr. Davide BENEVENTI and Dr. Hervé DUVAL, for your warm help to this thesis. Thank you very much Dr. Jean-Luc Trompette, and I appreciate your kind suggestions and useful comments which help to further improve and complete the dissertation. Thanks a lot Dr. TOURBIN Mallorie and Prof. Denis BOUYER for your participation of my Ph.D. defence and your encouragement of my work.

I am willing to thank the Chinese Scholarship Council for the financial support of my Ph.D. study. Surely, thank all my Chinese friends here, Yanping LIU, Weiwen CHEN, Shenwei BAI,

Jian LIU, Biao WANG, Ran LIU, Lixia YANG, Xiaomin XIE, Jin YAN, Haiyang WU, Ke CHEN… I will forever keep in mind each moment that we spent together.

I would also like to thank my supervisors in the Research Center of Eco-environmental Sciences of the Chinese Academy of Sciences, Professor Dongsheng WANG who is also the member of thesis' jury and Dr. Feng XIAO who firstly introduced me to the world of scientific research and also helped me to get the opportunity of studying in France.

I would like to dedicate this work to my dearest parents. Wherever I am and whenever I need to be backed up, their unconditional love and support can always find a way to me. Their never ending patience and understanding are the inspiration profoundly contributing to the completion of my Ph.D. study and encouraging me to confront every challenge and go through all the tough days.

Abstract

The removal of nanoparticles (NPs) from waters is a serious challenge in the water treatment field owing to the high stability and colloidal nature of particles. This study is devoted to develop effective flotation processes for NP separation. The investigation is firstly conducted to get a good knowledge of features and colloidal behaviors of NPs in suspension. Surface modification tests and adsorption-aggregation experiments are then carried out to understand the interaction mechanisms between NPs and flotation assisting reagents. Two types of flotation (dissolved air flotation (DAF) and colloidal gas aphrons (CGAs) involved flotation) were specially focused on: the former aims at using air bubbles to remove NP aggregates with the assistance of humic acid (HA), while the later employs the surface functionalized microbubbles, CGAs, to enhance the interaction of NP-bubble for the sake of high treating efficiency.

Results show that, on mixing with the highly basic HA solution (pH12.9), the surface charge of TNPs is primarily neutralized by OH^- and then screened by polyanions of HA. When the pH of TNP-HA suspension is lower than 3 by adding HA stock solutions at pH4.0~9.0, the electrostatic attraction between TNPs and anions becomes insufficient but the aggregation of TNPs-colloidal HA occurs. In continuous DAF trials, the appropriate pH of HA stock solution (pH $\leqq$ 9) and optimum HA concentration (11.1 mg/L DOC) for high TNP removals (> 95 %) are determined. The residual HA concentration remained in a low level even when HA is overdosed. When the pH of the TNP-HA suspension is highly acidic, most HA molecules are not really soluble and uncharged, and they may aggregate themselves and form hydrophobic colloidal precipitates to minimize the contact with the aqueous environment. As for the study of CGAs, the characterization results denote that introducing air flow during the CGA generation process can slow down the liquid drainage speed and may facilitate the particle separation performance; the stirring speed is a crucial parameter to create micron scale bubbles, and CGAs can be positively or negatively surface charged by using different surfactants. Different SiO_2 NP (SNPs) can be efficiently separated from aqueous suspensions by the continuous CGA generation-flotation process with the highest SNP removal close to 100 %. The comparison tests between CGA-flotation and DAF denote that the former take the greater advantage because of its better treating effect and less surfactant demand.

Keywords: Nanoparticle removal, Dissolved air flotation, Humic acid; Colloidal gas aphrons, Adsorption-aggregation, Interaction mechanisms

Résumé

La séparation de nanoparticules (NPs) contenues dans des milieux aqueux est un sérieux challenge pour le traitement des eaux à cause de la grande stabilité et de la nature colloïdale de ces particules. Ce travail concerne le développement de procédés efficaces de flottation pour la séparation de nanoparticules. La première partie du travail est conduite pour obtenir une connaissance plus étroite de la nature et du comportement colloïdal des nanoparticules en suspension. Des tests de modifications de leur surface et des expériences d'adsorption-agrégation sont ensuite menés pour comprendre les mécanismes d'interactions entre les NPs et des réactifs d'aide à la flottation. Deux type des techniques de flottation (la flottation à air dissout (DAF) et la flottation par des aphrons colloïdaux (CGAs)) sont utilisés : le premier type a ici pour objectif de séparer les nanoparticules par des bulles d'air avec l'aide d'acides humiques (HA), alors que le second utilise des microbulles dont la surface est fonctionnalisée par des tensioactifs (CGAs), dans l'objectif d'accroître l'efficacité de séparation. Les résultats montrent que, par mélange avec une solution basique de HA (pH 12.9), la charge de surface de nanoparticules de TiO_2 (TNPs) est d'abord neutralisée par des ions OH^- et ensuite écrantée par les polyanions de HA. Quand le pH des suspensions TNPs-HA est en dessous de 3 par ajout de solution mère de HA de pH 4.9-9.0, l'attraction électrostatique entre les TNPs et les anions est insuffisante, mais on observe quand même l'agrégation entre TNPs et la part colloïdale de l'HA. Par des essais de DAF en continu, le pH optimal de la solution mère de HA ($pH \leqq 9$) et la concentration optimale en HA (11.1 mg/L COD) permettent d'éliminer plus de 95% des nanoparticules. La concentration résiduelle de HA reste à un très bas niveau même quand l'acide humique est surdosé. Quand le pH des suspensions TNPs-HA est très acide, la plupart des molécules d'acides humiques ne sont pas solubles et ne sont pas chargées. Elles peuvent s'agréger entre-elles et former un précipité colloïdal hydrophobe pour minimiser leur contact avec le milieu aqueux. En ce qui concerne les CGAs, leur caractérisation montre que la vitesse d'agitation est un paramètre crucial pour créer des aphrons de l'ordre de la dizaine de micromètres. Les CGAs peuvent être chargés négativement ou positivement en utilisant des tensioactifs adaptés. Différentes nanoparticules de SiO_2 (SNPs) peuvent être efficacement (près de 100%) séparées de suspensions aqueuses par le procédé continu de flottation par CGAs. La comparaison entre flottation par CGAs et DAF montre l'avantage du premier procédé plus efficace avec une moindre quantité de surfactant.

Mots-clés: Séparation de nanoparticules, Flottation à air dissout, Acides humiques, Aphrons colloïdaux, Adsorption-agrégation, Mécanismes d'interaction

Résumé étendu

Introduction

La flottation est une combinaison complexe de chimie des surfaces, de dynamique des films minces et de mécanique des fluides. Le principal objectif de ce travail est d'utiliser la flottation pour séparer des nanoparticules (NPs) de l'eau. Comme il a été déjà montré, les collisions entre bulles et nanoparticules dues au mouvement Brownien et l'attachement des NPs à la surface des bulles sont difficiles, causes d'une efficacité de séparation toujours faible.

Deux méthodes sont proposées dans ce travail pour éliminer effectivement les NPs de suspensions aqueuses : (i) former de larges agrégats à l'aide d'un réactif assistant de flottation (collecteur de NPs) de manière à ce que le mécanisme d'interception devienne le mécanisme de collision prédominant entre bulles et nanoparticules ; (ii) utiliser des microbulles dont la surface est fonctionnalisée afin d'accroitre les interactions électrostatiques et l'attraction hydrophobe entre NPs et les bulles.

Deux type de NPs communes, d'oxydes de titane (TNP) et de silice (SNP), ont été choisis comme cibles à éliminer. Après une revue générale sur les dangers des effets des NPs dans l'environnement aqueux et sur la faisabilité de la séparation par flottation présentés dans le chapitre 1, les propriétés et le comportement colloïdal des NPs ainsi qu'une première analyse des caractéristiques des réactifs assistants de flottation sont étudiés dans le chapitre 2, à travers leur distribution de taille et leur potentiel zéta en fonctions du pH et de la force ionique. L'objectif de ces analyses est de comprendre les mécanismes interfaciaux entre les NPs et les collecteurs afin de mieux comprendre et/ou même de prédire les processus interfaciaux observés ensuite dans le travail sur la flottation.

Dans le 3ème chapitre, la flottation à air dissout (DAF) est utilisée pour séparer des TNPs avec l'assistance d'acide humique (HA) et/ou l'ajustement du pH. Au préalable, des

expériences de modification des propriétés de surface des NPs par des solutions alcalines de HA sont menées dans l'objectif de rechercher leurs mécanismes d'interaction. Grace à la détermination de la taille des agrégats, à des mesures de potentiel zéta, à une analyse FT-IR, à celle de la DOC résiduelle, il a été confirmé que l'interaction entre TNPs et HA est principalement le résultat d'une neutralisation des charges de surface accompagnée d'un échange de ligands, et d'autres mécanismes comme la formation d'une couche de HA sur la surface des nanoparticules. Des tests d'adsorption et d'agrégation ont ensuite été menés en contrôlant le pH des solutions de HA, montrant un mécanisme d'interaction entre HA et TNPs de type agglomération des TNPs avec de l'HA colloïdale précipitée. Ensuite, des essais de flottation continue ont été réalisés avec un pilote de laboratoire construit spécialement, sous différentes conditions physicochimiques (pH et concentration en HA) et opératoires (débits de suspension, d'eau pressurisée et d'effluent). Le pH de la suspension dans le flottateur est le paramètre essentiel, car il conditionne le comportement colloïdal des TNPs. La valeur appropriée du pH de la solution de HA et sa concentration optimale pour une grande efficacité de séparation des NPs et un faible résidu en HA ont été déterminées. Le précipité de HA pourrait être considéré comme un filet dans lequel les TNPs pourraient être piégées ou attrapées, l'ensemble étant ensuite capturé par les bulles, favorisant ainsi la flottation.

La deuxième partie de ce travail consiste à utiliser un système de microbulles (aphrons gazeux colloïdaux, CGAs) pour faciliter la séparation de SNPs par flottation (chapitre 4). Un générateur de CGAs de laboratoire a été imaginé et construit sur la base de la proposition de Flex et Sebba en 1985. Les propriétés des CGAs produits ont été déterminées en mode discontinu, ainsi qu'en mode continu, également mis en œuvre pour les tests de flottation. Le temps de demi-vie des CGAs τ_S a été mesuré ppour montrer la stabilité des CGAs ; les résultats expérimentaux sont lissés par l'équation de Hill permettant de représenter la cinétique de drainage des suspensions de CGAs. La taille des CGAs est mesurée par diffraction laser. Différents paramètres (vitesse d'agitation, débit et concentration d'air, et débit de solution de tensio-actifs) ont été testés pour déterminer des conditions optimales de

production des CGAs. De plus, leur potentiel zéta a été mesuré pour vérifier la fonctionnalisation de la surface des bulles, ceci avec deux tensio-actifs (CTAB et SDS). Le mécanisme d'interaction entre les molécules de tensio-actif et les SNPs, conduisant à l'adsorption et/ou à l'agrégation a été étudié. Différents mécanismes de flottation sont mis en exergue. Les SNPs sont séparées des suspensions aqueuses par le procédé de flottation avec production continue de CGAs. Les effets sur les performances de flottation de la concentration en tensio-actifs dans la cellule de flottation, de la concentration et de la taille des SNPs dans le courant d'alimentation et du pH sont examinés. Les mécanismes conduisant à la flottation par CGAs sont explorés. Ensuite, une comparaison entre la flottation par CGAs et la flottation par DAF est proposée pour des conditions identiques de concentration de tensio-actifs et de débits de suspension d'alimentation. Enfin, dans le dernier chapitre, des conclusions principales sont proposées ainsi que des perspectives pour ce travail.

Conclusion

Le traitement d'eaux usées polluées par des nanoparticules est un sérieux challenge dû à leur taille réduite (< 100 nm), à la stabilité des suspensions, et à leur comportement colloïdal. La flottation est un procédé de séparation liquide-particules reposant sur l'attachement ou l'adsorption des particules à la surface de bulles traversant la suspension. Ce travail a été dédié à l'amélioration de la séparation de nanoparticules par flottation. Or, il a été largement reporté dans la littérature que la flottation de nanoparticules est due à un mécanisme prédominant de transport des nanoparticules jusqu'à la surface des bulles par diffusion Brownienne.

Deux idées ont donc été poursuivies pour réaliser cet objectif : (1) accroitre la taille des particules de l'échelle nano à l'échelle micro de sorte que les NPs puissent être flottées comme des agrégats traditionnels microniques ; (2) diminuer la taille des bulles et fonctionnaliser leur surface afin de renforcer l'effet de la diffusion Brownienne et les interactions colloïdales entre bulles et NPs, et ainsi augmenter l'efficacité de capture des NPs.

Pour ce faire, deux études expérimentales ont été menées. Dans un premier temps, des essais ont été poursuivis pour effectuer la séparation des NPs par flottation à air dissout (DAF). Dans cette partie, les TNPs ont été choisies comme NPs cibles, et une matière organique dissoute, HA, a été sélectionnée comme agent assistant de flottation. Une série d'expériences d'agglomération a été menée suite à celle de flottation pour comprendre les mécanismes d'interaction entre TNPs et HA, et aussi pour tester la faisabilité de l'usage de HA pour la séparation des nanoparticules. Les résultats montrent la formation d'agrégats pendant la mise en contact résultant, après sédimentation, en un liquide surnageant le plus clair à 9.15 mg/L DOC, le dosage optimal de HA étant 7.8~9.15 mg/L. La neutralisation des charges entre OH^- et les TNPs joue le rôle principal induisant l'agglomération vraie des TNPs, alors que les autres anions (i.e. Cl^-, poly anions de molécules de HA) avec une densité de charges plus faible que OH^- aident à écranter les effets des charges de surface. Pour des valeurs de pH à l'équilibre inférieures à 3, les molécules de HA sont peu dissociées et un précipité colloïdal de HA est observé, qui ne produit pas une attraction électrostatique suffisante entre les poly anions de HA et les TNPs, mais conduit à une co-agglomération des TNPs et des précipités colloïdaux de HA. Une analyse de la dimension fractale des agrégats obtenus confirme que les agrégats de TNP-OH^-- poly anions de HA issus principalement du mécanisme de neutralisation sont de conformation compacte alors que ceux issus des interactions entre TNPs et colloïdes de HA sont plus ouverts.

Les procédés de flottation DAF par ajustement du pH et par ajour de HA ont été testés et comparés. L'ajustement du pH peut aider à éliminer les TNPs mais le rendement d'élimination n'a pas dépassé 65%. Un rendement d'environ 99% a été obtenu avec l'aide de HA quand le H de la solution de HA était entre 4.7 et 6.2.Cependant, avec des solutions basiques de HA, le rendement de flottation décroit même au dosage optimum. Un ratio élevé A/S peut améliorer la performance du procédé de flottation en fournissant une surface de capture plus importante à l'attachement des nanoparticules sur les bulles. Quand le pH final de la suspension flottée est supérieur à 4, la neutralisation des charges entre TNPs et OH- est

le mécanisme dominant de la formation des agrégats de TNPs. De plus, d'autres mécanismes peuvent intervenir dans l'élimination des TNP : l'échange de ligands, la création de liaisons entre HA et la surface des TNPs, des attractions hydrophobes accrues entre TNPs potentiellement dues à l'adsorption de HA sur la surface des TNP. Pour des pH de la suspension inférieurs à 4, la plupart des molécules d'HA ne sont pas réellement solubles et ne sont donc pas chargées. Elles peuvent former des agglomérats qui précipitent sous forme colloïdale pour minimiser leur interaction avec le milieu aqueux environnant. Le précipité colloïdal de HA peut agir comme un réseau colloïdal qui entraine les TNPs, résultant en flocs dont l'efficacité d'attachement sur les bulles est meilleure et plus stable. Il est important de noter, que ce soit par aggrégation ou par flottation, une faible quantité résiduelle en DOC de HA est toujours associée à une séparation efficace des TNPs. Ceci contribue à affirmer la participation des HAs au procédé de flottation des TNPs, conditionnée pas la formation des agrégats TNP-HA-Bulles. L'élimination efficace de la DOC indique également que le rejet des effluents du procédé DAF dans l'environnement aquatique ne causerait pas un problème environnemental.

La seconde partie du travail a été dédiée à l'utilisation, pour la flottation de nanoparticules, de microbulles dont la surface a été modifiée (CGAs). Les CGAs ont été créés à partir d'un tensio-actif cationique (CTAB) et d'un tensio-actif anionique (SDS), grâce à un générateur de CGA à l'échelle de la paillasse élaboré en s'inspirant des propositions de Felix Sebba en 1985. La morphologie des CGAs a été observée au microscope optique. Leur temps de demi-vie τ_S a été utilisé pour évaluer leur stabilité, il a été mesuré entre 80 et 150s en fonction des différentes conditions générées. Un drainage en deux étapes a été observé dans toutes les configurations de CGAs. La taille des CGAs a été mesurée par diffraction laser. La vitesse de rotation de l'agitateur influence fortement la taille. Une vitesse de 8000 rpm a été sélectionnée dans la suite de l'étude comme meilleur compromis entre une demande en bulles de petite taille et une consommation énergétique limitée. Dans la plupart des cas, la taille moyenne des CTAB-CGAs a été mesurée entre 35 et 45 µm, et celle des SDS-CGA entre 40 et 50 µm en mode continu alors qu'en mode discontinu, le diamètre moyen pour les deux

tensio-actifs est de l'ordre de 20 à 30µm. Augmenter la concentration et le débit de tensio-actif, ou le débit d'air diminue la taille des CGAs de façon très limitée. La modification de la charge de surface des bulles a été confirmée par la mesure du potentiel zéta des CGAs. Les mesures de potentiel zéta des CGAs confirment la modification des charges de surface. Les CGAs sont chargés positivement ou négativement en utilisant des tensio-actifs différents, ce qui peut conduire à renforcer l'attraction électrostatique entre bulles et particules de charges opposées pour la flottation. Les mécanismes d'interaction entre les SNPs et les molécules de tensio-actif ont été étudiés par des isothermes d'adsorption. Comparé avec le modèle de Langmuir, les modèles de Freundlich and de Langmuir-Freunlich permettent de mieux lisser les données expérimentales, en particulier le dernier modèle qui prédit la capacité maximale d'adsorption.

Suite à ces mesures préliminaires, la séparation de nanoparticules a été menée par flottation alimentée en micro-bulles CGAs. Trois types de SNPs de différentes tailles et chares de surface ont été sélectionnés comme particules modèles. A la concentration optimale en tensio-actif, quasiment 99% des SNPs ont pu être éliminés. Les influences de la concentration en tensio-actifs, de la taille des SNPs, de leur concentration et de leur pH sur les performances de flottation ont été examinées. Les résultats montrent que de hautes efficacités d'élimination peuvent être obtenues pour des concentratons de tensio-actifs même inférieures à 0.02mmol/L. De meilleurs résultats ont été obtenus avec une plus grande concentration initiale en SNP et avec des particules de plus petite taille. Un pH neutre ou basique de la suspension intitiale de SNP donne de meilleurs résultats pour la flottation avec le CTAB, alors qu'un pH autour de 3.5 peut résulter en une faible élimination des SNPs. Les CGAs obtenus avec le SDS ont permis d'obtenir de hautes valeurs d'efficacité pour tous les pHs considérés. L'effet d'attraction hydrophobe surpasse certainement celui de l'attraction électrostatique dans ce procédé de flottation avec des CGAs. La comparaison entre la flottation par CGAs et le procédé classique DAF a été faite dans les conditions de flottation optimale déterminées par les expériences précédentes en flottation continue avec des CGAs. Les CGAs peuvent éliminer les SNPs plus efficacement que la flottation DAF. Par rapport au procédé DAF dont l'efficacité dépend de l'hydrophobisation de la surface des particules par

les tensio-actifs, la flottation par CGAs peut agir également en absence de tensio-actifs adsorbés, par interaction avec ceux adsorbés sur la surface des bulles, ce qui au final nécessite une quantité moins importante de tensio-actif pour une efficacité équivalente.

Perspectives

Les résultats obtenus dans cette étude ont montré l'efficacité des HA comme assistant de flottation des nanoparticules et la capacité des CGAs pour l'élimination des NPs. Toutefois, plusieurs domaines demandent encore que des recherches soient poursuivies sur la base des résultats acquis dans ce travail :

- Des matières organiques naturelles comme les substances humiques extraites directement des sols ou des ressources aquatiques, du chitosane, et des substances polymériques extracellulaires (EPS) issues des usines de traitement biologique de l'eau, pourraient être utilisées pour faciliter la flottation des nanoparticules. Par l'attachement ou l'adsorption matières organiques-NPs et leur élimination par les bulles, les séparations simultanées des NPs et des matières organiques des eaux polluées pourraient être réalisées, autorisant ainsi le développement de procédés plus respectueux de l'environnement ;
- Des polyélectrolytes (par exemple des chlorures de polyaluminium) sont des additifs qui pourraient être combinés avec des tensio-actifs classiques pour la génération de CGAs afin de créer des aphrons avec des surfaces multi-fonctionnalisées. Il serait alors possible de traiter des eaux polluées contenant plusieurs types de nanoparticules ;
- La caractérisation in-situ des agrégats de flottation en termes de taille et de morphologie est toujours un problème dû à l'existence de fines bulles à l'intérieur des flocs qui les rendent instables. Une étude dynamique des flocs de flottation nécessite d'être mieux explorée par l'application de techniques différentes, comme la diffraction laser avec un matériel de type Sparytec ou Mastersizer, ou la diffraction de rayons X, etc… Les conditions de mesure restent à être déterminées et optimisées ;
- Utiliser la flottation par CGAs à l'échelle pilote puis industrielle reste à développer.

Ce procédé peut s'avérer économe en capital investi par rapport à la flottation DAF avec une haute efficacité à condition d'améliorer le dimensionnement du générateur de CGAs, de choisir ou de synthétiser des tensio-actifs pour fonctionnaliser les bulles, et d'optimiser les conditions de flottation.

- Using CGAs involved flotation in pilot- and plant- scale applications still remains to be developed. A capital-saving and high efficient process with CGAs needs to be worked out by improving the design of CGA generator, selecting or synthesizing functionalized surfactant, and optimizing flotation conditions.

Contents

List of figures

List of tables

Nomenclature

Latin letters

B The constant related to the heat of adsorption (-)

b The Temkin constant (J/mol)

b_L The Langmuir bonding term related to interaction energies (L/mg)

b_{L-F} The Langmuir-Freundlich bonding term related to interaction energies (L/mg)

C_0 The TNP concentration of influent (mg/L)

C_{0S} The initial concentration of surfactant solution (mg/L)

C_{0V} The volume concentration of influent (TNP suspension) (%)

C_3 The TNP concentration of effluent (mg/L)

$C_3^{'}$ The HA concentration of effluent (mg/L DOC)

C_D The TNP concentration due to the water dilution (mg/L)

$C_D^{'}$ The HA concentration due to the water dilution (mg/L DOC)

$C_{DOC}^{'}$ The dissolved organic matter existing in the TNP suspension (mg/L)

C_e The equilibrium concentration of surfactant solution (mg/L)

$C_{\max L}$ The Langmuir maximum capacity (mg/g)

$C_{\max L-F}$ The Langmuir-Freundlich maximum capacity (mg/g)

C_{HA_0} The initial HA concentration before HA-TNP interaction (mg/L DOC)

$C_{HAstock}$ The HA concentrations of HA stock solution (mg/L DOC)

C_{HA_t} The final HA concentration of TNP-HA mixed suspension at equilibrium (mg/L DOC)

C_{Δ} The amount of HA adsorbed on TNPs (mg/L DOC)

C_{SDS} The SDS concentration in the CGA generator (mmol/L)

C_{SNP} The volume concentration of SNP suspension (vol.%)

C_{CTAB} The CTAB concentration in the CGA generator (mmol/L)

C_{surf} The concentration of surfactant solution in the CGA generator (mmol/L)

C'_{surf} The surfactant concentration in the flotation cell (mmol/L)

D_f The fractal dimension (-)

d The diameter of CGAs (μm)

d_b The diameter air bubble in DAF (μm)

d_p The particle size (nm or μm)

d_{tube} The inner diameter of tube connecting CGA generator and measurement cell (m)

E The mean free energy of adsorption (KJ/mol)

E_{att} The attachment efficiency (-)

E_{capt} The capture/collection efficiency (-)

E_{coll} The collision efficiency (-)

E_{stab} The stability efficiency (-)

I The scattered light intensity (-)

K Equaling to half life of CGAs τ_s (s)

K_f The Freundlich affinity coefficient ($mg^{(1-n)}L^n/g$)

K_h The Henry constant ($mL \cdot L^{-1} \cdot atm^{-1}$)

K_T The equilibrium binding constant (-)

k The flotation rate constant (min^{-1})

k' The rate of change in size in the RLA regime ($nm\ s^{-1}$)

k_{fast} The rate of change in size in the DLA regime (nm s^{-1})

l The length of tube connecting CGA generator and measurement cell (m)

l' The thickness of dark layer in the optic microscopic image of CGA (m)

m The weight of SNPs (mg)

m_{air} The mass of air (Kg)

m_{TNP} The mass of TNPs (Kg)

N_b The bubble number per unit time (s^{-1})

N_p The nanoparticle number per unit time (s^{-1})

$N_{p/b}$ The number of particles captured by one rising bubble (-)

n The sigmoidal character of the Hill equation curve (-)

n_{air} The refractive index of air (-)

n_F The Freundlich linearity constant (-)

n_{L-F} The Langmuir-Freundlich linearity constant (-)

n_m The refractive index of the suspending medium (-)

n_{water} The refractive index of water (-)

p The pressure for dissolving air (atm)

Q The laser wavenumber, the difference between the incident and scattered wave vectors of the radiation beam in the medium (nm^{-1})

Q_1 The flow rate of influent (NP suspensions) (mL/min)

Q_2 The flow rate of pressurized water in DAF or CGA suspension in CGA-flotation (mL/min)

Q_3 The flow rate of effluent (mL/min)

Q_4 The flow rate of floats (mL/min)

Q_a The flow rate of flotation assisting reagent (mL/min)

Q_{air} The flow rate of air in CGA generation (mL/min)

Q_b The flow rate of bubbles (mL/min)

Q_{CGA} The flow rate of CGA suspension (equals to $Q_{surf.}$) (mL/min)

Q_{HA} The flow rate of HA stock solution (mL/min)

$Q_{surf.}$ The flow rate of surfactant solution (equals to Q_{CGA}) (mL/min)

q_{eD-R} The amount of surfactant adsorbed onto per unit dosage of SNPs (mol/g)

$q_{\max}$ The theoretical monolayer sorption capacity (mol/g)

R_{surf} The reduction of surfactant usage (%)

r The radius of CGAs (μm)

S_b The surface area of one bubble (m^2)

S_p' The projected area of one nanoparticle (m^2)

T The Temperature (K or ℃)

T_K The Krafft temperature (K or ℃)

t_T The CGA transporting time from generator to flotation cell (s)

U_b The relative velocity between water and a bubble (m/s)

V The volume of surfactant-SNP mixed suspension (mL)

$V_{generator}$ The volume of CGA generator (mL)

$V_{\max}$ The maximum volume of drained liquid (mL)

V_{TNPs} The volume of TNP suspension (mL)

$V_{(TNPs+HA)}$ The volume of TNP-HA mixed suspension (mL)

V_t The volume of drained liquid at time t (mL)

W The stability ratio (-)

Greek letters

β	The activity coefficient related to mean adsorption energy (mol^2/J^2)
$\beta^{'}$	The aggregation rate in the RLA regime (particle/s)
β_{fast}	The aggregation ratae in the DLA regime (particle/s)
ε	The Polanyi potential (-)
η	The NP removal efficiency (%)
θ	The scattering angle (°)
θ_{air}	The angle of refraction in air (CGA bubble) (°)
θ_{water}	The angle of incidence in water (°)
λ	The wavelength of the radiation in a vacuum (nm)
ρ_{air}	The density of air (Kg/m^3)
ρ_{TNP}	The density of TNPs (Kg/m^3)
τ_s	The half life (s)
τ_{Sm}	The measured half life (s)
τ_{Sp}	The predicted half life (s)
ν_L	The viscosity of water (m^2/s)
φ	The volume ratio between CGA suspension and dionized water (-)
ϕ	The package rate of attached particles at the bubble surface (-)

Introduction

Flotation is a complex combination of surface chemistry, thin-film dynamics, and fluid mechanics. The main objective of the current study is using the flotation technique to separate nanoparticles (NPs) from water. As has been previously recognized that the NP-bubble collision caused by Brownian motion and attachment are difficult, hence the NP removal efficiency is always poor. Two methods were proposed in this study to effectively remove NPs from aqueous suspension: (i) forming large aggregates by using flotation assisting reagent (NP collector) so that the interception can be the predominant collision mechanism between particles and bubbles; (ii) using surface functionalized microbubbles to enhance the electrostatic and hydrophobic attraction between NPs and bubbles in the flotation process.

Herein, two types of commonly seen NPs, titania (TNP) and silica (SNP), were chosen as representative treating targets. After a general review of the threat of NPs in the aqueous environment and the feasibility of particle separation by flotation in Chapter 1, properties and colloidal behaviors of NPs and characteristics of flotation assisting reagents were primarily studied in Chapter 2 via the analysis of particle size, zeta potential, pH value, and turbidity under different physiochemical conditions such as NP concentration, pH and additional ionic strength. Through this investigation, the understanding of interfacial mechanisms between NPs and collectors in the following interfacial processes could be better understood or even predicted.

In the 3rd chapter, dissolved air flotation (DAF) was employed to remove TNPs with the assistance of humic acid (HA) and/or pH adjustment. Before flotation, surface modification experiments were firstly conducted between TNPs and alkaline HA solution for the sake of their interaction mechanisms. Through aggregate size determination, zeta potential measurement, FT-IR analysis, and residual DOC detection, the interaction of TNP-HA was confirmed to be the result of mainly charge neutralization accompanied with ligand exchange, and other mechanisms such as the formation of HA layer on the particle surface. The adsorption-aggregation tests were then carried out controlling pH values of HA stock solution, through which the agglomeration of TNPs with precipitated HA colloids was declared for the TNP-HA interaction process. Thereafter, continuous flotation trials were performed on the particularly designed laboratory scale apparatus under different physiochemical conditions (pH and HA concentration) and operating conditions (flow rates of

influent, pressurized water and effluent). The pH value of flotation suspension was found to be significant in the flotation process by changing the colloidal behavior of TNPs. The appropriate pH value of HA stock solution and optimum HA concentrations for high TNP removals and low residual HA concentration were determined. The colloidal precipitate of HA might be considered as an extended fishnet where TNPs could be enmeshed or trapped, and hence the bubble capture in DAF was reinforced.

The other direction in this work is to employ a system of microbubbles (colloidal gas aphrons, CGAs) into flotation to facilitate the SNP separation (Chapter 4). A laboratory scale CGA generator was designed and fabricated based on the proposal of Flex Sebba in 1985. The batch generation mode was specially conducted for the study of CGA properties, and the continuous CGA production mode was used in both CGA characterization and flotation process. The half life τ_S was measured to represent the stability of CGAs; experimental data were fitted by the Hill equation which could figure out the drainage speed of CGAs. The CGA size was measured by laser diffraction. Different factors (stirring speed of agitator, air flow rate, and concentration and flow rate of surfactant solution) were tested to determine the optimum condition for the CGA creation. Moreover, the zeta potential of CGAs was also measured by NanoZS to verify that the bubble surface was functionalized by using different types of surfactant (CTAB and SDS in this study). Moreover, the interaction mechanism between surfactant molecules and SNPs were studied by adsorption-aggregation. Combined with different characteristics of SNP suspension, the specific interaction interpretation was given. Different flotation mechanisms of CGA-flotation and DAF were highlighted.

SNPs were separated from aqueous suspensions by the continuous CGA generation-flotation process. Surfactant concentration in the flotation cell, initial SNP concentration and size in the influent, and pH of SNP suspension were investigated for their effects on the flotation performance and also the exploration of CGA-flotation mechanisms. Then, the comparison between CGA-flotation and DAF at the same surfactant concentration and flow rate of influent was conducted in terms of the SNP removal efficiency and surfactant demand. Ultimately, main conclusions and prospects of this work are given in the last chapter.

Chapter 1

General review of nanoparticle in wastewater and relative separation techniques

Summary

Along with the growth of nanotechnology, materials including natural or manmade nanoparticles (NPs) have become widely used. This chapter firstly reviews possible sources of NPs in wastewater with respect to industrial sectors, household commodities and effluents of water treatment units. The specific environmental hazards and health threats of NPs in waters and wastewaters are demonstrated; thereafter, existing separation processes of NPs from aqueous suspensions and their treating efficiencies are comparatively reviewed, in which advantages of flotation, the essential technique in this Ph.D. study, is outweighted. The flotation separation mechanisms of NPs are depicted herein so as to propose strategies of improving the NP removal efficiency: (a) decreasing the bubble size by using different bubble generation methods, (b) increasing particle size with the aid of flotation reagents, and (c) combining (a) and (b) by modifying the bubble surface with flotation reagents. Based on the above principles, the design and application of different flotation processes and techniques are introduced.

1.1 Sources of nanoparticles (NPs) in the aqueous environment

Nanoscience involves the study of materials in the nano scale level between approximately 1 and 100 nm. Due to the high reactivity, large specific surface area, and the tuneable nature of nanomaterials, nanotechnology has widespread applications from industrial sectors such as energy, catalysts, pigments, electronics, remediation, and fuel additives, to household commodities such as food storage containers, cleaning supplies, bandages, clothing, personal care products, cosmetics, pharmaceutical formulations and washing machines (Ju-Nam and Lead, 2008). It has been reported that the engineered nanomaterials are currently used in around 1628 commercially available consumer products, and analysts estimate that the market for such products is currently around hundred of billions of euro and possibly rises to one trillion by 2015 (Groso et al., 2010; Chalew et al., 2013).

1.1.1 Classification of nanomaterials

The composition of nanomaterials differs according to their formulation, and generally can be classified into inorganics and organics as shown in Fig. 1.1: metals, metal oxides and quantum dots as semiconductors are considered as the former whilst fullerenes and carbon nanotubes belong to the latter (Peralta-Videa et al., 2011).

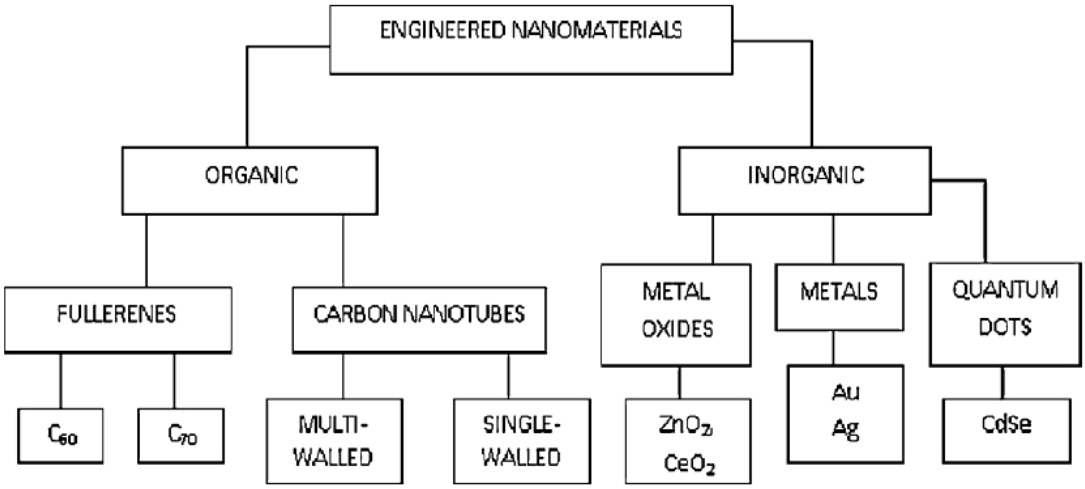

Fig. 1.1. Nanomaterial classification according to their composition. (Peralta-Videa et al., 2011).

As suggested by Foss Hansen et al. (2007), nanocommidities should be categorized depending on the location of the nanoscale structure in the system, which lead to a division of nanoproducts into three categories (Fig. 1.2): (1) being nanostructured in the bulk; (2) having nanostructure on the surface; and (3) being processed into nanostructured particles. 70 % of consumer products are in category 3 (as particles), which includes nanoproducts in forms of surface-bound nanomaterials, NPs suspended in liquids, NPs suspended in solids, and free airborne particles. Therein, NPs suspended in liquids were used in 37% of the consumer products (Bakker, 2012), and the current study was launched to figure out effective ways of removing these NPs from aqueous systems in order to avoid relative environmental problems caused by NPs.

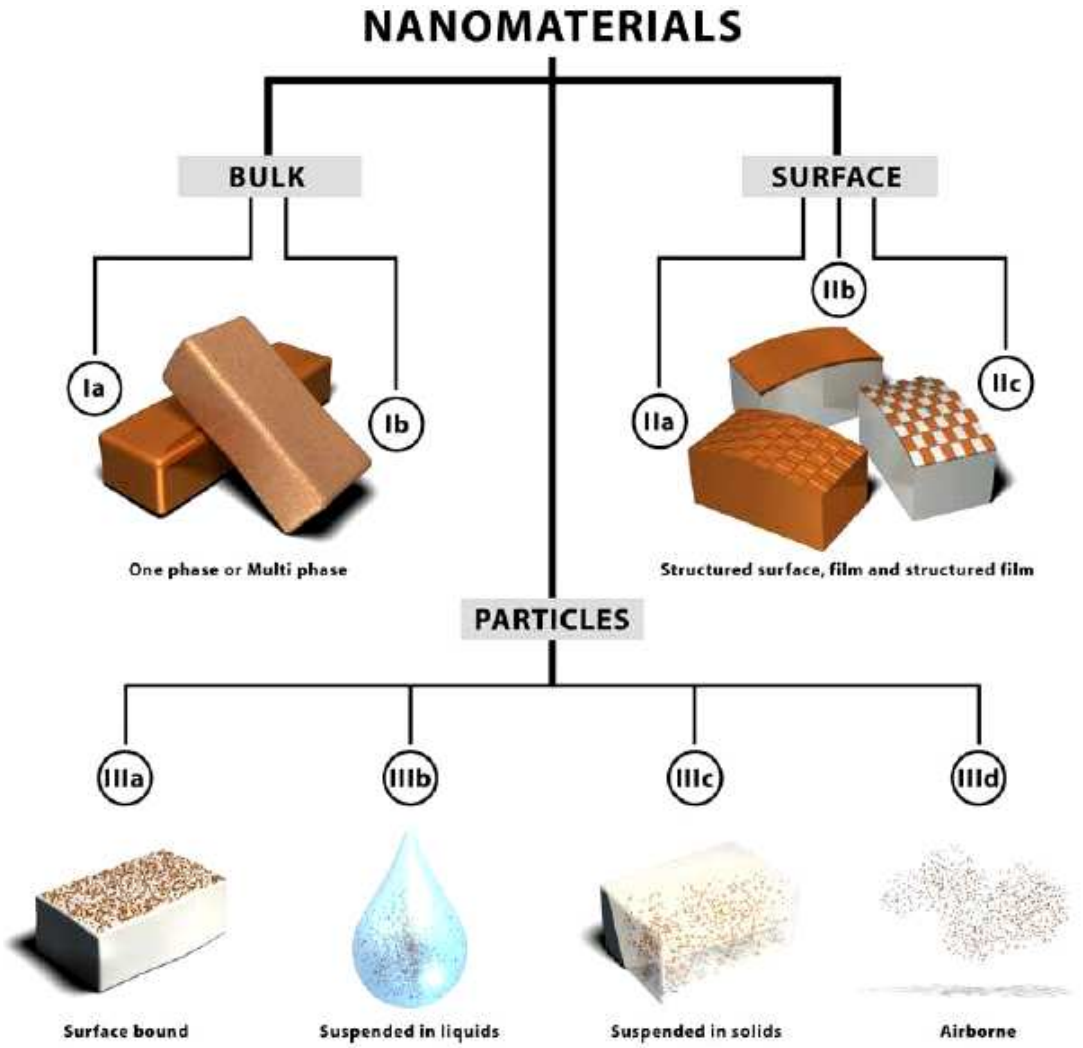

Fig. 1.2. The categorization framework for nanoproducts (Foss Hansen et al., 2007).

1.1.2 NPs from domestic and industrial wastewater

Carbon, silver, silica, titania, zinc and cerium dioxide are most commonly used among different types of NPs (see in Fig. 1.3). It is inevitable that those nanoscale products and their by-products find one release route among others into the aquatic environment via domestic and industrial wastewater discharges. Typically, there is a growing global demand on fuel additives, lubricants, and catalysts because of their enhanced performance achieved through the infusion of nanoscale cerium oxide particles. Generally, these nanotechnologically fuel additives, lubricants and catalysts are likely to be emitted through various waste streams into the air, water or soil systems. Ultimately, they will end up into the aquatic and terrestrial environments through surface-runoffs, spillages during use, and leakages from vehicles, or via sewage drainage systems. This raises serious concerns of dealing with nanowastes from both point and non-point sources.

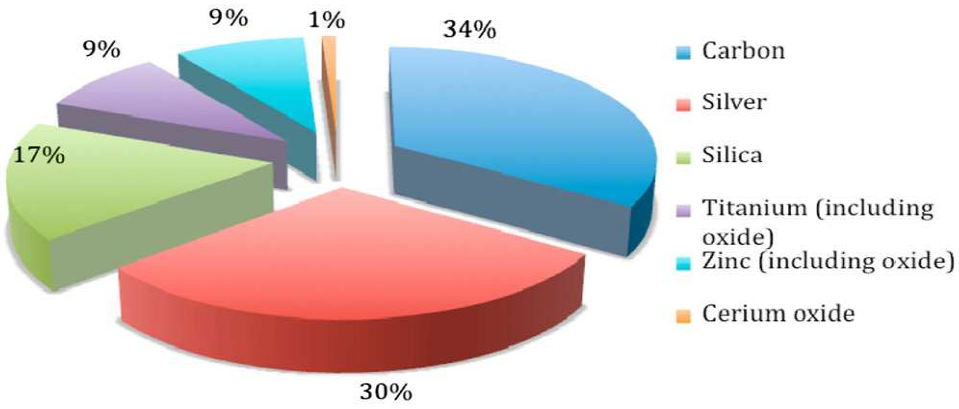

Fig. 1.3. Nanomaterials used in consumer products, 2006 (Maynard, n.d.).

Another instance is the cosmetics and personal care sector which constitute the largest number of nanoproducts (> 50 %) currently available in the global market (Musee, 2011). The usage of nanomaterials is favoured for the following reasons: ability to absorb and reflect UV light while remaining transparent (e.g. TiO_2), a better antioxidant than vitamin E (e.g. fullerene), antibacterial properties (e.g. nano-Ag), and anti-aging skin properties (e.g. nanosomes and gold particles) (Yang et al., 2007; Benn and Westerhoff, 2008; Labille et al., 2010). Consequently, the waste streams containing nanomaterials will be introduced directly to the aquatic environments at application phase -- through the sewage systems as a result of showering and washing process.

1.1.3 NPs from wastewater treatment plants (WWTPs) as second pollutants

Some metallic NPs may dissolve (e.g., silver-, zinc-, iron- or copper-based) or biodegrade (e.g., fullerenes) in wastewater, subsequently adsorb to settable biomass, and finally precipitate as inorganic solids or form stable aqueous complexes. Because of the dense biological communities in WWTP unit processes, under typical conditions, more than 90 % of the nanomaterials may attach to biomass and be removed in wastewater treatment plants (WWTPs). Inclusion of membrane filtration to strengthen gravity settling has the potential to increase NP removal (Springer et al., 2013; Westerhoff et al., 2013). However, after the biosolids are disposed to the land surface and spread to fields, landfills, or incineration, their fate needs to be further considered. From this standpoint, municipal WWTPs are particularly important sources of contaminant release into the environment, as they provide potential pathways of nanopollutants into surface waters, soils, and air through treated effluent, biosolids, and plant-generated aerosols (Kiser et al., 2010).

1.2 Threat of NPs to human beings and the aqueous environment

1.2.1 Pathways of NP entry into living bodies via the aqueous environment

As reported by Moore (2006), apart from the NP uptake by inhalation or ingestion which is the major route in terrestrial organisms, in the aqueous environment there may be more routes of entry such as direct passage across gill and other external surface epithelia. Ultimately, those NPs possibly accumulate in human bodies through the food chain. The natural propensity for many NPs to bind transition metals and organic chemical pollutants is believed to enhance the toxicity of some NPs; and the ability of those particles to penetrate the body and cell (e.g. through fluid-phase endocytosis and cavelae in Fig. 1.4) provides potential routes for the delivery of NP-associated toxic pollutants to sites where they would not normally go.

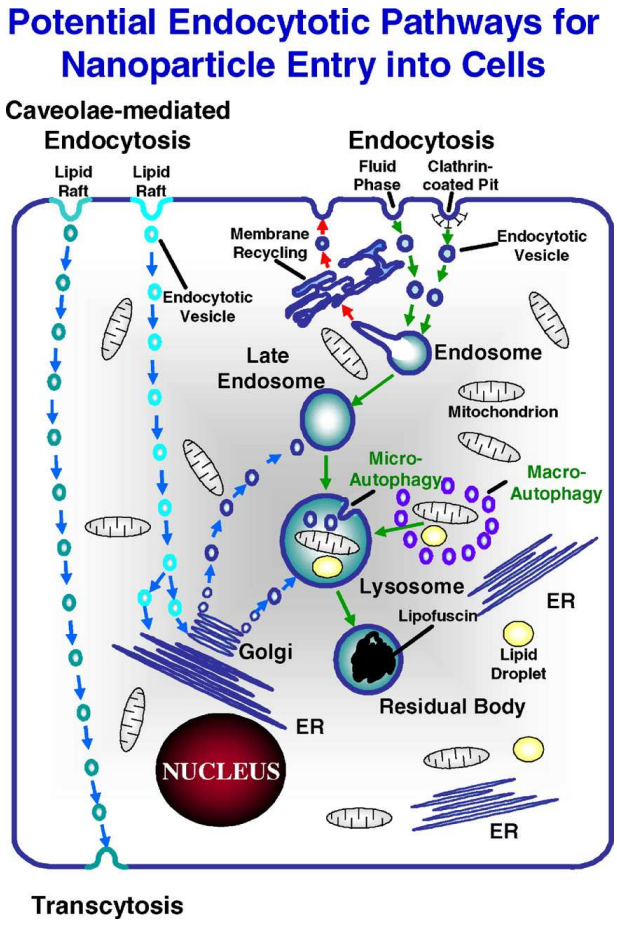

Fig. 1.4. Pathways for endocytosis in the cell which could be exploited by manufactured NPs. Endocytosis via clathrin-coated pits (receptor mediated) or uncoated pits (fluid phase) transfers materials to the lysosomal degradative compartment, while caveolar endocytosis can result in translocation to the endoplasmic reticulum (ER), Golgi or through the cell by trancytosis (Moore, 2006).

1.2.2 Hazard and toxicity of NPs

Any toxic effect of NPs will be very specific to their type of base material, size, substitute, and coating. One of the earliest findings confirmed that NPs (< 100 nm) showed greater toxicity than fine particulates (< 2.5 µm) of the same material on a mass basis. This has been observed with different types of NPs, including titanium dioxide, aluminum trioxide, carbon black, cobalt, and nickel (Hallock et al., 2009). For example, Oberdorster et al. (1994) found that 21 nm titanium dioxide particles produced 43 fold more inflammation (as measured by the influx of polymorphonuclear leucocytes, a type of white blood cell, into the lung) than 250 nm particles based on the same mass instilled into animal lungs.

The impact of nanomaterials on living cells can be broken down into the interactions between nanomaterials and individual cell components. The membrane interface is the first interactional medium between a material and a cell (Wiesner and Bottero, 2007). Yang et al. (2010) concluded that the long-term exposure (21 days) of low-level C60 caused significant cellular damage, leading to cell dysfunction and cell lysis or necrosis in *daphnia magna*. The very large surface area of ultra-small particles could result in the direct generation of harmful oxyradicals (ROS), causing cell injury by attacking DNA (Brown et al., 2001). Furthermore, nanomaterials that interact with proteins might alter the protein structure as well. Highly selective protein adsorption on NPs added to the fact that particles were capable of reaching subcellular locations, results in significant new potential impacts for NPs on protein interactions and cellular behaviours. The loss of secondary structure and consequent changes in the activity of proteins upon binding to NPs could be seen as a drawback or a potential source of NP toxicity (Lynch and Dawson, 2008).

In short, the potential advantages of nanomaterials are immense, however, so are their potential dangers. Some of the dangers might be induced by the application of NPs in the fields of medicine and personal care. In order to avert the risks, we must thoroughly understand the nanomaterial properties, and then develop comprehensive plans to prevent them. In the following part, we are going to discuss how to remove NPs from water. One simple way to prevent the risks is also to prevent the contamination by NPs, especially of water resources.

1.3 Techniques already applied in the NP wastewater treatment

1.3.1 Challenges in the NP wastewater treatment

The rapidly increasing production of engineered NPs has created a demand for particle removal from particularly industrial and communal wastewater streams. It is challenging and urgently necessary to develop effective techniques to clarify NP wastewaters considering their physiochemical properties and environmental threat of NPs. On the one hand, surfaces and interfaces of particles are crucial characteristics of nano scale materials. As the particle size decreases, the proportion of atoms found at the surface is magnified relative to the proportion inside its volume, resulting in more reactive NPs and possibly higher potential toxicity. On the other hand, in the NP application, surface coating can be utilized to alter surface properties so as to prevent aggregation or agglomeration with different particle-types, and/or serve to "passivate" the particle-type to mitigate their potential hazard on health (Warheit et al., 2008). Those well dispersed NP suspensions bring greater difficulties in the NP separation process. Even if the surface-functionalized NPs are likely to be removed by water treatment processes to sewage sludge (typically recycled to land), uncoated NPs will continue through the effluent steam (Jarvie et al., 2009). The study of Hwang et al. (2011) pointed out that aqueous engineered iron oxide NPs coated with a surfactant ($ENP_{Fe\text{-}surf}$) would be introduced into environmental receptors and potentially impact them through the treated effluent because they could deteriorate the water quality with respect to soluble chemical oxygen demand, turbidity, and apparent color. The large fractions of $ENP_{Fe\text{-}surf}$ could also go into sludge management processes, leading to the necessity of assessing secondary impacts of $ENP_{Fe\text{-}surf}$ on the sludge stabilization, composting, and landfill disposal.

1.3.2 Water treatment application and case study of the NP removal from aqueous body

A growing number of study and trials on laboratory and WWTP scales have been addressed to the NP release into aquatic environment via controlling the treated effluent discharge; meanwhile great efforts have been dedicated to govern the terrestrial environment via sludge disposal or application to land (Hwang et al., 2011). The efficient NP removal is particularly important in view of preventing the considerable NP ecotoxicity for a long-term persistence and evidence. Herein, several typical attempts and application on the NP wastewater treatment have been summarized in Table. 1.1. Traditional and improved techniques, such as flotation, coagulation, filtration, adsorption, were used to deal with different kinds of NP

suspensions or wastewater including chemical mechanical polishing effluent, municipal sewage, etc, and high treating efficiencies and helpful indications for further technical development were obtained.

Table. 1.1. Typical NP wastewater treatments.

Treating method	Target NP contaminant	Particle size	Type of treating water	Key results/findings	Reference
Foam flotation	Colloidal titanium dioxide (TiO_2)	50 nm	Simulated wastewater	TiO_2 separation was almost complete in optimum conditions. The coulombic interaction between charged TiO_2 surfaces and ionic collectors played a dominant role. Foam flotation might find application in the separation of submicron TiO_2 particles in suspend-photocatalyst systems.	Shen, 1998.
Foam Flotation	Colloidal silica alumina particle	40-150 nm	Simulated wastewater	Four techniques were employed to assess the rate of true flotation and entrainment in the flotation process. The proportion of the colloidal particles recovered by true flotation was quite high due to the fine bubble size. A smaller bubble size had a smaller associated wake and hence fewer particles were entrained into the froth.	George et al., 2004.
Electro-coagluation-flotation	Silica NP; Dissolved silicon	79.8 nm	Chemical mechanical polishing (CMP)	The surfactant CTAB was employed as both frother and collector in the process. Removal of turbidity and dissolved Si exceeded 90% given the charge loading	Hu et al., 2005.

			wastewater	applied over 2000 $C \cdot L^{-1}$ with 5mg$\cdot L^{-1}$ of CTAB. The sludge volume and the settling time were significantly less in the solution containing CTAB than in that without CTAB. No CTAB pollution problem existed after the ECF process.	
Dispersed air flotation	Silica NP	88.9 nm	CMP wastewater	Very effective removal of particles from wastewater was found when cationic surfactant CTAB, was used as collector. Both the change of interface properties and the aggregation of particles contributed to flotation removal of particles. When n-dodecyl amine chloride was used as collector, longer reaction time and higher dosage were needed owing to its relatively weak adsorption.	Lien and Liu, 2006.
Nano-bubble flotation technology (NBFT)	Silica NP; Dissolved silica NP and heavy metals	106 nm	CMP wastewater	PACl/NaOl was the best combination of activator/collector, and its application in the NBFT with coagulation process increased the clarification efficiency by 40 % compared with traditional processes. High efficiencies were also observed in the pilot-scale flotation experiments. Optimum treating	Tsai et al., 2007.

				conditions were determined. The cost and performance assessment reflected that the CMP wastewater could be treated efficiently at a minimum cost using NBFT.	
Dissolved air flotation	Silica NP	75 nm, 80 nm	Simulated wastewater	More than 99% of the nanosilica 30R50 can be removed by flotation with the addition of CTAB. Flotation without additives could not effectively work mainly due to the hydrophilic surface of silica particles.	Liu, 2010; Liu et al., 2012.
Biosorption	Cerium oxide NP	24.5 nm	Simulated wastewater	Certain part of the model cerium oxide was found in the exist stream. The NP surface charge and the stabilizing surfactants in the raw wastewater greatly influenced the treating effect. There were also complex interactions between dissolved species and NPs in the changing environment of the sludge.	Limbach et al., 2008.
Biosorption	Nanosilver	10-500 nm	Sock manufacturing wastewater	The adsorption of nanosilvers to biomass was used to develop a model. The high silver concentration might limit the disposal of the biosolids as agricultural	Benn and Westerhoff, 2008.

				fertilizer.	
Biosorption	Fullerene Titanium dioxide Silver	3-100 nm	Simulated wastewater	Increasing the biomass concentration to which NPs were exposed increased the NP removal. NOM and EPS had the most significant effect on fullerene and biosorption, decreasing aq-nC_{60} removal from water. The specific sorption mechanisms were expected to be uncovered.	Kiser et al., 2010.
Electrocoagulation	Fine oxide particles	100 nm	CMP wastewater	Al/Fe (anode/cathode) was a good electrode pair in terms of overall performances. 99% copper could be removed and 96.5% turbidity was reduced in less than 100 min, with an effluent COD below 100 mg/l. The wastewater quality exceeded the direct discharge standard and the effluent can be considered for reuse.	Lai and Lin, 2003.
Magnetic seeding aggregation	Silica NP	60 nm	CMP wastewater	The turbidity of the CMP wastewater was reduced from 110 NTU to 1 NTU in a magnetic field strength higher than 800 G. Magnetic seeds used in this study could be directly reused for 3 times.	Chin et al., 2006.

Coagulation-sedimentation	Silica NP	2-90 nm	Industrial wastewater	NPs were not effectively removed by the existing coagulation-sedimentation unit with PACl as coagulant. NPs agglomerated in approximately linear aggregates of sizes 100–300 nm. Prolonged contact between residual PACl and the nano-particles generated large aggregates.	Chang et al., 2007.
Flocculation-sedimentation	Silica NP with iron oxide core	110 nm	Domestic wastewater	The surface-functionalized SiO_2 NPs were likely to be removed by sedimentation to sewage sludge; Those uncoated continue through the effluent stream. This study shows new potential for exploiting surface functionalization of NPs to modify their environmental pathways.	Jarvie et al., 2009.
Electrically assisted cross-flow filtration	Synthetic nano-sized alumina (γ-Al_2O_3) and silica particles (SiO_2)	200 nm for γ-Al_2O_3; 84 nm for SiO_2	Aqueous suspension	The pH value played an important role in electrofiltration; meanwhile the conductivity primarily controlled the critical current via linearly correlation. Addition of salt to increase the conductivity could enhance the separation efficiency through increasing the cirtical current difference. Particles of different surface charges could be separated completely without	Sung et al., 2007.

				conductivity adjustment.	
Membrane filtration	Fullerol nC_{60}	252±132 for Fullerol; 160±64 for nC_{60}	Simulated wastewater	The molecular interactions that determine interfacial tension may play a key role to the bond strength between fullerol molecules in an aggregate. Beyond a critical pressure, ties between fullerol molecules might be weakened, allowing for aggregate deformation or break-up, and possible passage through the membrane. Electrolytes that favor stronger bonds in aggregates will exhibit greater removal by membranes.	Jassby et al., 2010.
Ultrafiltration	Silica NP	78 nm	Simulated wastewater	The 10 kDa cellulose membrane gave rise to the highest process efficiency under stirred conditions with the associated retention rate greater than 99.6 %. The 10 kDa membrane was subject to almost completely reversible fouling according to the unstirred filtration experiments.	Springer et al., 2013.
Full scale wastewater treatment plant	Titanium nanomaterial	4-30 nm	Municipal sewage	More than 96 % of the influent titanium could be removed. It appeared that microfiltration-treated	Westerhoff et al., 2011.

	wastewaters contain fewer NPs than conventionally settled wastewater.

Among all the NP separation methods mentioned above, flotation is focused as the essential technique in the current study to purify the NP polluted water, and high NP removal efficiencies are expected through the process control and/or the device improvement. Previous research studies in our laboratory concerning the particle-bubble interaction mechanism and NP aggregation led this dissertation to extend flotation as a clarification technology for removing NP from water, and relative details will be depicted in the following section.

1.4 Flotation in the NP separation from water

Flotation, the water purification process based on the adsorption or attachment of materials on the surface of gas bubble passing through a solution or suspension, has always been considered among the most effective techniques in particle separation (Ramirez et al., 1999). Its great potential on the NP and submicron particle removal from wastewaters has been proved via the successful application of carrier flotation, agglomerate flotation, emulsion flotation and oil-in-water flotation in increasing flotation rates of ultrafines (George et al., 2004). In our research group, work has been dedicated to the NP separation by flotation and aggregation. Liu et al (2010, 2012, 2013) developed a laboratory scale flotation apparatus for NP separation from liquid media, and also studied the interaction between silica NPs and additives ($AlCl_3$ and CTAB, respectively) by means of kinetics and thermodynamics aggregation researches. Flotation tests in the absence and presence of additives highlighted the importance of flotation assisting reagents on achieving high NP removal efficiencies. It was found that the charge neutralization dominated mechanism for the agglomeration of NP suspension in the presence of either $AlCl_3$ or CTAB. Besides, for the $AlCl_3$ involved NP aggregation, a possible “hair layer” for NP at the high ionic strength and sweep flocculation based on the precipitation of $Al(OH)_3$ could play leading roles at the thermodynamic equilibrium. For the NP-surfactant (CTAB) aggregation, “depletion flocculation” or “volume-restriction” was proposed to explain the aggregation of nanosilica at high zeta potential conditions apart from the electrostatic interaction. Critical coagulation concentrations of additive reagents were determined and high NP removals (> 99 %) were obtained.

1.4.1 Flotation mechanisms of the NP separation by flotation

1.4.1.1 General mechenisms of particle involved flotation process

It is extensively recognized that the key of flotation process is the bubble-particle capture which is the consequence of i) bubble particle collision, ii) particle attachment to the bubble and iii) the stabilization of particle-bubble aggregates: $E_{capt} = E_{coll} E_{att} E_{stab}$, where E_{coll} is the collision efficiency, E_{att} is the attachment efficiency and E_{stab} the stability efficiency of the particle-bubble aggregates (Huang et al., 2011). The transport of particles towards the bubble surface is shown schematically in Fig. 1.5. Without loss of generality, three predominant transport mechanisms are considered, including interception, gravity (sedimentation) and Brownian diffusion. The transport of particles by interception is due to the liquid flow, which carries the particles along the liquid streamlines. The particles come into contact with the bubbles because of their finite size. Transport by gravity is significant for solid particles which have a density greater than that of water. The influence of inertial forces and gravity on the particle transport is insignificant for NPs; and transport by Brownian diffusion is then the most important mechanism. The combination of these three transport mechanisms allows the determination of the transition between the Brownian diffusion and hydrodynamic-gravity collection mechanisms (A. V. Nguyen et al., 2006).

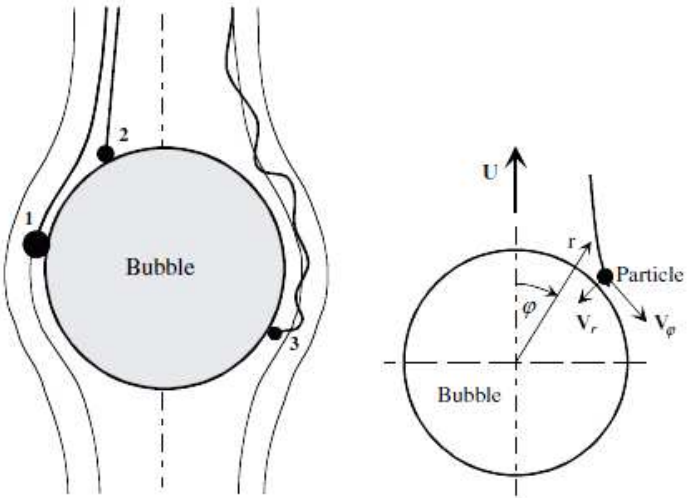

Fig. 1.5. Schematics of the (1) interception (2) gravity (3) Brownian transport mechanisms for fine particles towards a rising bubble in a rotationally symmetrical coordinate system (r, θ). The thick lines describe the particle trajectory while the thin lines describe the liquid streamlines (A. V. Nguyen et al., 2006).

In previous studies of our research group, much effort has been devoted to the bubble capture behavior and efficiency of microparticles in the flotation process. Sarrot et al. (2005) found

that the collision efficiency increased with the Reynolds number and significantly decreased with the level of bubble surface contamination; for clean and fully contaminated spherical bubbles, the efficiency evolved as d_p/d_b and $(d_p/d_b)^2$, respectively, whatever the bubble Reynolds number and the particle size, whereas for partially contaminated bubbles, the efficiency could be scaled with d_p/d_b or $(d_p/d_b)^2$ depending on both the level of contamination and the particle size (Legendre et al., 2009). In accordance with this direct numerical simulation (DNS), the capture efficiency of microparticles was then determined using a single bubble experimental device developed in the laboratory (Sarrot et al., 2007), demonstrating that the capture efficiency decreased with the bubble diameter at high bubble Reynolds number but increased with the bubble diameter at low bubble Reynolds number, and the particle hydrophobicity facilitated the collision of particle-bubble. Huang et al. (2011) continued this investigation and emphasized that, by measuring the evolution of bubble's rising velocity, the surface coverage could be determined, and the number of particle collected and carried by the bubble could be deduced. Different from the classical counting techniques, this technique based on measuring the bubble velocity was easy to be implemented, and its results could agree well with others. It has also been confirmed that the interface contamination impacted greatly the collision efficiency between bubbles and inertial particles; meanwhile, one model was proposed to describe collision efficiency for any clean or contaminated bubble, inertial or non-inertial particles (Huang et al., 2012).

1.4.1.2 Flotation of NPs

In the case of NPs and submicron particles involved flotation, in contrast to large particles, the aggregate of a particle with a bubble is stable (E_{stab}=1) since both the hydrodynamic and gravity forces are now negligible compared with the adhesion force. Thus the capture efficiency can be reduced to $E_{coll}E_{att}$. The attachment efficiency E_{att} takes values from 0 to 1, reaching the maximum when the energy barrier between interacting bubbles and particles is lower than the energy of thermal motion kT. When the energy barrier is higher than the energy of the thermal motion, the analysis of particle attachment becomes more complicated because the probability of overcoming the barrier is a function of surface forces and particle diffusivity (Mishchuk et al., 2012).

In the case of E_{att} =1, the capture efficiency is further reduced to the collision efficiency E_{coll}. As aforementioned, for NPs that approach large molecular dimensions, Brownian diffusion is the main collision operative mechanism. Diffusion is an effective mass transfer mechanism, and the loss of inertia associated with fine particles may enhance the collection by bubbles and thus becomes a positive advantage in Brownian motion. Spiclman and Goren (1970) were probably the first to consider the influence of both the colloidal interaction and the microhydrodynamic interaction on the deposition of Brownian particles as found in filtration. The flotation recovery of nano and submicron particles was primarily qualitatively explained by Reay and Ratcliff (1973) who determined the collection efficiency by including Brownian diffusion using a formulation of Levich. However, the Levich theory failed to consider the microhydrodynamic interaction between a particle and a bubble surface at close approach, which changed the Stokes drag force.

The study and practice of NP involved flotation processes have established that the recovery of particles by flotation is most successful in the 10~200 μm size range (Ahmed and Jameson, 1985). The poor collection of NPs from aqueous suspensions has become a significant challenge of flotation due to the significant decrease in the collision rate and encounter efficiency as the particle size decreases (A. V. Nguyen et al., 2006; Tatu Miettinen et al., 2010). Reay and Ratcliff (1973) found that the collection efficiency have a minimum at a particle size in the order of 100 nm; with a size smaller than the transition size, Brownian diffusion and colloidal forces (electrical double-layer and non-DLVO hydrophobic forces) controlled the particle collection, whereas the interception and collision mechanisms predominate with larger particles (Nguyen et al., 2006; T. Miettinen et al., 2010; Mishchuk et al., 2012). It indicates that the separating efficiency of NPs can be improved via using small bubbles so as to enhance Brownian diffusion and thus the collision efficiency, and/or reinforcing colloidal forces between NPs and bubbles in order to increase the attachment efficiency. Additionally, it is worth noting that, in addition to treating the NP wastewater, the research of NP involved flotation can also be indicative in the collection and purification of NPs after preparation (Chungchamroenkit et al., 2008).

1.4.2 Approaches of improving the NP removal efficiency in flotation

To increase the bubble capture efficiency of NPs and thereby improve the flotation performance, flotation techniques have been developed from two approaches, either

decreasing bubble size or increasing apparent particle size by NP surface modification. The specific description is given down below.

1.4.2.1 Decreasing the bubble size

Smaller bubbles are preferred in treatment techniques due to both their high surface area-to-volume ratio and their increased bubble volume fraction at a fixed flow rate due to lower rising velocity. Compared with large bubbles, their low rise velocity allows long residence time in the flotation column, which enhances the attachment between particles/flocs and bubbles. Additionally, as the gas in the microbubbles dissolves into the treated water, their zeta potential increases rapidly because of a reduction of the bubble surface area (Wen et al., 2011). A large number of mechanical and physiochemical approaches have been employed for tiny bubble (microbubble and nanobubble) production so as to improve the NP collection efficacy in flotation:

(1) Generation of microbubbles

For the generation of micro-sized bubbles with diameters on the order of several tens of microns, a large body of mechanical approaches have been used, including improving the design of flotation cells (i.e., the shape of the rotor and stator) and the gap size between the rotor and stator so that the gas bubbles produced at the bottom of the flotation cell can be dispersed into smaller bubble sizes. The venturi-type microbubble generator has also been widely accepted in use (Terasaka et al., 2011). It has the advantages of compact size, low pump power and high-density bubble generation normally with a mean diameter below 100 μm. The venturi-type generator consists of three main parts, i.e. inflow, tubule and tapered outflow (Agarwal et al., 2011). Morever, a microporous material can be used at the bottom of the cell, through which the gas bubbles are produced. James Hanotu, et al.(2012) used the fluidic oscillation for microbubble generation, which converted continuous air supply into oscillatory flow with a regular frequency to generate bubbles (around 50 μm) of the exit pore.

In addition to those mechanical production of microbubbles, different physiochemical methods, typically dissolved gas flotation (DAF) and electroflotation (EF), are extensively applied. DAF is the technique to generate small bubbles and improve the floatability of fine particles. The most common dissolved gas is air which is also one of the main flotation approaches in this Ph.D. study. DAF is based on Henry's law, where the solubility of air in an

aqueous solution is proportional to the partial pressure of air at constant temperature. Bubbles are formed by a reduction in pressure of water pre-saturated with air at pressures higher than atmospheric. The air-supersaturated water is forced to go through needle-valves or special orifices, and clouds of bubbles with average diameter of 30~100 µm (60~70 µm in our case) are then produced in the down stream of the constriction. The schematics can be seen in Fig. 1.6.

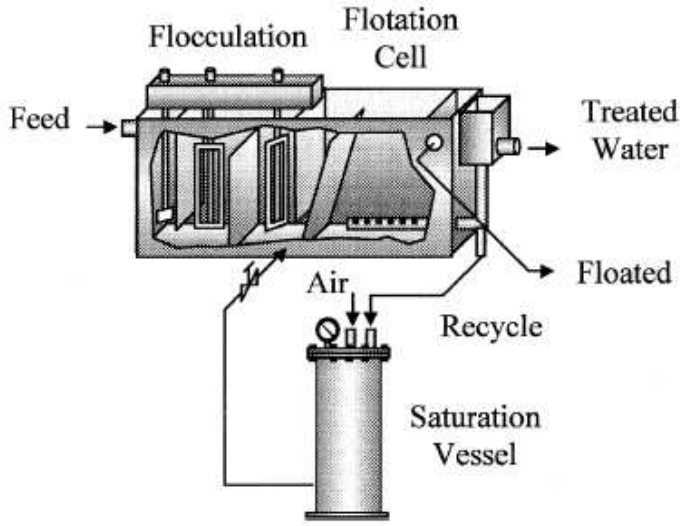

Fig. 1.6. The conventional DAF unit, with water recycle to the saturator (Rubio et al., 2002).

EF is based on the use of hydrogen and oxygen bubbles formed by the electrolysis of water. Oxygen is formed at the anode, Eq. (1.1), and hydrogen is formed at the cathode, Eq. (1.2). These two gases may be used either separately or together, or in combination with air bubbles in electroflotation.

$$H_2O \leftrightarrow 2H^+ + \frac{1}{2}O_2(g) + 2e^- \qquad \text{Anode (+)} \tag{1.1}$$

$$2H_2O + 2e^- \leftrightarrow 2OH^- + H_2(g) \qquad \text{Cathode (-)} \tag{1.2}$$

In most cases ‘‘electrolytic oxygen and hydrogen” do not have any specific effect on the surface of minerals and their flotation rate depends mainly on the bubble size (Chen, 2004). The effective EF obtained is primarily attributed to the generation of uniform and tiny bubbles. The sizes of the bubbles generated by EF were found to be log-normally distributed with over 90% of the bubbles in the range of 15~45 µm for titanium-based DSA® anode (Chen et al., 2002). In contrast, typical bubble sizes range from 30 to 100 µm for DAF.

(2) Generation of nanobubbles

As for nanobubbles, their interface consists of hard hydrogen bonds similar to those found in ice and gas hydrates, leading to reduced diffusivity which helps to maintain adequate kinetic balance against high internal pressure of bubbles (Ohgaki et al., 2010). Compared with microbubbles that tend to gradually decrease in size and subsequently collapse due to long stagnation and dissolution of interior gases into the surrounding water, nanobubbles remain stable in water (Zimmerman et al., 2011). The formation, growth and collapse of nanobubbles in solution are often referred to cavitation which can be defined as the formation of tiny bubbles filled with vapour/gas or their mixture and the subsequent activities such as growth, collapse and rebound in liquids (Fan et al., 2010). Based on the mode of generation, cavitation is broadly classified into four categories, i.e. hydrodynamic, acoustic, optical and particle cavitation (Agarwal et al., 2011b). Hydrodynamic cavitation can provide a simple and practical method to create tiny bubbles in situ in flotation systems by way of mechanical agitation or fast liquid flow (Zhou et al., 2009). Cavitation occurs when decreasing static pressure of the pressurized fluid entering a tubule part (Agarwal et al., 2011b). It has been reported that nanobubbles with a mean diameter of 400~700 nm could be created by ultrasonication of a mixed surfactant solution with constant purging using a steady gas stream (Oeffinger and Wheatley, 2004). Cavitations also can be achieved in nature by local energy deposit: either by photons of laser light (optical cavitation) or by other elementary particles (e.g. protons in a bubble chamber, particle cavitation) (Fan et al., 2010). The bubbles generated on a particle surface by cavitation naturally attach to the particle, eliminating the collision and attachment process which is always the rate-determining step for flotation (Tatu Miettinen et al., 2010).

It has to be noted that the use of small bubbles also involves disadvantages. Due to the low rising velocity of rather small bubbles with attached particles, very long flotation times result and hence require a substantial residence time in flotation circuits. Another disadvantage is that the lifting force of small bubbles may be too low to ensure process selectivity. Furthermore, it has been observed that tiny bubbles may cause high water recovery which increases the entrainment of gangue minerals (Schwarz and Grano, 2005).

1.4.2.2 Enhancing the particle-bubble interaction

(1) NP aggregation

For fine particles, it has been clear that the flotation rate increases with increasing particle size (Duan et al., 2003; Pyke et al., 2003). Many techniques have been developed to increase particle size and mass, and to decrease the surface energy. Fine particles are thereby induced to form flocs or aggregates. Depending on the mechanisms of aggregate formation, these techniques can be divided into three classes: selective flocculation, coagulation and hydrophobic aggregation.

In the selective flocculation, flocs are formed through the bridging ability of long-chain polymer molecules or ions. These polymers first adsorb onto mineral surfaces by the electrostatic attraction, specific chemical interaction and/or hydrogen bonds followed by bridging other mineral particles and forming loose flocs (Gregory and O'Melia, 1989). It has often been claimed that the selective flocculation is a promising technique for fine mineral particles. However, it is yet to find general application because the entrapment of gangue still remains as a major issue.

Coagulation is a much more widely used technique in the water purification where no selectivity is required. Coagulation of tiny particles can be achieved by the addition of electrolyte which decreases the electrostatic repulsion between charged particles. The hybrid system of the coagulation and flotation processes can be very effective when the system is correctly conditioned with respect to gas flow rate, pH value and chemical addition (Painmanakul et al., 2010). The different chemical agents (coagulants, flocculants, polymers, surfactants, etc.) have been studied in batch systems in order to analyze the optimum dosage, pH value and operation time for mixing and settling (Lien and Liu, 2006).

With the hydrophobic aggregation, tiny particles are selectively hydrophobised, similar to the conventional froth flotation. In order for the particles to be held together by the hydrophobic force, they need to be in very close proximity achieved by intense agitation. Non-polar oils are often added into the solution to increase the strength of the aggregates. The hydrophobic aggregation can be further divided into shear flocculation, emulsion flotation, carrier flotation, oil extended flotation, spherical agglomeration and two-liquid extraction (Subrahmanyam and Forssberg, 1990; Rao, 1997).

In all those particle aggregation processes, it is interesting to introduce less hazardous and more ambient-friendly reagents, and the natural organic matter (NOM) such as humic substances (HS) is among the potential choices. Brown and black biopolymers associated with soil, sediment, and particles suspended in water, and consisting of material derived from the degradation of animals and plants, are referred as HS; and HS involved interfacial processes are drawing more and more attention (Tschapek et al., 1981; Rebhun et al., 1998; Gai et al., 2011). Humic acid (HA), one of the main components of HS, is apt to interact with nano-oxides (Yang et al., 2009): firstly, the large surface area of nano-oxides provides space for HA adsorption; secondly, low hydrophilicity of nanoparticles allows HA molecules to approach to their surfaces; moreover, HA is composed of a large number of aromatic rings linked together by long alkyl chains of different lengths, resulting in a flexible skeleton that can help making bridges between NPs or NP-bubble surfaces. The structure of HA is shown in Fig. 1.7. Strong interactions such as the electrostatic attraction and the ligand exchange between HA and nano-oxide surfaces will induce the HA adsorption.

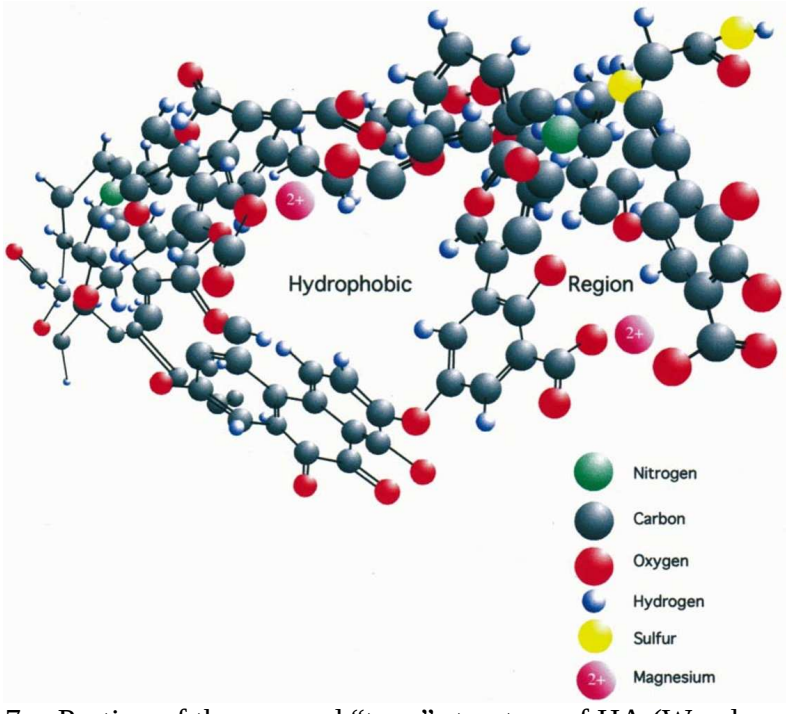

Fig. 1.7. Portion of the propsed “type” structure of HA (Wandruszka, 2000).

The study of Dos Santos and Oliveira (2007) suggested that HA could be used as an alternative for starch in the iron ore flotation process and obtain a higher floatability of hematite and quartz. Reyes-Bozo et al. (2011a) found that biosolids that contains both HA and

phosphorus compounds could interact with copper sulfide ores surfaces through a complex mechanism involving both inner and outer-sphere linkages; the film flotation tests showed that biosolids adsorbed on the surface of copper sulfide ores and changed their hydrophobicity. The research of this group also indicated that HA has more affinity for copper-containing mineral species and could be used as both collector and frother in the sulphide mineral concentration process by froth flotation, compared with biosolids and traditional surfactants (Lorenzo Reyes-Bozo et al., 2011). Nevertheless, the mechanisms involved have not been completely understood yet, particularly with reference to the phenomena observed in alkaline media (Kumpulainen et al., 2008).

(2) Bubble surface modification/ functionalization

To reinforce the bubble-NP interaction and improve the flotation process, bubble surface modification is also a promising way. Gas bubbles are reported to be generally negatively charged in pure water and in solutions of inorganic electrolytes. One objective is to reverse the surface charge of bubbles aiming for the capture of negatively surface charged particles. Li C. and Somasundaran P. (1991; 1992; 1993) found that bubbles can be positively charged in electrolyte solutions of multivalent salts (including metal ions solutions) depending on the concentration of the dissolved species, which in turn will depend on the salt concentration and solution pH. With a prior knowledge of the species distribution, bubbles can be made to acquire the desired sign and magnitude of surface charge by adding the required amounts of appropriate salts. The other approach is to create a functionalized bubble surface using a chemical additive dosed into the bubble generator. Specifically, positively charged bubble surfaces can be produced which are able to attract negatively charged NPs without the requirement for particle agglomeration – a technique being termed as PosiDAF. Although many studies have investigated the charge of bubbles treated with a variety of chemicals including cationic surfactants (Cho et al., 2005), metal coagulants (Li and Somasundaran, 1992), very few of them have actually been applied in DAF for the particle removal: for instance, .Rita K. Henderson (2009, 2010, 2014) used polyDADMAC as PosiDAF chemical to achieve high algae cell removals. The flotation performance could be attributed to the bubble surface modification through which positive sites were created as bridge between the bubble and cell surface and thereby the attachment efficiency increased.

In the present study, a system of microbubbles, colloidal gas aphrons (CGAs), is proposed to facilitate the flotation efficiency. CGAs, firstly defined by F. Sebba (1982), can be described as a system of microbubbles (10-100 μm) with colloidal properties. The structure of CGAs (seen in Fig. 1.8) consists of a gas core covered by a multi-layer of surfactant though the conclusive evidence of structural confirmation is still needed (Waters et al., 2008; Hashim et al., 2012).

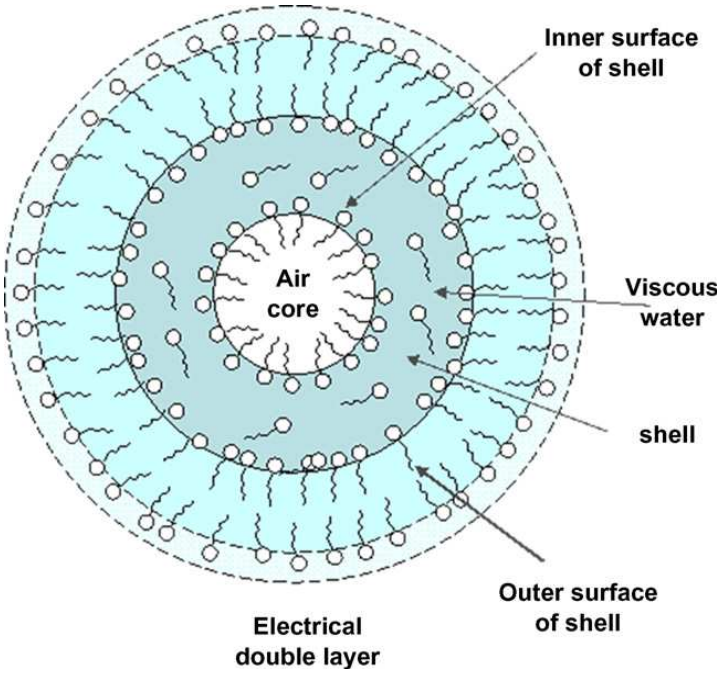

Fig. 1.8. Proposed CGA structure by F. Sebba (Platz, 1989).

The classical CGA generation (shown in Fig. 1.9) is to stir the surfactant solution at high speed (> 4000 rpm) in a baffled vessel (Sebba, 1985); many other methods have also been employed in the production of microbubbles (Hashim et al., 2012), such as sonication (Xu et al., 2008), dispersed air flotation (Ahmed and Jameson, 1985), electroflotation (Ketkar et al., 1991), dissolved air flotation (Henderson et al., 2010), etc. Depending on the type of surfactant used for generation, CGAs can be electrically surface charged or uncharged. CGAs possess unique properties which may facilitate the flotation separation of NPs: (i) high interfacial area for particle-bubble contact; (ii) electrostatic attraction between bubbles and particles with opposite surface charges; (iii) hydrophobic bubble surface facilitating the NP adhesion; (iv) high stability comparing with conventional foams; (v) allowing to be pumped from the generation point to the point of use without loss of their original structure (Hashim and Gupta, 1998; Spigno et al., 2014).

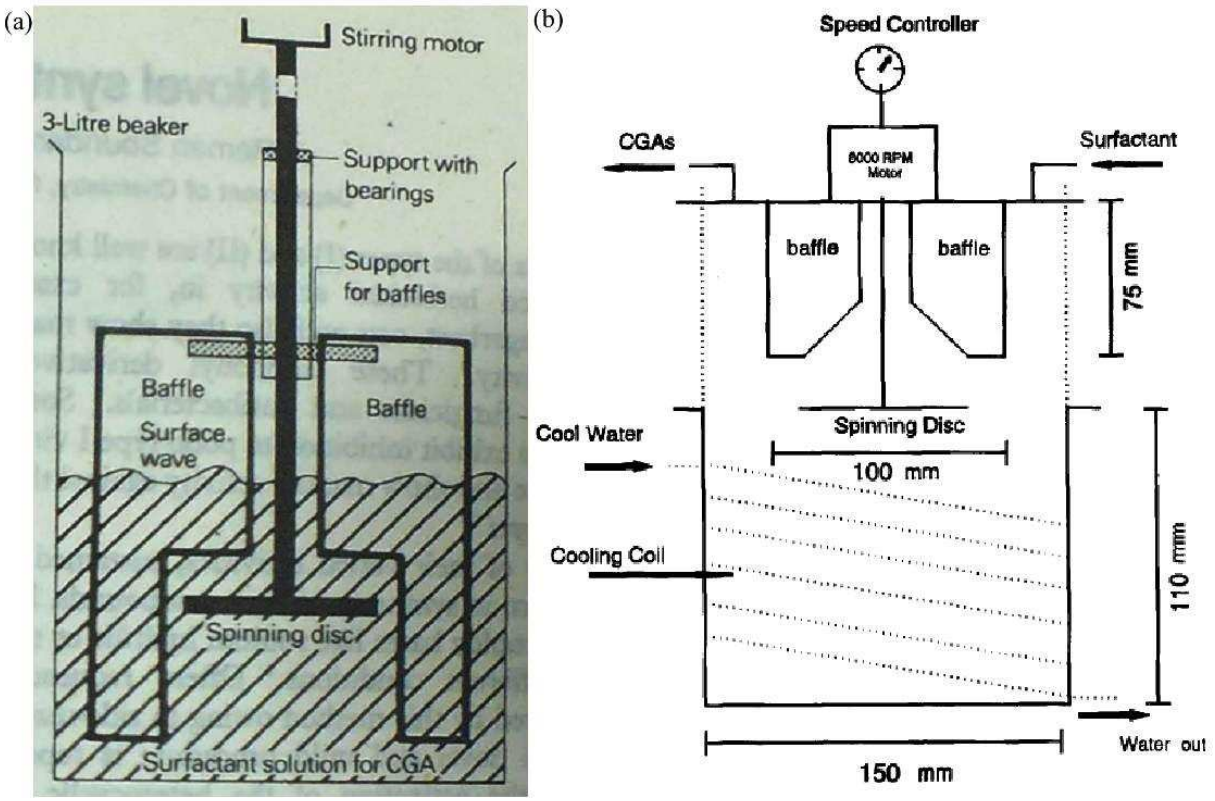

Fig. 1.9. Typical CGA generators: (a) Spinning disc generator by F. Sebba (1985); (b) generator designed by Chaphalkar et al. (1993; 1994).

The application of CGAs in the flotation process has been reported in the field of fine particle separation. Hashim, M.A. and Gupta, B.S. (1998) recovered up to 70 % fine pulp fibers (with the average size of around 1.7 µm) as foamate from the paper mill wastewater by CGAs. The oxygen demand and the sludge volume in the treating process could be reduced, and the application of CGAs was found to be inexpensive and feasible. The study of Mansur et al. (2006) showed that the high removal of fine particles could be obtained at the surfactant concentration close to the critical micelle concentration (CMC); since small bubbles were not able to provide sufficient buoyancy to lift large solid particles, there should be optimum particle and bubble sizes, individually, to achieve high removal efficiencies for particular separation problems. Waters et al. (2008) found that the attraction between CGAs and fine particles was initially caused by electrostatic interaction, suggesting the potential of CGAs for the selective separation of fine mineral feedstocks. However, to the authors' knowledge, there have not been any scientific reports concerning the removal of NPs (the average size < 100 nm) by CGA involved flotation.

1.5 Conclusions

This chapter provides a general scope of NP pollution in the aqueous environment, necessity of treating the NP contaminated water, and techniques applied in relative water treatment units; the significance of flotation in separating NPs from water is specifically highlighted.

The increasing usage of NPs inevitably leads to their release into the aquatic environment and causes the exposure to living organisms. Researchers have shown some relations between NPs and the health hazard which is resulted from active physiochemical properties of NPs. By now, a wide number of water treatment techniques, including adsorption, coagulation, filtration and as well as those improved and/or integrated processes, has been applied in different types of NP contaminated water, such as chemical mechanical polishing wastewater and municipal sewage, etc. Nano sized Ag, TiO_2, SiO_2, CeO_2 and carbon tube are among the most commonly seen NPs during those separation and purification processes.

Flotation is drawing increasing attention in the NP removal owing to its advantage upon fine particle separation. Mechanisms concerning the NP collection efficiency have been studied in 1960s. In practice, the flotation of NPs can be improved by either reducing the bubble size so as to enhance the impact of Brownian diffusion or forming large NP aggregates for the greater collision efficiency of bubble-particle; moreover, the bubble surface modification has also been studied to reinforce the colloidal force (charge neutralization) and non-DLVO (hydrophobic attraction) between bubbles and NPs.

Considering the development of flotation separation of NPs aforementioned and as well as the research advantage in our team, this Ph.D. study essentially works on increasing the NP removal by means of flotation. After the investigation of NP properties and the colloidal behaviour of NPs in suspension (Chapter 2), a series of work is carried out from two aspects: (i) the NP aggregation by way of changing the physiochemical condition of suspensions (pH adjustment and/or organic matter assistance) and the removal of NP aggregates using DAF; experimental methods and results will be presented in Chapter 3; (ii) the production of surface modified microbubbles (CGAs) including the design of bubble generator, the application of those microbubbles in NP separation from aqueous body, the comparison of NP flotation efficiency between CGA-flotation and DAF, and the mechanistic exploration of NP-surfactant; relative experiments and result analysis will be shown in Chapter 4.

Chapter 2

Properties of NP suspensions and flotation assisting reagents

Summary

This study examines the flotation removal efficiency and separation performance of two commercial NPs in dispersion (TiO_2 and SiO_2, shortly named as TNPs and SNPs, respectively) with the assistance of flotation reagents (so-called flotation assisting reagents or collectors). The former is used in the HA assisted flotation experiments so as to investigate the effect of organic matter on the aggregation and flotation process, and relative results are presented and discussed in Chapter 3. As for the latter, three kinds of SNPs (30R50, 30R25 and 30CAL50) with either similar size but opposite surface charges (30R50 and 30CAL50) or same surface charge but different particle diameter (30R50 and 30R25) are chosen in all the CGA involved trials such that the influence of NP features on CGA-NP interactions can be completely studied and understood; corresponding experimental results are shown and analyzed in Chapter 4.

For the sake of specific interpretation of NP-collector interaction in the following experimental sections, it is quite necessary to figure out the characteristics and colloidal behaviors of NPs in suspension as well as the properties of flotation assisting reagents (i.e. HA and surfactants), which is the main objective of this chapter.

2.1 An overview of characterization techniques

A series of tests were conducted upon NPs with respect to particle size, zeta potential, mass content, morphology, turbidity, pH value, and conductivity. Thereafter, influences of NP concentration, pH value and additional ionic strength (IS) on NP suspensions were then investigated. The initial NP suspension was sonicated for 15 min in an ultrasonic bath (Branson ultrasonic) and allowed to cool to room temperature for 30 min prior to measurement or experiment. The sample suspensions with different NP concentrations or pH values or additional NaCl concentrations were vigorously mixed on the vortex mixer (Fisher Scientific FB15024, UK) for 1 min and then kept 24 h for equilibrium. The duration has been confirmed to be sufficient by French et al. (2009) and Keller et al. (2010) in their studies of the NP suspension stability with the effect of IS and pH. Besides, properties of HA solution and surfactant solution were also examined. Techniques used herein are listed as follows. Principles and procedures of all analytical techniques above (excluding ICP-AES and ICP-MS) have been specifically described in Chapter 2 of Liu's Ph.D. dissertation (2010).

- Particle size and size distribution were analyzed by either dynamic light scattering (DLS) or laser diffraction scattering (LDS) considering their different measurement ranges. For NPs and small aggregates, the Nanotrac NPA250 with an external probe (Microtrac Inc., USA, the measurement range of 0.8~6500 nm) was used for the size determination by means of DLS; the Mastersizer 2000 (Malvern Instruments Ltd, UK, the measurement rang of 0.2~2000 μm) was used for greater particle size analysis by way of LDS.
- Zeta potential was determined by electrophoresis on Zetasizer NanoZS (Malvern Instruments Ltd, UK);
- Ti mass content (thus TNP mass concentration) of TNP suspension Lot #1 was measured by the inductively coupled plasma atomic emission spectroscopy (ICP-AES, Ultima2, Jobin-Yvon Horiba, USA) which was undertaken by Mrs. Marie-Line de Solan Bethmale at Service Analyses & Procédés of Laboratoire de Génie Chemique de Toulouse. The Ti detection limit was 0.78 ppb. As for Ti mass content of TNP suspension Lot #2 and Si mass content (thus SNP mass concentration), they were measured via the inductively coupled plasma mass spectrometry (ICP-MS, 7700 Series ICP-MS, Agilent Technology, USA) by Ms. Florence LERAY in LISBP of INSA de Toulouse. The Ti and Si detection limits were 4 ppt and 0.5 ppb, respectively.
- Transmission electron microscopy (TEM) was used for TNP morphology and size estimation. A droplet of diluted suspension was put on a carbon coated copper grid dried under vacuum before observation and then observed by TEM JEOL 100CX and Philips CM20 (200 kV);
- Turbidity was measured with a 2100N-IS Turbidimeter (Hach, USA);
- pH value was measured by a pH-539 PH meter (WTW) with a SenTix 41 pH-electrode;
- Conductivity was measured with a LF 538 conductivity meter (WTW) and a Tetracon 325 probe which has 4-electrode cell with built-in temperature sensor;
- Dissolved organic carbon (DOC) was determined by the TOC analyzer (Shimadzu corporation, Japan) for the HA concentration;
- Surface tension of HA and surfactant solutions was measured on Tensiometer (GBX, France).

All chemicals used in this study were analytical reagent grade products. The deionized water with conductivity lower than 1.7 μS/cm water was used for all experiments and produced by

an AQUASOURCE system, where water was filtered for particles larger than 1 µm and deionized through an ion exchange resin.

2.2 TNP suspension and HA solution

2.2.1 TNPs and TNP suspension

2.2.1.1 Characterization of TNPs in the initial suspension

One commercial TNP water dispersion (TiO_2, Rutile, 5-30 nm, density 4.2 $g.cm^{-3}$ at 20°C, 15 wt.%, Nanostructured & Amorphous Materials, Inc, USA) was employed in the present work. There were two series of TNP suspension with different Lot numbers: the one bought in 2010 (Lot #7102R-011110, briefly named as Lot #1 in the following text) was used in TNP-HA agglomeration experiments and as well as preliminary HA assisted DAF tests; the other ordered in 2012 (Lot #7102R-062212, briefly named as Lot #2 hereafter) was used in adsorption-aggregation experiments and the main part of HA assisted and pH adjusted DAF trials.

The mean hydrodynamic diameters of TNP Lot #1 and Lot #2 are determined to be 41.6 nm and 14.5 nm, respectively. As shown in Fig. 2.1, two peaks (around 21.5 nm and 72.3 nm) of the particle size distribution (PSD) curve denotes two TNP size populations in the TNP suspension Lot #1 whilst the PSD of TNPs Lot #2 is nearly monomodal.

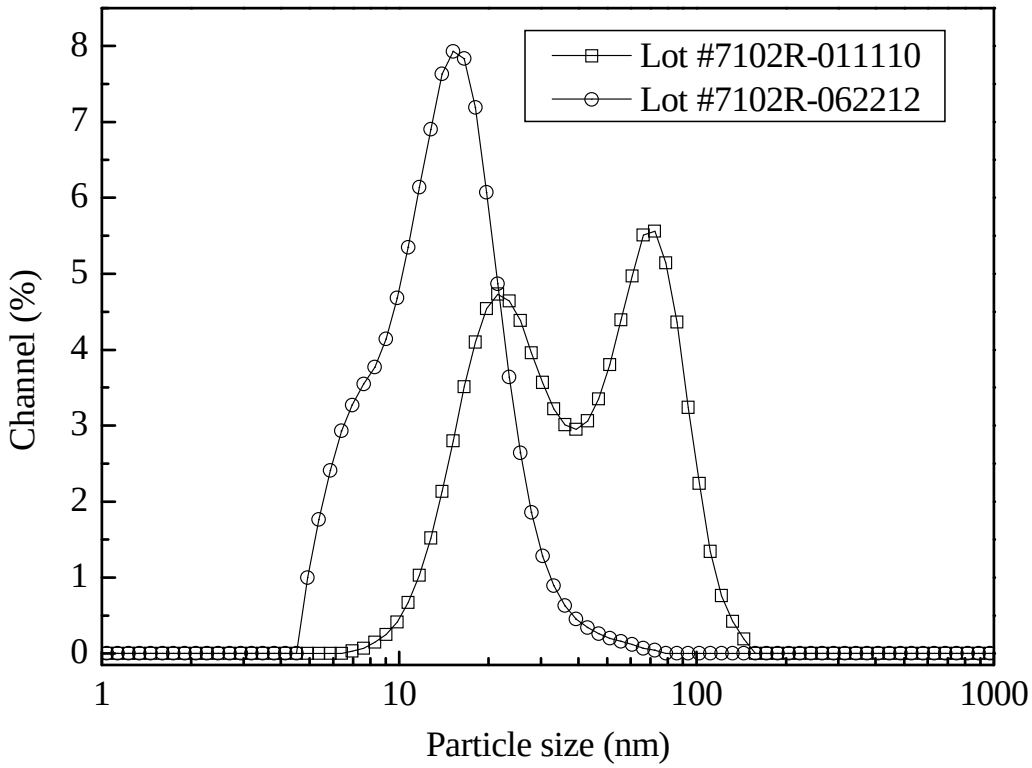

Fig. 2.1. Particle size distributions of two TNP suspensions (Lot #1 and Lot #2).

TEM images of TNP product Lot #1 exhibit the particle morphology; meanwhile the NP size can be roughly estimated using the scale (Fig. 2.2). TNPs in the suspension are round in shape with a coating layer which might result from certain additives added during the suspension producing process. The visual observation also confirms TNPs of Lot #1 are not monodispersed since two particle size populations are seen: about 20~30 nm to 70~80 nm in diameter, in accordance with the conclusion drawn from the DLS measurement (Fig. 2.1).

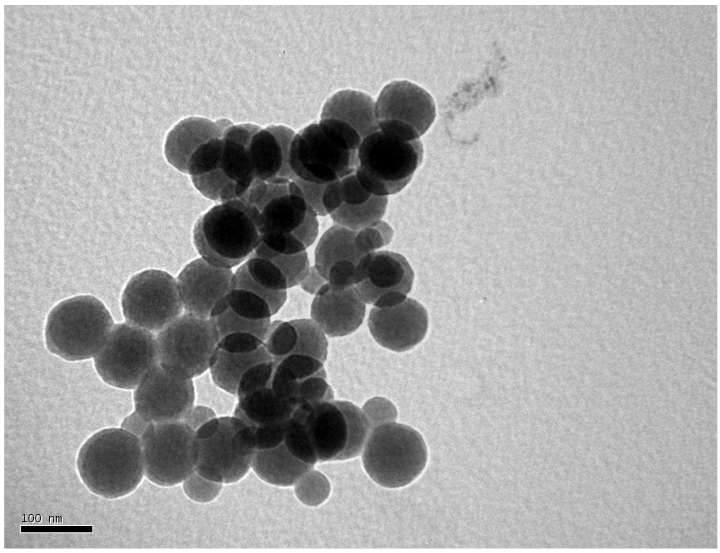

Fig. 2.2. TEM observation of TNP suspension Lot #1.

Other results obtained in the laboratory and provided by producer are given in Table 2.1. Comparing with the TNP suspension Lot #2, the TNP suspension Lot #1 is of higher turbidity, TNP concentration and conductivity possibly due to the quality variation caused by the long-time storage, but of similar values of zeta potential and pH because of the same TNP material and producing method. Concentrations of trace elements (Si, Mg, Ca, and Pb) provided by the producer are the same. In the following investigation of suspension properties, results obtained from the product Lot #2 is depicted as representative.

Table 2.1. Physicochemical characteristics of TNP suspensions (0.15 wt.%).

Data from the laboratory analysis			Data offered by the producer	
Item	Lot #1	Lot #2	Lot #1 and Lot #2	
Turbidity (NTU)	23.2	10.9	Si (ppm)	≤ 0.55
Zeta potential (mV)	+42	+39.8	Mg (ppm)	≤ 0.45
pH (Temperature, °C)	2.96 (22.4)	2.88 (22.0)	Ca (ppm)	≤ 0.60
Conductivity (mS/cm)	0.832	0.701	Pb (ppm)	≤ 0.002
Ti (TiO_2) mass content (ppm)	844.0 (1406.7)	703.5 (1172.5)		

2.2.1.2 Colloid behaviors of TNP suspensions

Several physiochemical factors, including NP concentration, pH value, additional salt concentration, may greatly impact the NP properties (such as particle size and zeta potential) and hence influence interface behaviors of NPs to some extent. In view of this consideration, the colloid behaviors of suspension with a controlled TNP concentration of 0.15 wt.% are investigated.

(1) Effect of TNP concentration on suspension properties

Fig. 2.3 shows the variation of pH value, TNP size, and zeta potential versus the weight concentration of TNP suspension. The pH of suspension slightly increased from 1.2 to 2.9 along with the dilution of TNP suspension from 15 wt.% to 0.15 wt.% (Fig. 2.3(a)). The zeta potential of TNP suspensions remained around +38 mV with small drift over the concentration range, indicating the surface charge being little affected by the dilution of deionized water, as shown in Fig. 2.3(b). The stable zeta potential and pH value implied the sound dispersion to the investigated dilution extent and no aggregation occurred. The particle

size kept stable within the range of 0.1~0.75 wt.%, and slightly decreased when the TNP concentration was higher than 1 wt.%. In the concentration of 0.1~0.75 wt.%, the particle interaction can be neglected and the mean hydrodynamic diameter is calculated by directly applying the Stokes-Einstein law. The reduction of particle size at higher TNP concentrations can be attributed to the modification of the structural factor caused by the particle-particle interaction and/or to the multi-scattering of light in the colloidal suspension (Xu, 2000; Tourbin, 2006; Tourbin and Frances, 2007; Liu, 2010). Therefore, it is inferred that good results for the particle size determination by DLS is in diluted conditions, and the TNP concentration of 0.15 wt.% is used in all the following experiments.

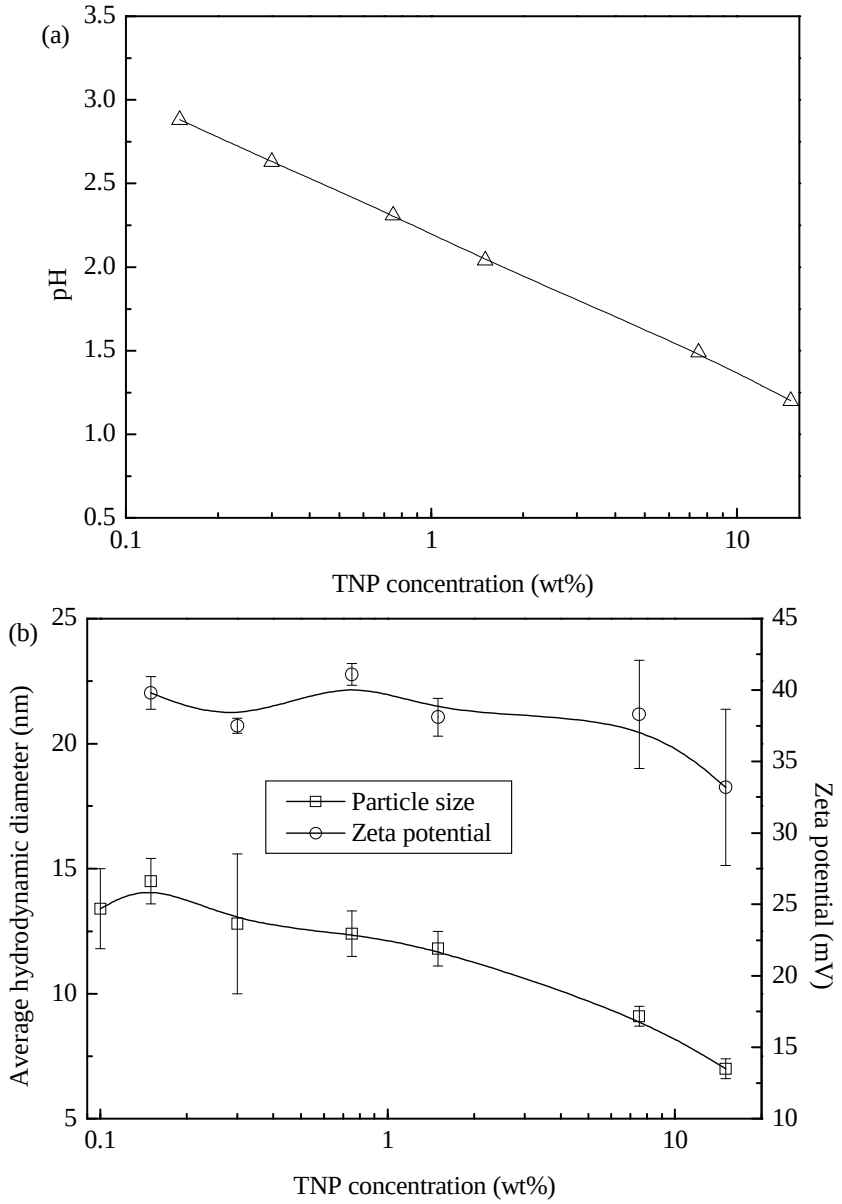

Fig. 2.3. Properties of TNP suspension varying with different TNP concentrations: (a) pH; (b) particle size and zeta potential.

(2) Effect of pH value on zeta potential and particle size of TNPs in suspension

The pH-dependence of zeta potential and particle size can be seen in Fig. 2.4. As illustrated in Table 2.1, the initial zeta potential and pH value of 0.15 wt.% TNP suspension was around +40 mV and 2.9, respectively. The pH was adjusted by adding NaOH solution (AR, Carl ROTH, Germany). The zeta potential began to sharply decrease at pH higher than 4, and remained at around -45 mV when the pH value was higher than 8. The isoelectric point (IEP) was found to be at approximately pH 5.7.

The particle size grew along with the pH increase. When the pH was higher than 4, the particle size jumped into the micron scale (> 20 μm), far beyond the DLS detection limit. Thereafter, the particle size was determined by LDS on Mastersizer 2000. The particle size kept 55±5 μm within pH5~10. The maximum particle size firstly appeared at IEP which could be attributed to the charge neutralization on the NP surface by OH^-: aggregates were favorably formed since they did not appeal to one another. At pH11, the particle size decreased to about 25.5 μm possibly due to the fact that the OH^- adsorbed on the NP surface resulted in the re-stabilization of suspension by electrostatic repulsion.

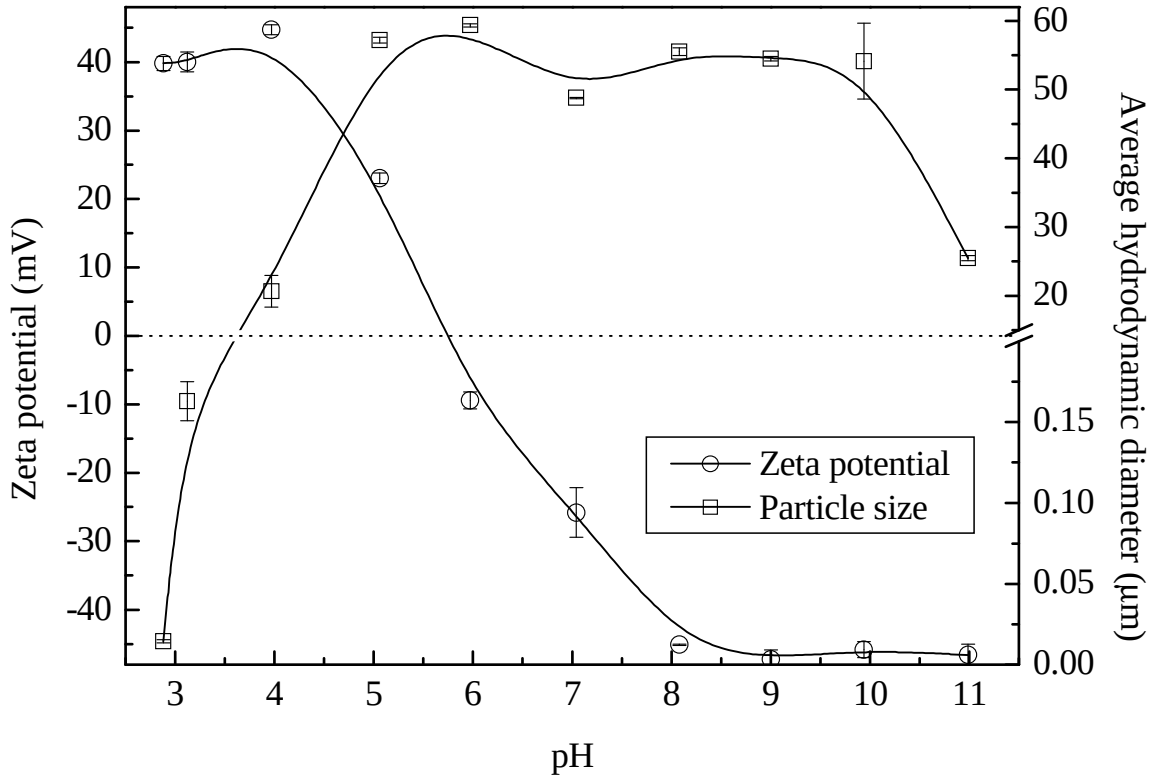

Fig. 2.4. Zeta potential and particle size varying with pH values of TNP suspension.

Since metal oxides such as TiO_2 and SiO_2 are well known to contain numerous surface MeOH groups that favorably create hydrogen bonds with water, the charging behavior of those metal oxides can be given as below so as to better interpret their species variation at different pH values:

at pH<IEP, $Me-OH+H_3O^+ \Rightarrow Me-OH_2^+ + H_2O$;

at pH>IEP, $Me-OH+OH^- \Rightarrow Me-O^- + H_2O$.

When the pH of suspension gets close to IEP moving from acidic value to basic value, it turns to be $Me-OH_2^+ + OH^- \Rightarrow Me-OH+H_2O$.

(3) Effect of additional IS on TNP suspension

The IS of the initial dispersion product is not provided by producer. In the current study, an additional salt effect was investigated by adding NaCl (AR, Carl ROTH, Germany)-deionized water solution in the suspension. The 0.15 wt.% TNP suspension was adjusted to different additional NaCl concentrations (0, 0.005 mol/L, 0.01 mol/L, 0.03 mol/L, 0.05 mol/L, 0.07 mol/L, and 0.10 mol/L, respectively) which were in accordance with the concentration range of other investigations concerning the IS effect on the TNP or NP aggregation process (Saleh et al., 2008; French et al., 2009; Keller et al., 2010).

The conductivity, a cumulative parameter for the ionic concentration in water, may greatly affect the stability of NP suspension. The more salt in a solution or suspension, the greater its conductivity. The conductivity of initial TNP suspension (0.15 wt.%) was around 0.701 mS/cm (Table 2.1), much higher than that of the deinoized water (0.0017 mS/cm), confirming the existence of certain ionic additive reagent in the TNP suspension product. As shown in Fig. 2.5, adding NaCl into the TNP suspension led to a linearly increase of conductivity: from 0.701 mS/cm to 11.3 mS/cm when the additional NaCl concentration increased from 0 to 0.10 mol/L.

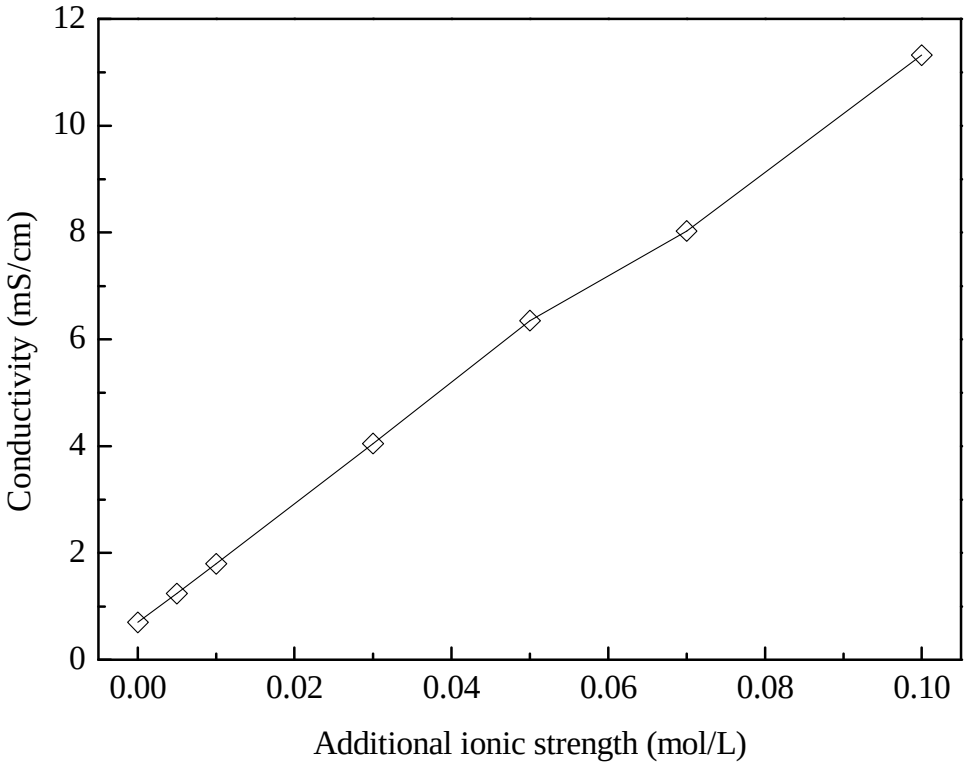

Fig. 2.5. Conductivity of TNP suspension varying with different additional IS.

TNP suspensions were not buffered, and there was only little drift (from pH 2.79 to pH 2.82) in investigated NaCl concentrations as shown in Fig. 2.6(a), revealing that NaCl did not modify the pH of TNP suspension since no release of either H^+ or OH^- should be observed by adding this salt. It is presented in Fig. 2.6(b) that, in the lower additional NaCl concentration range (≤ 0.03 mol/L), the DLS measurement did not denote any significant aggregation, and the particle size centered around 14.5~15.5 nm, close to that of the initial TNP suspension. In the medium additional NaCl concentration range (from 0.05 mol/L to 0.07 mol/L), TNPs slightly agglomerated, forming aggregates with an average particle size of 20 nm. When the added NaCl reached 0.1 mol/L, the particle size jumped into the micron scale (about 22 μm) that was far beyond the DLS detection limit, in which case the particle size determination switched to LDS by Mastersizer 2000.

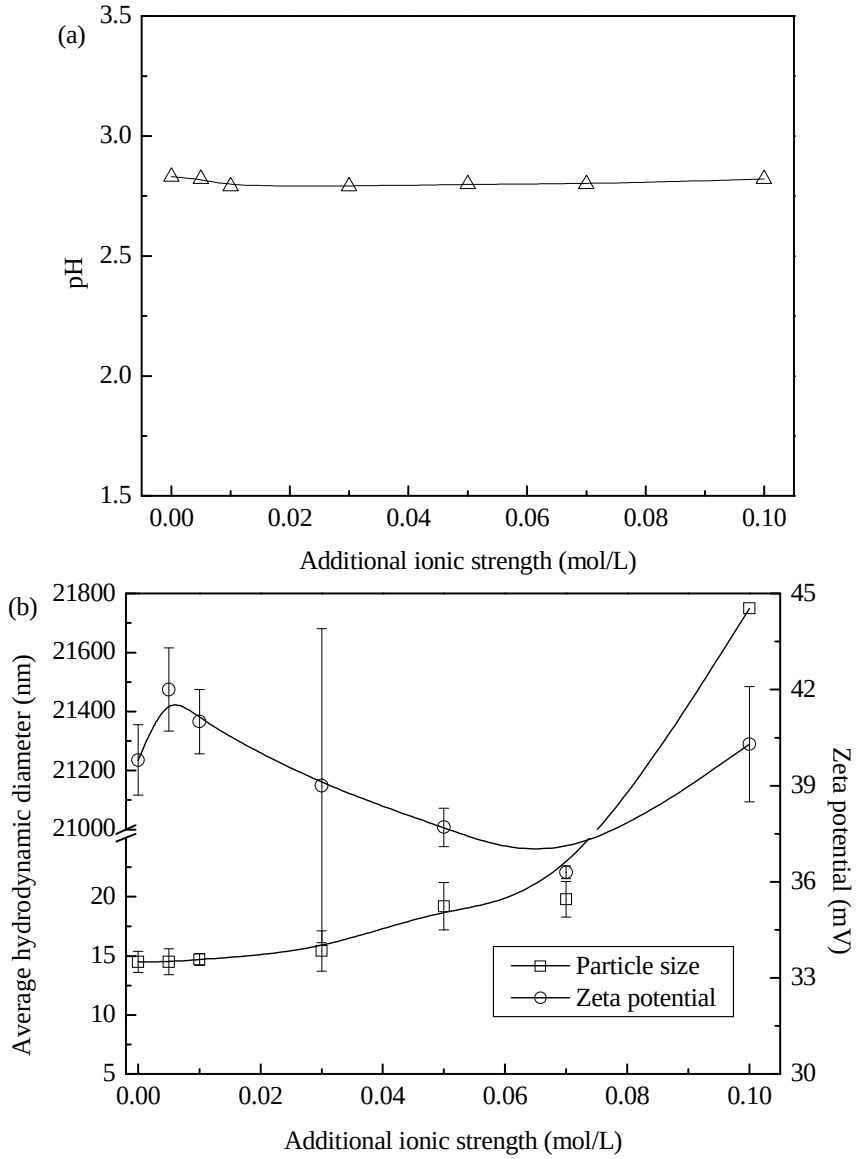

Fig. 2.6. Properties of TNP suspension varying with different additional IS: (a) pH; (b) particle size and zeta potential.

Since the pH value of TNP suspension remained approximately 2.8 (Fig. 2.6(a)), lower than the pH_{IEP} of 5.7, particle surfaces were therefore bearing positive charges, compensated by Cl^- ions in solution. At the additional IS ≤ 0.07 mol/L, the particle size increased from about 14.5 nm to 20 nm and zeta potential remained almost constant (fluctuating between +40 mV to +36 mV), as the NaCl concentration rose. This could be interpreted by the classical DLVO theory, which predicted that any increase in the IS of the electrolyte solution in which particles are suspended should compress the diffuse layer associated with the particles, diminish interparticle repulsion, and therefore promote aggregation (French et al., 2009). The slight increase of NP size attained by DLS at added NaCl concentrations lower than 0.01 mmol/L might be caused by (i) the too low salt concentration to give rise to large aggregates

and (ii) the underestimation of smaller particles of DLS analysis: according to Rayleigh's approximation, the intensity of light scattered by a particle (or aggregate) is proportional to the sixth power of its diameter causing large particles to scatter far more light than small ones; the software used to analyze the DLS data takes differential scattering into account, but some underestimation of small-size particles is still likely to occur (French et al., 2009). However, as for the highest additional IS (0.10 mol/L), the zeta potential rebound to approximately +40 mV while the largest particle size was obtained.

2.2.2 Properties of flotation assisting reagent -- HA

2.2.2.1 Preparation of HA solution

HA is the alkali soluble but acid insoluble fraction of humic substances (Hiraide et al., 1993). A commercial sodium salt of HA (Carl ROTH, Germany) was used in this research. The HA stock solution was prepared as follows: certain amount (1 or 2 g) of HA powder was dissolved in 1 L of 0.1 mol/L NaOH solution, stirred for 6 h to make sure it fully dissolved, and finally filtered through 0.45 μm membrane to remove residual non-dissolved HA powder. The molecular weight of the HA used in this study was measured to be approximately 17.3 kDa (17300 g/mol) via high performance size exclusion chromatography, and the relative experimental protocol and results are shown in Appendix A.

2.2.2.2 Characterization of HA and HA solution

(1) Determination of HA concentration

The amount of HA is related to its mass in general. The milligram of either its carbon content or the dried HA sample is usually used to give the concentration of HA solution in mg/L unit (Kretzschmar et al., 1998; Rebhun et al., 1998; Illés and Tombácz, 2006). In this experiment, the HA concentration was determined by the TOC analyzer with regard to DOC, mg/L DOC. The stock solution was diluted according to required HA concentrations in experiments. The relationship between DOC and the dilution factor is shown in Fig. 2.7, from which the HA concentration of stock solution can be inferred. In the present study, four HA stock solutions were successively prepared in the same way as aforementioned in Section 2.2.2.1 and used in the surface modification experiments and DAF trials, and their concentration were determined to be 405.3 mg/L DOC, 586.9 mg/L DOC, 653.0 mg/L DOC (when 1 g HA powder was

dissolved during preparation) and 1084 mg/L DOC (when 2 g HA powder was dissolved during preparation), respectively.

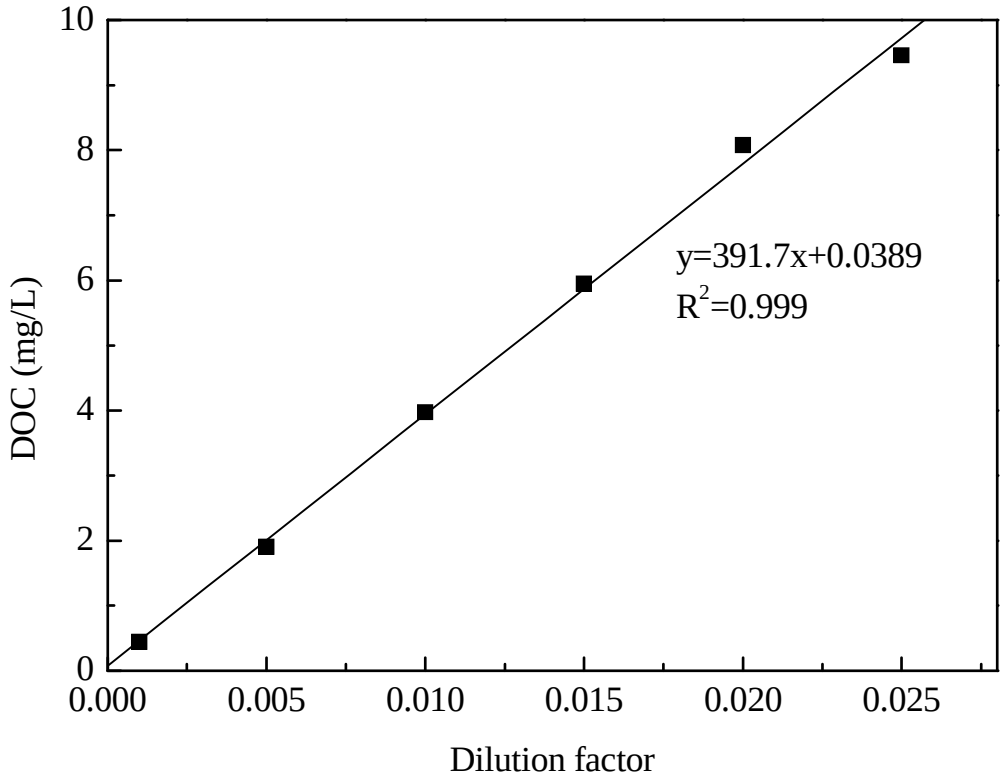

Fig. 2.7. DOC as a function of HA concentration.

(2) HA concentration as a function of pH

The effect of pH on the solubility of HA solution was tested by adding HCl (AR, Carl ROTH, Germany) and then measuring the variation of HA concentration. It is shown in Fig. 2.8 that the HA concentration remained around 525±25 mg/L DOC in a wide pH range of 4~13, and only when the pH decreased to 3.3, the HA concentration reduced to about 206.5 mg/L DOC and the precipitates could be visually observed at the bottom of the vessel. This decrease of solubility as a function of pH value can be explained: the extent of carboxylate groups of HA molecules decrease along with the decrease of pH, and thereby HA molecules exhibit weaker repulsion between each other. Owing to the presence of their large hydrophobic moieties, HA molecules will thus tend to aggregate so as to reduce their contact with the surrounding aqueous phase, and finally the sediment can be obtained. Consequently, in the highly acid solution (pH lower than 4), it could be supposed that all the HA molecules were not really soluble.

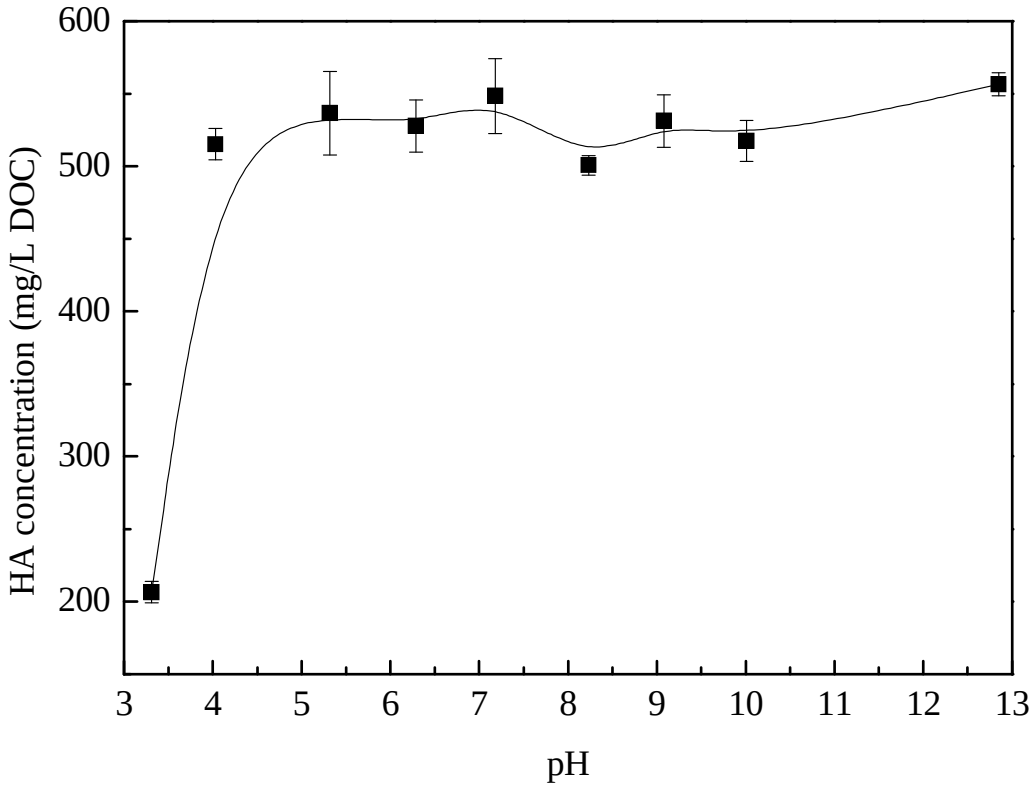

Fig. 2.8. HA concentration varying with pH value of HA solution.

(3) Verification of CMC

The surfactant properties of HA has been recognized (Tschapek et al., 1981; Guetzloff and Rice, 1994; Agarwal et al., 2010). As a surface modifier of TNP and also flotation assist, HA may spontaneously form micelles beyond a certain concentration and thus may not play the role we expect in aggregation. For this reason, the critical micelle concentration (CMC) of HA is verified by measuring the surface tension (Tensiometer, GBX, France) at the room temperature of approximately 22 °C (295.15 K). A CMC of 290±5 mg/L DOC can be observed in Fig. 2.9, which is much lower than those reported elsewhere (4~40 g/L) (Tschapek et al., 1981; Guetzloff and Rice, 1994; Conte and Piccolo, 2002), possibly due to different representations of HA concentration unit and as well as different amounts ionogenic and non-ionogenic molecules in the HA product caused by the HA extraction process and resulting in the HA nature variation.

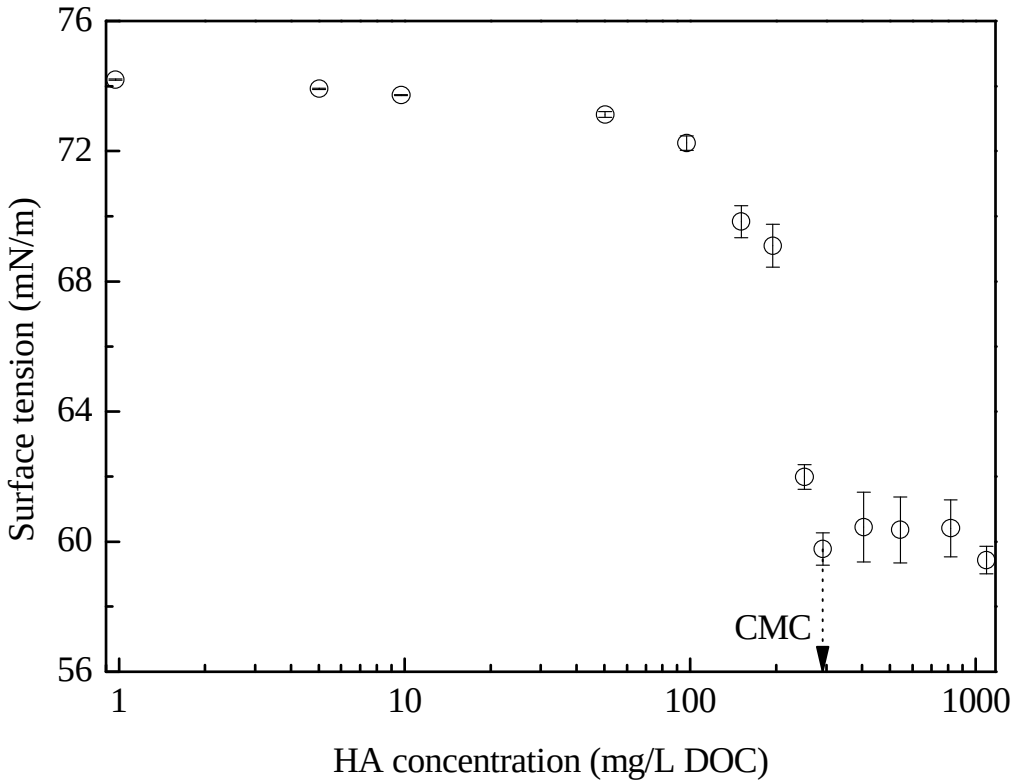

Fig. 2.9. Determination of CMC by surface tension measurement.

(4) Characterization of HA solution

The particle size (determined by DLS, Nanotrac) and turbidity curves at different HA concentrations are shown in Fig. 2.10(a). Fig. 2.10(b) displays representative PSD patterns of HA from 0.54 mg/L DOC to almost 80 mg/L DOC, and those of TNPs are also presented as comparison. It is worth noting that, at the HA concentration lower than 10.5 mg/L DOC, the particle size and turbidity measured in the HA solution were about 1 nm and lower than 1 NTU, respectively, much lower than those values attained in TNP suspensions (see in Section 2.2.1.1), which could be considered to have no great impact on the measurement size of TNP-HA aggregates. When the HA concentration was higher than 10.5 mg/L DOC, the particle size and turbidity jumped sharply. The turbidity kept rising and reached close to 14 NTU at the CMC of HA. The average "particle" size was approximately 176 nm at the HA concentration of 80 mg/L DOC and kept around 167±7 nm thereafter. As interpreted by Tschapek et al. (1981), when the HA powder are alkali-treated in water, the Na^+-humate sol forms which is soluble spontaneously colloidally and, evidently, molecularly (because it lowers the surface tension of water). This solubility is known as "peptisation" with the average sol size from one nanometer to hundreds of nanometers. When the HA concentration exceeds the CMC, it is inferred that the Na^+-humate sol contains both micelles and

amphiphilic molecules. In the HA concentration range higher than 10.5 mg/L DOC, the HA sol is of close or much larger size than TNPs, and thereby the interfacial process between TNPs and HA will not be recognized merely as HA molecules adsorbing toward the TNP surface any more, but it is also necessary to consider the possible co-precipitation between those TiO_2 and HA sol.

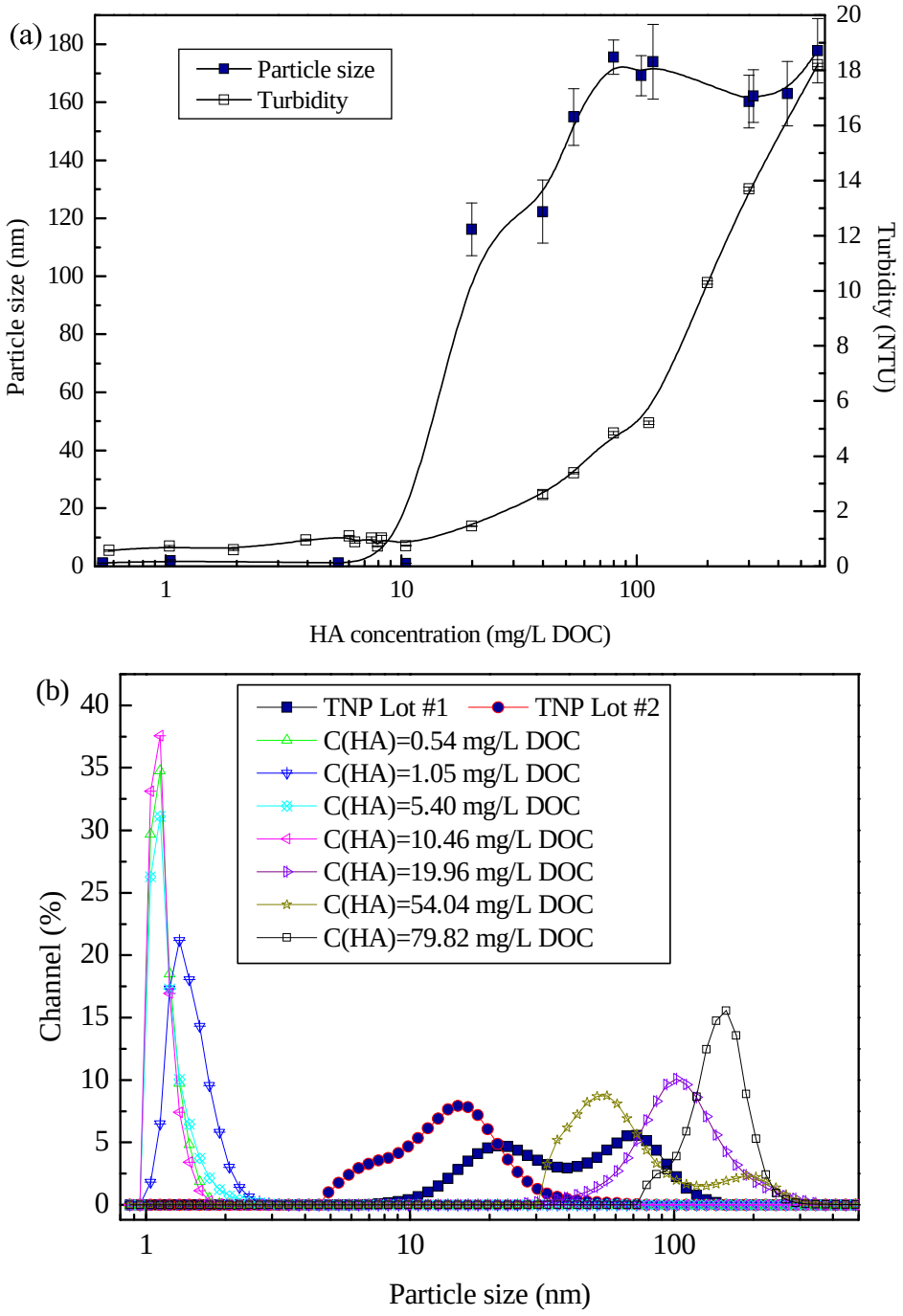

Fig. 2.10. (a) Particle size and turbidity varying with HA concentrations; (b) PSD patterns of TNPs and HA.

As presented in Fig. 2.11, the zeta potential fluctuated around -15 mV at HA concentrations lower than 10 mg/L DOC; it greatly reduced to approximately -40 mV within the HA concentration range of 20~310 mg/L DOC. The pH value of HA solution was also influenced by HA concentration, decreasing from 11.6 ([HA]=113 mg/L DOC) to 4.4 ([HA]=0.58 mg/L DOC) along with dilution.

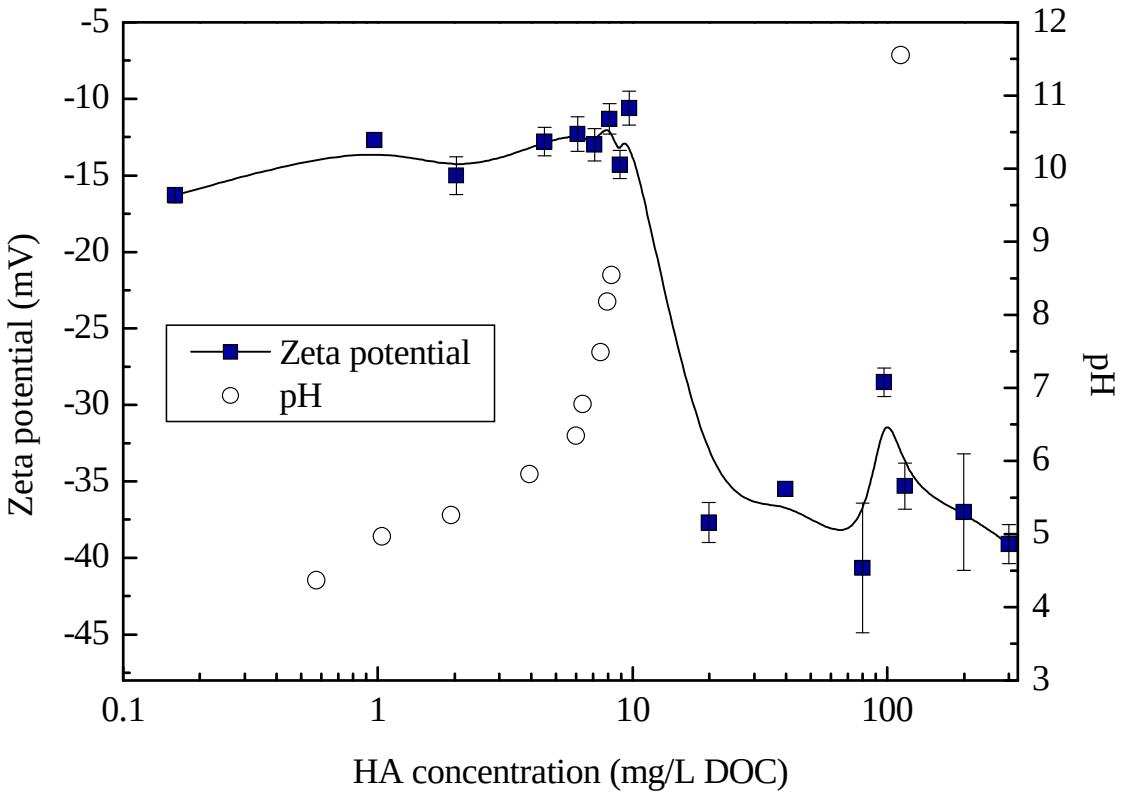

Fig. 2.11. Zeta potential and pH value varying with HA concentrations.

2.3 SNP suspensions and surfactant solutions

2.3.1 SNPs and SNP suspensions

2.3.1.1 Characterization of SNPs in the inital suspension

SNPs, the main particulate component of chemical mechanical polishing wastewaters, have drawn serious attention in the NP separation study as reviewed in Chapter 1. Herein, three kinds of commercial SNP suspensions were employed as treating targets in the investigation of CGA-flotation: the negatively surface charged 30R50 and 30R25 with an average particle size of approximately 80 nm and 30 nm, respectively, and the positively surface charged 30CAL50 of around 77 nm in diameter. Their PSDs measured by Nanotrac are shown in Fig. 2.12, all of which are monomodal even though Liu observed two size populations for 30R50

by TEM (Liu, 2010; Liu et al., 2012). Since Liu also used the same 30R50 and 30R25 dispersions in her Ph.D. research, specific properties of those two SNPs can be referred to the relative dissertation and publications (Liu, 2010; Liu et al., 2012; Liu et al., 2012; Liu et al., 2013). The characterization of SNP suspensions was made and results attained are presented in Table 2.2.

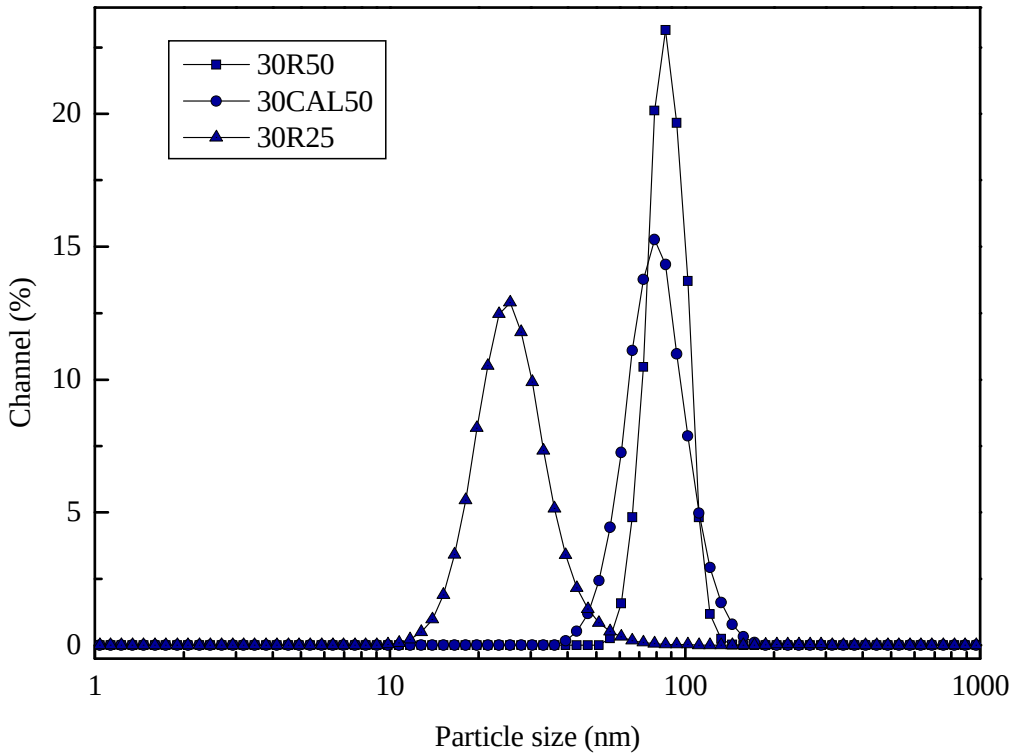

Fig. 2.12. Particle size distributions of different SNPs.

Table 2.2. Characteristics of three types of SNP suspensions.

	SNP Concentration * (vol.%)	SNP concentration by ICP-MS (mg/L)	Zeta potential (mV)	Turbidity (NTU)	pH
30CAL50	0.015	422.40	+53.3	23.1	4.9
	0.005	133.84	+52.1	8.08	5.2
30R50	0.015	505.52	-27.6	32.8	6.4
	0.005	155.40	-27.2	11.0	6.5
30R25	0.015	352.65	-29.6	1.41	6.8

* The SNP concentration is used in both flotation and adsorption-aggregation experiments.

2.3.1.2 Colloid behaviors of SNP suspensions

Similar to the investigation of colloidal characteristics upon the TNP suspension, SNP suspensions with a controlled concentration of 0.15 vol.% were studied with respect to impacts of NP concentration, pH value and additional salt concentration on physiochemical properties of SNPs.

(1) Effect of SNP concentration on SNP particle size measurement

The variation of particle size of 30R50 and 30R25 (0.15 vol.%) along with the SNP concentration has been extensively discussed in Liu's Ph.D. study (Fig. 2.13(b) and (c)) and as well as the research of Tourbin (2006), and here Fig. 2.13(a) gave supplementary data of 30CAL50 (0.15 vol.%).

As demonstrated by Tourbin (2006) and confirmed by Liu (2010), at low SNP concentrations ([30R50] < 0.5 vol.% and [30R25] < 0.15 vol.%), the average size determined by DLS (Nanotrac) is almost independent of concentration because of the negligible particle interaction, while above certain SNP concentration range, the mean size decreases with silica concentration increasing possibly due to a modification of the structural factor caused by the interaction between particles and/or by multi-scattering of light in the colloidal suspensions. It was concluded that good results for the particle size determination by DLS only be achieved in diluted conditions. As for the case of 30CAL50, the average particle size was measured to be approximately 77 nm. No great size fluctuation was found in the SNP concentration ≤ 0.5 vol.%, agreeing well with the size variation of 30R50 in diluted SNP concentrations. At higher SNP concentrations (> 0.5 vol.%), the size measurement experienced small decrease, as has been observed for other SNPs by Tourbin (2006) and Liu (2010).

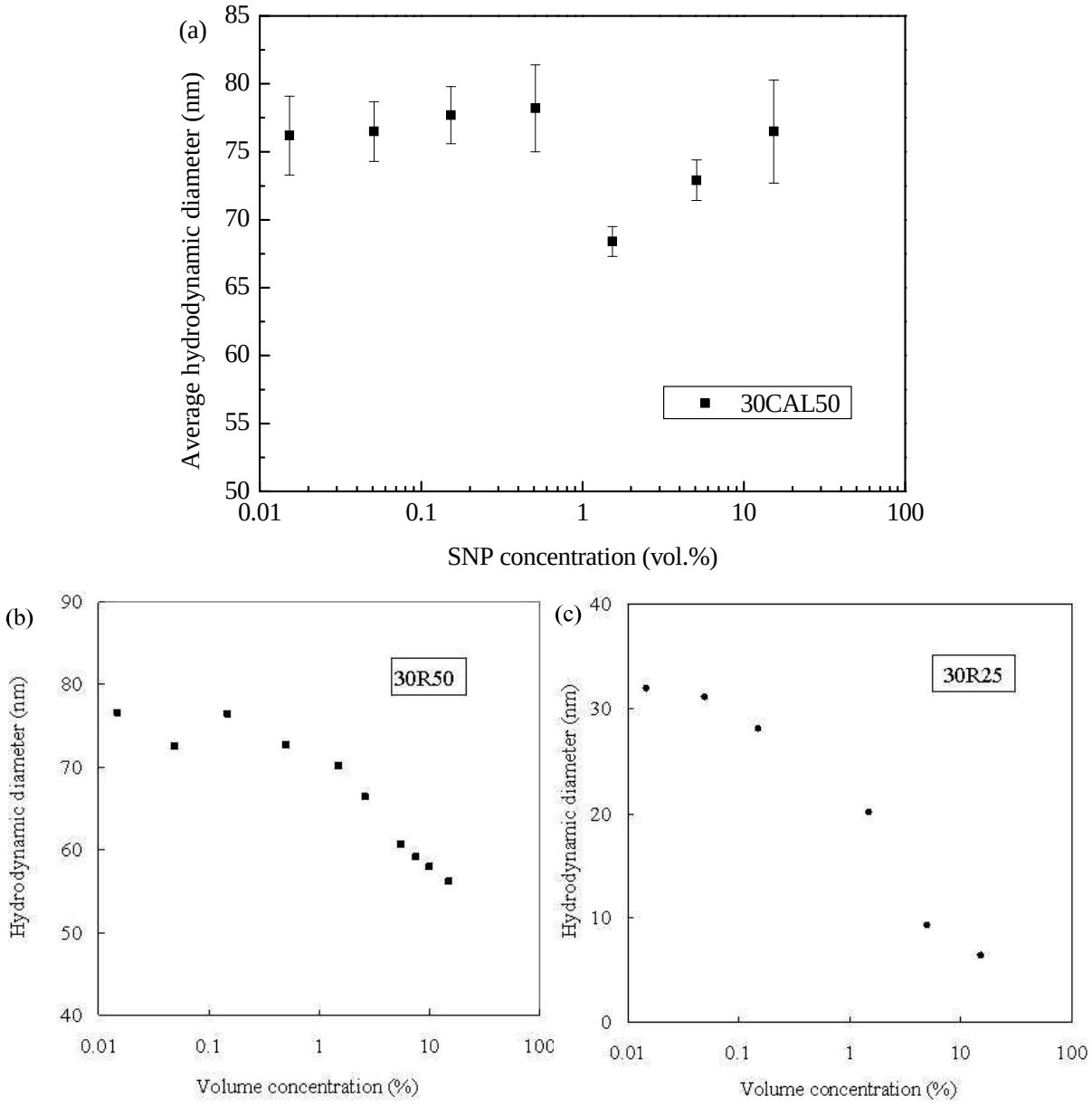

Fig. 2.13. Particle size varying with SNP concentration: (a) 30CAL50 (measured in this study), (b) 30R50 and (c) 30R25 (measured by Liu (2010)).

(2) Effect of pH on the particle size and zeta potential

Since the pH value of NP suspension can greatly affect the agglomeration behavior of NPs by way of changing their surface charges due to gain or loss protons (H^+), thus, zeta potential and particle size as a function of pH value was investigated herein. Certified analytical grade sodium hydroxide (NaOH) solution (2 mol/L, free of carbonate, Fisher Scientific, UK) and hydrochloric acid (HCl) solution (1 mol/L, Carl ROTH, Germany) were diluted to 0.1 mol/L and used as pH regulators.

Liu (2010) reported that the commercial 30R50 and 30R25 SNP suspensions were of high and negative zeta potential (< -30 mV). In the present work, the zeta potential of 0.15 vol.% 30CAL50 suspension was as high as +50 mV. It confirmed the stability of those aqueous suspension systems by electrostatic repulsion. The IEPs of 30R50 and 30R25 were around pH1~1.5 whilst that of 30CAL50 was approximately pH9.8 (Fig. 2.14). The absolute values of zeta potential were higher than 30 mV at pH values higher than 3 (30R50) and 6 (30R25) or lower than 8 (30CAL50), revealing a moderate colloid stability of suspensions. The pH_{IEP}≈2 for 30R50 and 30R25 is expected for silica, whilst the pH_{IEP}≈9.8 for 30CAL50 may stem from the presence of a grafted polycation at the silica surface: Liu (2010) pointed out that the stabilizer of Klebosol colloidal silica 30CAL50 is an Al derivative.

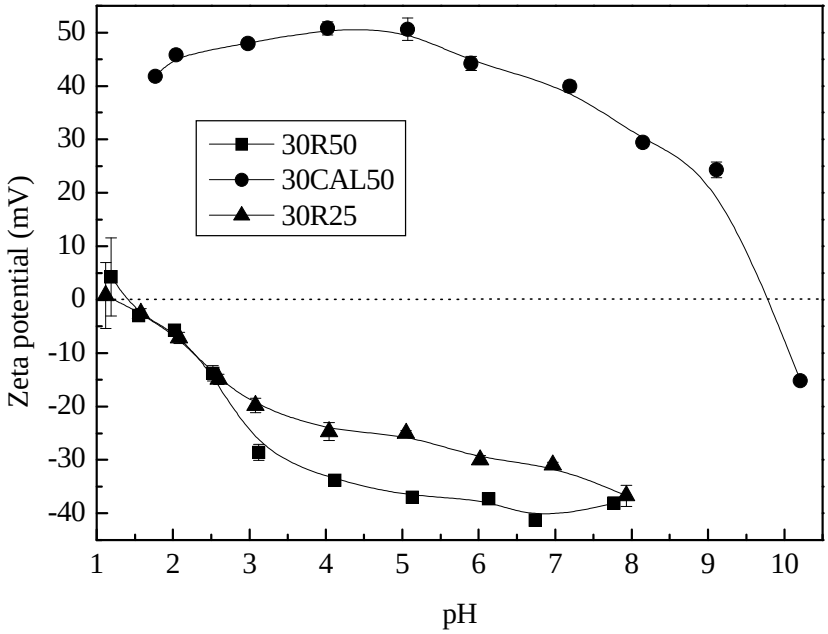

Fig. 2.14. Zeta potential of suspensions varying with pH value at the SNP concentration of 0.15 vol.%.

The variation of particle size of 30R50 and 30R25 (0.15 vol.%) along with pH was demonstrated in Liu's Ph.D. study, and Fig. 2.15. is presented here to offer the supplementary data of 30CAL50 (0.15 vol.%). The average sizes of 30R50 and 30R25 0.15 vol.% close to their IEPs were about 90 nm and 37 nm, respectively, compared with approximately 80 nm (30R50) and 30 nm (30R25) under other pH conditions (Liu et al., 2012; Liu, 2010). The particle size of 30CAL50 0.15 vol.% greatly increased to around 1 μm at IEP, and kept in the range of 75~89 nm at pH values lower than 6. The large particle size obtained at IEPs for all the three types of SNPs was consistent with the fact that the charge neutralization could lead to the unstable colloid suspension and thus be apt to form particle aggregates.

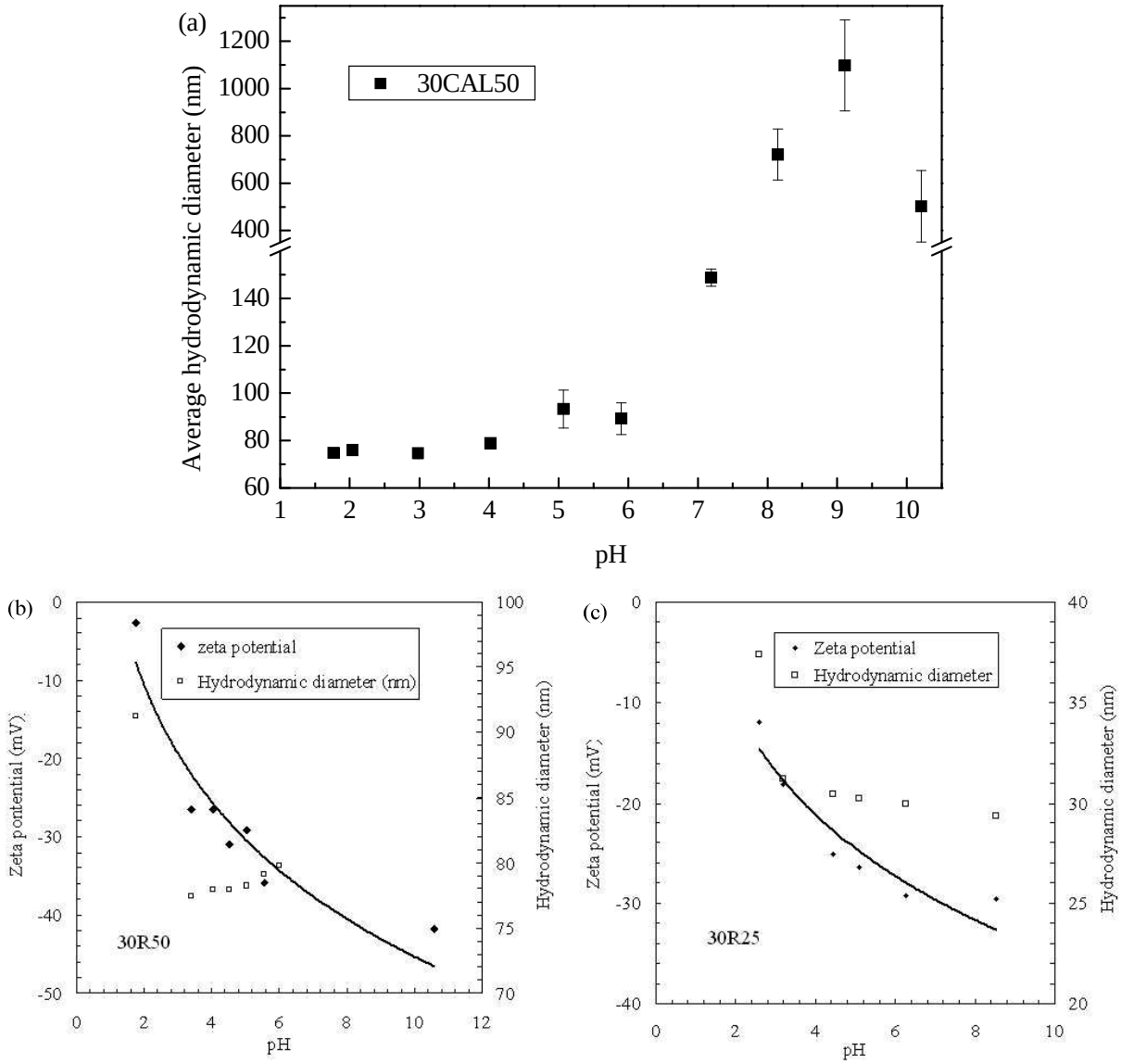

Fig. 2.15. Particle size varying with pH at the concentration of 0.15 vol.%: (a) 30CAL50 (measured in this study), (b) 30R50 and (c) 30R25 (measured by Liu (2010)).

(3) Effect of additional IS on the particle size and zeta potential

The specific information of additive reagents in those commercial SNP suspensions is unknown from the producer. Similar to Section 2.2.1.2(3), the additional salt concentration is investigated here for its impact on the stability of NP suspension by adding NaCl (AR, Carl ROTH, Germany)-deionized water solution in suspensions within the additional NaCl concentration (additional IS) range between 0~200 mmol/L NaCl.

The initial conductivities of 0.15 vol.% 30R50, 30R25 and 30CAL50 suspensions were measured to be 49.5, 45.6 and 164.8 μS/cm, respectively, by the conductivity meter

mentioned in Table 2.2, whereas that of the deionized water was about 1.7 μS/cm, denoting that the addition of ions into the initial suspension during the production process caused the IS increase of suspension. The extra NaCl addition into the suspension could give rise to the linearly increase of conductivity, and the resulting conductivities of the three SNP suspensions were close at high NaCl concentrations higher than 5 mmol/L (Fig. 2.16).

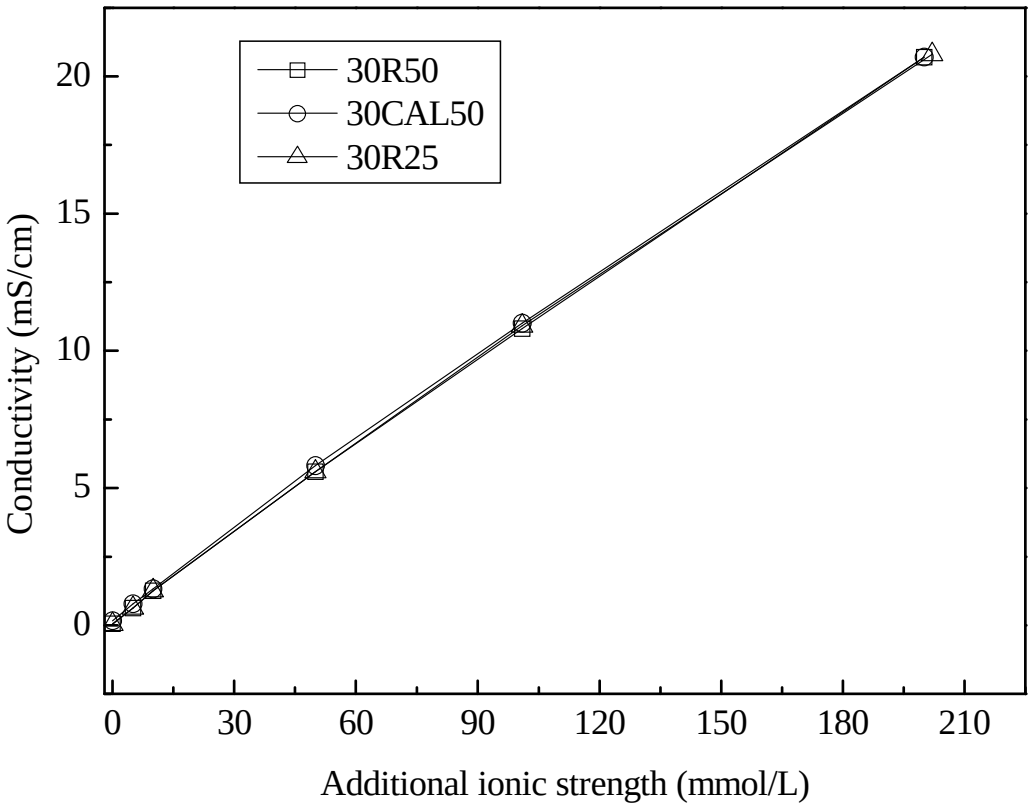

Fig. 2.16. Conductivity of SNP suspension varying with additional IS.

Particle size, zeta potential and pH versus additional IS are shown in Fig. 2.17, individually. 30R50 and 30R25 kept uniform particle size of 80~87 nm and 26~30 nm, individually, in the investigated additional IS range. The particle size of 30CAL50 0.15 vol.% was around 80 nm at additional IS ≤ 100 mmol/L; for a higher additional IS of 200 mmol/L NaCl, the particle size rose to 106 nm. The interpretation of that size increase observed by DLS here could be referred to Section 2.2.1.2(3).

The absolute values of zeta potential reduced with the increase of NaCl concentration for all the three types of SNPs as shown in Fig. 2.17(b): dropping from around 40 mV to 19 mV for 30R50 0.15 vol.%, from about 32 mV to 16 mV for 30R25 0.15 vol.%, and from about 50 mV to 31 mV for 30CAL50 0.15 vol.%, agreeing well with the trend found in the research of

Saleh et al. (2008). As illustrated by Saleh et al. (2008), the particle-particle interaction energy affected by IS could be approximated by DLVO theory that assumed van der Waals attractive and electrostatic repulsion: at low IS below 10 mM, the energy barrier of particles was difficult to overcome, whereas the electrostatic repulsion would less effectively hinder particles approaching to each other. The study of Yotsumoto and Yoon (1993) also denoted the interesting phenomena that NaCl destabilized silica suspensions.

The pH values of 30R50, 30R25 and 30CAL50 suspensions stayed always around 7.6±0.6, 8.2±0.6, and 4.5±0.1, respectively (Fig. 2.17(c)). That subtle drift in pH values could be ascribed to no release of H^+ or OH^- by adding the salt NaCl. H^+ and OH^- are well known as ions determining the zeta potential of particle surfaces due to their high charge density, while Cl^- and other anions can just screen the surface charge.

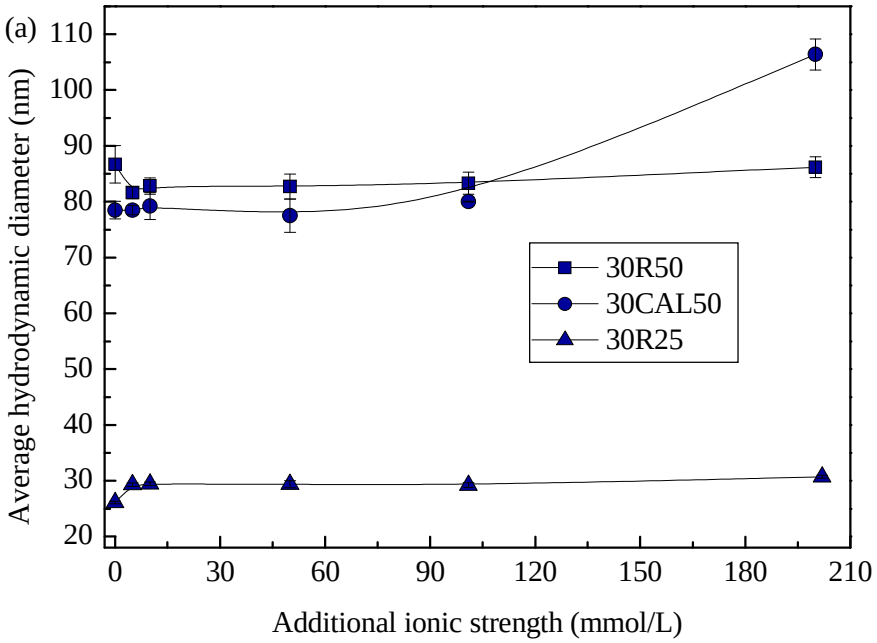

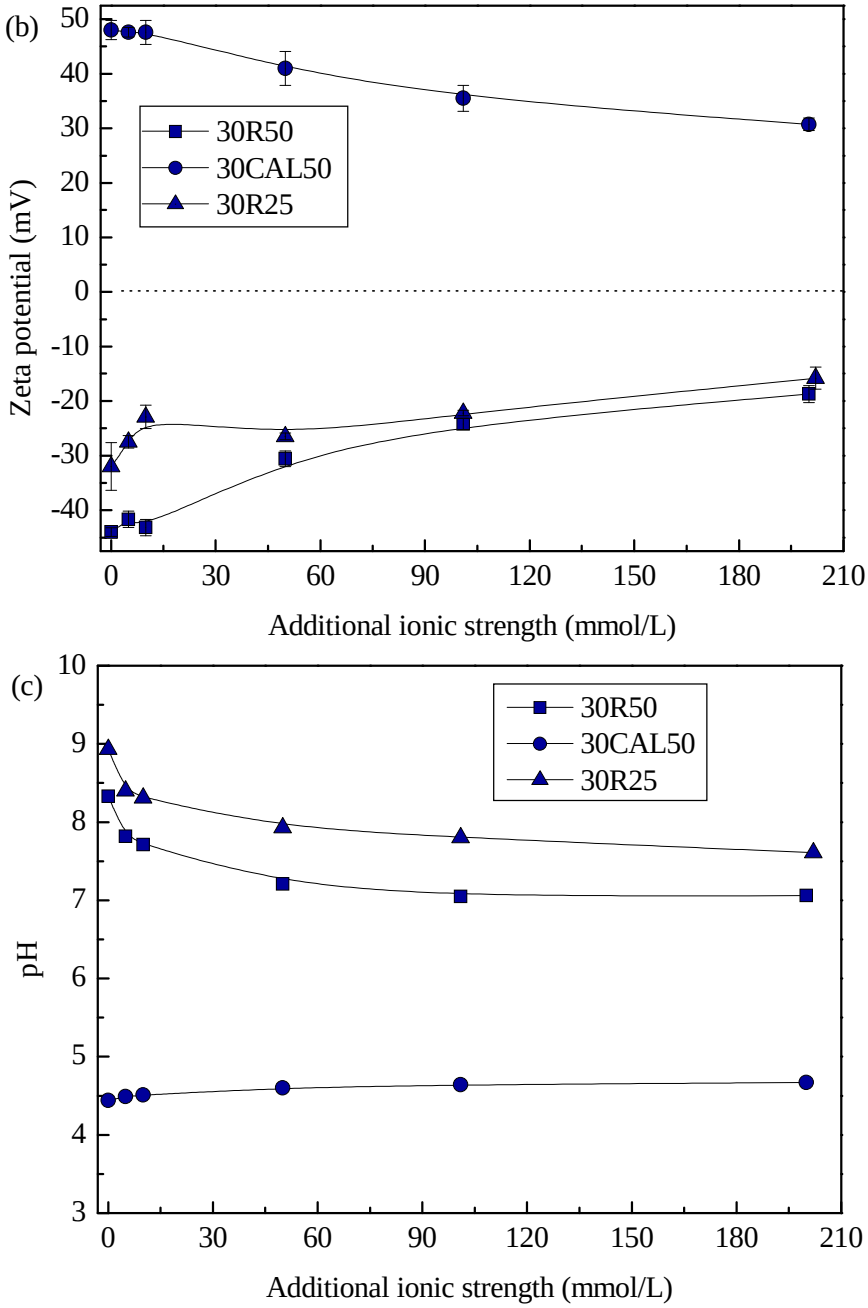

Fig. 2.17. Effect of additional IS on properties of SNP suspension: (a) particle size, (b) zeta potential; (c) pH value.

2.3.2 Properties of flotation assisting reagent -- surfactant

CGAs were generated using sodium dodecyl sulfate (SDS, Sigma-Aldrich, U.S.) and cetyl trimethylammonium bromide (CTAB, Carl ROTH, Germany). SDS, an anionic surfactant (MW=288.37 g/mol), is a salt of an organosulfate consisting of a 12-carbon tail attached to a sulfate group that gives the material the amphiphilic properties (its structural formula is shown in Fig. 2.18(a)). CTAB is a cationic surfactant with a chain of 16 carbon atoms (MW=364.45 g/mol) (its structural formula is presented in Fig. 2.18(b)).

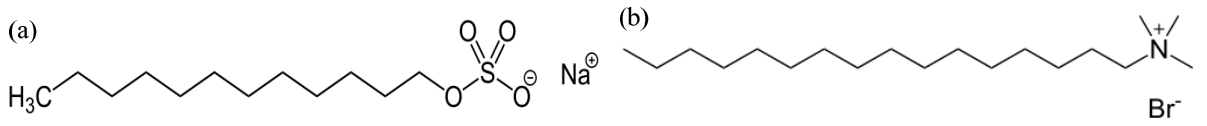

Fig. 2.18. Structural formula of (a) SDS and (b) CTAB.

The CMCs of CTAB and SDS, above which micelles spontaneously formed, were verified to be approximately 0.98 mmol/L and 7.7 mmol/L, respectively, by measuring the conductivity and the surface tension at the room temperature of approximately 25 °C (298.15 K) (Fig. 2.19): for the surface tension measurement, the CMC corresponded to the concentration above which the surface tension remained constant; for the conductivity measurement, the CMC was determined by the intersection of two straight lines below and above the CMC. The CMCs of CTAB and SDS obtained here agreed well with the values in others' reports (Kile and Chiou, 1989; Fuguet et al., 2005). Another important parameter of surfactant is the Krafft temperature (T_K) below which the surfactant remains in crystalline form and even in aqueous solution and micelles cannot form. The T_K values of CTAB and SDS were found to be approximately 25~26 °C and 14~16 °C, respectively (Rico and Lattes, 1986; Qian et al., 2005). All experiments with CTAB and SDS were thereby conducted above T_K. Additionally, the pH value of surfactant solutions kept stable in the investigated concentration range (Fig. 2.20), fluctuating within 6.19~6.41 for SDS ranging from 0.01 mmol/L to 17 mmol/L and varying around 6.15~6.37 for CTAB ranging from 0.01 mmol/L to 15 mmol/L.

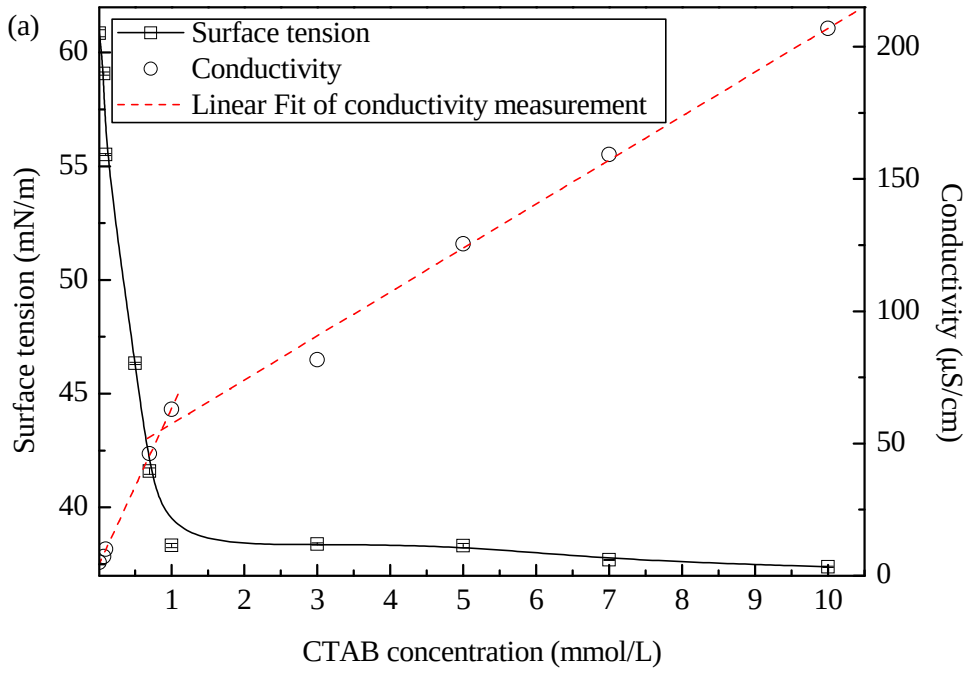

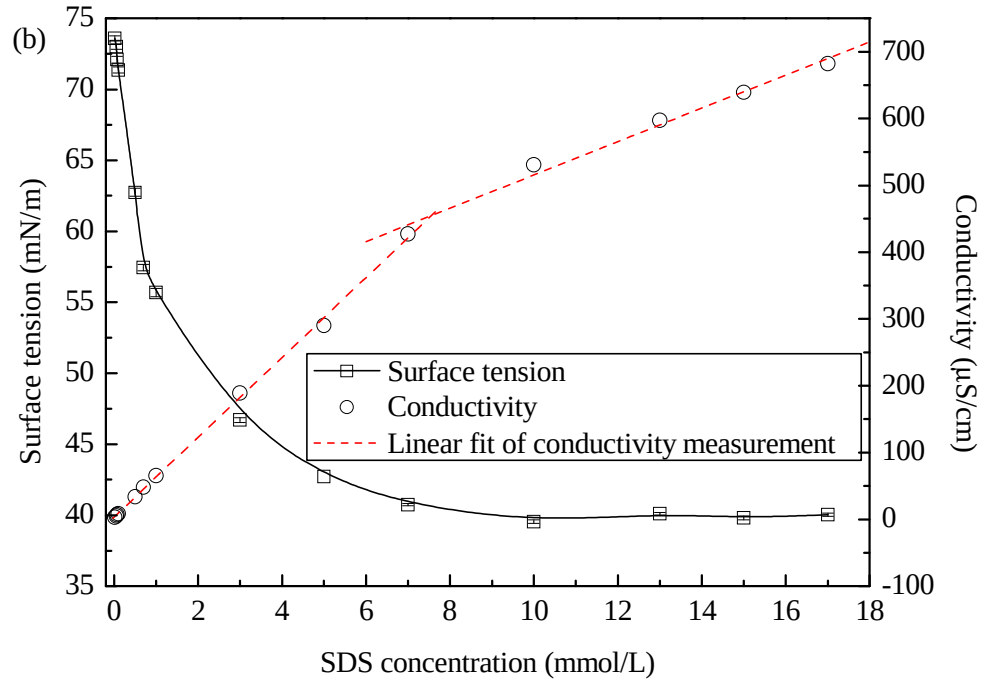

Fig. 2.19. Determination of CMCs by measuring surface tension and conductivity: (a) CTAB; (b) SDS.

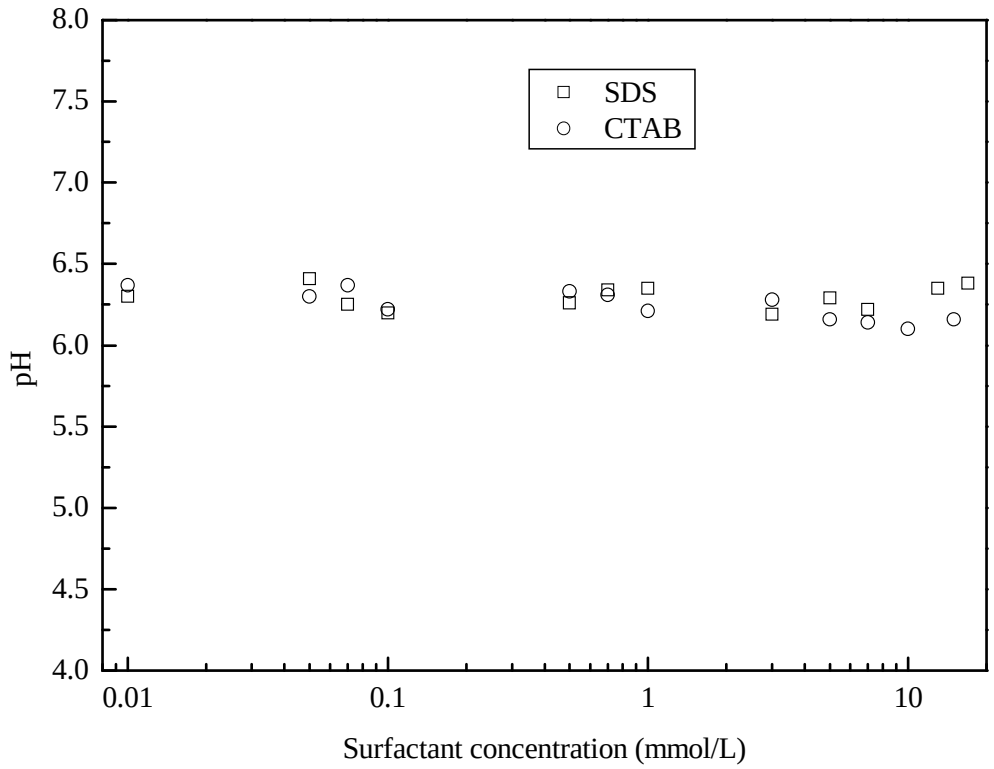

Fig. 2.20. The pH value of surfactant solution varying with surfactant concentrations.

2.4 Conclusions

The features of NPs (TNP and SNP) and flotation assisting reagents (HA, CTAB and SDS) were explored in this chapter as fundamental study before the following flotation, aggregation and adsorption experiments, such that specific interfacial mechanisms between NPs and collectors in those processes can be well explained and understood. Effects of NP concentration, pH value, and IS on the colloidal behavior of NP suspension were investigated apart from the NP characterization. The preparation of flotation assisting reagent solution and the particular properties were studied as well. Relative conclusions have been drawn down below:

- TNP and TNP suspension:

The acidic commercial TNP suspension with the average particle diameter of 41.6 nm (Lot #1) and 14.5 nm (Lot #2), respectively, was employed in the current study. Over the investigated TNP concentration range, the pH slightly increased (< pH3) due to the dilution effect and the zeta potential remained constant at around +38 mV. The concentration of suspension was fixed to be 0.15 wt.% in all the following experiments.

Metal oxides such as TiO_2 and SiO_2 are known to be representative hydrophilic solids owing to the presence of numerous surface MeOH groups that favorably create hydrogen bonds with water. The TNP suspension was susceptible to the pH variation: the zeta potential decreased with increasing pH value from 3 to 11, the surface charge reversing from positive to negative at pH_{IEP} (5.7). TNP aggregates formed due to the charge neutralization. The maximum particle size firstly appeared at pH_{IEP} and the size kept 55±5 μm within pH5~10; at pH11, the particle size decreased to about 25.5 μm possibly resulting from the particle re-stabilization by electrostatic repulsion.

Adding salt would give rise to large aggregate in the suspension without greatly changing the zeta potential and the pH value, agreeing well with the classical DLVO theory which leads to the prediction that any increase in the IS of the electrolyte solution in the particle suspension will compress the diffuse layer associated with the particles, diminish interparticle repulsion, and therefore promote aggregation.

- HA used as TNP collector and surface modifier

The HA solution was prepared by dissolving the HA powder into the highly basic solution, and the dissolved HA could keep the soluble state at pH ≥ 4. The CMC of HA was determined to be 290±5 mg/L DOC in this study. The HA solution at the concentration lower than 10 mg/L DOC was of average particle size smaller than 1 nm and turbidity lower than 1 NTU, while for higher HA concentration, the particle size and turbidity got sharp increase, which might influence the interfacial mechanisms between HA and TNPs. In the following chapter, HA concentrations below and above 10.5 mg/L DOC are tested in surface modification and adsorption-aggregation experiments, respectively. When the HA concentration is higher than 10.5 mg/L DOC, the TNP-HA interfacial process will not be recognized merely as HA molecules adsorbing toward the TNP surface any more, but it is also necessary to take the possible co-precipitation between those TiO_2 and the colloidal precipitates of HA molecules into account.

- SNP and SNP suspension

Three types of SNPs (30R50, 30R25 and 30CAL50) were employed in order to obtain the completely understanding of NP properties on the NP-CGA interaction in either flotation or adsorption-aggregation which will be particularly in Chapter 4. The negatively surface charged 30R50 and 30R25 with an average particle size of approximately 80 nm and 30 nm, respectively, and the positively surface charged 30CAL50 of around 77 nm in diameter. Rather different from TNPs, all the SNPs were less pH sensitive over the pH range of 2~6 where the particle size fluctuated around their average value. The IEPs of 30R50 and 30R25 were around pH1~1.5 whilst that of 30CAL50 was approximately pH9.8. Adding salt would result in the slight reduction of absolute zeta potential of all SNPs, and as well as the increase of particle size for 30CAL50 whereas the other two SNP kept constant.

- Surfactant (CTAB and SDS) used as SNP collector and CGA generating solution

The CMCs of CTAB and SDS were verified as approximately 0.98 mmol/L and 7.7 mmol/L, respectively. The Krafft temperature T_K values of CTAB and SDS were found to be approximately 25~26 °C and 14~16 °C, respectively (Rico and Lattes, 1986; Qian et al., 2005), above which all experiments with CTAB and SDS were conducted. The pH value of surfactant solutions kept stable in the investigated concentration range.

Based on the properties of NPs and relative collectors figured out in this chapter, successive investigations of NP-collector interaction in the surface modification and adsorption-

aggregation processes will be focused on for the mechanical interpretation of NP separation in flotation, and the flotation removal efficiency of NPs will be tested thereafter.

Chapter 3

DAF of TNPs with HA assistance

Summary

In search of environmentally-friendly reagents, this chapter aims at evaluating the feasibility of using HA as an assisting reagent to remove TNPs from aqueous suspension. Experiments are divided into three parts:

(1) Primary surface modification experiments of TNPs by alkaline HA solution leaving the pH of HA stock solution free. Specific tests are carried out for the sake of agglomeration behaviors and interaction mechanisms of TNP-HA resulting from both HA molecules and OH^-.

(2) Adsorption-aggregation experiments with controlling pH of HA stock solution. Adsorption characteristics of HA molecules on the TNP surface are studied at different pH values of HA stock solution and HA concentrations, and properties of resulting aggregates are investigated in terms of particle size and fractal structure. Thus, interaction mechanisms between TNPs and HA molecules can be further investigated.

(3) Laboratory scaled continuous DAF of TNPs with HA assistance and pH adjustment, individually. The high TNP removal efficiency is expected to be attained and ways of flotation condition optimization are then proposed.

3.1 TNP surface modification with alkaline HA solution

3.1.1 Experimental method

Before flotation tests, TNP surface modification experiments with HA were firstly carried out without controlling the pH value of HA stock solution so as to explore the interaction between TNPs and HA in water dispersion. Various amounts of alkaline HA stock solution was added directly into the 0.15 wt.% TNP suspension (Lot #1), and the TNP-HA suspension was then vigorously mixed on the vortex mixer (Fisher Scientific FB15024, UK) for 1 min, and then kept 24 h to reach the complete adhesion of TNP-HA. The reaction duration was confirmed to be sufficient by relative studies dedicated to the TNP surface modification with NOM (Kim et al., 2009; Zhao et al., 2012).

- Surface charge measurement was carried out to obtain the information on the state of charge at the solid-liquid interface by Zetasizer NanoZS.
- Particle size and PSD of supernatant and sediment were characterized by DLS (Nanotrac) and LDS (Mastersizer 2000), respectively, due to different measurement ranges of the two

techniques and the various diameters of NPs and larger aggregates as mentioned in Chapter 2.

- Functional groups of the modified TNP surface were investigated by FT-IR performed on TENSOR 27 FT-IR Spectrometer (Bruker Optics Corporation, Germany) at Service Analyses & Procédés of Laboratoire de Génie Chemique de Toulouse. The infrared spectra were recorded from 4000 to 400 cm^{-1}, using a 4 cm^{-1} resolution. The samples were pressed with dried KBr pellets at a ratio of approximately 1:100 w/w.
- The small angle laser light scattering (SALLS) method has been used in the determination of aggregate fractal dimension. Particles in the sample scatter light proportionally to their size and at a constant angle independent of which part of the particle is hit by the beam. Small particles scatter light at the high angles while large particles scatter at low angles (Jarvis et al., 2005). The Malvern Mastersizer 2000 has an array of photosensitive detectors at different angles between 0.01° and 40.6° that detect the light scattered by the sample. In the light scattering study, the total scattered intensity I is a function of the scattering vector Q, where Q is the difference between the incident and scattered wave vectors of the radiation beam in the medium, which is given below:

$$Q = \frac{4\pi n_m \sin\left(\theta/2\right)}{\lambda} \tag{3.1}$$

where, n_m is the refractive index of the suspending medium, θ is the scattering angle, and λ is the wavelength of the radiation in a vacuum. It has been shown that for a mass fractal aggregate, which satisfies conditions for Rayleigh-Gans-Debye (RGD) regime, its scattered intensity I is related to Q and the fractal dimension by D_f:

$$I \propto Q^{-D_f} \tag{3.2}$$

On a log-log plot there is a linear region, with a slope of $-D_f$ (Bushell et al., 2002). This relationship holds provided that the length scale of investigation is much larger than the primary particles and much smaller that the aggregates (Guan et al., 1998). This condition is largely fulfilled in our case where the primary NP size is around 14.5 nm meanwhile the floc size can be at least 10 μm.

3.1.2 Surface charge of TNP-HA aggregates

The surface charge is of great importance to know the dispersion characteristic of the TNP system. The amount of charge on the surface can dictate many ultimate uses, as NPs are very

reactive in aqueous suspension (Singh et al., 2012). The effect of HA concentration on zeta potential of TNPs was investigated for the surface modification study. The HA (0.57~9.15 mg/L DOC) modified the TNP surface from positively to negatively charged (Fig. 3.1), and the zeta potential reverses near the HA concentration of approximately 7.8 mg/L DOC, which was considered to be the optimum HA dosage for the TNP aggregation. The pHs of suspensions were not higher than 6.1 (when the HA concentration is 9.15 mg/L DOC). It should be noted that, when the HA addition was less than 6.5 mg/L DOC and the correspondingly pH value of the HA solution was lower than 4, HA molecules were not absolutely soluble as formerly demonstrated in Section 2.2.2.2(2); hence, the polyanions of HA molecules could not de-stabilize the TNP suspension.

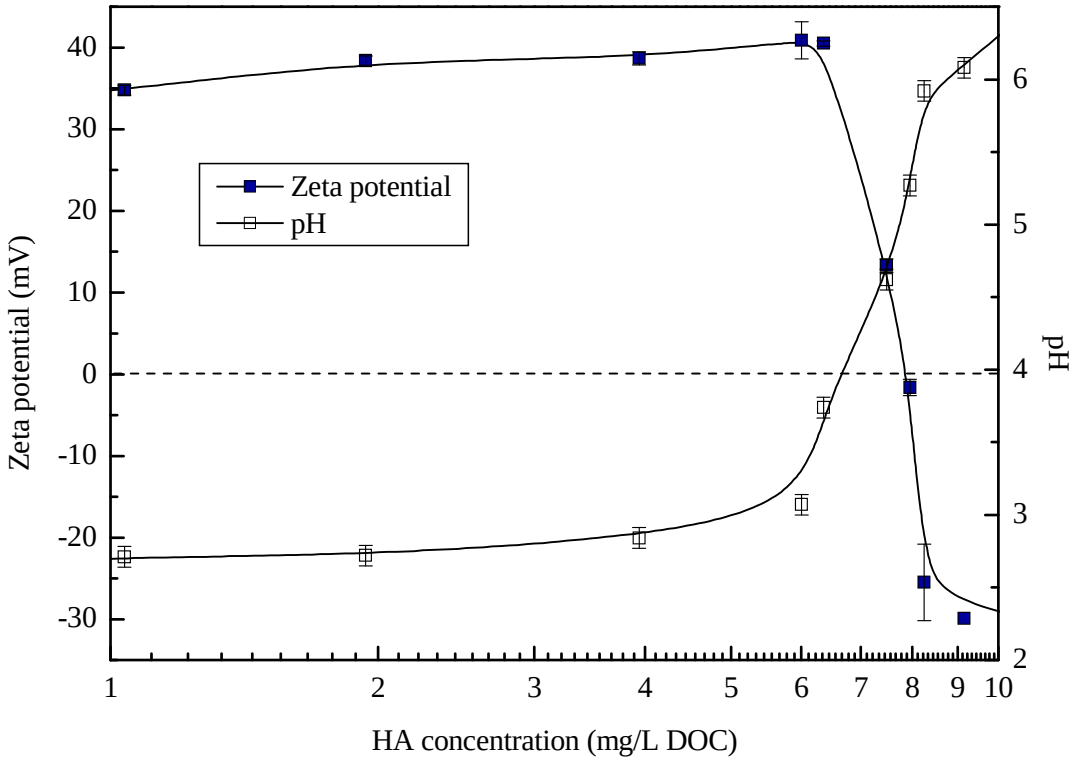

Fig. 3.1. Zeta potential and pH profiles of TNPs (0.15 wt.%) at different HA concentrations.

Since the HA solution used in this study was an alkaline solution, the effect of pH on zeta potential should also be considered in order to differentiate it from the effect of HA and clarify the surface interaction mechanism as well. The pH-dependence of zeta potential determined in the 0.15 wt.% TNP suspension with and without HA can be seen in Fig. 3.2. It denoted that the IEP of the NaOH-adjusted curve was at pH 5.9, while that of the HA-adjusted curve was at pH 5.2, shifting to a lower pH with the presence of HA. It was noting that the zeta potential value of TNP suspension in the absence of HA was +24.1 mV at the

pH_{IEP} (5.2) of suspension in the HA presence, implying the repulsive interparticle interaction. In the process of TNP surface modification with basic HA, the OH^- from NaOH could neutralize positive charges on TNP surface first, and then the further adsorption of HA-polyanions led to the over-compensation of positive charges on the oxide surface. Due to this polyanionic coating layer on TNPs with HA addition, the measured values of zeta potential became more negative than that at the pH_{IEP} in the absence of HA. It is worth noting that OH^- resulting from NaOH in the HA stock solution played leading roles in the TNP aggregation from the respect of electrostatic interaction, and the polyanions of HA contributed to the screening of TNP surface charge when HA molecules were ionized. Similar explanation of humic substances on nanoaprticle surface charge was given in the case of HA adsorption and aggregation of magnetite NPs (Illés and Tombácz, 2006).

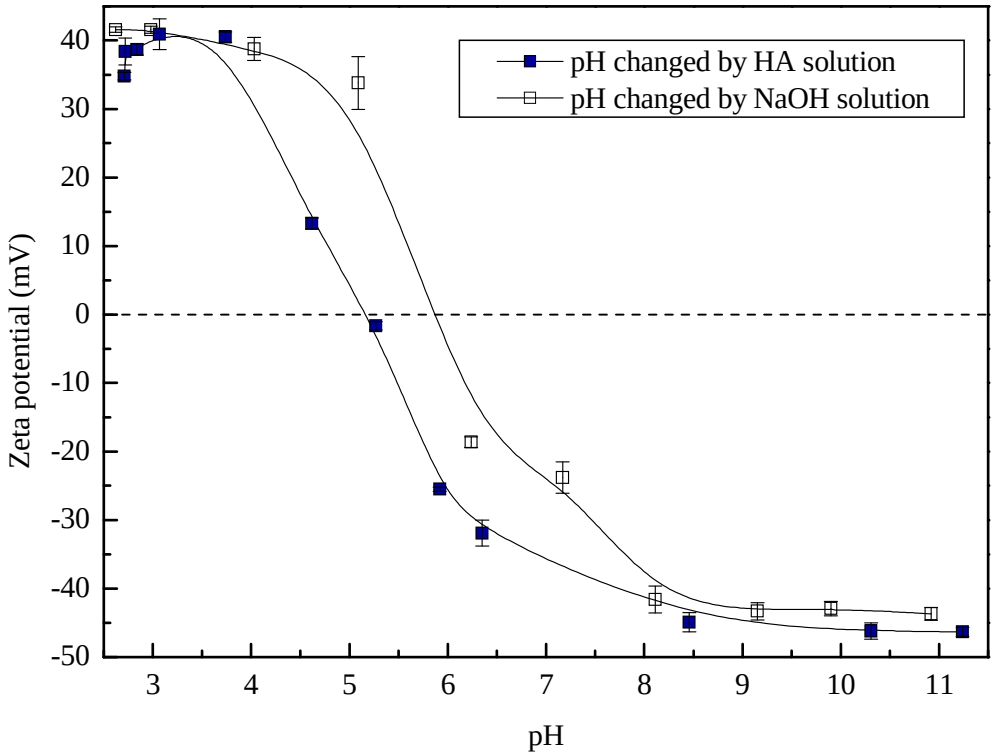

Fig. 3.2. Zeta potential as a function of in the presence and in the absence of HA.

As presented in Fig. 3.3, when adjusting the pH of HA stock solution to different values (pH4.6, 6.0, 8.2 and 12.7, in which the HA could be well dissolved as illustrated in Section 2.2.2.2(2) of Chapter 2), the HA dosage for neutralizing the surface charge of TNPs greatly increased, from 7.8 mg/L DOC for pH 12.7, to 62 mg/L DOC for pH 8.2, 98 mg/L DOC for pH 6.0, and 105 mg/L DOC for pH 4.6.

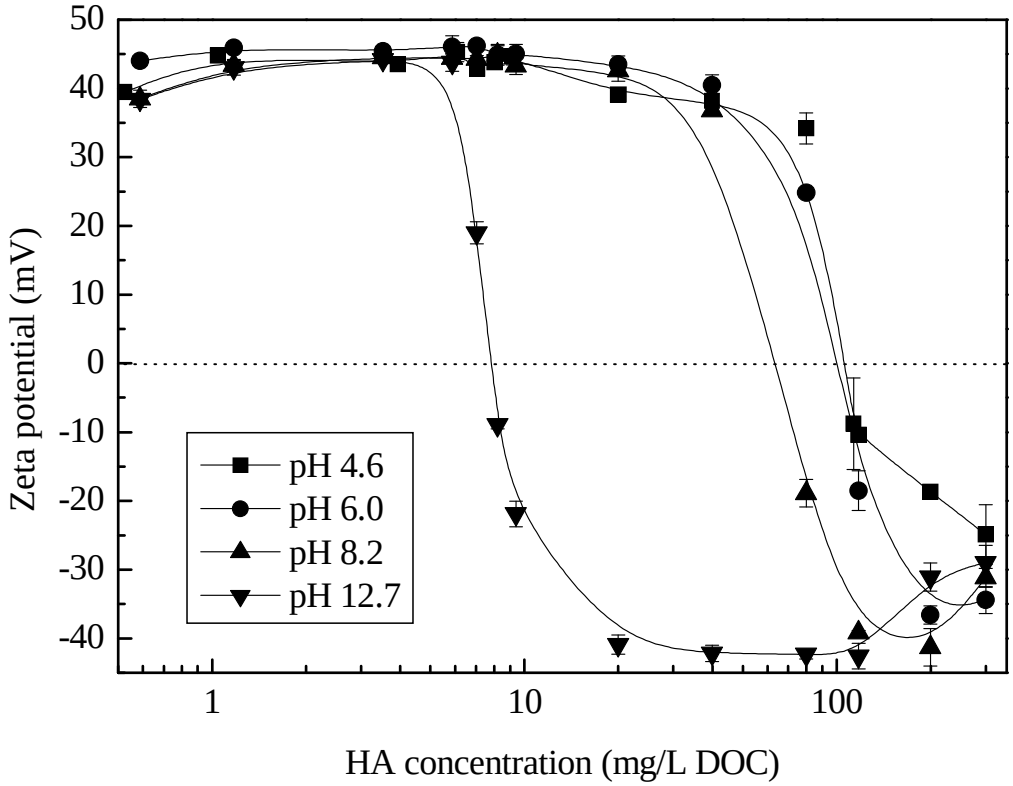

Fig. 3.3. Zeta potential as a function of HA concentration under different pH conditions.

3.1.3 PSD pattern of TNP-HA suspension

Four HA concentrations close to the optimum HA dosage were chosen to compare and study the PSD pattern of the TNP suspension. Fig. 3.4 shows photographs of the HA modified TNP suspension, and size distributions of supernatants and sediments are presented in Fig. 3.5. In the investigated HA concentration range, the solid-liquid stratification appeared, and supernatants turned from clouded to clear, along with the increasing of the HA concentration. The phenomenon agrees well with what is shown in Fig. 3.5: in Fig. 3.5(a), the average particles sizes with HA concentrations of 6.10 mg/L DOC to 9.15 mg/L DOC were 237.5 nm, 228.2 nm, 197.4 nm, and 0.930 nm, individually, and in Fig. 3.5(b), the average sizes of sediments were 8.6 μm, 19.4 μm, 26.1 μm, and 133.6 μm, respectively. The decrease of particle size in supernatants and increasing of particle size in precipitants demonstrated that that HA facilitated the formation of TNP-HA aggregates. Increasing the HA dosage, the TNP-HA aggregates were apt to settle down because they were getting large, compact and dense. The largest aggregates were obtained at 9.15 mg/L DOC which was higher than the optimum HA dosage (7.8 mg/L DOC) resulting from the zeta potential investigation. Since both ligand exchange and electrostatic interaction had been employed to explain the NOM adsorption by nano-oxides (Gu et al., 1994; Yang et al., 2009), our result illustrated that the interaction

between the functional groups of HA and TNPs made TNPs difficult to re-stabilize, even if zeta potential became more negative.

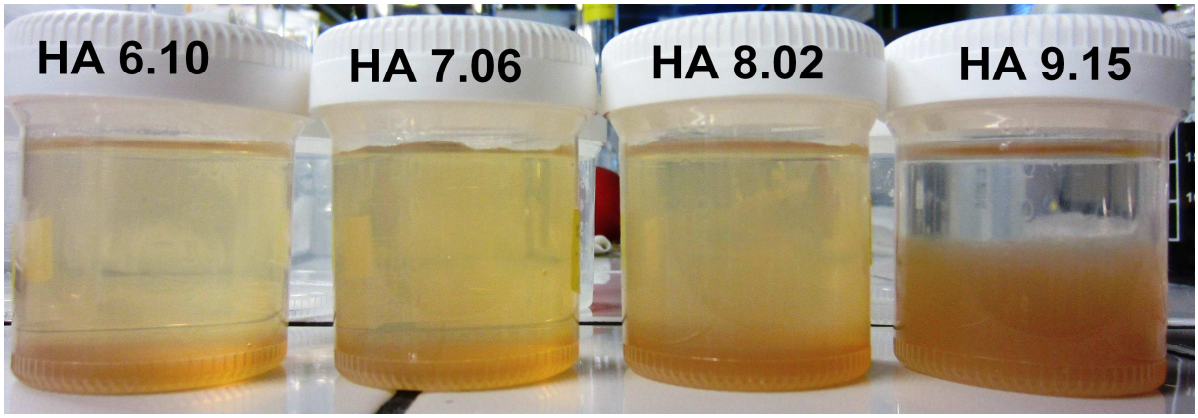

Fig. 3.4. Photos of surface modified TNP suspensions at different HA concentration (The number on the capsule stands for the HA concentration (mg/L DOC).).

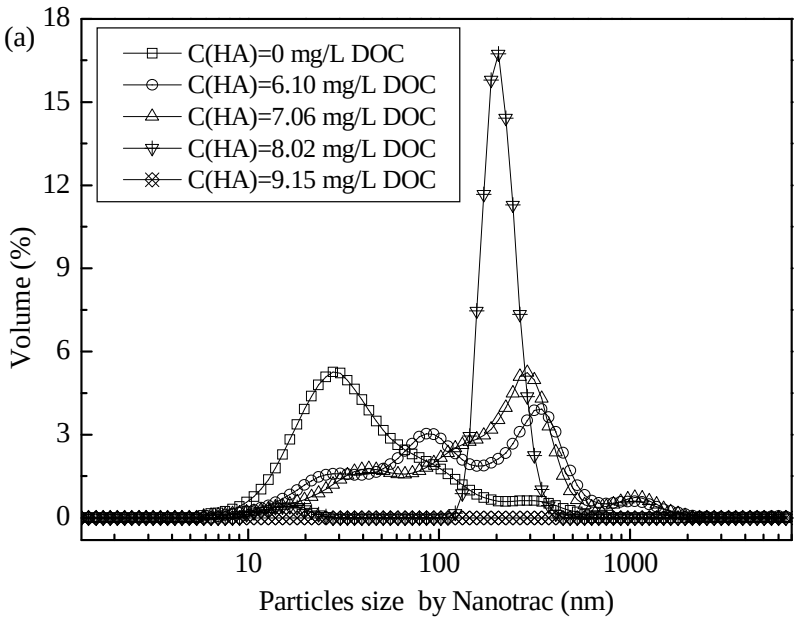

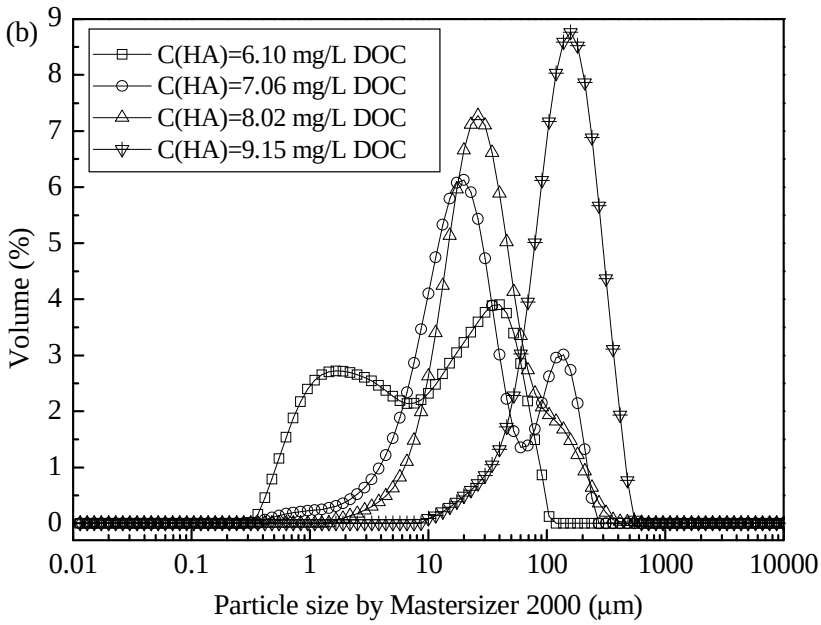

Fig. 3.5. PSD of surface modified TNP suspensions: (a) supernatant by DLS; (b) precipitates/flocs by LDS.

3.1.4 FT-IR analysis

In order to verify the interaction type between HA and TNPs, FT-IR studies were conducted on samples of TNPs conditioned with HA. Fig. 3.6 shows the FT-IR spectra of TNPs modified by different concentrations of HA. For HA, the broad bands at around 3400 cm^{-1} could be assigned to OH stretching of the carboxylic groups, phenolic, alcohol or bonded water; the 1773 cm^{-1} peak could be attributed to the C=O stretching of COOH groups (de Moraes and Rezende, 2005); peaks around 1600 cm^{-1} were produced by stretching of C=C linkages of the aromatic groups; the sharp band observed at 1432 cm^{-1} corresponded to the O-H bending vibrations of alcohols or carboxylic acids deformation of carboxyl groups (De Moraes and Rezende, 2005; Agarwal et al., 2010). For TNPs, the major peaks (3277 cm^{-1} and 1617 cm^{-1}) were retained but presented systematic frenquency shifts (red shifts) with stronger intensity, revealing the strong interaction between TNPs and HA due to adsorption of HA molecules (Yang et al., 2009; Iijima et al., 2009; Singh et al., 2012). The appearance of the peak at around 1390 cm^{-1} (the O-H bending vibration of alcohols or carboxylic acids) in the (TNP+HA) mixtures indicated the interaction of HA-OH with TNP surfaces.

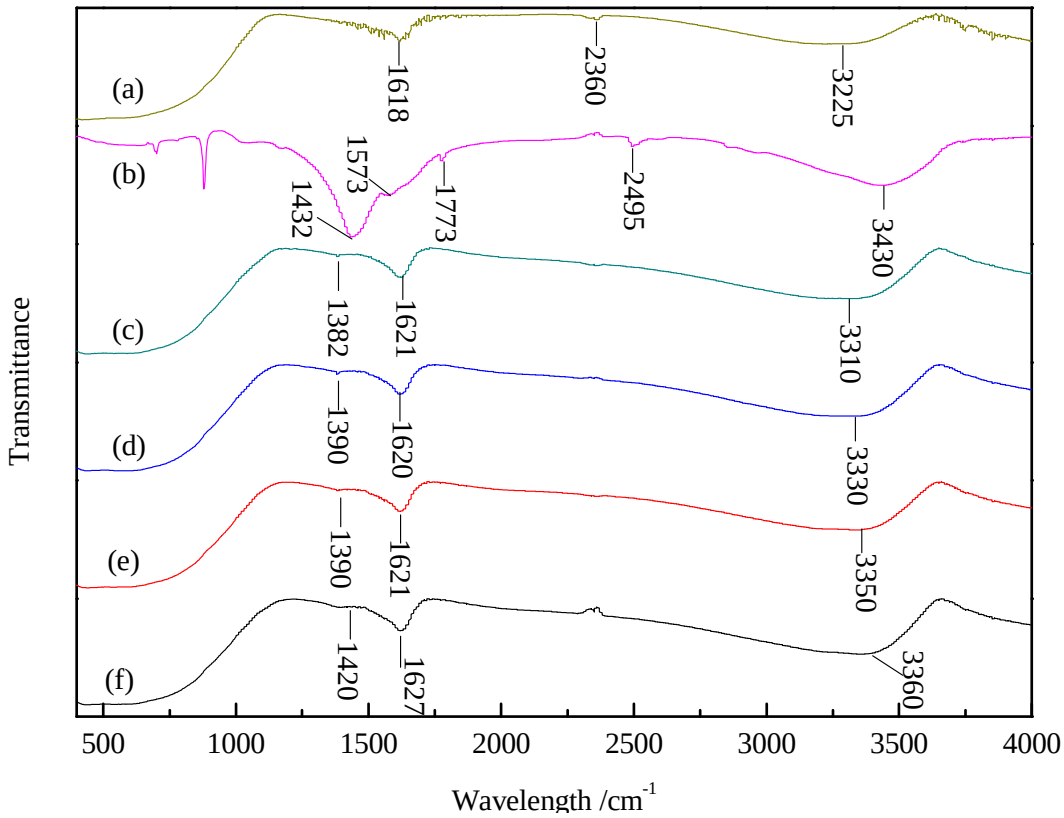

Fig. 3.6. FT-IR spectra of TNPs before and after surface modification by HA with various additive contents: (a) TNPs, (b) HA, (c) TNPs + 6.10 mg/L DOC HA, (d) TNPs + 7.06 mg/L DOC HA, (e) TNPs + 8.02 mg/L DOC HA, (f) TNPs + 9.15 mg/L DOC HA.

3.1.5 Residual DOC and turbidity in the TNP-HA suspension

Quantities of studies have proved that the DOC in natural water sources may react with disinfectants to form disinfection by-products, and reduce the effectiveness of water treatment by interfering with fouling membranes and adsorbents (Kitis et al., 2001; Huang et al., 2012); moreover, the dissolved HA may enhance the solubility of some organic pollutants and pesticides (Chiou et al., 1986). Therefore, the high HA concentration will not be environmentally friendly. The residual DOC and turbidity of TNP-HA suspension after a long time (24 h) until the equilibrium are shown in Fig. 3.7. The 0.15 wt.% commercial TNP suspension (Lot #1) used in this study had the DOC of around 0.95 mg/L possibly caused by the unknown organic additive for the good dispersion. The residual DOC kept increasing until the HA dosage was 6 mg/L DOC; thereafter, it sharply decreased along with the increase of HA concentration and maintained around 1 mg/L at the HA dosage $\geq$ 7.5 mg/L DOC. As for the residual turbidity, it presented the worst result at the HA concentration around 6.3 mg/L DOC. That might be attributed to the aggregated TNP-HA particles are not dense, compact and large enough to settle down. When the HA concentration was higher than 7.5 mg/L DOC, the residual turbidity in supernatants was close to 0 NTU, matching well with the zeta

potential (close to 0 mV at HA concentration of 7.8 mg/L DOC). A transparent supernatant with the highest adsorbing amount of HA on TNPs could be obtained at the HA concentration of 9.15 mg/L DOC. For the aim of low residual DOC and turbidity in the resulting suspension, an optimum HA concentration range of 7.8~9.15 mg/L DOC was determined. In that HA dosage range, almost all HA aggregated with TNPs, leaving only little in the solution, which was also confirmed by results presenting in Fig. 3.4 and Fig. 3.5. Therefore, the residual HA in water would not be a threat to the environment.

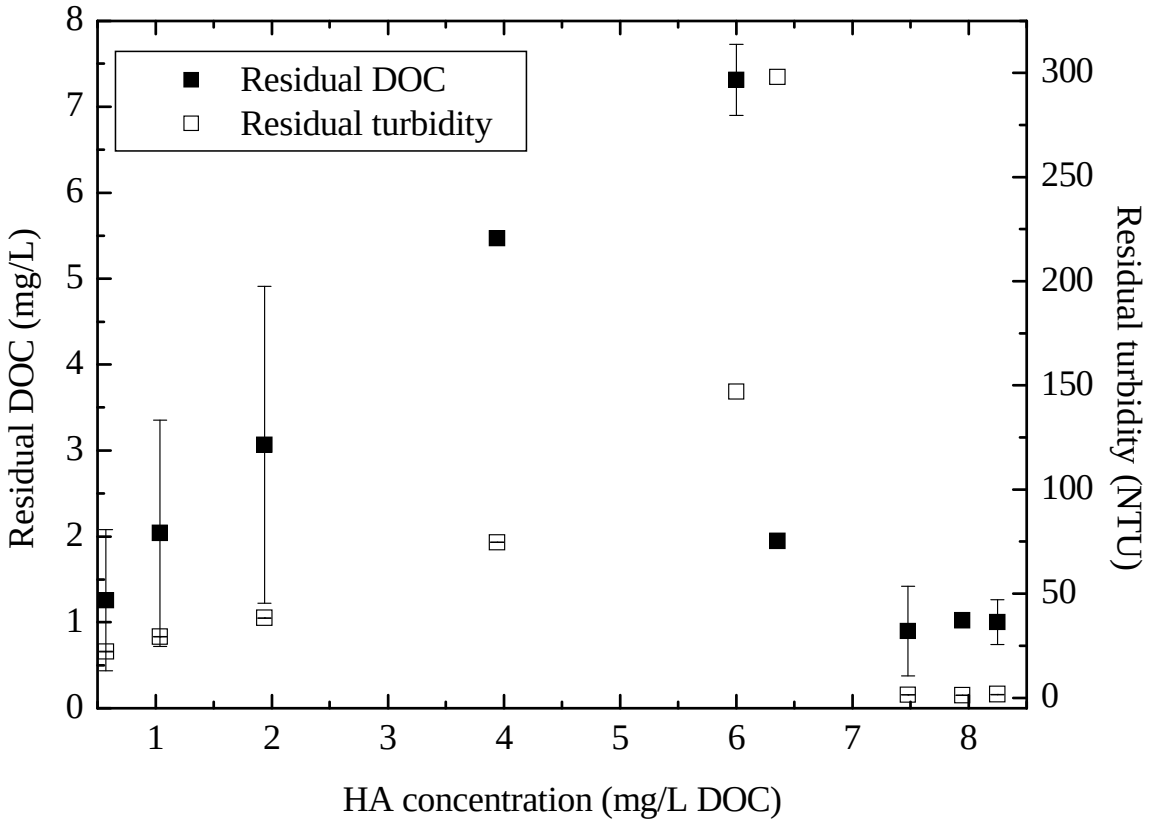

Fig. 3.7. Residual HA and residual turbidity as functions of HA concentrations.

3.1.6 Discussion of the TNP surface modification with alkaline HA solution

The leading mechanisms of controlling NOM (such as HA) adsorption on metal oxides (i.e. iron oxide) include electrostatic interactions, ligand exchange, hydrophobic interactions, and van der Waals interactions (Gu et al., 1994; Arnarson and Keil, 2000; Yang et al., 2009 Ding and Shang, 2010). Due to the heterogeneity and complexity of NOM and adsorbent surfaces, combinations of different adsorption mechanisms have been suggested to occur in reality. In the basic HA solution, OH^- acts as ions neutralizing the surface charge of TNPs owing to its greater affinity with positively charged surfaces, and the polyaions of HA molecules (i.e. –

COO^-) further compress the TNP surface charge. Besides, the functional groups of HA are capable of interacting with metal species in solution or suspension. It is therefore possible that TNPs may interact with either the polyanions of soluble and ionized HA, or colloidal fraction of HA, or both (Baek and Yang, 2005). It is worth noting that, when alkali treated, the M_e^{2+}, M_e^{3+}-humates and HA become M_e^{+}-humate, a colloidal and molecular water soluble substance. Its surface activity is related to the colloidal part, although they are not surface active themselves, however, through peptisation, generate the surface active components.

Due to the presence of ionogenic (acids and their salts) as well as non-ionogenic (alcohol functional groups in HA) molecules, the Me^+-humate is surface active, whereas due to the presence of micelles it behaves as a colloid with properties such as coagulation, peptisation, ion exchange, and coagel formation (Tschapek et al., 1981). Since the sodium hydroxide solution is usually used for dissolving the commercial HA, the surface active Na^+-humate is therefore easily formed in the HA alkali solution, and thereafter interacts with TNPs.

In the surface modification experiment, the HA solution with a concentration lower than 10 mg/L DOC was applied. Flocs, which were easy to precipitate when they were large, dense and compact enough, formed with the increase of HA dosage, resulting in clear supernatants. Characterizations of zeta potential, PSD, FT-IR and HA-TNP adhesion show that the aggregation might be due to the electrostatic attraction, ligand exchange, hydrophobic and van der Waals interaction resulting from the addition of HA molecules and the existence of OH^-. An optimum dosage range of HA was determined to be 7.8~9.15 mg/L DOC.

3.2 TNP-HA adsorption-aggregation experiments with controlling pH

Results in Section 3.1 clearly show that the interaction between TNP and HA refers to the total depletion of the latter from the bulk suspension and the pH value of TNP-HA mixed suspension made great effect. Therefore, it is necessary to further study the TNP-HA interfacial process in view of both adsorption and aggregation (so-called adsorption-aggregation) at controlled pHs of HA stock solution and the fixed pH of TNP suspension.

Therefore, this part of work focuses on (i) adsorption isotherms being used to deeply investigate the adhesion of HA on the TNP surface, and (ii) particle size and fractal dimension

of aggregates formed during batch adsorption tests in order to understand properties of NP-collector aggregate which may give an indication of NP-involved interfacial processes.

3.2.1 Experimental procedure

A series of adsorption batch tests were carried out using 150 mL glass bottles with Teflon-lined screw caps to avoid the undesirable surfactant adsorption by container. 50 mL 0.3 wt.% TNP suspension (Lot #2) was mixed with 50 mL HA stock solutions of different concentrations ranging from 1 mg/L DOC to 25 mg/L DOC so as to give varying concentrations in the bottle. The suspensions were mixed by means of end-over-end rotation (Reax 20/8, Heidolph Instrument GmbH & Co. KG, Germany) at the constant rotating speed of 15 rpm. As indicated in former studies where the equilibrium could be reached within 18 hours under similar experimental conditions (Vermeer et al., 1998; Vermeer and Koopal, 1998), the mixtures were agitated for 18 hours at the room temperature of approximately 22 °C (295.15 K) to ensure that the equilibrium was achieved. Thereafter, 30 mL supernatant was carefully withdrawn and separated by centrifuging at 8000 rpm for 20 min. The final sample was analyzed by TOC analyzer for HA concentration. The amount of adsorbed HA (q_e, μg DOC/g TNPs) at equilibrium were obtained by the following equation:

$$q_e = \frac{(C_{0S} - C_e)V}{m} \tag{3.3}$$

where C_{0S} and C_e (mg/L DOC) are initial and equilibrium concentrations of HA, respectively. V (mL) is the volume of the TNP-HA mixed suspension, m (mg) is the weight of TNPs. All samples were collected and measured in the same way described above for the HA concentration after 72 hours of adsorption tests. The concentration kept constant and no desorption was found.

3.2.2 Adsorption isotherms

It has been extensively known that HA remains in solution at pH ≥ 2 and is composed of the higher molecular weight fraction of the humic matter (Vermeer and Koopal, 1998). The HA concentration remained constant at pH ≥ 4 in the current investigation as aforementioned in Chapter 2. Herein, the HA stock solution was pre-adjusted into pH4.0, 6.3, 9.1 and 12.9, individually, and then interacted with TNPs such that the pH influence of HA stock solution on adsorption-aggregation could be particularly studied. Experimental results were fitted by

classical adsorption isotherm equations Langmuir, Freundlich, Langmuri-Freundlich (L-F) and Temkin.

- The Langmuir model assumes monolayer adsorption onto a homogeneous surface with no interactions between the adsorbed molecules (Ho et al., 2002), and this classical isotherm equation is:

$$q_e = \frac{b_L Q_{\max L} C_e}{1 + b_L C_e} \tag{3.4}$$

where b_L represents the Langmuir bonding term related to interaction energies (L/mg) and $Q_{\max L}$ denotes the Langmuir maximum capacity (mg/g).

- The Freundlich model is valid for non-ideal sorption on a heterogeneous surface with interaction between adsorbed molecules where the distribution of sorption heat is non-uniform. It assumes that the adsorption is more difficult as more and more binding sites are occupied by adsorbates and multilayer adsorption can occur (Jiang et al., 2013). The Freundlich equation can be expressed as follows:

$$q_e = K_f C_e^{n_F} \tag{3.5}$$

where K_f represents the Freundlich affinity coefficient ($mg^{(1-n)}L^n/g$), indicating the adsorption capacity of the adsorbent, and n_F is the Freundlich linearity constant related to sorption intensity or surface heterogeneity. For n_F > 1 the adsorption is considered to be poor; for n_F between a value of 0.5 and 1, adsorption is defined as moderately difficult; with n_F values between 0.1 and 0.5, it shows favorable adsorption.

- The L-F model is an empirical equation often used to describe chemisorption onto heterogeneous surface.

$$q_e = \frac{b_{L-F} Q_{\max L-F} C_e^{n_{L-F}}}{1 + b_{L-F} C_e^{n_{L-F}}} \tag{3.6}$$

where $Q_{\max L-F}$ is the total amount of binding sites on the adsorbent surface, b_{L-F} is related to the mean association constant K_0 ($K_0 = b_{L-F}^{1/n_{L-F}}$), and n_{L-F} represents the heterogeneity index of the binding site energy; as the value of n_{L-F} approaches to 1, the adsorbent is homogeneous and the L-F equation is reduced to Langmuir isotherm. For a heterogeneous material, n_{L-F} <1. When either n_{L-F} or b_{L-F} is 0, the L-F equation can reduced to Freundlih.

Thereby, the L-F isotherm is able to model both of homogeneous and heterogeneous adsorption systems (Jiang et al., 2013).

- The Temkin isotherm assumes that the heat of adsorption of all the molecules in the layer decreases linearly with coverage due to adsorbent-adsorbate interactions, and that the adsorption is characterized by a uniform distribution of the binding energies, up to some maximum binding energy (Ho et al., 2002). The Temkin isotherm equation is applied in the following form:

$$q_e = B\ln\left(K_T \cdot C_e\right) \tag{3.7}$$

where K_T is the equilibrium binding constant; B is related to the heat of adsorption, and can be calculated from $B = RT/b$; T is the absolute temperature in Kelvin; b is the Temkin constant (J/mol).

Based on the regression coefficient (R^2), only Freundlich and L-F models exhibited good fits with R^2 situating within the range of 0.940~0.999, and specific modeling outcomes are shown in Fig. 3.8 and Table 3.1. The low regression coefficient R^2 obtained from the Langmuir fitting suggested that the model was too simple to describe the adsorption of HA on TNPs, and thus it could be inferred that both aggregation and sorption probably involved in the interplay between TNPs and HA (Abraham et al., 2013). The Freundlich isotherm equation constant n_F can be used to explore the favorability of adsorption process, and the favorable adsorption happens when the n_F value falls in 0~1. However, all n_F vales were higher than 1 in the present study, showing the difficult and poor adsorption but probably indicating other aggregation interaction process, rather than adsorption, played the dominant role of TNP-HA interaction. It could be inferred that the aggregation process of TNP-HA was led by agglomeration of TNPs with precipitated HA particles. The following DAF experimental results of TNP separation with the HA assistance will further study whether both HA and TNPs will be well removed by flotation. The good agreement between fitting results and experimental data indicated that the heterogeneous interaction between HA molecules and the TNP surface. As for the L-F model, the parameter $Q_{\max L-F}$ could predict the total amount of binding sites on the adsorbent surface. As shown in Table 3.1, the binding sites on the TNP surface decreased along with the pH value of HA solution increasing. HA adsorption data were not modeled well across the HA concentration range and pH values of HA stock solution by Temkin isotherm.

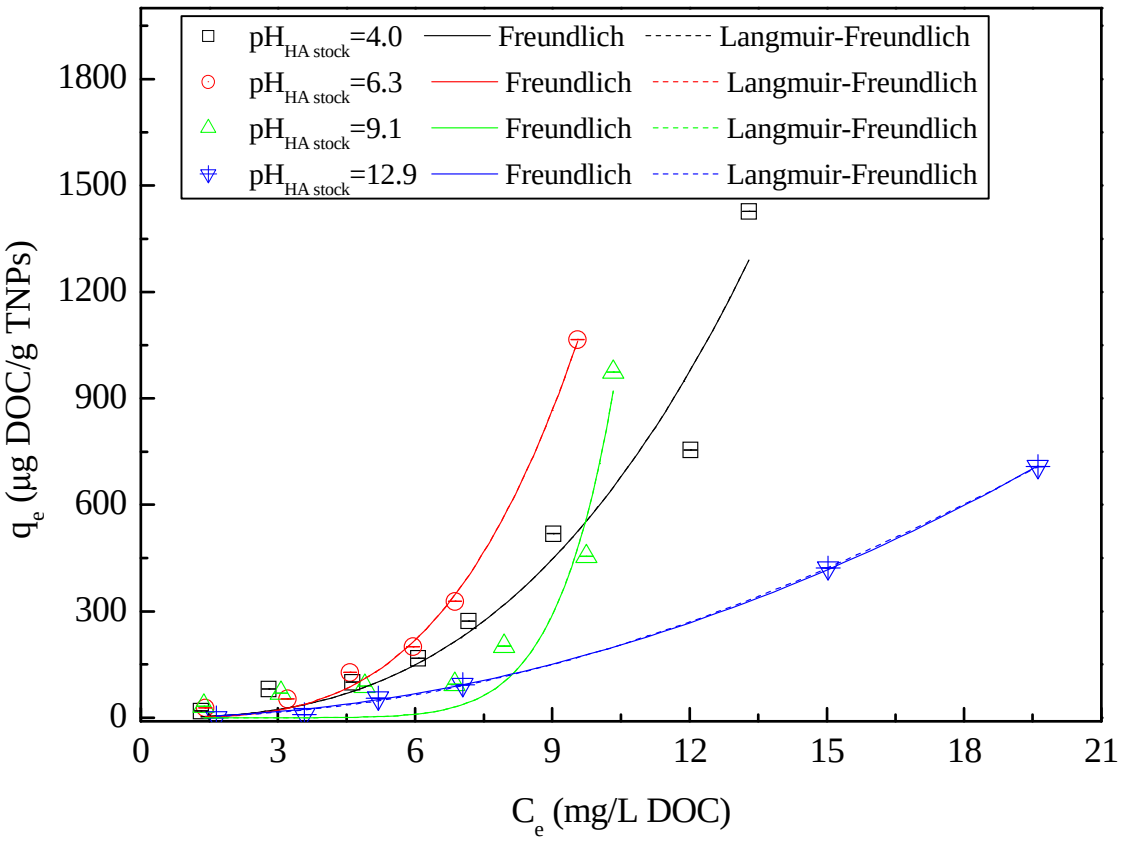

Fig. 3.8. Experimental data and fitting curves of Freundlich and L-F adsorption results of 0.15 wt.% TNP+HA.

Table 3.1. Fitting results from Langmuir, Freundlich, and L-F models.

	Langmuir model			Freundlich model			Langmuir-Freundlich model				Temkin model			
	$Q_{\max L}$ (μg/g)	b_L	R^2	K_f	n_F	R^2	$Q_{\max L-F}$ (μg/g)	b_{L-F}	n_{L-F}	R^2	B	K_T	b (J/mol)	R^2
$pH_{HA\ stock}$=4.0	1.54E+08	4.52E-07	0.716	1.1	2.715	0.950	6.72E+07	1.70E-08	2.716	0.950	470.49	0.428	5.27	0.587
$pH_{HA\ stock}$=6.3	3.16E+08	2.20E-07	0.607	0.5	3.398	0.995	2.38E+08	2.09E-09	3.398	0.995	418.32	0.458	5.93	0.525
$pH_{HA\ stock}$=9.1	1.07E+10	4.68E-09	0.506	2.7E-06	8.409	0.940	1.91E+09	1.44E-15	8.408	0.940	301.22	0.470	8.23	0.413
$pH_{HA\ stock}$=12.9	1.02E+08	2.96E-07	0.876	1.9	1.989	0.999	6.43E+03	2.30E-04	2.110	0.999	276.38	0.343	8.97	0.773

3.2.3 Properties of HA-TNP aggregates obtained from adsorption-aggregation

3.2.3.1 Zeta potential and pH value

The electrophoretic mobility data for TNPs in the presence of HA is presented in Fig. 3.9. It can be seen that the addition of HA with pH values of around 4.0, 6.3 and 9.1 led to little change in the absolute magnitude of pH and zeta potential as a function of increasing HA initial concentration. The pH of suspensions kept constant significantly lower than 3 and thus the ionization of HA molecules was weak, giving rise to the fact that the electrostatic attraction with the positively surface charged TNPs was far from being enhanced. This indicated no evidence for any charge neutralization of the TNP surface for these cases. However, on addition of highly basic HA solution (pH=12.9), the zeta potential of TNPs was then considerably altered synchronously with pH value of suspension especially at HA equilibrium concentrations higher than about 7 mg/L DOC. The zeta potential of TNPs became zero when the equilibrium concentration was around 10.8 mg/L DOC and the pH value of suspension turned to be about 6.7. Thereafter, the surface charge reversed to negative and the absolute value increased along with the HA equilibrium concentration.

HA adsorption by nano-oxides depended on three factors (Yang et al., 2009): (1) large surface area of nano-oxides, which provides space for HA adsorption; (2) low hydrophilicity and few negative charges on nano-oxide surface, allowing HA molecules to approach to the particle surface; and (3) strong interactions, such as electrostatic attraction and ligand exchange between HA and nano-oxide surfaces, which induced the HA adsorption. As studied by Vermeer et al. (1998), on increasing the pH value of mixture suspension, both the hydrodynamic layer thickness of adsorbed HA and the adsorbed amount decreased but the reducing magnitude of the former was less than that of the latter. That is the case of $pH_{HA\ stock}$=12.9 in Fig. 3.9 when the pH of adsorption-aggregation suspension rose along with the addition of HA solution.

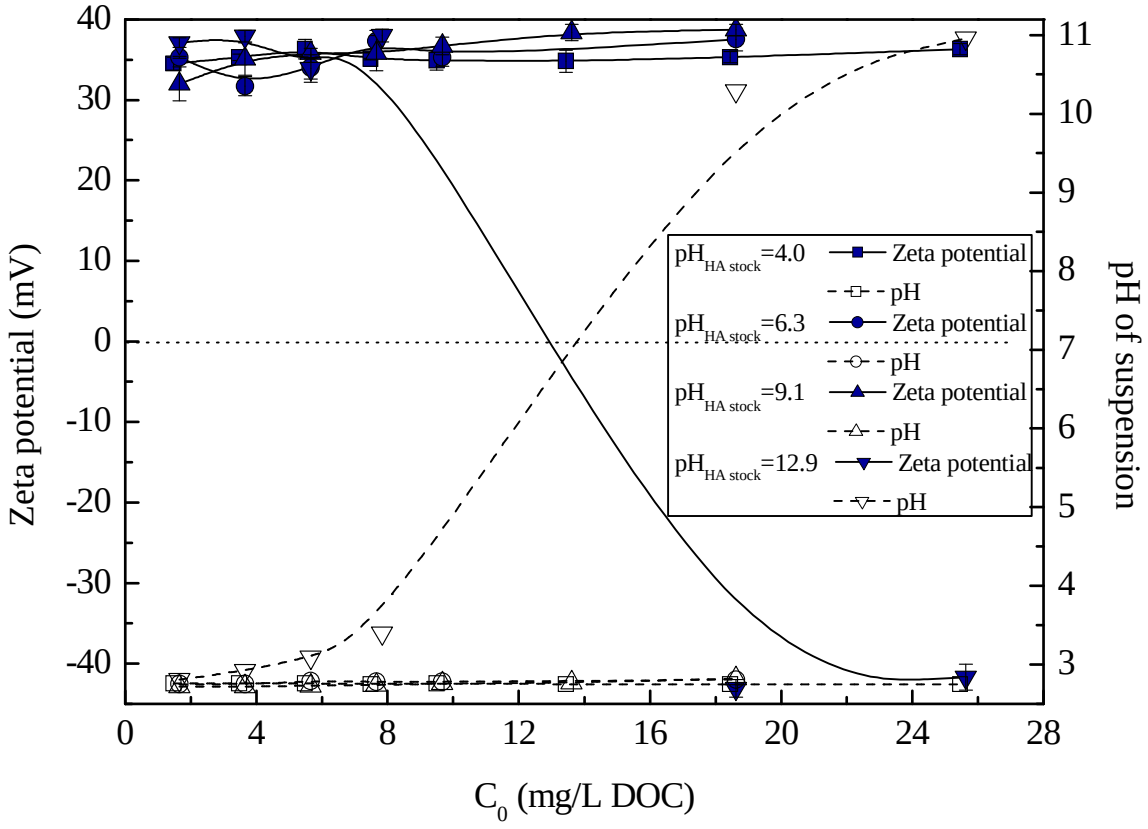

Fig. 3.9. Zeta potential and pH value of post-(adsorption-aggregation) suspension as a function of initial HA concentration.

3.2.3.2 Aggregate size

Particle size of aggregates (in the sediment) formed by adsorption-aggregation was measured by DLS (Nanotrac) or LDS (Mastersizer 2000) according the magnitude of their particle size. Average particle size and PSD attained are shown in Fig. 3.10(a). For different pH values of HA solutions, the increasing HA addition could result in larger aggregates, and particularly, the high basic HA solution (pH_{HA}=12.9) lead to micron aggregates at HA concentrations of 9 and 13 mg/L DOC but the aggregates turned to be in nanoscale at higher HA dosage due to the re-stabilization of TNPs. With the stock HA solution at pH 4.0, 6.3 and 9.1, the equilibrium pH values of TNP-HA suspension was lower than 3 (Fig. 3.9) and the size of the sediment fraction was always smaller than 1 μm (Fig. 3.10(a)), which might correspond to the presence of colloidal precipitates of HA molecules and as well as their adhesion with TNPs; comparatively, TNP-HA aggregates in the presence of HA stock solution at pH12.9 were formed through the electrostatic interaction. At lowest HA concentration of 1 mg/L DOC, the PSD exhibited monomodal; as the HA concentrations rose, multimodal could be obtained (Fig. 3.10(b)~(e)).

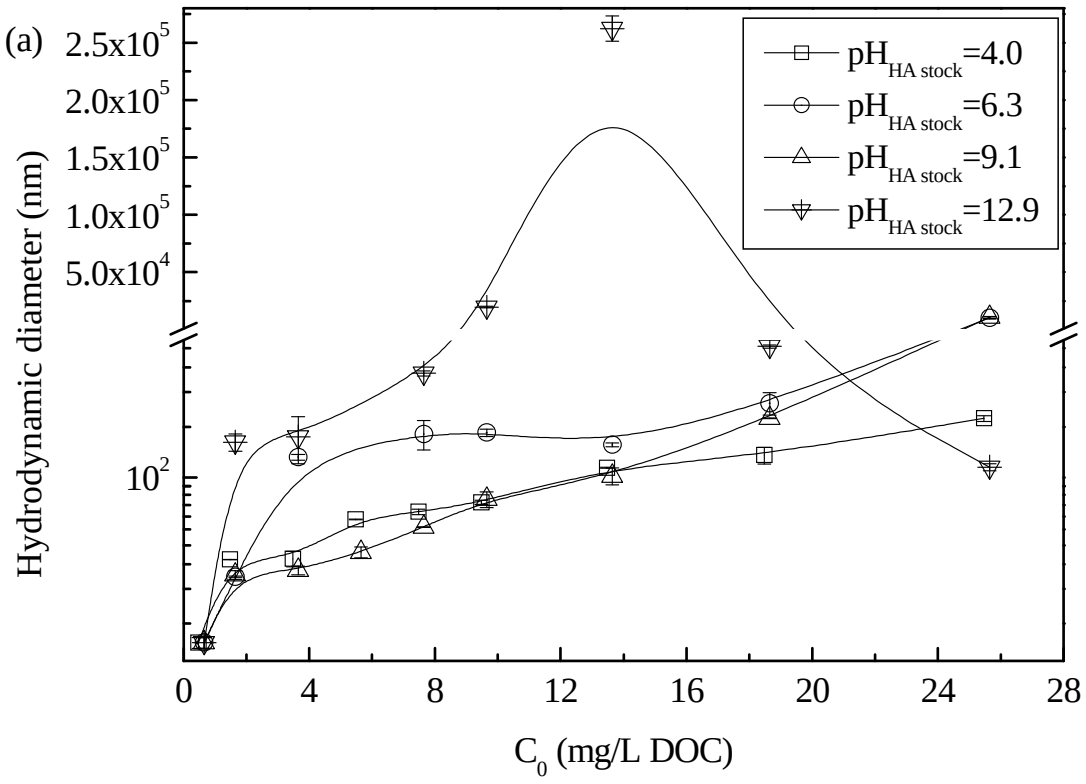
(a)
Hydrodynamic diameter (nm)
2.5x10^5
2.0x10^5
1.5x10^5
1.0x10^5
5.0x10^4
10^2
0
4
8
12
16
20
24
28
C0 (mg/L DOC)
pHHA stock=4.0
pHHA stock=6.3
pHHA stock=9.1
pHHA stock=12.9

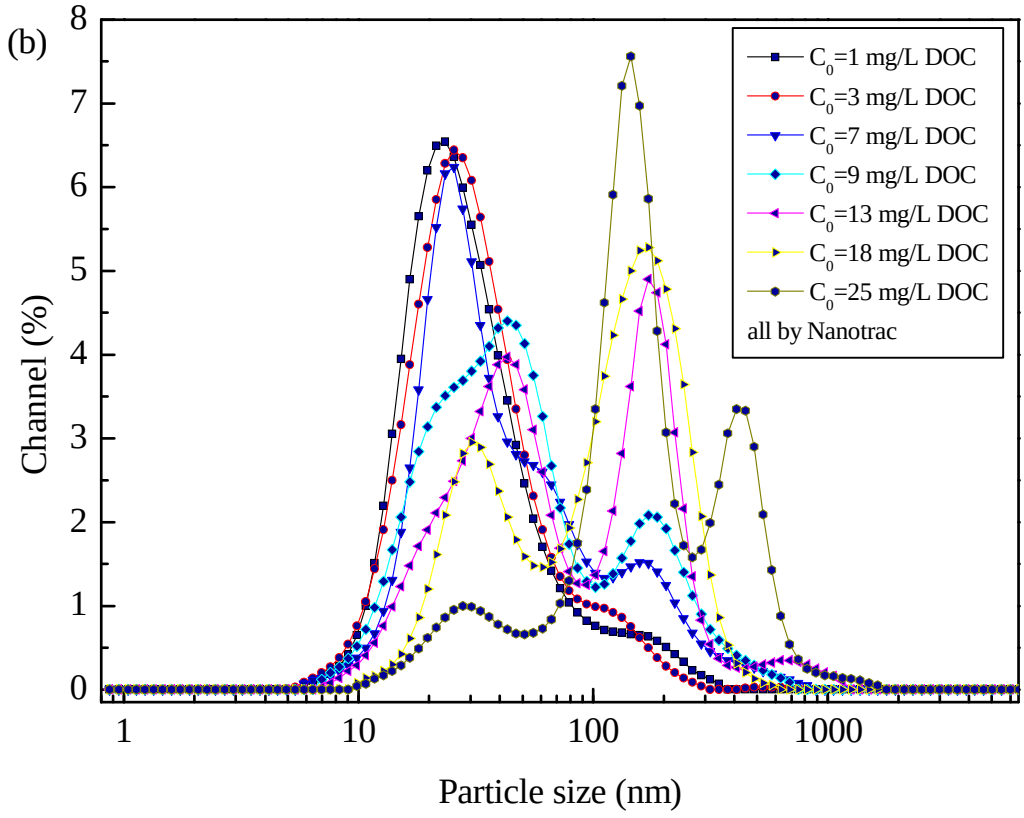
(b)
Channel (%)
0
1
2
3
4
5
6
7
8
1
10
100
1000
Particle size (nm)
C0=1 mg/L DOC
C0=3 mg/L DOC
C0=7 mg/L DOC
C0=9 mg/L DOC
C0=13 mg/L DOC
C0=18 mg/L DOC
C0=25 mg/L DOC
all by Nanotrac

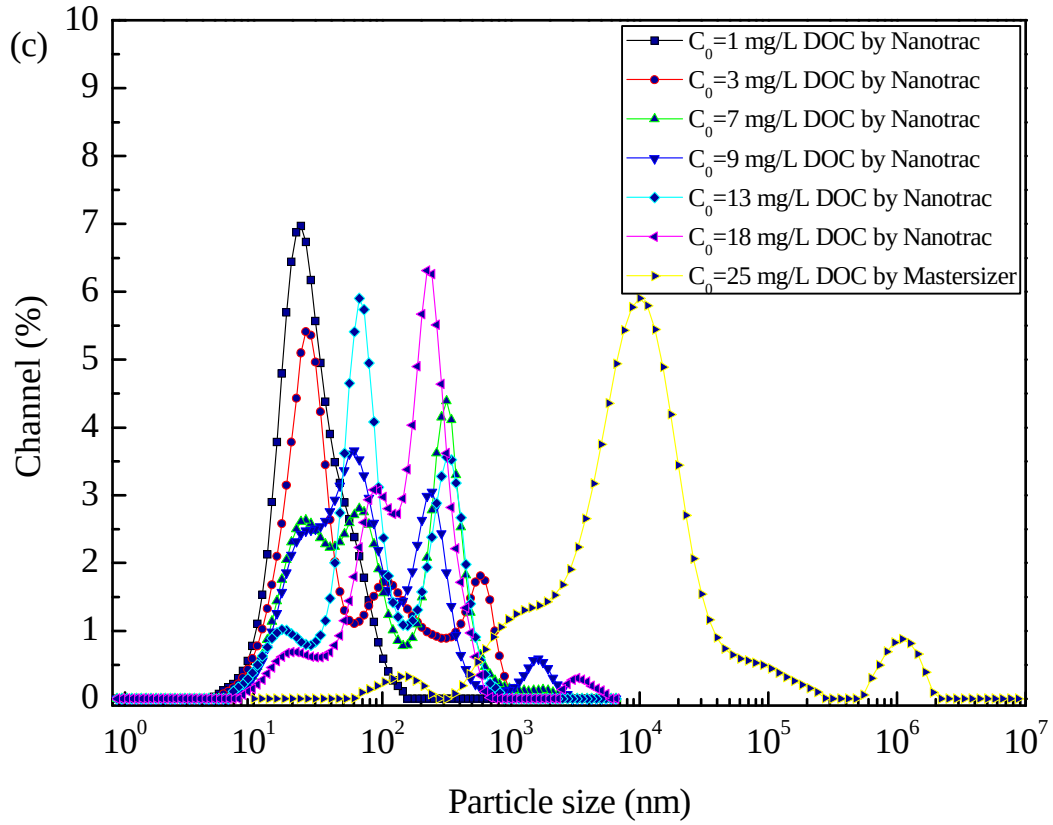
(c)
Channel (%)
Particle size (nm)
C0=1 mg/L DOC by Nanotrac
C0=3 mg/L DOC by Nanotrac
C0=7 mg/L DOC by Nanotrac
C0=9 mg/L DOC by Nanotrac
C0=13 mg/L DOC by Nanotrac
C0=18 mg/L DOC by Nanotrac
C0=25 mg/L DOC by Mastersizer

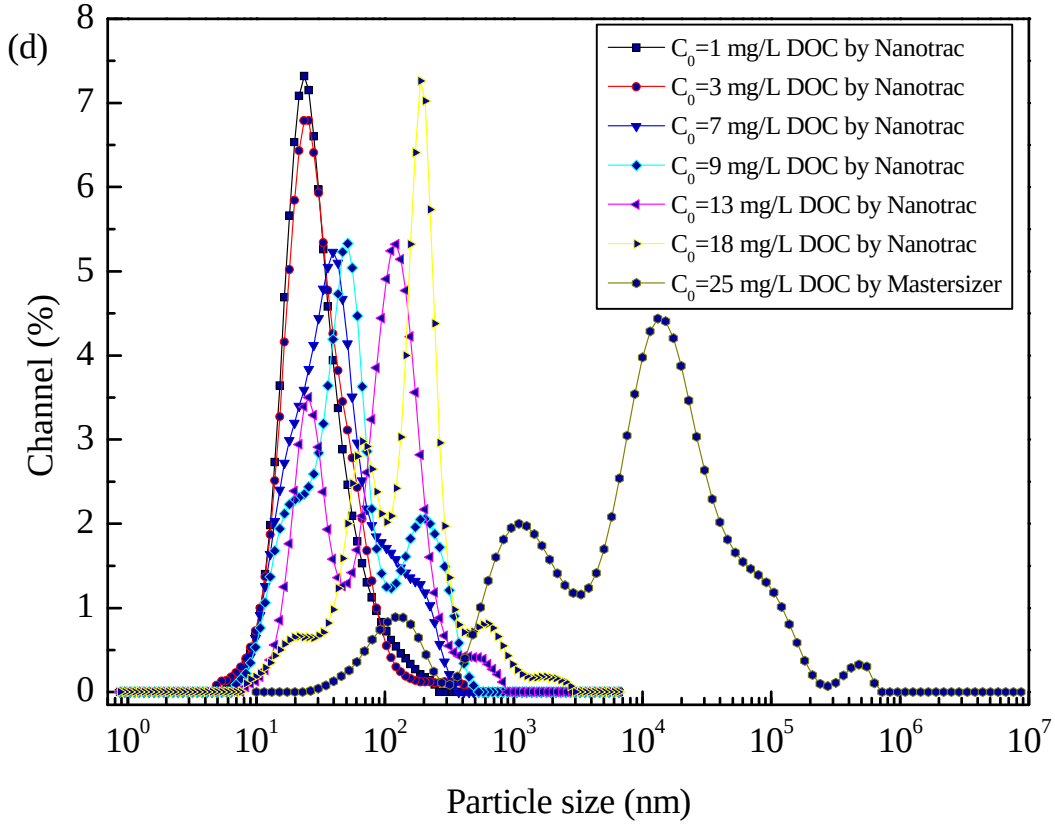
(d)
Channel (%)
Particle size (nm)
C0=1 mg/L DOC by Nanotrac
C0=3 mg/L DOC by Nanotrac
C0=7 mg/L DOC by Nanotrac
C0=9 mg/L DOC by Nanotrac
C0=13 mg/L DOC by Nanotrac
C0=18 mg/L DOC by Nanotrac
C0=25 mg/L DOC by Mastersizer

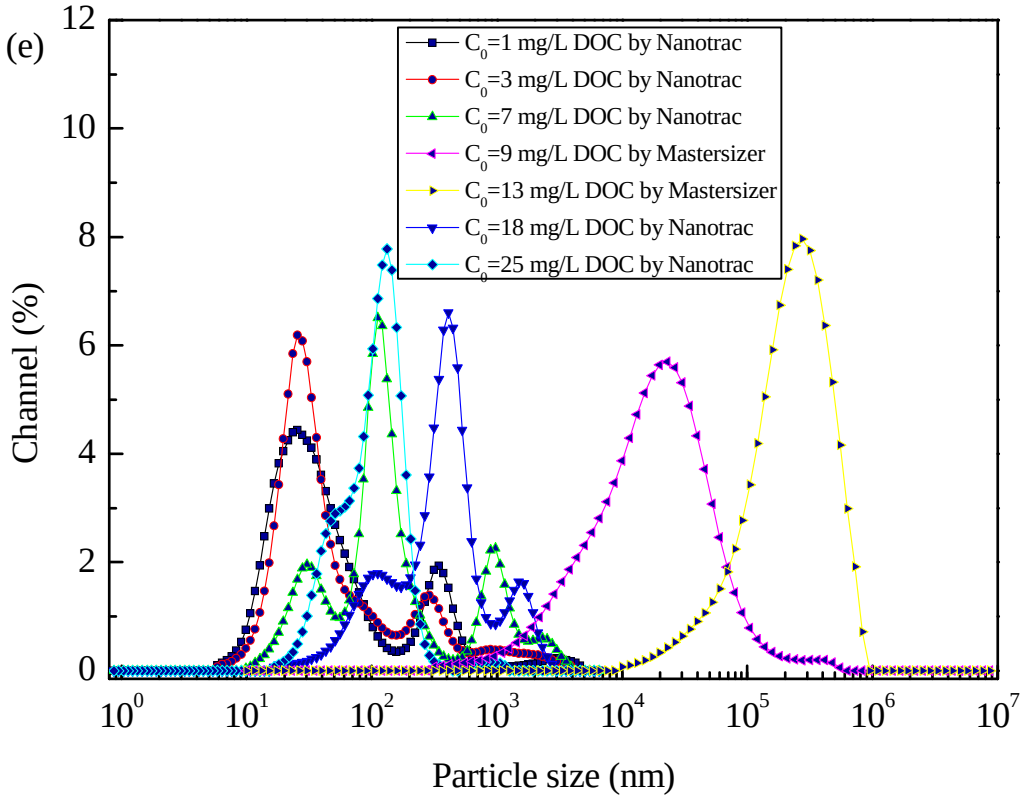

Fig. 3.10. Particle size measurement of TNP-HA aggregates after adsorption-aggregation: (a) variation of particle size with initial HA concentration; PSD patterns at different pH values of HA stock solution (b) pH_{HA}=4.0, (c) pH_{HA}=6.3, (d) pH_{HA}=9.1, (e) pH_{HA}=12.9.

3.2.3.3 Fractal structure

The morphological structure of aggregates could be achieved by SALLS via Mastersizer 2000, and herein, for the four different pH values of HA solution, the fractal structure of four TNP-HA aggregates were measured: TNPs formed at pH_{HA}=6.3 (C_0=25 mg/L DOC), pH_{HA}=9.1 (C_0=25 mg/L DOC), and pH_{HA}=12.9 (C_0=9 mg/L DOC and 13 mg/L DOC). It can be seen from Fig. 3.11 that for the weakly acidic and basic HA solution, the D_f of TNP-HA aggregate were lower than 2, presenting an open and loose structure; when the pH of HA solution reached as high as 12.9, compact and dense TNP-HA aggregates formed with D_f higher than 2 and even close to 3 (C_0=13 mg/L DOC). On the one hand, based on the analysis in Section 3.2.3.1: TNP-HA aggregates at the equilibrium pH lower than 3 (using the HA stock solutions at pH 6.3 and 9.1, according to Fig. 3.9) were formed probably by the adhesion between HA colloidal precipitates and TNPs, whereas those TNP-HA flocs at the equilibrium pH higher than 5 (using the HA stock solution at pH12.9, according to Fig. 3.9) was attained via the charge neutralization; the latter floc gave rise to the firmer aggregate configuration than the former which could be attributed to the stronger TNP-HA combination

through the electrostatic attraction. On the other hand, at a given pH value, the HA molecules might be flattened on the TNP surface after adsorption. The adsorbed HA layer thickness was largely determined by "tails" of the adsorbed HA molecules protruding into the solution. The degree of flattening increases with increasing pH. Some parts of HA molecules protruded relatively far into the solution (Vermeer et al., 1998) resulting in the formation of large aggregates. At high pH a significant part of the adsorbed molecule is in close contact with the surface (Vermeer et al., 1998). As a consequence, the TNP-HA flocs at high pH of 12.9 were of more compact morphology.

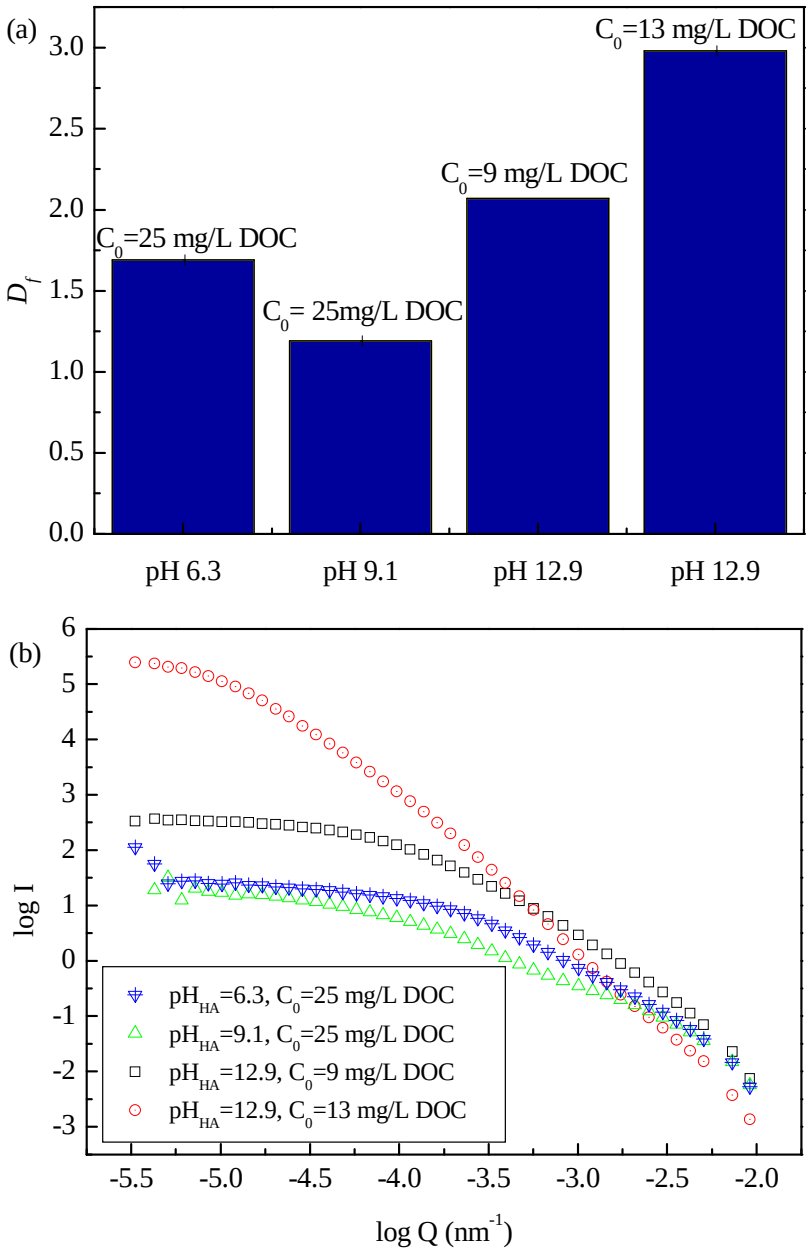

Fig. 3.11. Fractal dimension of TNP-HA aggregates at different pH of HA stock solution: (a) D_f variation; (b) log I as a function of log Q.

Given the adsorption-aggregation analysis of this section and the HA sol obtained in Chapter 2, there could be three types of aggregates formed in the adsorption-aggregation: (i) TNP-HA flocs resulted from agglomeration of TNPs with precipitated HA particles by interacting with small HA molecules or large HA sols, (ii) TNP-TNP flocs, and (iii) HA sols/colloids, all of which had the potential of being separated by flotation. Their flotation performance is about to be tested in the following section.

3.3 Laboratory scale continuous DAF experiments

3.3.1 Experimental device, methods and procedure

3.3.1.1 Description of laboratory scale continuous DAF apparatus

Experiments were carried out in a continuous flotation device designed in our lab (Liu, 2010), shown in Fig. 3.12. Before each experiment, the flotation device is totally cleaned with de-ionized water. The TNP suspension is prepared in the feed tank (b in Fig. 3.12) with continuous agitation in order to well disperse TNPs. When the DAF test starts, the TNP suspension is pumped into the flotation cell and meanwhile the pressurized water is injected into the cell from saturation tank (c in Fig. 3.12) to create bubbles. The flotation cell (a in Fig. 3.12) is divided into two zones, one for the NP suspension being mixed with the tiny bubbles and the other for the disengagement of bubbles. The flotation cell has glass windows in order to visually follow the flotation process and the separation of bubbles from the clean water exit, and to perform the in-situ bubble size measurement. Bubbles capture particle in the first zone. When bubbles come to the surface, they may create foam. The foam moves from first zone to the second and can be recovered by draining-off. For HA involved flotation experiments, the HA stock solution was injected at the bottom of the first zone by peristaltic pump. After the first zone of the flotation cell is full, the peristaltic pump controlling the flow rate of clarified water after flotation is switched on. Clear water is recovered at the bottom of the second cell (d in Fig. 3.12). The liquid flow rates of TNP wastewater Q_1, pressurized water Q_2, effluent (the clarified water) Q_3 and additive solution Q_a (NaOH or HA) are controlled for different operating conditions by the same type of peristaltic pump (Masterflex L/S, with pump head, HV-7518-00, Cole-Parmer Instrument Company, USA), individually.

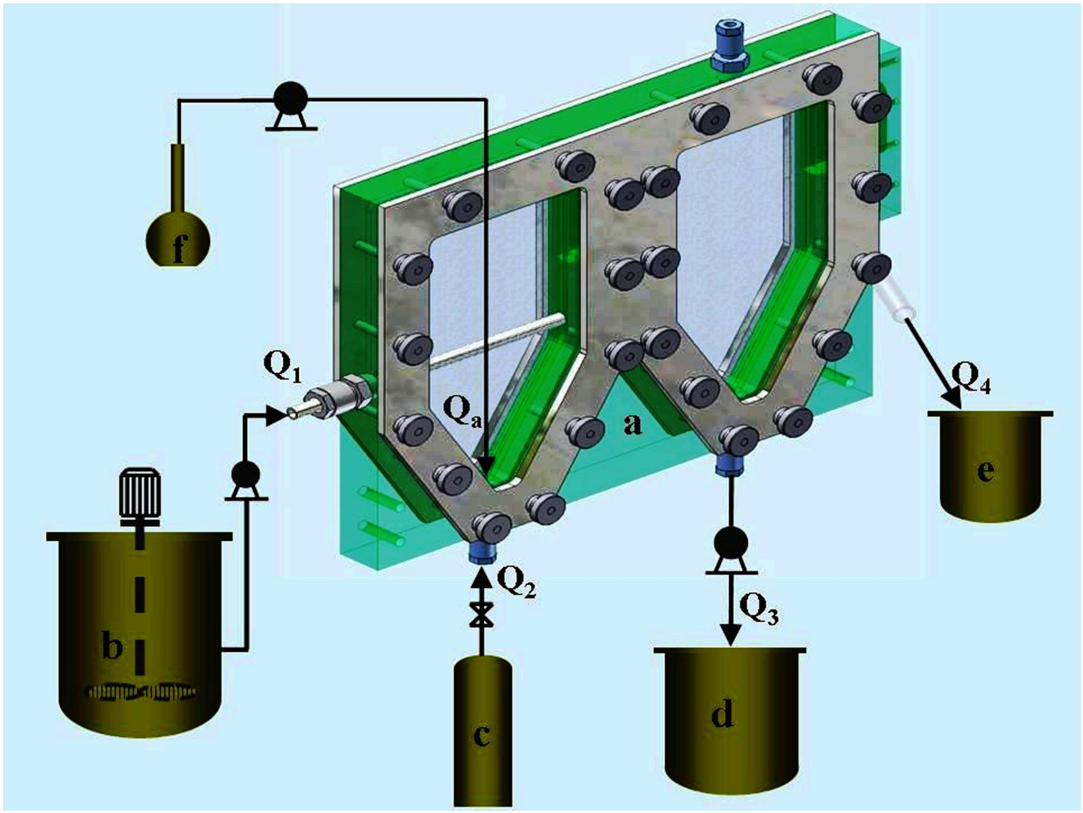

Fig. 3.12. Schematic representation of the laboratory scale continuous DAF device: (a) Flotation cell (200×105×18 mm^3), (b). Feed tank (40 L), (c) Saturation tank with pressurized water (20 L, the maximum tolerated pressure is 7 bars), (d) Tank for clean water (20 L), (e) Tank for foam (5 L), (f) Flask for the additive solution (500 mL).

3.3.1.2 Bubble production

Air is dissolved into the deionized water inside the saturation tank (c in Fig. 3.12) by adding air under pressure. To ensure small bubbles, pressure differences of 400 to 600 kPa are recommended (Edzwald, 1995). Herein, a relative pressure of 6 bars was set for all DAF experiments in this study. Then, the pressurized water flow is injected through the valve at the bottom entrance to the contact zone and microbubbles are produced. The small bubbles give the water a milky appearance, and so the term white water is used to describe the bubble suspension in the DAF tank (Edzwald, 2010). The measurement by Laser Diffraction Sizing (Malvern Spraytec) denotes that bubbles produced in the saturator have an average diameter d_b of about 70 µm (Liu, 2010). The zeta potential of air bubbles was not characterized in this work but it has been measured to be negative between pH 2.0 and 12.0 in the DAF study of Kubota et al. (1983), Li and Somasundaran (1992), Han and Dockko (1998), Han et al. (2004) and Oliveira and Rubio (2011).

3.3.1.3 Capacity of the DAF system

The capacity of the DAF system in this study was estimated in the same way as Liu et al. did (2012): the maximum relative velocity between water and a bubble U_b was determined to be 14.4 m/h ($\mathrm{Re} = U_b d_b / \nu_L = 0.28$) by solving the force balance on the bubble (70 μm in diameter) among the buoyancy, gravity and the drag force in the Stokes regime; then, the theoretical maximum effluent flow rate Q_3 of 453.6 mL/min could be obtained by multiplying the velocity U_b with the cross-section area of the flotation cell. In the DAF study of Liu et al. (2012), the real maximum Q_3 was also investigated by testing the maximum experimental flow rate under which no bubble was trapped in the exit flow. The maximum experimental Q_3 was found to be 440 mL/min, very close to the theoretical value showing that the hydrodynamic effectiveness of this continuous DAF cell is quite good for a so small system.

Liquid flow rates in the DAF process satisfy Eq. 3.8:

$$Q_1 + Q_2 + Q_a = Q_3 + Q_4 \tag{3.8}$$

where Q_4 represents the float-liquid flow rate whose minimum value can be figured out when Q_1, Q_2 and Q_a are fixed, and the maximum Q_3 is already known.

3.3.1.4 Determination of hydraulic retention time (HRT)

Preliminary flotation tests were carried out to explore the variation of water quality along with flotation time and determine the HRT of DAF in this investigation. DAF experiments were conducted as described in Section 3.3.1.1, and tracing particles subjected to flotation was a mean to identify the steady state, whereas tracing inert substances (ions) was used to determine the HRT. Thereby, turbidity and conductivity of clarified water were measured at different time intervals. These two parameters were chosen as representatives of treated water properties because of their instant availability in the working scene. Results in Fig. 3.13 showed that the effluent could reach a steady state after 4.5 min. Accordingly, samples of clarified water were taken 5 min after DAF started so as to evaluate the flotation performance.

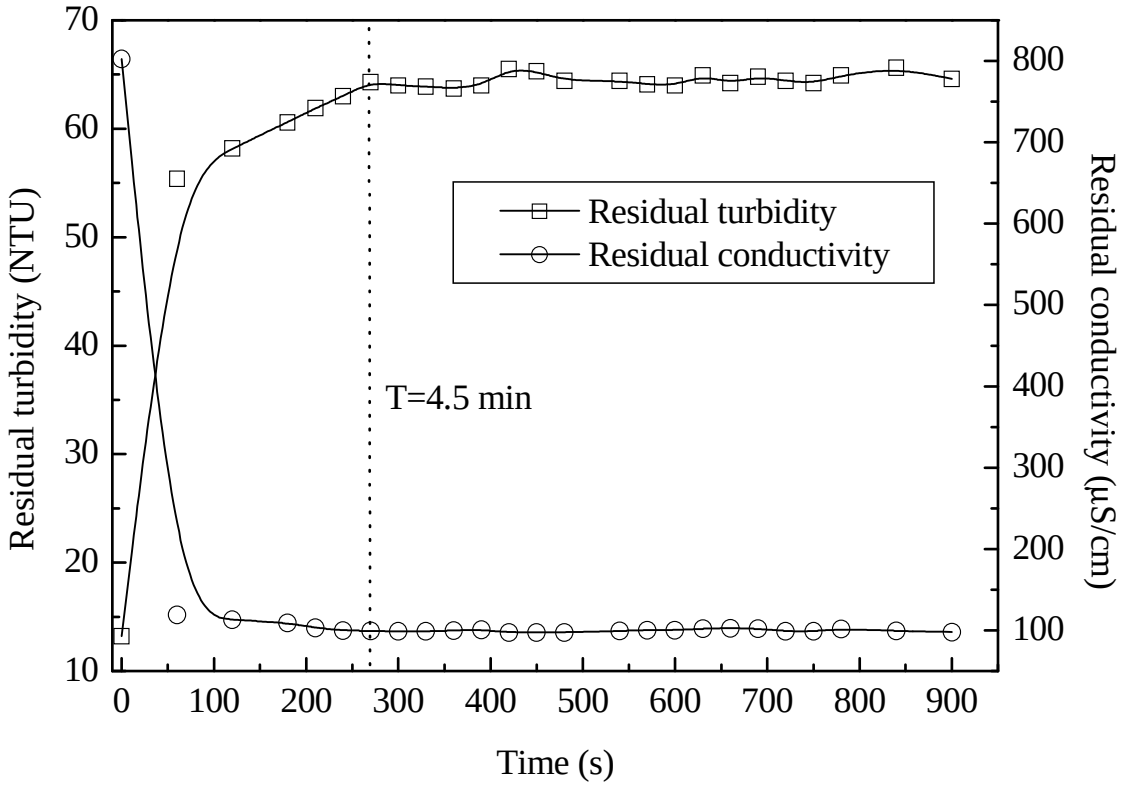

Fig. 3.13. Residual turbidity and residual conductivity varying with the flotation time.

3.3.1.5 Evaluation of DAF performance

The Ti content in the effluent and influent was analyzed by ICP-AES or ICP-MS for the TNP removal efficiency η; zeta potential, pH and residual DOC concentration were also measured to characterize the water quality before and after DAF.

(a) *TNP removal efficiency* η

This parameter was figured out in the same way as Liu et al. (2012) and Zhang and Guiraud (2013), in which the dilution effect caused by pressurized water was excluded:

$$\eta = \left(\frac{C_D \times Q_3 - C_3 \times Q_3}{C_D \times Q_3} \right) \times 100\% = \left[1 - \frac{C_3 \times (Q_1 + Q_2 + Q_a)}{C_0 \times Q_1} \right] \times 100\% \quad (3.9)$$

where C_0 and C_3 are TNP concentrations of the influent and effluent, respectively. C_D is considered to be the TNP concentration absolutely resulted from the dilution of the pressurized water, and can be calculated as follows:

$$C_D = \frac{C_0 \times Q_1}{Q_1 + Q_2 + Q_a} \quad (3.10)$$

(b) *HA removal* η'

HA is expected to facilitate the TNP removal process by forming TNP-HA-bubble aggregates, and thereby the residual HA in the DAF effluent should be as little as possible.

Besides, considering that HA may complex with metal ions, leading to unexpected metal transport and release in waters and soils (Zouboulis et al., 2003; Brum and Oliveira, 2007), the excess HA-release along with wastewater can be problematic. In this study, η' is used to estimate the amount of HA removed from the stock solution by flotation.

$$\eta' = \left(\frac{C_D^{'} \times Q_3 - C_3^{'} \times Q_3}{C_D^{'} \times Q_3} \right) \times 100\% = \left[1 - \frac{C_3^{'} \times (Q_1 + Q_2 + Q_a)}{C_{HAstock} \times Q_a} \right] \times 100\% \quad (3.11)$$

where $C_{HAstock}$ and $C_3^{'}$ are HA concentrations of the HA stock solution and the DAF effluent, respectively. $C_D^{'}$ is the HA concentration caused by the dilution effect:

$$C_D^{'} = \frac{C_{HAstock} \times Q_a}{Q_1 + Q_2 + Q_a} \quad (3.12)$$

3.3.2 Tentative theoretical determination of operating conditions

The performance of DAF unit mainly depends on the ratio of the amount of gas to the amount of suspended solids applied to the unit (Wang et al., 2005). Injection of the pressurized water stream into the flotation cell causes air bubbles to be released. The bubble flow rate Q_b affects particle-bubble collisions, particle separation and removal, and thus is an important design and operating parameter (Edzwald, 1995; Edzwald, 2010). In this study, the mass ratio of air to solids (Air-to-Solids ratio, A/S) can be expressed as:

$$A/S = \frac{m_{air}}{m_{TNP}} = \frac{\rho_{air} \times V_{air}}{\rho_{TNP} \times V_{TNP}} = \frac{\rho_{air} \times Q_b}{\rho_{TNP} \times Q_1 \times C_{0V}} \quad (3.13)$$

where ρ_{air} =1.21 kg·m^{-3}, ρ_{TNP} =4.2 g·cm^{-3} (20 °C, 1 atm); the flow rate Q_1 and the volume concentration C_{0V} of the simulated TNP wastewater have been predetermined to be 70 mL/min and 0.04 % (being converted from the weight percentage 0.15 %, assuming that the volume change of the mixed suspension can be negligible), respectively. A theoretical A/S value, under which condition all TNPs could be effectively captured by bubbles, is decided by Q_b.

A crude hypothesis is used here, assuming that the fully efficient collision and attachment of NPs on the bubble surface occurs and leads to the bubble surface completely covered by one single layer of NPs. Accordingly, the bubble flow rate Q_b has to provide a sufficient area of air-liquid interface to capture all the particles.

The NP number per unit time can be calculated by Eq. 3.14,

$$N_p = \frac{Q_1 \times C_{0V}}{\frac{\pi (d_p)^3}{6}} \tag{3.14}$$

where C_{0V} =0.04 % and d_p =41.6 nm (TNP Lot #1) or 14.5 nm (TNP Lot #2) as aforementioned in Chapter 2.

The bubble number per unit time can be evaluated by Eq. 3.15:

$$N_b = \frac{N_p}{N_{p/b}} \tag{3.15}$$

if the number of particles captured by one rising bubble $N_{p/b}$ is known. Since the maximum number of NPs captured by one bubble still remains to be studied, here we only try to roughly assess this number by assuming that each bubble is covered with a NP monolayer. $N_{p/b}$ can then be calculated by Eq. 3.16:

$$N_{p/b} = \frac{\phi \times S_b}{S_p'} \tag{3.16}$$

where $S_p' = \frac{\pi (d_p)^2}{4}$ is the projected area of NPs and $S_b = \pi (d_b)^2$ is the surface area of one bubble. ϕ stands for the effect of the highly packed arrangement of the attached particles at the bubble surface, and has been experimentally determined in the study of micro-particles in flotation by Huang et al., and it could reach 80 % (Huang et al., 2011). This value is kept and applied in our case.

Q_b (mL/min) can be then calculated as follows:

$$Q_b = N_b \times \frac{\pi (d_b)^3}{6} \tag{3.17}$$

The pressurized water flow rate Q_2 (mL/min) is calculated from the bubble flow rate Q_b by Henry's Law which states that the solubility of a gas in a liquid is directly proportional to the partial pressure of the gas above the liquid at a constant temperature:

$$Q_b = K_h \times p \times Q_2 \tag{3.18}$$

where K_h is the Henry constant (18 mL·L^{-1}·atm^{-1}, 20 °C) (Blazy and Jdid, 2000); p is the relative pressure between the applied pressure and the atmospheric pressure for dissolving air (6 bars in this study).

3.3.3 Preliminary DAF tests (using Lot #1)

Results of surface modification and adsorption-aggregation experiments have shown that TNPs interact with HA by forming aggregates, and TNPs are not easy to re-stabilize in the entire HA dosage studied. To validate that this surface interaction can help to improve the efficiency of removing TNPs in DAF process, the DAF test was carried out to quantify the effect of different HA concentrations on the floatability of TNPs. Considering the optimum HA dosage range obtained from surface modification experiments, four HA concentrations (4.5, 6.5, 8.5 and 10.5 mg/L DOC) were chosen to investigate the DAF process with the HA assistance.

Q_1 was pre-determined to be 70 mL/min, and based on the tentative theoretical calculation in Section 3.3.2, flow rates of DAF experiments were figured out as follows: Q_2 was 166.7 or 250 mL/min, and Q_3 was 100 or 200 mL/min, and Q_{HA} varied according to investigating HA concentrations. The initial TNP concentration C_0 was fixed to be 0.15 wt.% (equally 1406.7 mg/L TNP by ICP-AES). Table 3.2 and Fig. 3.14 present the TNP removal of DAF tests by ICP-AES. In Table 3.2, positive values of TNP removal efficiency η demonstrate that DAF could effectively eliminate TNPs in the suspension, a higher value of η representing a higher DAF efficiency, while the sign "-" denotes ineffective DAF treatment.

It can be found that, without the HA addition, DAF was poorly effective in the investigating Q_2 and Q_3 ranges. For low pressurized water flow rate Q_2 =166.7 mL/min, higher HA dosages (≥ 7.9 mg/L DOC) could better improve the TNP removal, and the maximum removal efficiency of 91.4 % was achieved when C_{HA}=9.3 mg/L DOC. For high pressurized water flow rate Q_2 =250 mL/min, the DAF failed to have any treating effect when HA concentration was lower than 6.3 mg/L DOC; but for the HA concentration of 7.9 mg/L DOC, better TNPs removal efficiency of higher than 70 % were obtained. Table 3.2 and Fig. 3.14 denotes that high efficiencies of 91.4 % and 86.4 % were obtained at points of HA dosages 7.9 and 9.3 mg/L DOC, whereas their pressurized water flow rates and effluent flow rates

were quite different, indicating that the effect of HA outweighed that of bubble flow rate (Q_b, and thus also Q_2) and also effluent flow velocity (Q_3).Therefore, higher TNP removal efficiencies could be obtained by applying higher dosages of HA (increasing Q_{HA}). From the respect of higher TNP removal and lower dilution effect, the optimum operational condition for TNPs removal by DAF process in this study was determined to be (C_{HA}=7.9~9.3 mg/L DOC, Q_2=166.7 mL/min and Q_3=100 mL/min).

Table 3.2. TNP removal by ICP-AES (TNP Lot #1).

	Q_2=166.7 mL/min, Q_3=100 mL/min					Q_2=166.7 mL/min, Q_3=200 mL/min				
C_{HA} (mg/L DOC)	0.0	4.5	6.3	7.9	9.3	0.0	4.5	6.3	7.9	9.3
C_3 (mg/L DOC)	443.3	300.0	363.3	203.3	33.3	373.3	/	310.0	216.7	263.3
C_D (mg/L DOC)	416.0	402.8	397.2	391.7	386.4	416.0	402.8	397.2	391.7	386.4
η (%)	-	25.5	8.5	48.1	91.4	10.3	/	21.9	44.7	31.8
	Q_2=250 mL/min, Q_3=100 mL/min					Q_2=250 mL/min, Q_3=200 mL/min				
C_{HA} (mg/L DOC)	0.0	4.5	6.3	7.9	9.3	0.0	4.5	6.3	7.9	9.3
C_3 (mg/L DOC)	353.3	336.7	210.0	86.7	166.7	326.7	316.7	326.7	40	176.7
C_D (mg/L DOC)	307.7	300.4	297.3	294.2	291.2	307.7	300.4	297.3	294.2	291.2
η (%)	-	-	29.4	70.5	42.8	-	-	-	86.4	39.3

/: Ti (TNPs) concentration that was not detected by ICP-AES;

-: ineffective DAF treatment.

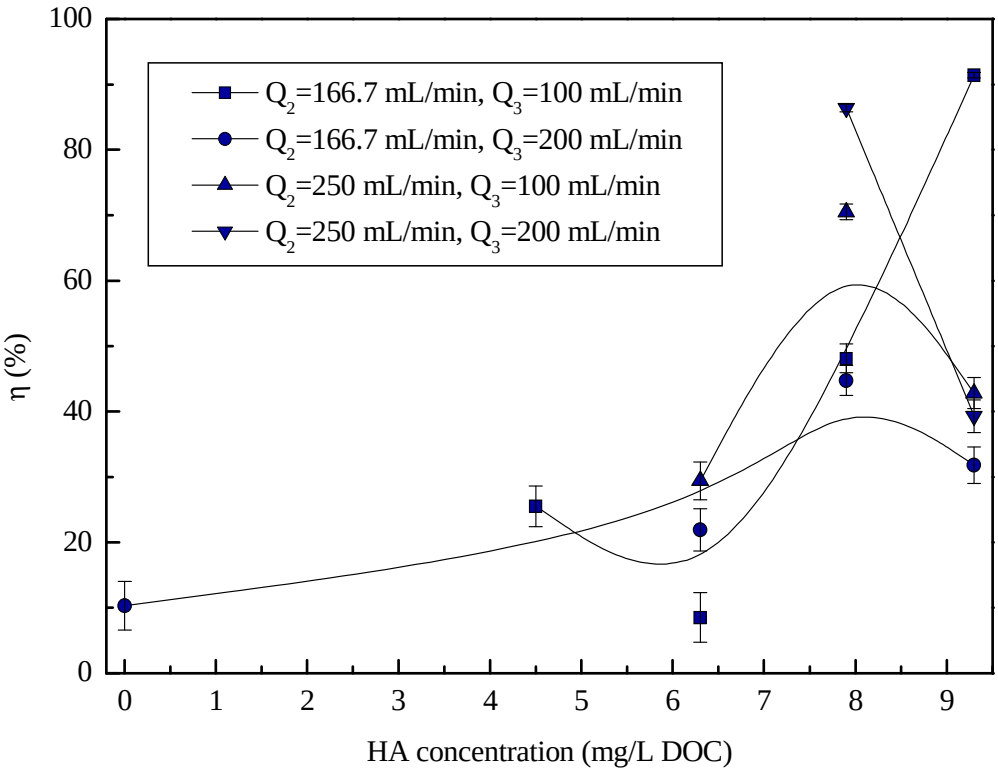

Fig. 3.14. Effect of HA concentration on TNP removal efficiency.

Zeta potential of the effluent was also measured to get a complete comprehension of the effect of HA on TNP removal efficiency (Fig. 3.15). It denotes that the zeta potential of the flotation suspension kept highly positive when HA dosage was lower than around 6.3 mg/L DOC. With the increasing of HA concentration (> 6.3 mg/L DOC), this stability was undermined, and the TNP removal correspondingly increased. In Fig. 3.14, the removal exhibited a deceasing trend when the HA dosage was higher than 7.9 mg/L DOC (for (Q_2 =166.7 mL/min, Q_3 =200 mL/min), (Q_2 =250 mL/min, Q_3 =100 mL/min), (Q_2 =250 mL/min, Q_3 =200 mL/min)), which might result from particles re-stabilization due to the formation of negatively charged small flocs.

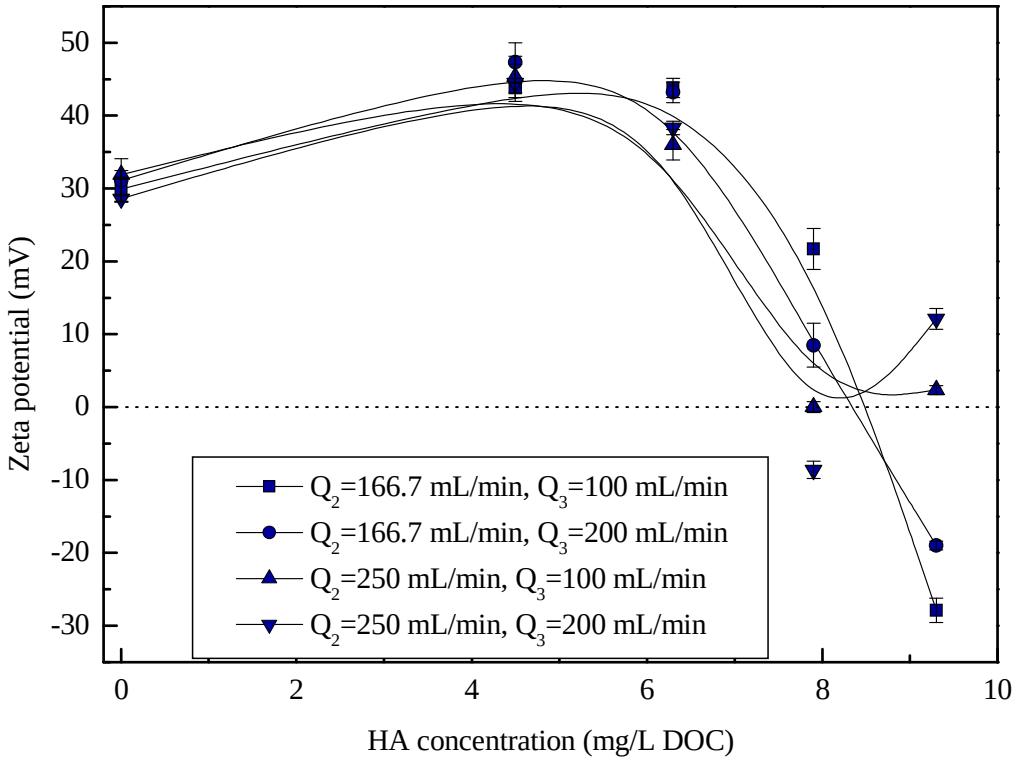

Fig. 3.15. Effect of HA concentration on zeta potential of treated TNP suspensions.

Based on data of Table 3.2 and the measurement of the treated suspension, the flotation performance is also expressed as Fig. 3.16. It is indicative that the TNP removal was only around 40 % at the zeta potential of 0 mV, and got higher than 60 % even when zeta potentials were negative. This was because TNP removal efficiency was achieved due to not only the electrostatic attraction between negative polyanions of HA, bubbles and surface positive TNPs, but also the hydrophobic interaction of TNP-HA. The assistance of HA to TNP removal efficiencies in the DAF process could be understood from the physiochemical interaction among TNPs, HA and bubbles. According to the discussion in Section 3.1, TNPs and HA were able to form flocs because of charge neutralization, ligand exchange, hydrophobic interaction, and van der Waals interactions when they contacted each other. In the DAF process, air bubbles with negative surface charges and small size (approximately 70 μm) were introduced (Edzwald, 2007; Oliveira and Rubio, 2011), and subsequently, bubble-TNP-HA or bubble-TNP aggregates were generated due to the collision of bubbles, TNPs and HA.

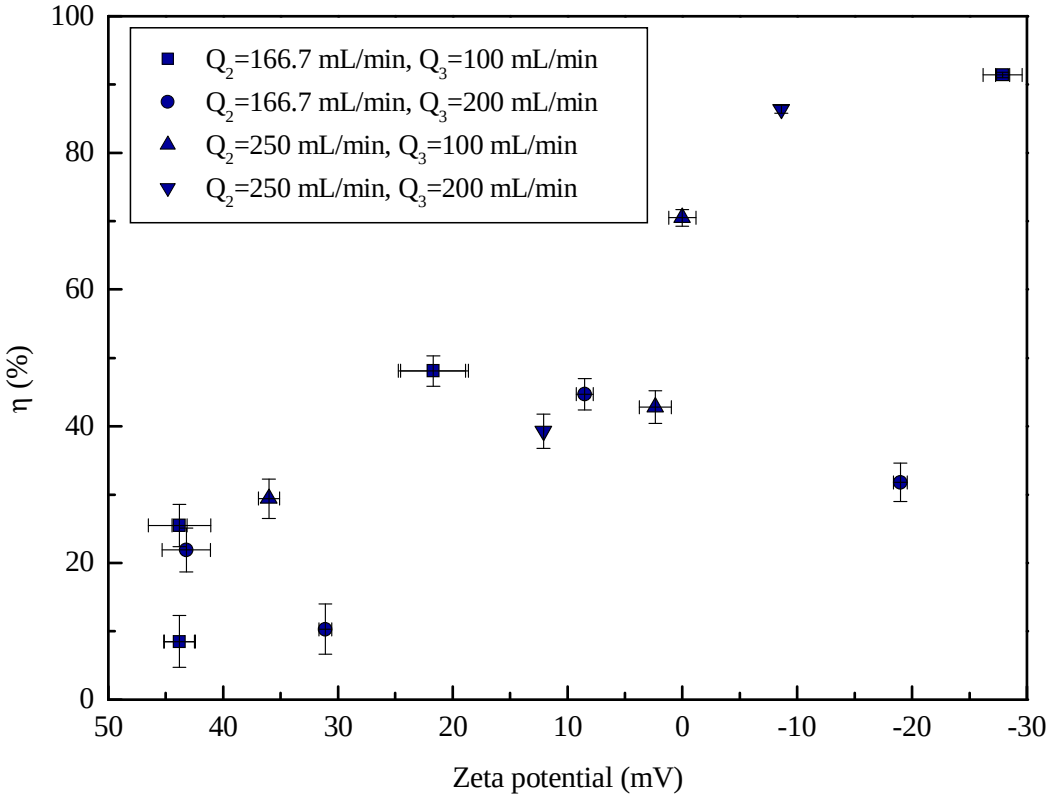

Fig. 3.16. Relationship between TNP removal efficiency and zeta potential of the flotation suspension. (Negative efficiencies are omitted.)

3.3.4 Expanded DAF tests (using Lot #2)

The preliminary trials in Section 3.3.3 confirmed the effectiveness of TNP separation by DAF with the assistance of dissolved HA (using the alkaline HA stock solution). However, it also pointed out the fact that the pH significantly affects the TNP aggregation behavior in the highly acidic TNP suspension (< pH3) by changing the zeta potential of TNPs. Studies of Guzman et al (2006), Pettibone et al. (2008), and French et al. (2009) denoted that the pH significantly could influence the stability, the surface adsorption and reactivity of the TNP suspension. Hence, it's of great importance to investigate the role of pH in the TNP flotation in the absence of HA. Hence, further investigation ought to be conducted to figure out the DAF performance on the TNP removal in the absence and presence of HA with pH controlled, which is the objective of Section 3.3.4.

In this part of experiments, Q_1 was firstly fixed to be 70 mL/min, and thereby Q_b and Q_2 were derived to be 17.8 mL/min and 167 mL/min, respectively. According to Eq. 3.13, a "theoretical" A/S value is then calculated to be 0.18. That is to say, when the bubble surface is completely covered by NPs, in order to capture all TNPs in the influent, the A/S value ought

to be 0.18. As shown in Table 3.3, the three investigated A/S values were determined to be no higher than 0.18, leaving the possibility of enhancing the DAF efficiency by improving physiochemical conditions (pH and DAF assisting reagent). Using an assisting reagent increases the size of the particles by coagulation so decreases the necessary quantity of air-water interface.

Table 3.3. A/S values in DAF experiments (TNP Lot #2).

No.	Q_1 (mL/min)	Q_2 (mL/min)	Q_2/Q_1 (%)	Q_b* (mL/min)	Q_b** (g/min)	Q_3 (mL/min)	A/S
1	70	167	238.6	17.8	0.0214	100	0.18
2	70	100	142.9	10.7	0.0129	60	0.11
3	140	100	71.4	10.7	0.0129	100	0.06

* The relationship between Q_b and Q_2 obeys Henry's Law in Eq. 3.18.

** at 20 °C and 1.013 bar.

3.3.4.1 DAF of TNPs with pH adjustment

The operating condition No. 2 in Table 3.3 (A/S=0.11, Q_1=70 mL/min, Q_2=100 mL/min, Q_3=60 mL/min) was used to examine this effect. Experiments were performed at different pH values (from 3.2 to 9.9) by adding the pH regulator (NaOH solution) into the contact cell during the experiment process. Flow rates of NaOH (Q_a) were determined by required pH values. Results obtained are depicted in Fig. 3.17.

The TNP removal efficiency η increased with the increase of pH, and high removals were achieved at pH values of approximately 5.5 and 6.4 (63.8 % with the zeta potential of +34.5 mV and 56.5 % with the zeta potential of -11.8 mV, respectively); then, η got a decreasing trend as pH values continued to rise. The removal efficiency stayed above 10 % within the tested pH range. Simultaneously, the variation of the zeta potential went through three stages: (i) keeping positive at around +40mV and even slightly increasing from pH 3.2 to 4.6, (ii) sharply dropping and encountering a reversal from pH 4.6 to 8.8, and (iii) finally staying at an average level of approximately -38 mV from pH 8.8 to 9.9. The IEP occurring at around pH 6.1 was just in Stage ii where about 60 % TNP could be removed, pointing out that the addition of OH^- destabilized the positively surface charged TNPs probably by neutralizing

the surface charge: when there was no more repulsive interaction between TNPs, the formation of aggregates would be enhanced, and those resulting large aggregates were thus more easily captured by bubbles. The specific mechanisms will be further discussed later (Section 3.3.4.3).

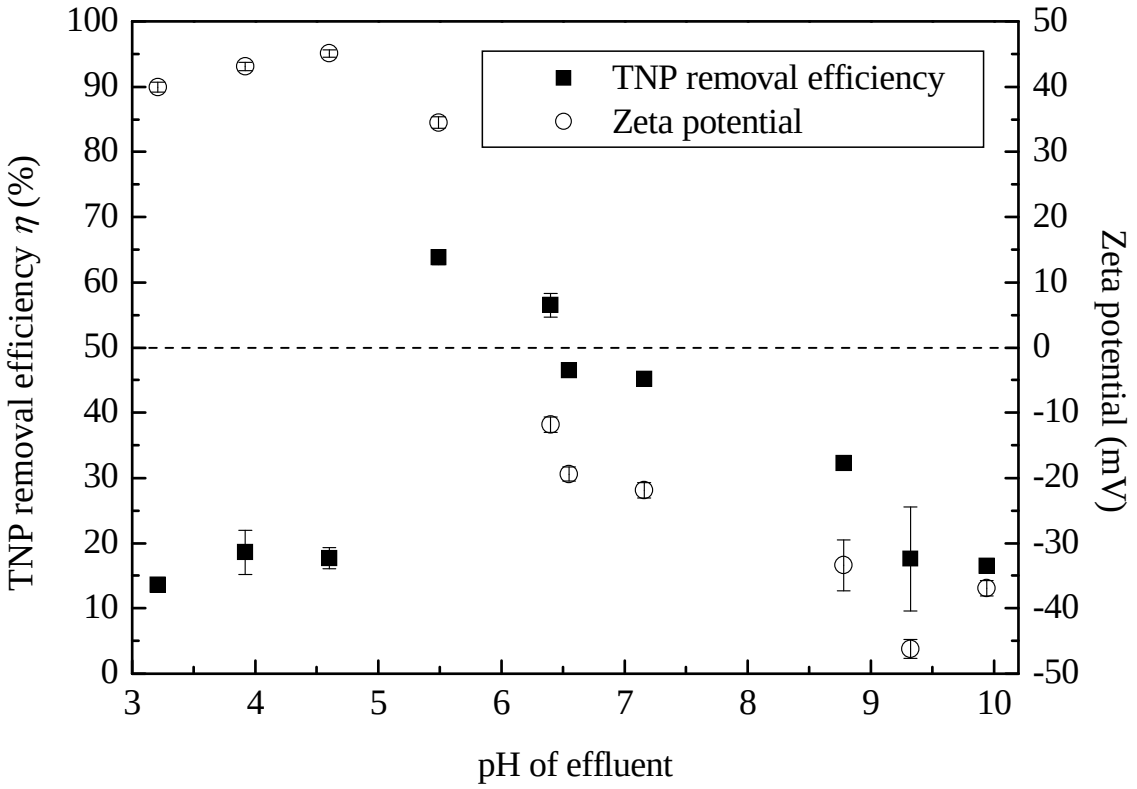

Fig. 3.17. TNP removal efficiency and zeta potential varying with pH of effluent.

3.3.4.2 DAF of TNPs with HA assistance

(1) Effect of the HA concentration

The influence of HA on the DAF performance (TNP removal efficiency, HA removal, zeta potential and pH of flotation effluent) was studied under the same operating condition mentioned in Section 3.3.4.1. The HA dosage ranging from 0 to 21 mg/L DOC was controlled by changing the flow rate of HA stock solution. Since pH has great influence on the flotation efficiency according to the experimental results of Section 3.3.4.1, HA stock solutions were adjusted to 4.7, 6.2, 8.9 and 12.1, respectively, by HCl solution before adding into the flotation aqueous system.

As described in Fig. 3.18, it is worth noting that, when $pH_{HA\ stock}$ was 4.7, the TNP removal efficiency in excess of 92 % was achievable at the HA dosage higher than 11.1 mg/L DOC.

With a maximum TNP removal of 99.6 %, using approximately 20.8 mg/L DOC of HA, 94.2 % of HA was also separated; meanwhile, the zeta potential of flotation aggregates was -14.5 mV, and pH of flotation suspension was around 3.58. For $pH_{HA\ stock}$=6.2, when dosing more than 11 mg/L DOC of HA, TNP and HA removals kept around 99 % and 91 %, respectively, with the zeta potential declining from +18.5 mV to -24.7 mV and pH slightly rising from 3.6 to 4.1. When further increasing the pH value of HA stock solution to alkaline range (8.9 and 12.1), optimum TNP removals fell to 72.7 % ($pH_{HA\ stock}$=6.2, HA dosage=11.1 mg/L DOC) and 40.4 % ($pH_{HA\ stock}$=12.1, HA dosage= 8.7 mg/L DOC), respectively, and HA removals were around 85.7 % and 93.3 %, correspondingly; the pH value of effluent rose considerably with the increasing dosage of HA, from acid to base, due to the addition of alkaline HA stock solutions. Obviously, increasing pH of HA stock solution decreased the TNP removal efficiency, though it reduced the HA demand for the optimum TNP removal. As denoted in Fig. 3.17, TNPs would be negatively surface charged if the pH of the flotation suspension was higher than 6.1 (IEP). On using the basic HA stock solutions, the electrostatic repulsion could occur between TNPs and polyanions of HA when the pH of the flotation suspension increased to IEP (Fig. 3.18), corresponding to the unfavorable aggregation and thus DAF performance.

The favorable HA removals obtained from experiments revealed the participation of HA in the DAF process. That was in agreement with what we found in the previous study of the TNP surface modification by HA, which confirmed the strong interaction between TNPs and HA molecules via the analysis of FT-IR, aggregate size distribution, and HA adsorption on TNPs (Zhang and Guiraud, 2013). The removal of TNPs by DAF was therefore yielded by the formation of TNP-HA-bubble aggregates. The high removal of DOC also indicated that the release of those DAF effluents into aqueous environment would not be an environmental problem. More systematical analysis will be given in Section 3.3.4.3.

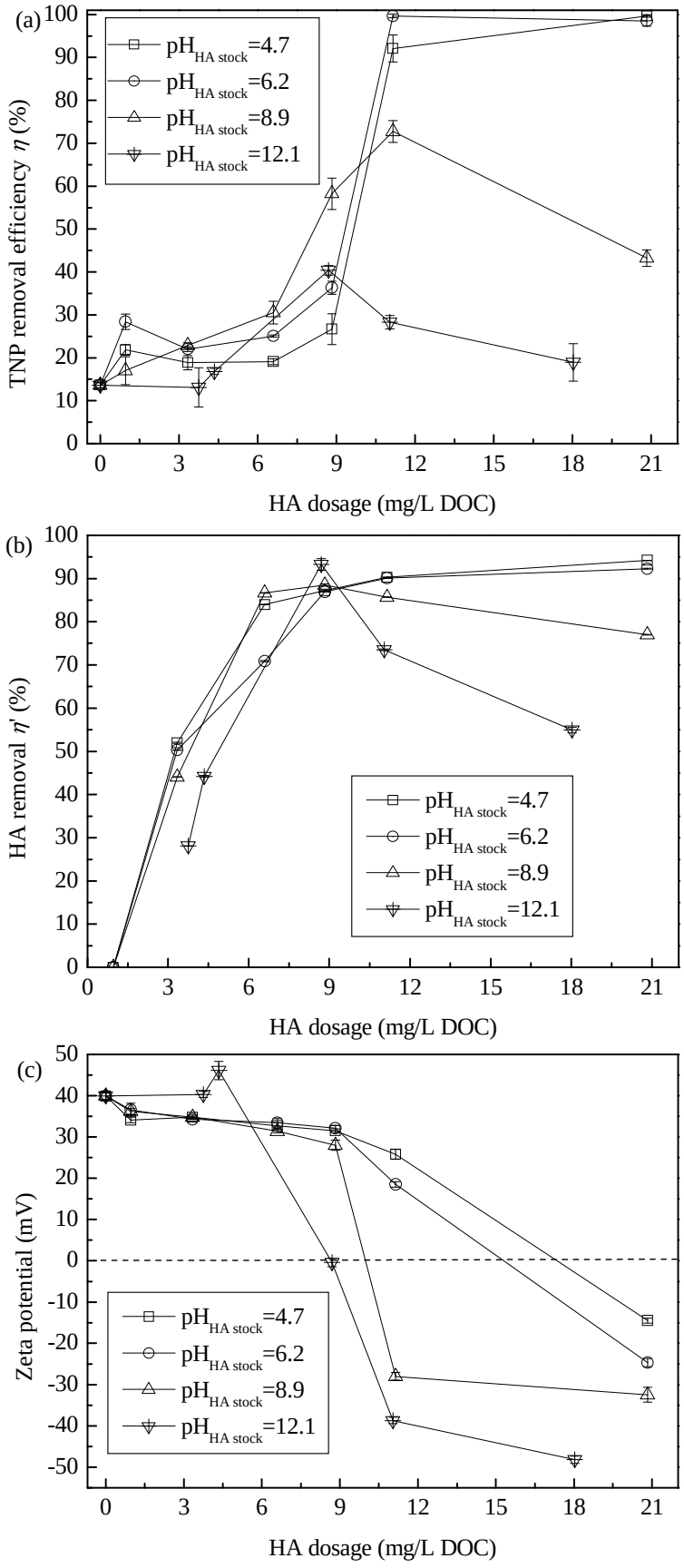
(a)
TNP removal efficiency η (%)
HA dosage (mg/L DOC)
pH_HA stock=4.7
pH_HA stock=6.2
pH_HA stock=8.9
pH_HA stock=12.1
(b)
HA removal η' (%)
HA dosage (mg/L DOC)
pH_HA stock=4.7
pH_HA stock=6.2
pH_HA stock=8.9
pH_HA stock=12.1
(c)
Zeta potential (mV)
HA dosage (mg/L DOC)
pH_HA stock=4.7
pH_HA stock=6.2
pH_HA stock=8.9
pH_HA stock=12.1

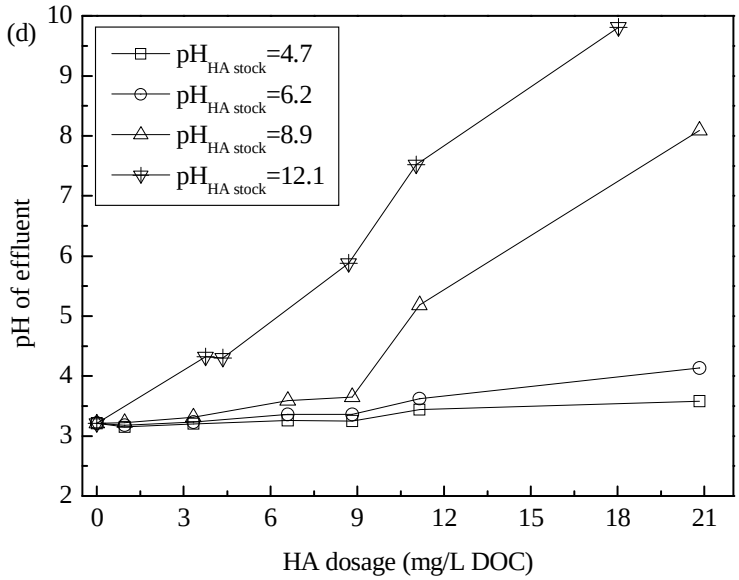

Fig. 3.18. Flotation behavior varying with HA dosage (The pH value of HA stock solution was adjusted to 4.7, 6.2, 8.9 and 12.1, respectively): (a)TNP removal efficiency, (b) HA removal, (c) zeta potential, and (d) pH of effluent.

(2) Effect of A/S ratio

DAF tests were conducted at three A/S values (0.06, 0.11 and 0.18 in Table 3.3) in order to investigate the influence of operating conditions on the flotation efficiency. In this series of DAF tests, the pH of HA stock solution was determined to be approximately 12.1 because of the lowest TNP removal efficiency obtained in this situation (aforementioned in Section 3.3.4.2(1)) and thereby a great "space" for the efficiency improvement. The DAF performance as a function of HA dosage for each A/S are displayed in Fig. 3.19, indicating that, for A/S values of 0.06, 0.11 and 0.18, (1) the use of DAF assisting reagents is necessary because, without the HA addition, TNP removal efficiencies were as low as 4.5 %, 13.6 % and 17.7 %, respectively; (2) optimum HA concentrations for these three A/S values were 11.8, 8.7, and 6.8 mg/L DOC, respectively. Fig. 3.19(a) (b) and (c) clearly showed that all the optimum HA dosages for both high TNPs and HA removals were attained at the zeta potential close to 0 mV and the pH value between 5~7, confirming that the charge neutralization predominantly decided the separation efficiency when using highly alkaline HA solution in the DAF process. The TNP-HA flotation suspension would be re-stabilized at higher HA concentrations.

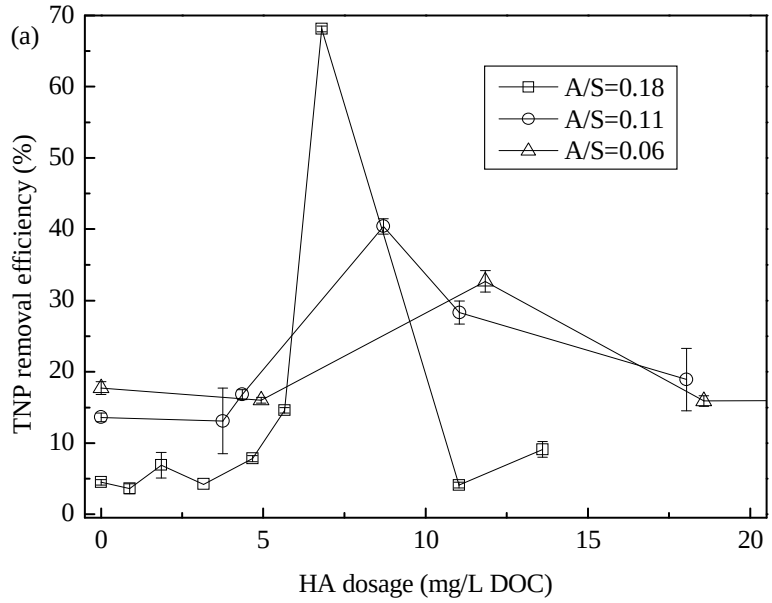
(a)
TNP removal efficiency (%)
HA dosage (mg/L DOC)
A/S=0.18
A/S=0.11
A/S=0.06

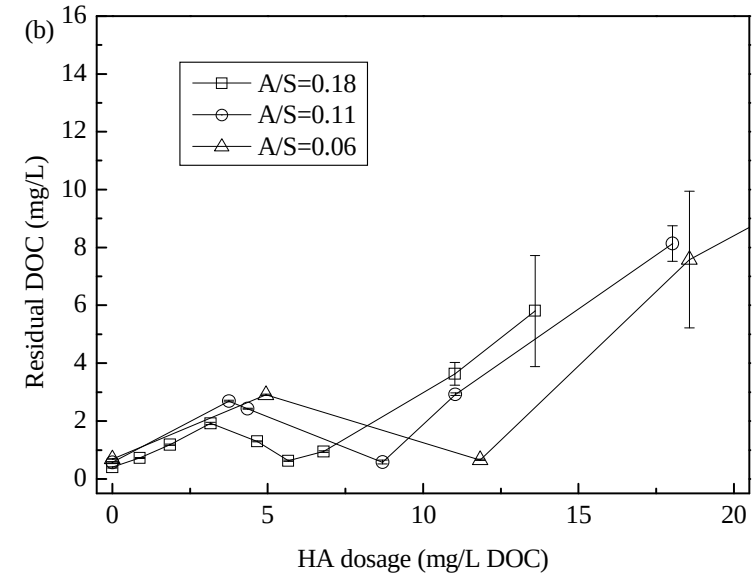
(b)
Residual DOC (mg/L)
HA dosage (mg/L DOC)
A/S=0.18
A/S=0.11
A/S=0.06

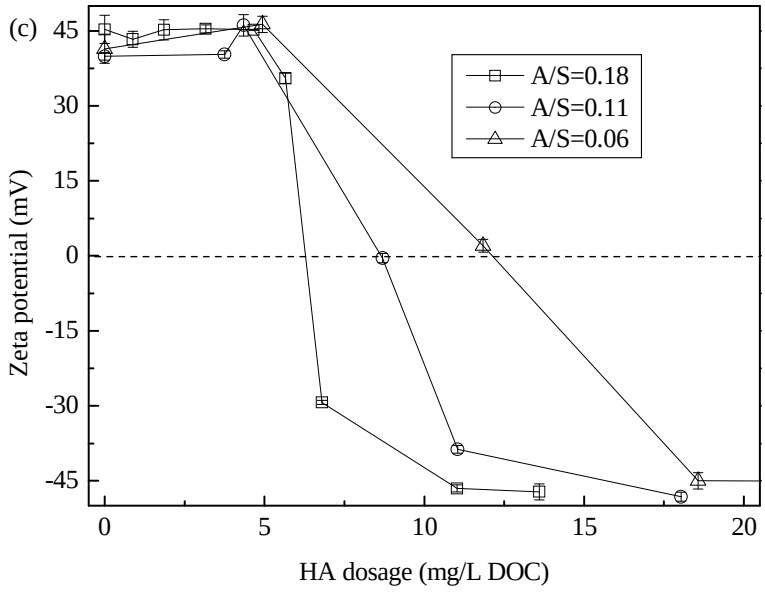
(c)
Zeta potential (mV)
HA dosage (mg/L DOC)
A/S=0.18
A/S=0.11
A/S=0.06

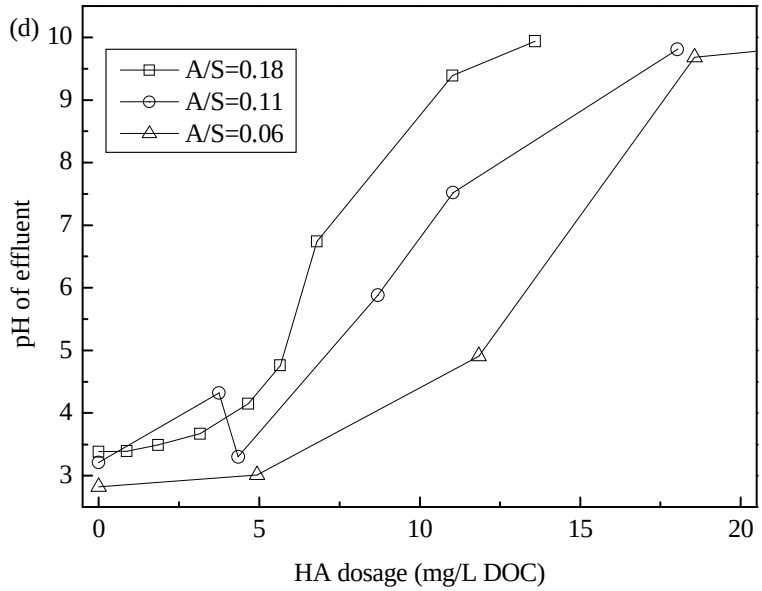

Fig. 3.19. Comparison of DAF performance under different A/S ratios: (a)TNP removal efficiency; (b) residual DOC; (c) zeta potential; (d) pH values.

Subsequently, DAF performances are compared at these three optimum HA dosages (Fig. 3.20). The TNP removal efficiency grew from less than 33 % (A/S=0.06) to almost 68.1 % (A/S=0.18). For A/S of 0.06 and 0.11, pH values of the flotation system were 4.9 and 5.8, respectively, and both of their zeta potentials approached zero. It demonstrated that, when the quantity of air bubbles was at a low level, the electrostatic attraction might play a leading role in the formation of TNP-HA-OH^- aggregates by heterocoagulation betwen TNPs and HA (or TNPs and HA-OH^-). When the air input further increased (A/S=0.18), a greater TNP removal was obtained since more air bubbles were introduced into the DAF system which gave rise to a greater bubble surface area available for collecting TNPs. In this case, the zeta potential exhibited a highly negative value of -29.3 mV, revealing that other mechanisms also contributed to the TNP removal in addition to the electrostatic interaction. Further discussion is given in the following section.

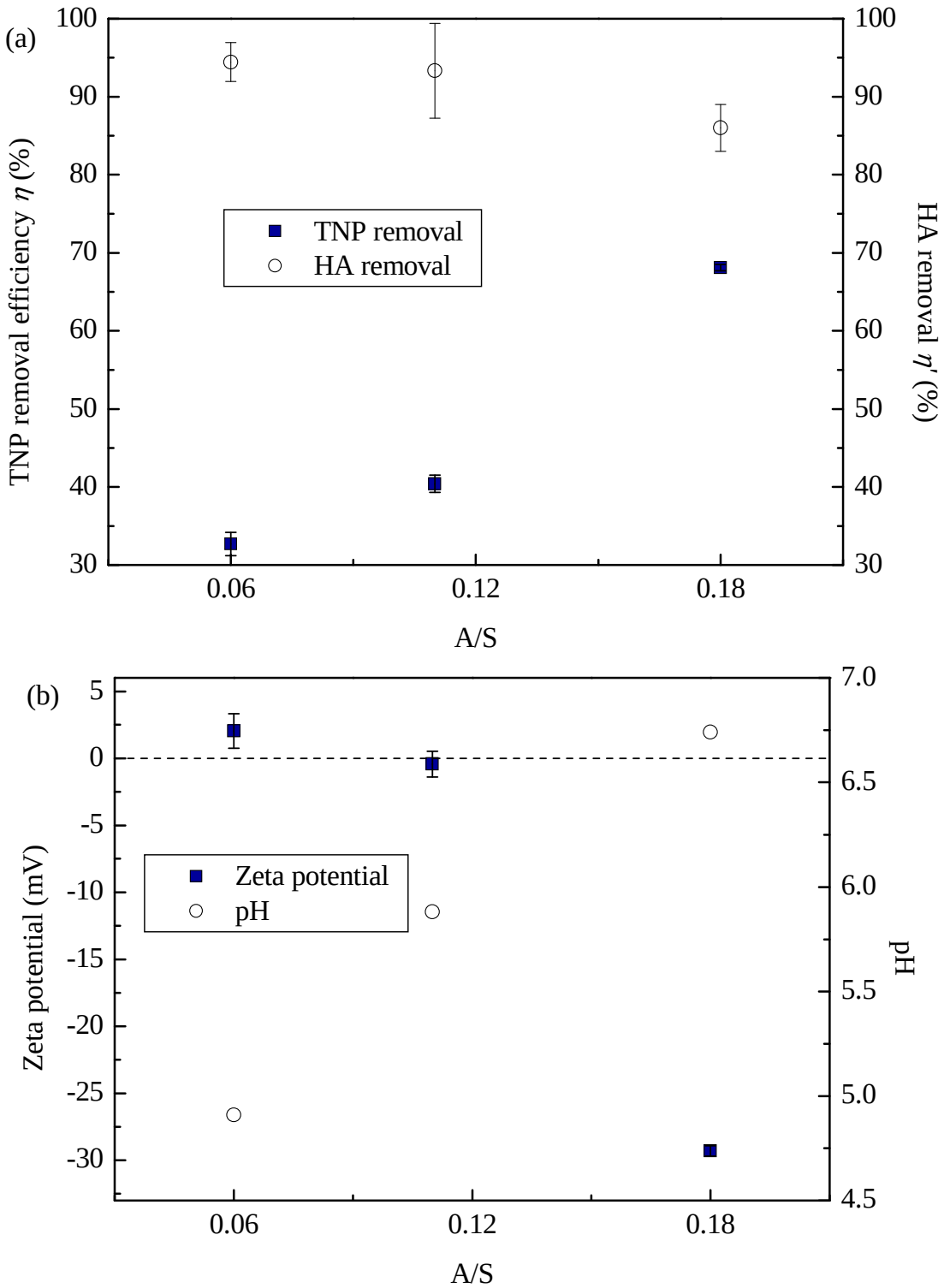

Fig. 3.20. Comparison of flotation performances at different A/S ratios: (a) TNP and HA removal, (b) Zeta potential and pH of effluent.

3.3.4.3 Discussion of flotation mechanisms

(1) Interaction mechanisms in DAF processes

Photos of the separation zone at pH 4.6, 5.9 and 8.8 in Fig. 3.21(a), (b) and (c) were taken immediately after DAF tests and are shown as representative of those three stages: for the either low or high pH, no obvious flocs were observed in the flotation suspension; whereas for the optimal pH value of 5.9, the TNP-bubble aggregates formed and floated on the surface of the suspension. The flotation phenomena in the presence of HA at different HA concentrations (pH_{HA}=12.1) are presented in Fig. 3.21(d), (e) and (f). Similarly, brown TNP-HA-bubble aggregates could be found at the optimum HA dosage, and for the below and above concentrations, there were no large flocs due to the stability and re-stability of the flotation suspension. Specific explanations and possible mechanisms will be discussed below.

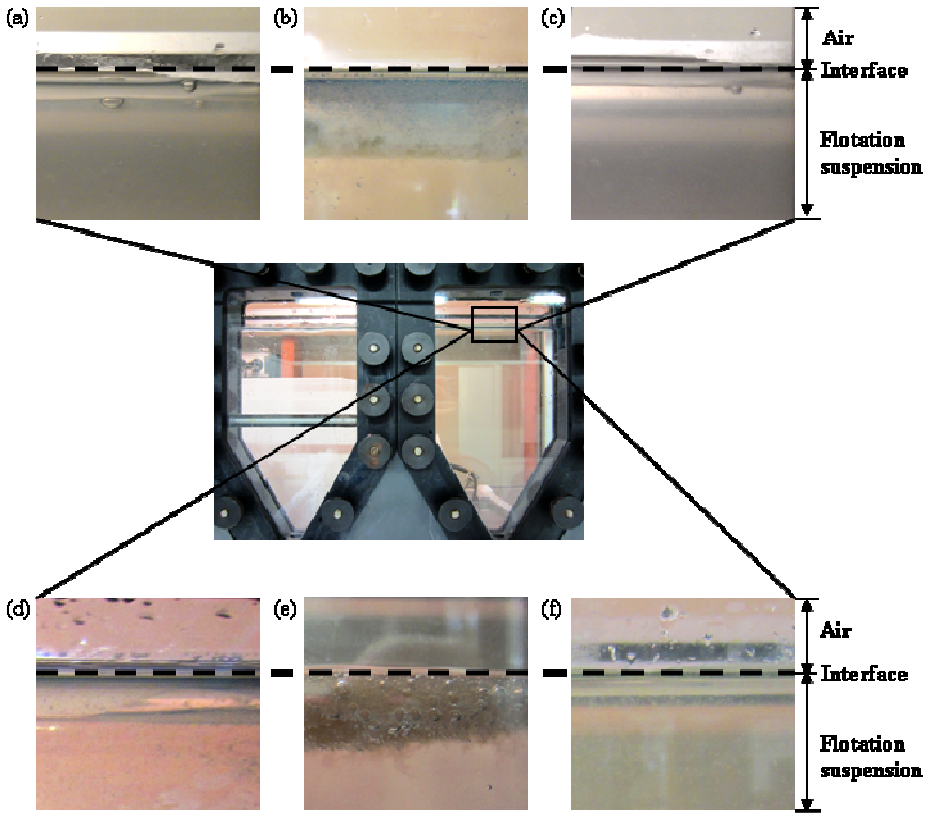

Fig. 3.21. Representative photos of the contact zone under the operating condition of Q_1=70 mL/min, Q_2=100 mL/min, Q_3=60 mL/min, at different pH values, (a) pH =4.6, (b) pH=5.9, (c) pH=8.8, at different HA concentrations, below (d), around (e), and above (f) the optimum concentration.

Given that the zeta potential relates to the degree of electrostatic interaction between suspended particles and other charged surfaces (i.e. the bubble surface) in the suspension, it is

the main parameter determining the flotation efficacy. To further understand possible interaction mechanisms in both pH adjusted and HA assisted DAF processes, the flotation performance was plotted as a function of zeta potential of the flotation aqueous suspension (Fig. 3.22).

Electrostatic forces When the zeta potential of flotation suspension was around zero, favorable TNP removals of all investigated flotation processes were achieved (Fig. 3.22(a)), so the charge neutralization may be one of the leading aggregation and flotation mechanisms. The charge type determines the formation of NP aggregates and particle-bubble aggregates; the charge magnitude predominates the extent of charge neutralization: high absolute values provide greater colloidal stability by way of increasing electrostatic repulsion between charged surfaces, while the lowest stability, appearing in the IEP area, offers more chances of TNP aggregation (Simate et al., 2012; Zhang and Guiraud, 2013). The zeta potential of positively surface-charged TNPs began to decrease when the OH^- concentration was great enough to neutralize the surface charge of TNPs, then switched to negative values and turned to be more negative with the dosage increase. On the other hand, the zeta potential of negatively surface-charged bubbles went more negative because of the "negative adsorption" or "exclusion" of protons from the bubble interface (Najafi et al., 2007).

Bonding action of HA on bubble surface Apart from the IEP area, high TNP and HA removals were also found when the flotation suspension was of incipient instability (±10 mV ~ ±30 mV) (Fig. 3.22(a) and (b)), indicating that the electrostatic interaction should not be the only interaction mechanism. When acid or weak acid HA stock solutions were dosed, the zeta potential of flotation suspension went from positive to negative without greatly changing the pH value (Fig. 3.22(c)), revealing that the variation of zeta potential was resulted from not only OH^- ions but also HA molecules which helped to compress the surface charges of TNPs. In the HA adjusted DAF, the ligand exchange, mainly resulting from the HA phenolic OH and COOH groups, could facilitate the adhesion of HA molecules onto TNP surfaces (Yang et al., 2009; Zhang and Guiraud, 2013). It has been confirmed that a HA layer could form on the surface of mineral particles (Vermeer et al., 1998; Vermeer and Koopal, 1998). That HA layer exerted influence in keeping the stability of particle-bubble aggregates by the bonding action of HA.

Hydrophobic attraction of TNP-bubble As stated by A. V. Nguyen et al. (2006), besides the electrical double-layer, the non-DLVO force is also one of the principal colloidal forces functioning in the particle flotation process. The attractive force between hydrophobic surfaces is one of the non-DLVO forces relevant to the bubble-particle collection interaction. It is pretty worth noting that when the pH of the flotation suspension was around 4 or less (using HA stock solutions with pH 4.7 and 6.2), a number of HA molecules were not really soluble and uncharged according to the analysis in Section 2.2.2.2(2), and they might aggregate to form colloidal precipitates in order to minimize the contact with the surrounding aqueous environment. Those colloidal precipitate possessing hydrophobic moieties could be considered as an extended colloidal fishnet in which TNPs were enmeshed or trapped. Their structure might greatly enhance the bubble-particle attachment and stability in DAF since the TNP and HA removal efficiencies higher than 95% were attained. Moreover, as for cases of pH adjusted DAF and HA assisted DAF using the HA stock solutions with pH 8.9 and 12.1, it is highly possible that the HA layer endowed the TNP surface with higher hydrophobicity, and it could be anticipated that the hydrophobic coagulation between TNPs and bubbles occurred considering that the zeta potential of particles in dilute electrolyte was lower than that of bubbles (Gochin and Solari, 1983; Paulson and Pugh, 1996). Meanwhile, the aggregated TNPs would probably entrap air bubbles on the surface, aggregate/particle bridging between two gas-nuclei might reinforce that hydrophobic effect and contribute to the maximum flotation efficiency.

Additionally, it is worth noting that the HA solution of stronger base caused worse TNP removals whereas high HA removals were still reached. It denoted that overdosed OH^- ions might hinder the adhesion of HA on the TNP surface, thus prevent the formation of TNP-HA aggregates, and as a result, stunt the collision between bubbles and particles; meanwhile, a large amount of HA molecules were possibly collected and removed by bubbles.

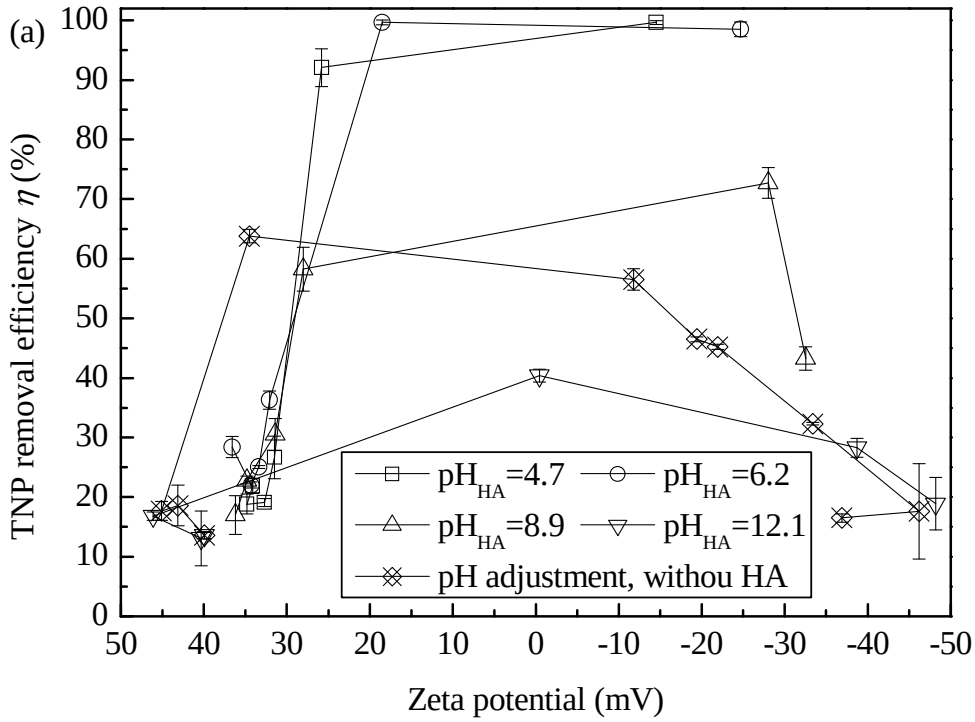
(a)
TNP removal efficiency η (%)
Zeta potential (mV)
pH_HA=4.7
pH_HA=6.2
pH_HA=8.9
pH_HA=12.1
pH adjustment, withou HA

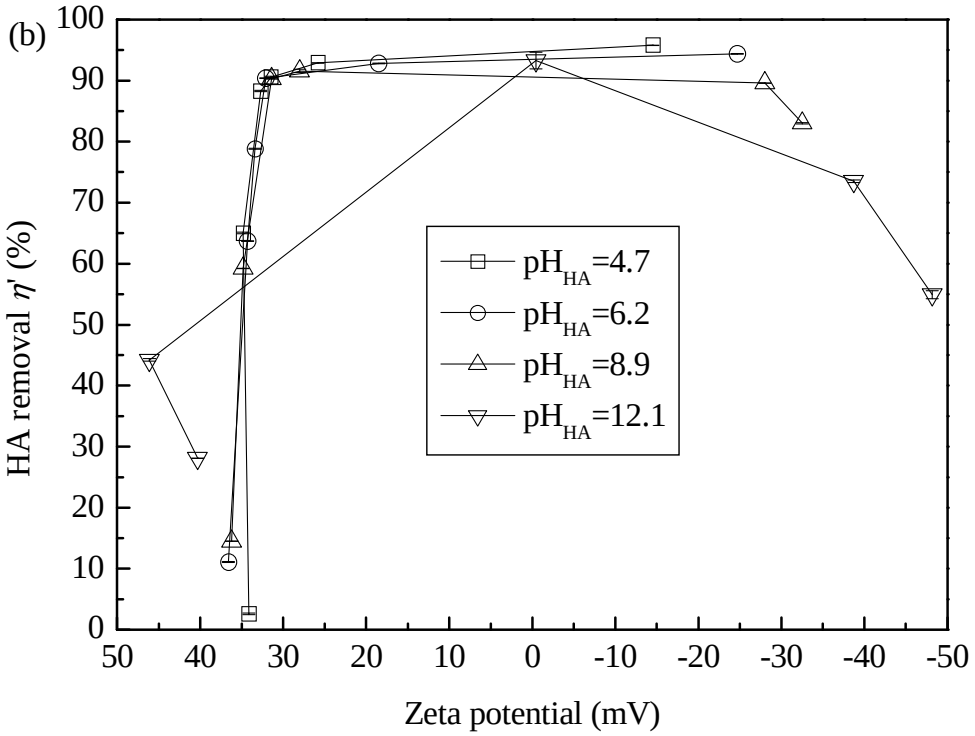
(b)
HA removal η' (%)
Zeta potential (mV)
pH_HA=4.7
pH_HA=6.2
pH_HA=8.9
pH_HA=12.1

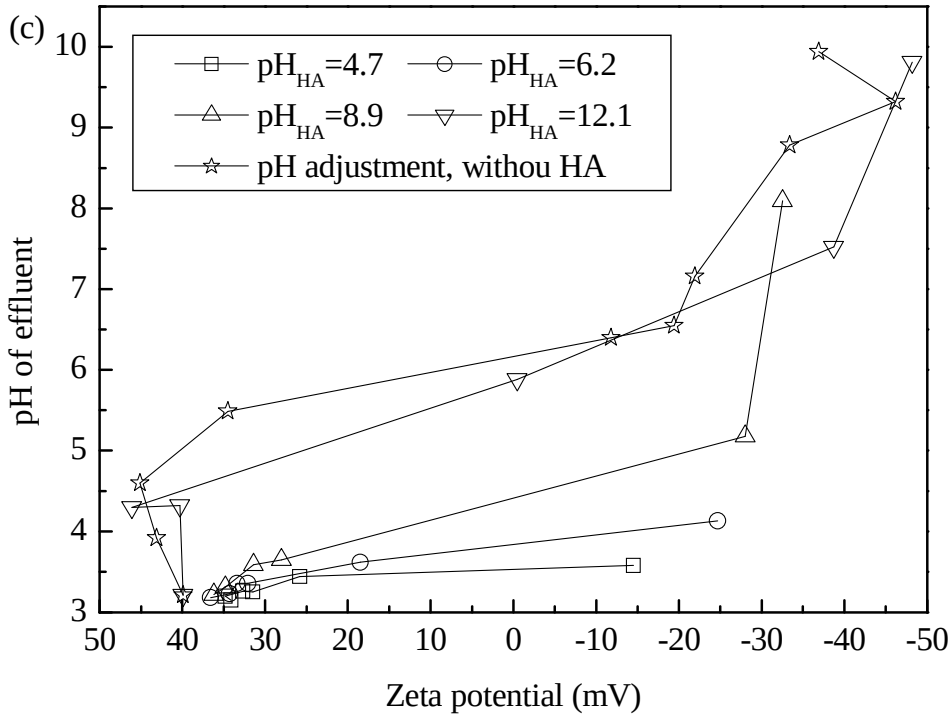

Fig. 3.22. Relationship between DAF performance and zeta potential of flotation suspension: (a) TNP removal efficiency, (b) HA removal, and (c) pH of effluent.

(2) Aggregate size distribution and fractal structure

It is well known that the aggregate (particle) size affects the collision efficiency in the flotation process, and thus influences the removal efficiency. The addition of HA or OH^- ions resulted in the formation of large TNP aggregates (d_p varying from 19 μm to 136 μm, as presented in Fig. 3.23). The aggregate size entered the interception regime, and went beyond nanoscale in which the Brownian diffusion motion controlled the collision efficiency (Reay and Ratcliff, 1973; Nguyen et al., 2006). Since it has been established that the recovery of particles by flotation is most successful in the 10~200 μm size range, the flotation assisting reagents (HA or pH regulator) used here could facilitate the TNP removal.

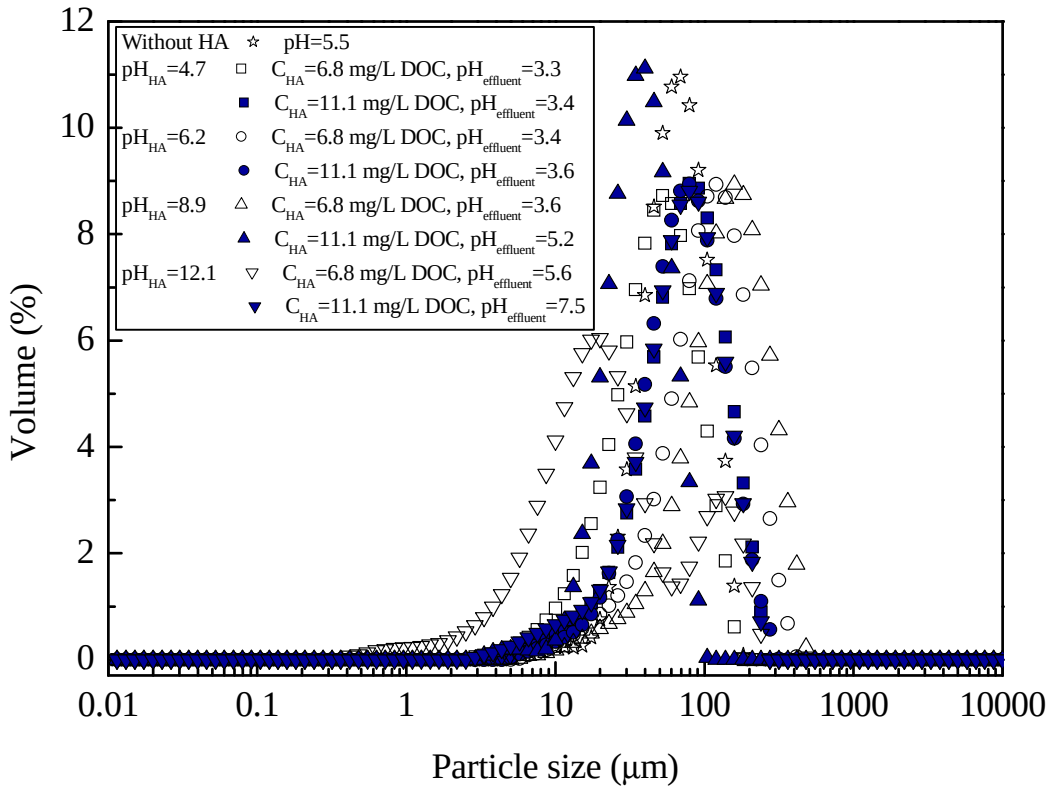

Fig. 3.23. Aggregate size distribution under different conditions.

Fractal structure is among the crucial physical properties having impact on the efficiency of unit processes in water treatment works (Chau, 2004). TNP aggregates in the presence and absence of HA generated in the DAF process were compared in terms of fractal dimension D_f (Fig. 3.24). Relationship between the scattered light intensity (I) and wavenumber (Q) (Eq. 3.4) on a log-log scale for the D_f determination is given in Fig. 3.24(b). D_f is restricted to the same range of Q values. For all D_f calculations, the correlation coefficient of the regression line was high (R^2>0.99). Herein, it was evident that the flotation flocs under investigation exhibited scattering behavior typical of mass fractal objects. The D_f values were in the region of 1.8~2.9. As a direct comparison, the increased D_f of flocs resulting from the higher HA concentration (11.1 mg/L DOC) signified that more HA molecules brought about more compact structures ($D_f \geq 2.65$) possibly through increased attraction between particles. Accordingly, under the same operating condition, flocs with close conformation rather than loose flocs appeared to give more benefit in DAF from a combined view of particle removal and floc structural character.

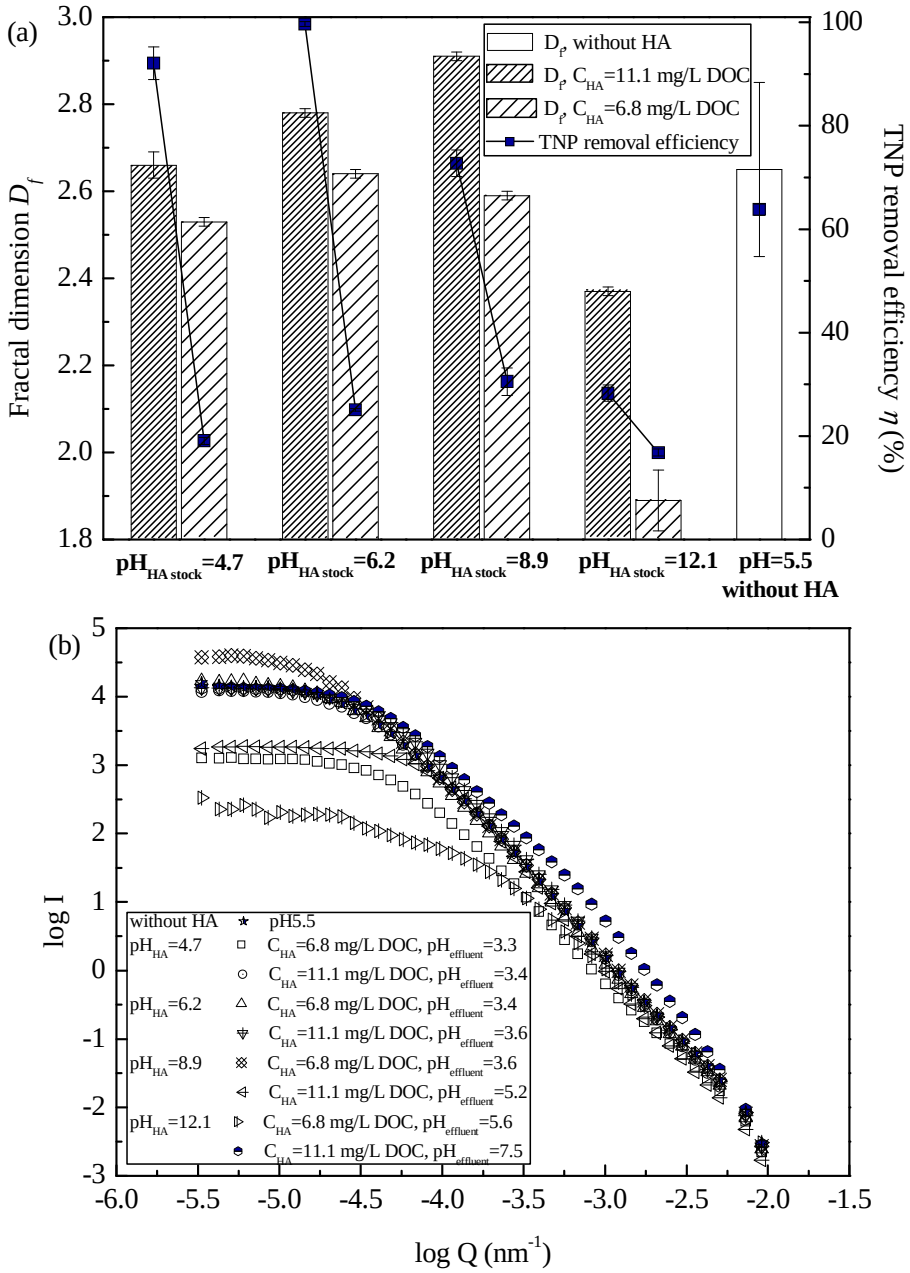

Fig. 3.24. (a) Comparison of fractal dimension values of flotation aggregates under different conditions (corresponding to Fig. 3.23); (b) Static light scattering plots of flotation flocs formed in different physiochemical conditions.

(3) Comparison between pH adjusted DAF and HA assisted DAF

The possible flotation interfacial process of pH adjusted DAF can be summarized as Route (a) in Fig. 3.25, where a1 and a2 depict the TNP aggregation and the bubble collection of TNPs, individually. The optimal flotation removal efficiency appears at the pH value close to IEP. After that pH area, the repulsive force gradually strengthens due to more negative surface charges of both TNPs and bubbles, resulting in the re-stabilization of TNPs. With the increase of pH values, the positively charged TNP surface is neutralized by OH^- and the aggregation

of TNPs is enhanced (a1 in Fig. 3.25), which facilitates the capture of TNPs by bubbles (a2 in Fig. 3.25). As further increasing the pH value, more OH^- anions are apt to be adsorbed on the TNP surface making them hydrophilic again, and thus the hydrophobic adhesion gets weak.

As for the HA assisted DAF process, the TNP removal efficiency is higher at the optimum HA dosage when the pH value of the flotation suspension is about 3~4. HA molecules probably precipitate as fibrous colloidal fishnet by which TNPs can be effectively enmeshed and the TNP-HA aggregates are thereby formed (b1 in Fig. 3.25). The adhesion of those aggregates onto the hydrophobic air bubble surface is strengthened due to the existence of hydrophobic portions of HA molecules (b2 in Fig. 3.25). Moreover, the electrostatic interaction also plays a key role in the TNP separation by HA assisted DAF owing to the attractive force between the positive surface charge TNPs and anions/polyanions of HA: The ligand exchange, mainly resulting from the COOH and phenolic OH groups of HA, is another significant effect proposed for adsorption of HA onto TNP surfaces. A HA layer formed on the surface of NPs can exert influence in keeping the bubble-particle aggregate stability by the bonding action of HA. It is worth noting that the separation efficiency of HA keeps high even if the TNP removal decreases when using the basic HA stock solution, revealing that HA can be eliminated by either agglomerating with TNPs or the bubble capture.

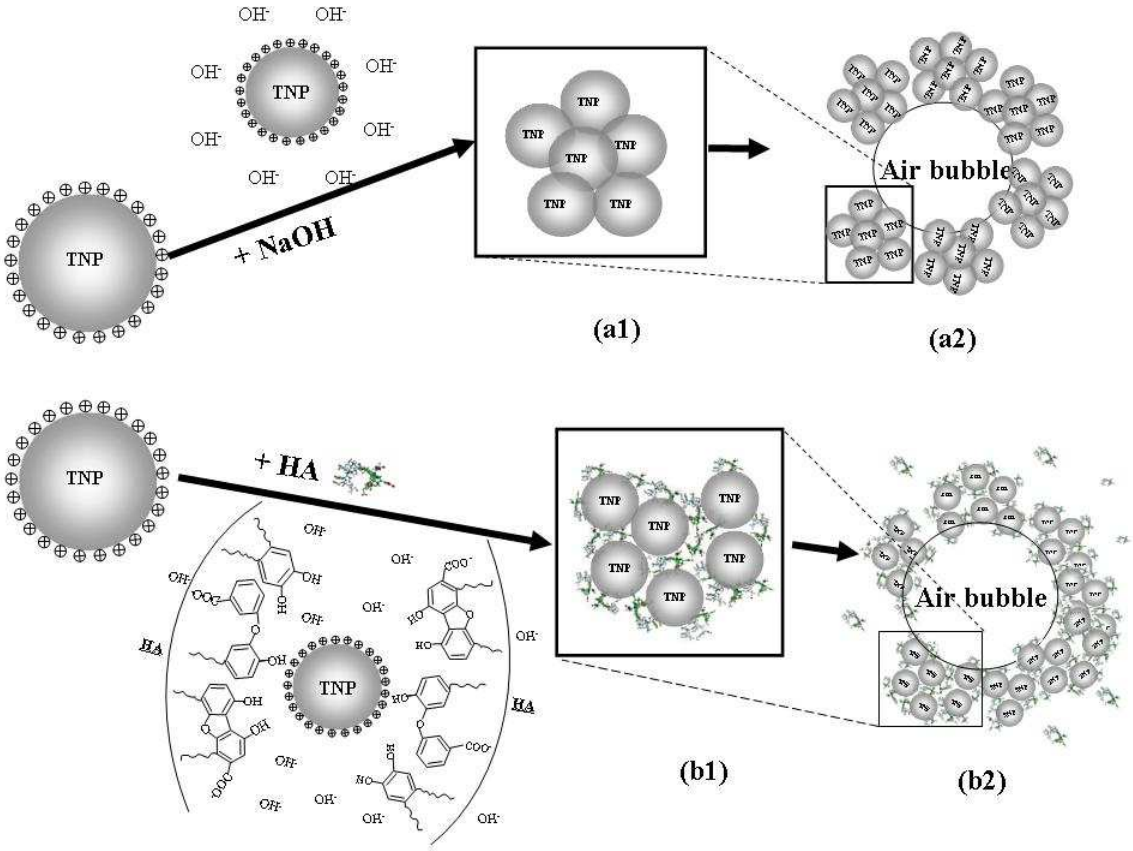

Fig. 3.25. Possible interaction schematic illustration between pH adjusted and HA assisted DAF processes (The scheme is drawn out of size proportion.).

3.4 Conclusions

This chapter specially dealt with the mechanism exploration of TNP-HA interactions and the DAF separation efficiency and performance in the absence and presence of HA under different pH conditions.

In the study of TNP surface modification with alkaline HA solution, TNP-HA aggregates were obtained and the optimum HA dosage range was determined to be 7.8~9.15 mg/L DOC in which the clearest supernatant was achieved at the HA concentration of 9.15 mg/L DOC. It had been known that the pH value of TNP suspension greatly affected the TNP aggregation process, and thereby adsorption-aggregation tests between TNPs and HA were then conducted at different pH values of HA stock solution. In the HA medium, the HA adsorption onto the TNP surface was a heterogeneous and difficult process regardless of adding HA stock solutions at different pH, according to the modeling fitting results of Langmuir, Freunlich and L-F equations. The L-F prediction of the maximum HA adsorption capacity implied that the amount of adsorbed HA on the particle surface became lower when the highly basic HA

solution was used. The pH of post-(adsorption-aggregation) suspension showed that the equilibrium pH of TNP-HA mixture suspension was always lower than 3 when adding HA stock solutions with pH values of approximately 4.0~9.0. Under these conditions, the ionization of HA molecules was weak and HA colloidal precipitates were present, resulting in the insufficiently electrostatic attraction between polyanions of HA and TNPs but the aggregation between TNPs and colloidal HA. As for the addition of highly basic HA solution (pH 12.9) into the TNP suspension, the surface charge of particles was primarily neutralized by OH^- and then screened by polyanions of HA. The fractal dimension analysis corroborated that aggregates of TNP- OH^- -HA polyanions being attained mainly by the charge neutralization were of dense configuration whereas the interaction between TNPs and HA colloid was open in view of morphological structure.

Thereafter, the feasibility of TNP removal from aqueous suspensions with a small scale continuous DAF apparatus was investigated. The pH value of flotation suspension greatly impacted the TNP removal efficiency because the electrostatic interaction (represented by zeta potential) was pH-dependent. It has been found that a highest TNP removal of approximately 64% could be obtained at pH5.5. With respect to higher TNP removal efficiency, the addition of DAF activator is necessary and HA was proofed to be a good choice: the use of HA resulted in TNP removal efficiencies as high as 99 % and simultaneously HA removals in excess of 90 % when the HA solution with low pH values (i.e. 4.7 and 6.2) was used. When the pH of the TNP-HA suspension was no higher than 4, most HA molecules were not really soluble and thus uncharged, and they might aggregate themselves and form colloidal precipitates to minimize the contact with the surrounding aqueous environment by making their hydrophobic moieties outwards. The colloidal precipitate of HA could act as and extended colloidal fishnet where TNPs would be enmeshed or trapped, then leading to a greater bubble-particle attachment efficiency and stability. Drinking water and natural water exhibits a pH range because it contains dissolved minerals and gases: surface waters typically range from pH 6.5 to 8.5 while the groundwater ranges from pH 6 to 8.5 (“What Is the pH of Water?,” n.d.). By adding those waters into the highly acidic TNP wastewater, the resulting water with favorable pH values may be achieved. Therefore, the surface water or groundwater containing HA may be recommended to facilitate the flotation separation of NPs.

The DAF efficiency could also be improved by optimizing the operating condition (A/S ratio). The HA assisted DAF efficiency could be enhanced by applying a higher A/S condition of 0.18 at $pH_{HA\ stock}$=12.1, which might be attributed to a greater bubble surface provided. Large TNP aggregates formed by the HA assistance or pH adjustment increased the interception collision efficiency between bubbles and particles, and therefore contributed to the improvement of DAF performance. When the optimum TNP removal efficiency was achieved, flotation aggregates were of higher fractal dimension under a fixed operating condition, illustrating that flocs with close conformation were preferable in DAF.

Base on results of this chapter, the large amount of water introduced along with the inputting of gas bubbles results in a considerably dilution effect. Thereby, it is imperative and interesting to reduce the dilution effect resulting from Q_2 by changing the way of producing bubbles and meanwhile further increasing the NP removal efficiency, which will be the essential goal in next chapter – the generation and flotation utilization of surface functionalized microbubbles (CGAs).

Chapter 4

CGA-flotation of SNPs

Summary

The fundamental reason for the low flotation rate of NPs is primary due to their low collision (Brownian diffusion) efficiency with conventional gas bubbles at a given size and velocity, as aforementioned in Chapter 1. In this work, the efforts have been dedicated on (i) increasing the particle size by forming NP aggregates with the assistance of HA such that the interception becomes the leading particle-bubble collision mechanism and the flotation separation can be facilitated, which is the main objective of Chapter 3; (2) enhancing the bubble-NP interaction by way of using surface functionalized microbubbles, CGAs, so that the electrostatic and hydrophobic attractions between NPs and bubbles can be greatly reinforced, which is the principal goal of this chapter.

Herein, a laboratory fabricated CGA generator is employed in the bubble generation, and the created CGAs are characterized in view of morphology, stability, size, and zeta potential for the understanding of their properties and performance in the following adsorption-aggregation and flotation processes. Thereafter, as has been done in Chapter 3, the adsorption-aggregation experiments were carried out in order to explore the surfactant-SNP interfacial mechanisms. A series of CGAs involved flotation trials are then conducted aiming at evaluating the SNP removal efficiency and preferable flotation conditions, and a short mechanism discussion follows. Finally, under the same collector dosage and flow rates, the comparison between CGA-flotation and DAF are carried out with respect to the SNP removal, and the mechanism difference between the two flotation approaches are discussed.

4.1 CGA generation and characterization

4.1.1 Design of laboratory scaled CGA generator and CGA generation

Based on the method suggested by F. Sebba (1985), a unit was fabricated in our laboratory for the continuous production of CGAs (A in Fig. 4.1). A high-speed agitator (B in Fig. 4.1, T25 digital ULTRA-TURRAX® - IKA, Germany, the motor speed is in the range of 3400~24000 rpm) is fitted on top of a cylindrical container (Ø60, 230 mL) and goes through the center of the lid. The generator, including the container and the agitator, are well sealed to avoid any liquid or gas leak. A gas inlet (3 in Fig. 4.1) is set at the center of the container to provide sufficient gas during the CGA generation process. Three flat baffles (6 in Fig. 4.1) are fixed at equal intervals to the inner wall of the container. When rotated at very high speeds, the agitator creates strong waves on the liquid surface. They strike the baffles, re-enter the water, and entrain the gas in the form of very small bubbles. Moreover, the baffles can reduce the

tendency to form a vortex as gas entrained in a vortex tends to form bubbles with a large distribution of size, whereas CGAs are expected to be as uniform as possible in size.

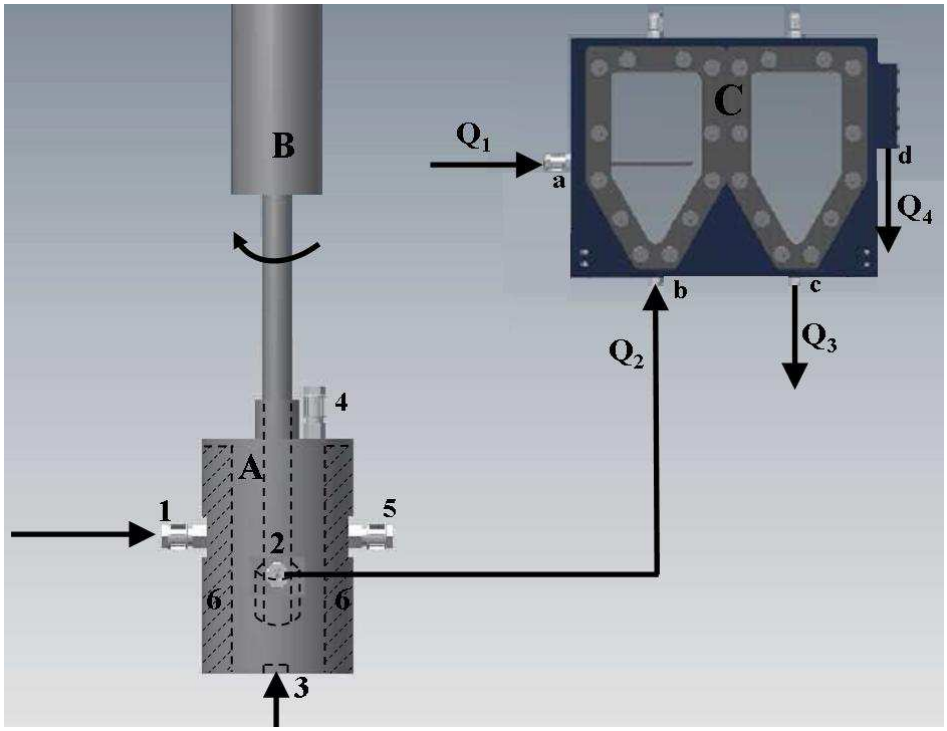

Fig. 4.1. Schematic diagram of the CGA generator and flotation setup. (A) CGA generator (230 mL): 1, 5- inlets of surfactant solution, 2- CGA outlet, 3- air inlet, 6- three baffles; (B) high speed agitator; (C) flotation cells (200×105×18 mm^3 for each zone): a- influent (NP suspension) inlet, b- CGA inlet, c- clarified water outlet, d- float outlet.

The agitator schemes of CGA generators used in this study and proposed by F. Sebba are individually presented in Fig. 4.2. For the IKA T25 digital agitator presented as B in Fig. 4.1, the surfactant solution to be processed is automatically drawn axially into the dispersion head and then forced radially through the slots in the rotor/stator arrangement at the high rotation speed, as shown in Fig. 4.2(b)② and Fig. 4.2(c). The high velocities acting on the surfactant solution can produce extremely strong shear and thrust forces. In addition, high turbulence occurs in the shear gap between rotor and stator, which provides the optimum mixing state. The dispersion effectiveness is heavily dependent on the result of the shear gradient and the time spent in the shear zone. The optimum range for the circumferential velocity of the rotor/stator arrangement is 6~24 m/s. As suggested by the producer of the agitator, a processing time of a few minutes is usually sufficient. A long processing time brings only an insignificant improvement, and the energy expended serves merely to increase the temperature of the medium. The speed is set by using the differently adjusting wheel.

Comparatively, the mixer used by F. Sebba (Fig. 4.2(d)) comprised a thin solid disc of metal approximately 5 cm diameter which was fixed to a vertical shaft connected to an electric motor capable of thousands of rpm. It could create CGAs with diameters between 30~300 μm, rarely falling below 30 μm (Chaphalkar et al., 1994).

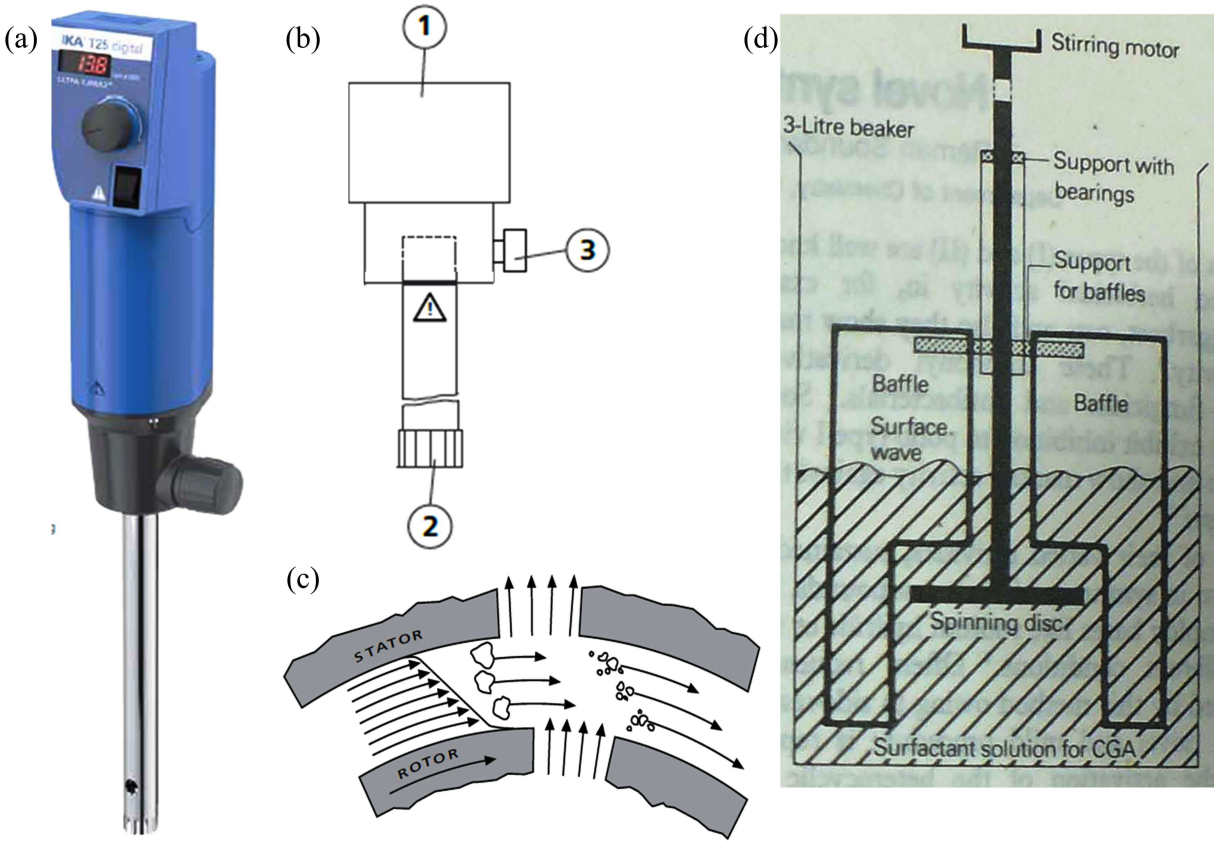

Fig. 4.2. Schematic illustration of agitators: (a) photo, (b) geometric graph (① - the drive unit, ② - the dispersing element, ③ - the knurled screw) of the high-speed agitator in this study, and (c) cross-sectional view of ②; (d) classical stirring motor fixed with spinning disc (Sebba, 1985).

CGAs that were created from the CTAB or SDS solution were named as CTAB-CGA and SDS-CGA, respectively. The pH of surfactant solution was stable in the investigated concentration range (Fig. 2.20). Hence, the pH of surfactant solution was not specially controlled in this study. Container A (Fig. 4.1) was filled with 200 mL surfactant solution before agitation. The batch generation mode was specially conducted for the study of CGA properties (size, half life, zeta potential, optical microscopic observation), during which the uncovered generator was fiercely agitated for 1.5 min and the CGA sample was obtained for characterization as soon as CGAs were generated. The continuous CGA production mode was used in both CGA characterization (size) and flotation. In that process, the whole generator

are well sealed to avoid any liquid or gas leak; after pre-agitating the surfactant solution for 1.5 min, the continuous generation started: the same type of peristaltic pump as aforementioned in Chapter 3 (Masterflex L/S, with pump head, HV-7518-00, Cole-Parmer Instrument Company, USA) was used to inject the surfactant solution into Container A from Inlet 1 and control the flow rate simultaneously; the air flow governed by a gas flow meter was input from the bottom center of the container (Inlet 3), and the generated CGA suspension went out from Outlet 2. In this case, the flow rate of surfactant solution Q_{surf} equals to that of CGA suspension Q_{CGAs}.

4.1.2 CGA characterization

The properties of CGAs were investigated in the current study in terms of optic microscopic visualization, half life, bubble size, and zeta potential. The batch and continuous generation modes were used and compared. The concentration, pH value and flow rate of surfactant solution, and as well as air flow rate were all investigated for their influences on CGA characteristics. Results attained and relative analysis and discussion are given in this part. Fig. 4.3 presents photos of CGA suspension during and after the generation process, clearly showing a milky appearance as “white water” which is often observed in the case of microbbuble suspension with an average bubble diameter of 10~100 μm in flotation (Edzwald, 2010).

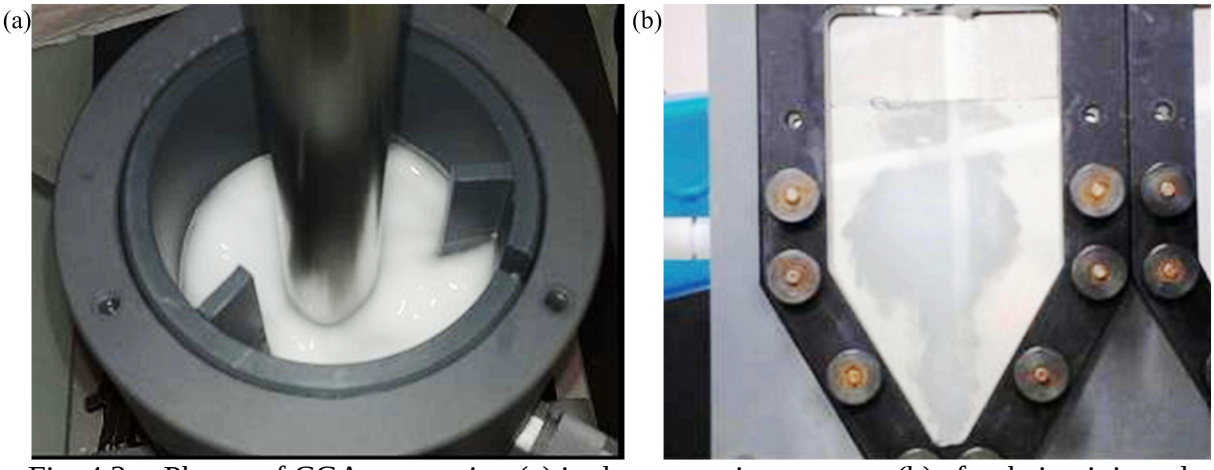

Fig. 4.3. Photos of CGA suspension (a) in the generation process, (b) after being injected into the measuring chamber from the bottom entrance.

4.1.2.1 Visual observation

The visualization of CGAs was performed on an optical microscope (Leica DM1000, Germany) with a CCD camera (Guppy PRO, Allied Vision Technology, Germany) installed on the phototube and linked to the computer. The CGA suspension was carefully collected by plastic Pasteur pipette immediately after production and dropped on the glass slide. Digital images of CGAs were then obtained.

The visual observation was made for CTAB-CGAs and SDS-CGAs produced at different surfactant concentrations. Images in Fig. 4.4 showed the morphology of CGAs immediately after generation, and a rather similar CGA photo was also obtained by Johnson et al. (2009) using a conventional light microscope. Optic microscope photos of regular bubbles were also given in Fig. 4.5 as comparison. For an ordinary gas bubble in water as Fig. 4.5(a) (CO_2 bubbles in a cola drink), it can be treated as a cavity enclosed by water; as for a soap bubble, any cavity introduced in water creates a water-gas interface where surfactants are adsorbed (Fig. 4.5(b)) (Chaphalkar, 1994). In the case of CGAs, as suggested by Sebba, they should be encapsulated by a layer of soapy shell. The soapy shell has an inner as well as an outer surface and both of them have surfactant monolayers adsorbed on them. The inner surface has oriented surfactant molecules that are hydrophilic pointing inward and hydrophobic outward, and the outer surface has surfactant molecules that are hydrophobic outward. The hydrophobic outer surface adsorbing surfactant ions from bulk water is electriferous to form diffuse electrical double layers. If the cationic surfactants are used to form CGAs, the outer surface of the gas bubble may be positively charged due to the ionization of surfactants (Dai and Deng, 2003). According to the scale on the photo, the apparent diameters of CTAB-CGA and SDS-CGA were in the range of 30~180 μm and 30~160 μm, individually. The microphotography could provide the morphology of CGAs, but the microbubble might suffer a distortion and the size possibly deviated from the truth caused by the disturbance during the bubble's transportation from the generator to the microscope. Thereby, in the following work, it is necessary to use LDS to obtain the CGA size distribution.

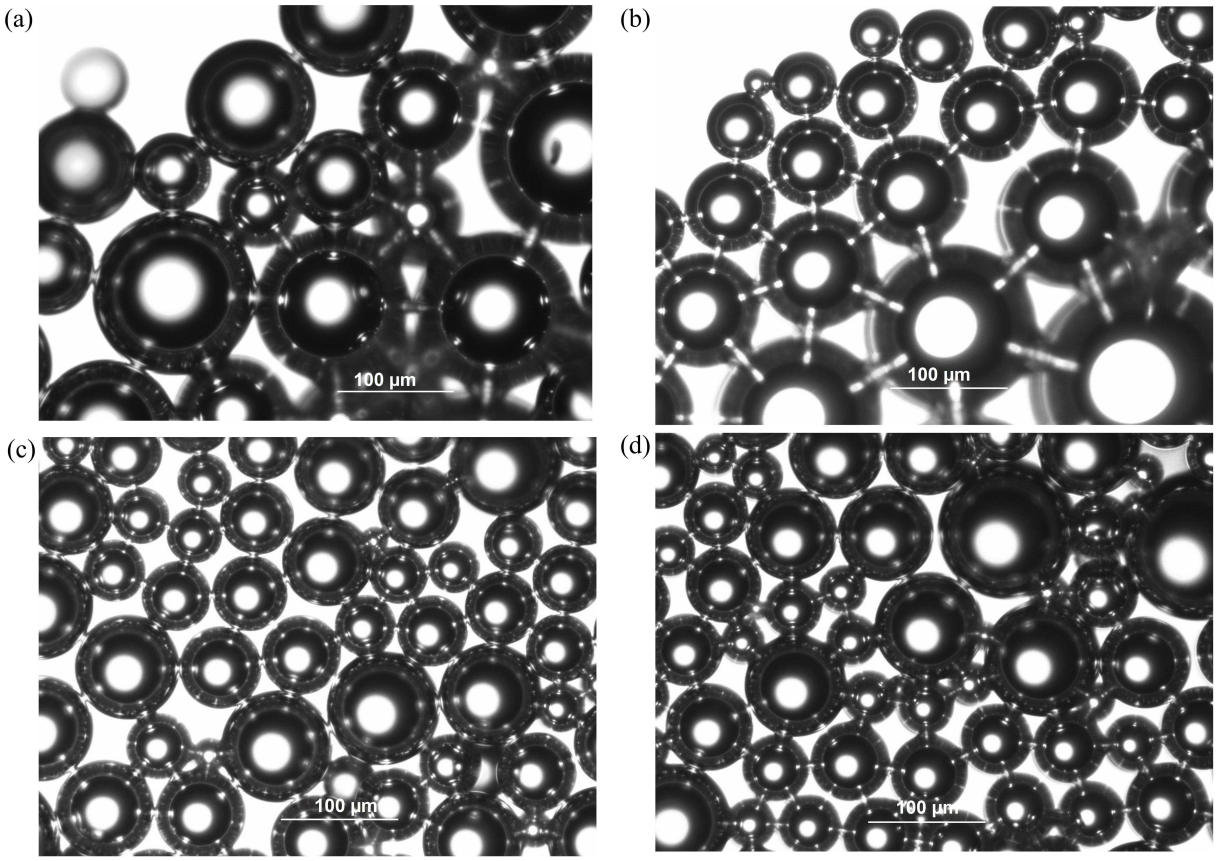

Fig. 4.4. CGA images of microscope obtained immediately after generated from (a) 0.6 mmol/L CTAB solution; (b) 1.0 mmol/L CTAB solution; (c) 4 mmol/L SDS solution; (d) 8 mmol/L SDS solution.

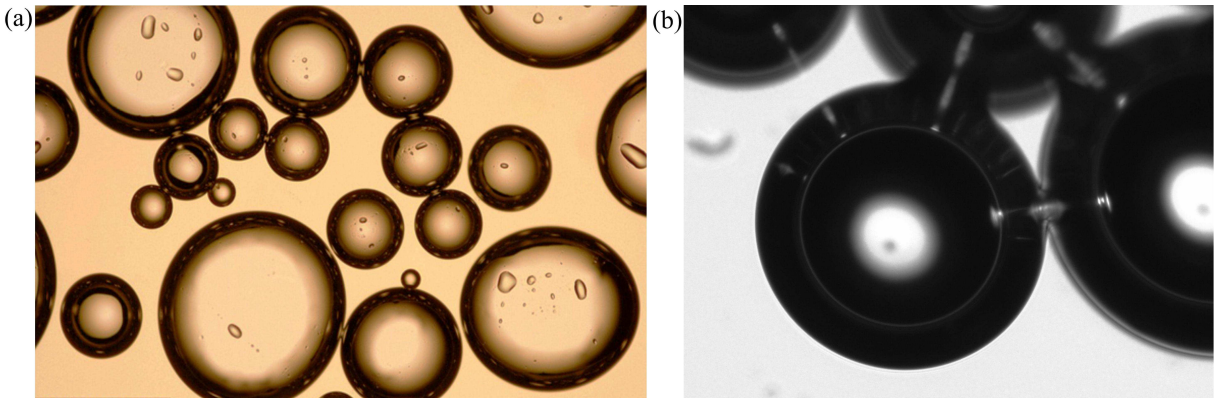

Fig. 4.5. Optic microscope images of regular bubbles: (a) CO_2 bubbles in a cola drink ("The true colours of fizzy drinks," n.d.), (b) soap bubbles by handshake.

A dark layer was always found in the CGA image of optic microscope due to the light refraction (shown in Fig. 4.6(a)), which was quite similar to the observation attained by Johnson et al. (2009). The following discussion aimed at figuring out whether this dark layer was caused by the surfactant layer encapsulating the air core of CGA. As stated by Snell's law, the ratio of sine angles of incidence and refraction is equivalent to the opposite ratio of

refraction indices. In the case of optic microscopic observation of gas bubbles, lights went thought the water-bubble interface from the water medium into the gas medium inside bubble:

$$\frac{\sin\theta_{water}}{\sin\theta_{air}} = \frac{n_{air}}{n_{water}} \tag{4.1}$$

with θ_{water} and θ_{air} as the angles of incidence and refraction, respectively, and n_{water} and n_{air} as the refractive indices of water and air that equal to 1.33 and 1.00, respectively. When the θ_{air} reaches 90° ($\sin\theta_{air}$ =1) and thus θ_{water} can be calculated as 48.8° by Eq. 4.1, the light refraction will not happen on the water-bubble interface and thereby the incident ray will be totally reflected (the red arrow in Fig. 4.6(b)). Hence, one dark layer forms between the incident ray with the angle of incidence of 48.8° and the ray passing tangentially the bubble.

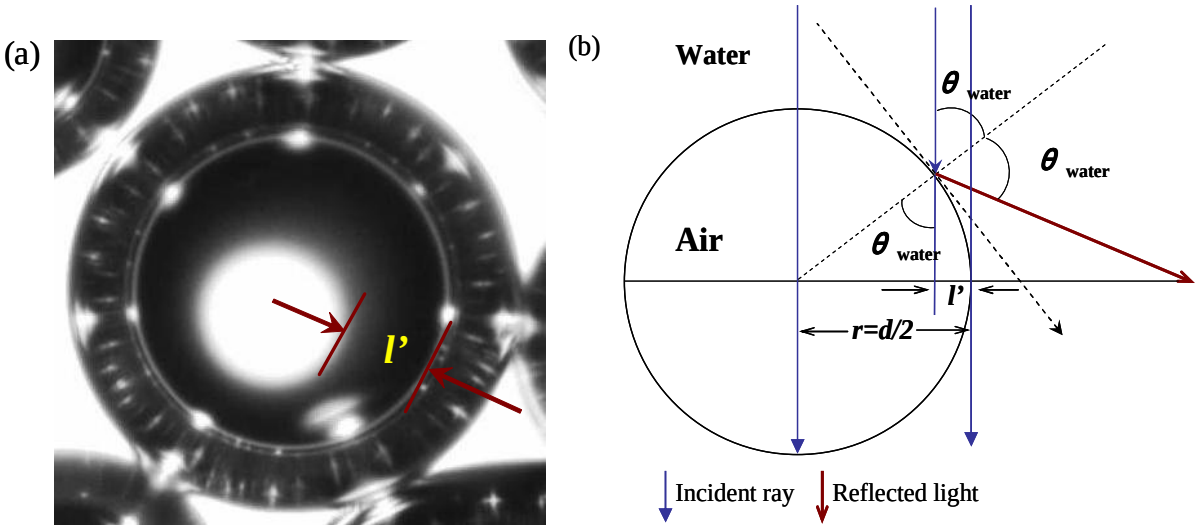

Fig. 4.6. Formation of the "dark layer" on the bubble image of optic microscope: (a) CGA photo; (b) schematic calculation of the dark-layer thickness.

Here, the thickness of this layer is presented as l' (see in Fig. 4.3). On knowing the average bubble size, l' can be easily figured out via the following way:

$$l' = r - r\times\sin\theta_{water} = \frac{d}{2} - \frac{d}{2}\sin\theta_{water} = \frac{d}{2}\left(1-\sin\theta_{water}\right) = 0.124d \tag{4.2}$$

where, $\sin\theta_{water}$ =1/1.33; r and d are the bubble radius and diameter, respectively. The CGA diameter normally falls in the range of 10~100 μm (Jauregi et al., 2000; Molaei and Waters, n.d.), and thereby l' can be calculated to be 1.24~12.4 μm (This rough calculation does not take into account the postulated double layer of surfactant and the refractive index of inside surfactant solution.). As summarized in the review of CGAs by Hashim et al. (2012), the possible thickness of surfactant double layer was measured or estimated to be from 96 nm to

750 nm for different surfactants, much smaller than the thickness of dark layer l' obtained in the present work. Therefore, this dark layer is not the double layer which is featured with highly concentrated surfactant solution inside and surfactant molecules on both inner and outer surfaces as proposed by Sebba (Platz, 1989). Herein, the dark layer was rather possibly resulted from the attachment of CGAs on the surface of glass slide.

4.1.2.2 Stability of CGAs -- half life τ_S

CGAs have to be pumped into the solution for the purpose of separation or flotation, and therefore a study of their stability is important under conditions when CGAs are pumped and mixed with an aqueous stream. "Stability" of the microbubble dispersion can be defined as the length in time over which the number of bubbles and their size distribution remains constant (Chaphalkar, 1994). The stability was measured with regard to half life (τ_s), the time required for half of the liquid content to drain. It depicts primary drainage during which the aphron structure is maintained. This was measured by transferring certain amount of CGA suspension into a 250-mL graduated cylinder and monitoring the drainage with time. The volume of CGA suspensions defined as the gas fraction was calculated from the final liquid volume and the total volume (Kommalapati et al., 1996).

The stability of CGAs may be affected by the interaction of surfactant molecules on the aphron surface, which is quite related to the surfactant concentration. The impact of air flow on the bubble stability has not been reported in any other research of CGAs and should be estimated here. Given the consideration above, the surfactant concentration and the air flow rate were investigated here for their influence on the CGA stability.

(1) Effect of surfactant concentration

The liquid drainage of CGAs as a function of time is depicted in Fig. 4.7. Different surfactant concentrations (below, close to and above the CMC) were investigated. CGAs herein were created in the batch mode without air input, and the initial volume of surfactant solution was approximately 150 mL. It could be seen that all the diverse surfactant concentrations tested resulted in drainage curves of the same form which exhibited an "S"-shaped profile. It can be inferred that the basic mechanism of drainage was similar in all the cases, and did not vary

with the solution composition. To describe the drainage kinetic curves, a three-parameter equation (Hill equation) was used (Yan et al., 2005):

$$V_t = V_{\max} \frac{t^n}{K^n + t^n} \tag{4.3}$$

where V_t refers to the volume of drained liquid at time t, $V_{\max}$ refers to the maximum volume of drained liquid, n describes the sigmoidal character of the curve, and K is equal to the τ_S of drainage. It has been long known that the Hill equation often gives a good approximation to more realistic and much more complex models, and many experimental cases have been characterized only in terms of the Hill equation (Hofmeyr and Cornish-Bowden, 1997). The parameters $V_{\max}$, K (τ_S') and n were estimated using nonlinear least squares regression, and the fitting curves are presented in Fig. 4.7 and those three statistical parameters and the half life values τ_S attained from experiments are given in Table 4.1.

As shown in Fig. 4.7 and Table 4.1, different surfactant concentrations are corresponding to different τ_S values: for both CTAB and SDS, τ_S increased when the concentration grew from half of CMC to around CMC, but further increasing the concentration affected the CGA stability slightly. Generally, the CGA drainage rate would reduce because of greater surface viscosity and surface elasticity which could be achieved by packing higher concentrations of surfactant (or particles) on the surface and resulting in high adhesive or cohesive bonding. The difference among τ_S values for different surfactant concentrations was thought to be the result of CMC. When the surfactant concentration was below the CMC, there were insufficient surfactant molecules present in the bulk to stabilize the large amount of interfacial area, whereas the τ_S value rose when the concentration was equal or close to CMC. As the surfactant concentration grew and exceeded the CMC, further addition of surfactant had a negligible effect because the additional surfactant molecules remained in the micelle suspended in the fluid film surrounding CGAs (Yan et al., 2005). It is seen from Fig. 4.7 that the drainage curves for all concentrations of CTAB and SDS displayed a similar variation trend: the τ_S of drainage from CTAB-CGAs ranged between 124 s and 170 s while for SDS-CGAs the range was 147~180 s. This indicated that CGAs produced from both these two surfactants had stability degrees alike, which was consistent with earlier findings by Chaphalkar et al. (1993) and Yan et al. (2005). Comparing the experimental results with the fitting curves by Eq. (4.3), it could be found that the Hill equation does not always

approximate the liquid drainage of CGAs. The fitted half life K was not far from the experimental result τ_S mainly at the beginning of the drainage process.

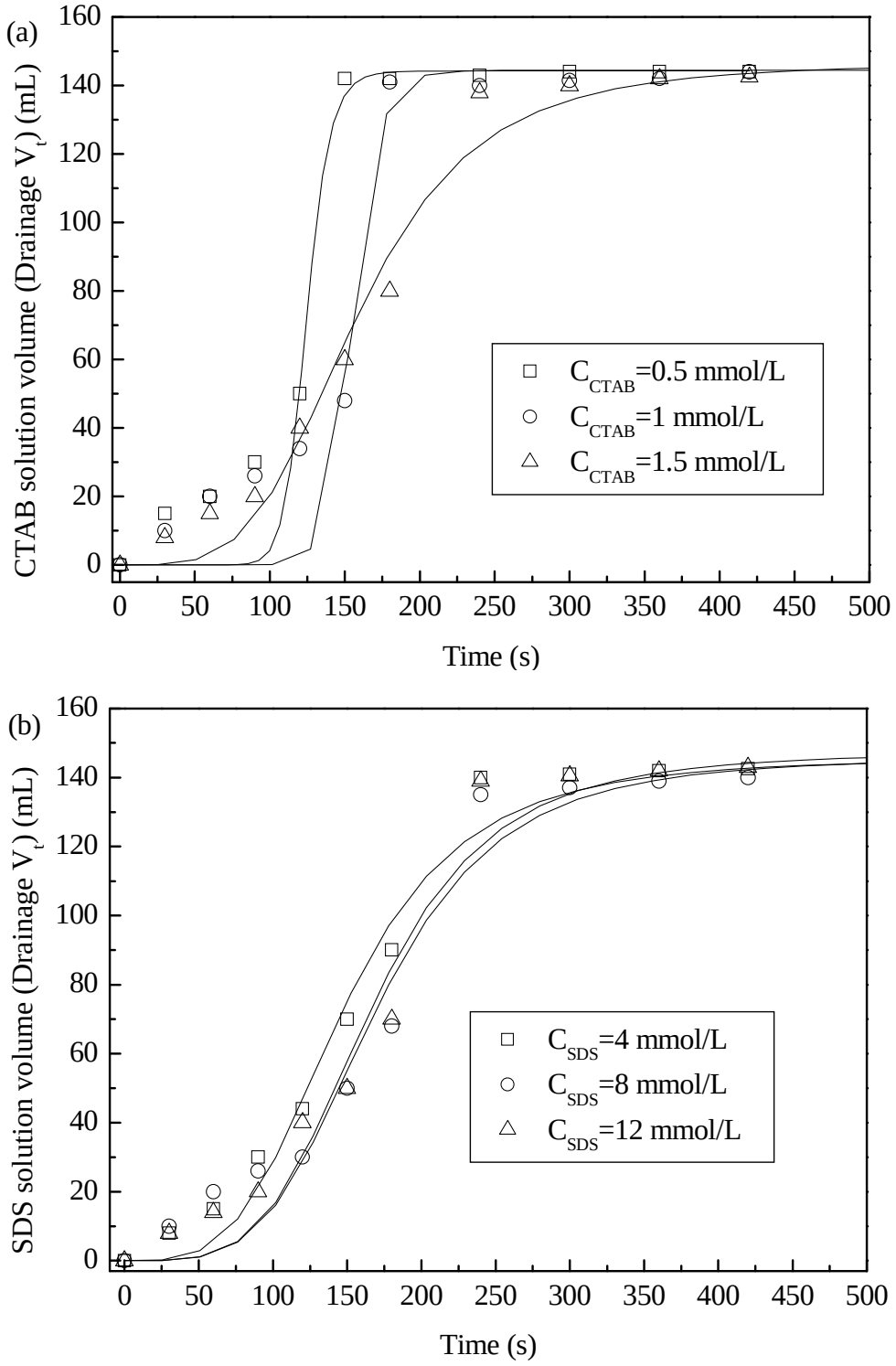

Fig. 4.7. Comparison between experimental data (scatters) and fitting drainage curves (curve) at different surfactant concentrations: (a) CTAB-CGAs, (b) SDS-CGAs.

Table 4.1. Parameters by Hill equation fitting and experimental values at different surfactant concentrations.

Surfactant solution	$V_{max} \pm \sigma_V$ (mL)	$K \pm \sigma_K$ (τ_s') (s)	$n \pm \sigma_n$	R^2	τ_S (s)
0.5 mmol/L CTAB	144.3±6.7	124.5±4.4	15.9±10.6	0.953	125.3
1.0 mmol/L CTAB	144.4±3.3	155.2±3.5	17.1±7.0	0.954	155.4
1.5 mmol/L CTAB	146.6±2.1	158.9±4.4	4.0±0.4	0.987	168.3
4 mmol/L SDS	145.8±2.0	147.4±4.2	3.6±0.4	0.987	154.7
8 mmol/L SDS	145.8±2.8	169.7±6.4	4.1±0.6	0.976	181.7
12 mmol/L SDS	147.3±2.6	166.8±5.7	4.1±0.5	0.980	179.6

(2) Effect of air input

The effect of air flow on the CGA stability was studied by investigating different flow rates in the generation process at the fixed surfactant concentration. The initial volume of surfactant solution turned to be approximately 90 mL since the volume of the generator was restricted but the volume of CGA suspension grew much faster and larger compared with the case without air input. Experimental results and fitting curves from Eq. 4.3 are depicted in Fig. 4.8 and parameters obtained by modeling fitting are given in Table 4.2. Compared with the fitting curves in Fig. 4.7, the experimental data of CGA generation in the presence of air flow were better fitted by the Hill equation. It seems that the τ_S of CGAs in the presence of air flow during creation process is specific to different surfactants: for CTAB-CGAs, the τ_S value decreased to some extent (from around 120 s to 98 s by modeling fit and from 130 s to 74 s by experiments) as the air flow rate increased. The air injection speeded up the drainage of liquid content and led to less stable CGAs. To the contrary, as for SDS-CGAs, the stability was largely enhanced along with higher air flow rates.

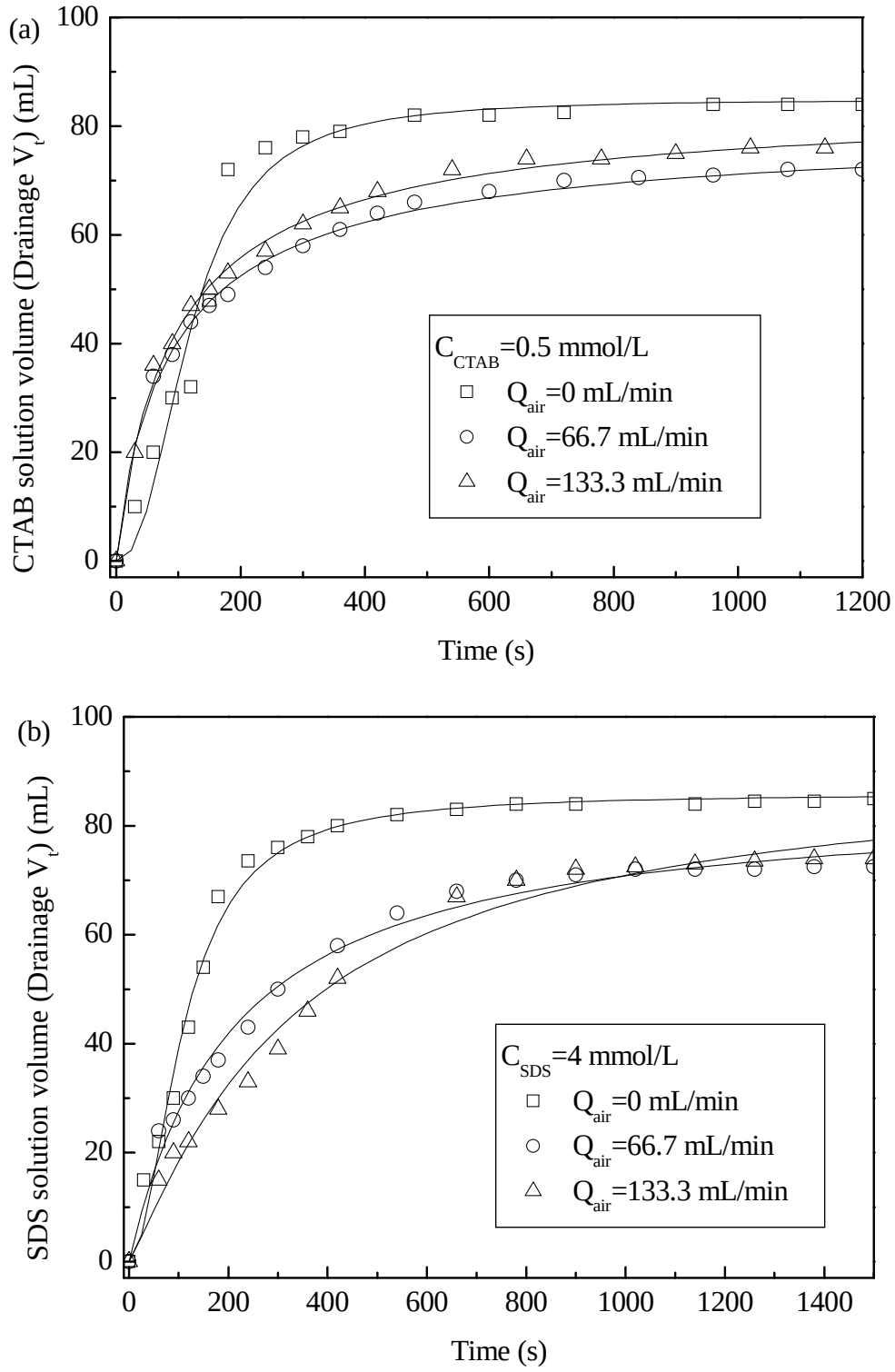

Fig. 4.8. Comparison between experimental data (scatters) and fitting drainage curves (curve) at different air flow rates: (a) CTAB-CGAs, (b) SDS-CGAs.

Table 4.2. Parameters by Hill equation fitting and experimental values at different air flow rates.

Surfactant solution	$V_{max} \pm \sigma_V$ (mL)	$K \pm \sigma_K$ (τ_S') (s)	$n \pm \sigma_n$	R^2	τ_S (s)
0.5 mmol/L CTAB + 0 mL/min air	84.9±2.1	119.1±6.9	2.4±0.3	0.966	138.0
0.5 mmol/L CTAB + 66.7 mL/min air	80.5±1.9	97.5±5.4	0.9±0.1	0.992	79.2
0.5 mmol/L CTAB + 133.3 mL/min air	84.7±1.9	97.8±5.9	0.9±0.1	0.994	74.4
4 mmol/L SDS + 0 mL/min air	85.9±1.4	109.7±4.7	1.9±0.2	0.984	118.8
4 mmol/L SDS + 66.7 mL/min air	85.2±4.4	206.7±26.3	1.0±0.1	0.986	172.5
4 mmol/L SDS + 133.3 mL/min air	91.4±6.9	336.6±56.8	1.1±0.1	0.983	280.3

(3) Drainage mechanism discussion

The rate and time of CGA drainage can be derived by differentiating Eq. 4.3 along with time t, which yields (Yan et al., 2005):

$$\frac{dV_t}{dt} = \frac{nV_{max}K^n t^{n-1}}{\left(K^n + t^n\right)^2} \tag{4.4}$$

The drainage data of CTAB-CGAs and SDS-CGAs were selected at the fixed surfactant concentration (half of CMC) in the absence and presence of air flow during the generating process, respectively (Fig. 4.9). At Q_{air} =0 mL/min, drainage curves for both CTAB-CGAs and SDS-CGAs exhibited rapid increasing rates from the beginning of drainage until their maximum, and then declined toward zero with time. However, when keeping inputting air into the generator during the CGA creation (Q_{air} =66.7 mL/min), both kinds of CGAs showed a short and sharp drop in the drainage rate from the initial value, and thereafter reduced slowly to zero along with time increasing.

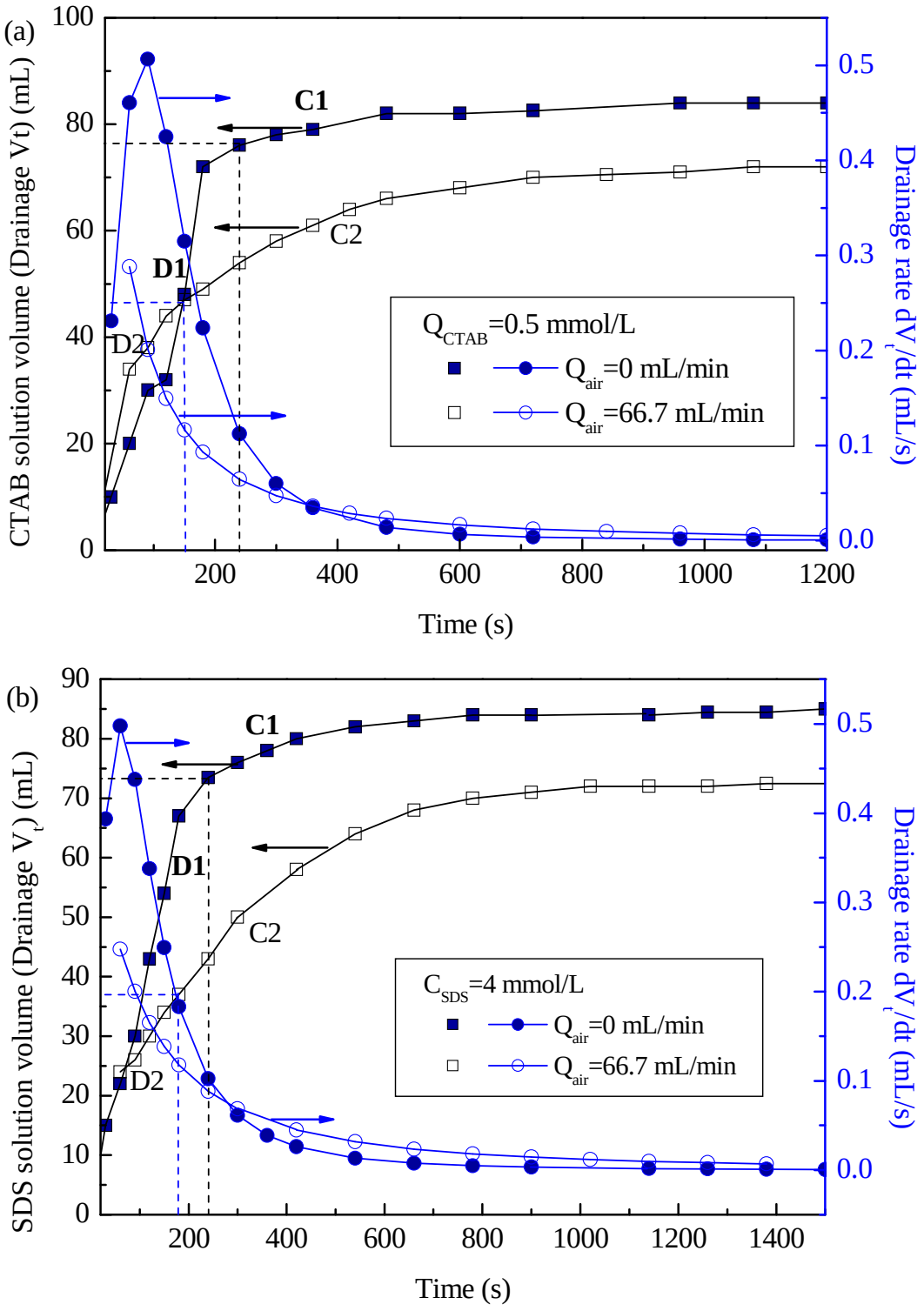

Fig. 4.9. Liquid drainage rate as a function of time: (a) CTAB-CGAs; (b) SDS-CGAs (C_{surf} ≈0.5CMC). Arrows indicate corresponding axis.

According to Yan et al. (2005), the drainage process can be divided into two stages. The first stage is rapid and almost linear with time till the formation of conventional foam, being dominated by gravity driven liquid drainage. In the absence of air input, the removal of more

than 90 % (for CTAB-CGAs) or 86 % (for SDS-CGAs) of the total liquid could be achieved (Region D1), while approximately 65 % and 50 % of the total liquid in CTAB-CGAs and SDS-CGAs would drain in the presence of air during the CGA production (Region D2). The secondary drainage involving the thinning of films is comparatively much slower as seen from Fig. 4.9 (Region C1 and C2). Further drainage of the liquid in the lamellae and plateau borders continues under the influence of capillary pressure and plateau border suction. When the liquid film becomes sufficiently thin (< 0.1 µm) the effect of London-van der Waals forces and the repulsive force of any electrostatic double layer also become important. Eventually, the films rupture and the bubbles coalesce. Inputting air during generation slowed down the drainage speed of CGAs especially in the first stage, and this reinforced stability might help CGAs to capture more NPs in suspension by retarding the deformation and collapsing of these aphrons.

4.1.2.3 Size measurement

(1) Spraytec setup and experimental procedure

The size measurement of CGAs was conducted via laser diffraction by Spraytec (Fig. 4.10) which is specially conceived to investigate highly transient dense sprays (Malvern, UK). Similar practices concerning the size determination of CGAs or colloidal liquid aphrons (CLAs) can be found in others' study (Chaphalkar et al., 1993; Kommalapati et al., 1996; Lye and Stuckey, 1998). As shown in Fig. 4.11(a), the CGA size measurement is performed in a chamber equipped with glass windows through which a low power He-Ne laser could pass. This chamber is also used as flotation cell in the following flotation experiments of this study and other previous DAF trials (Liu 2010; Liu et al., 2012; Zhang and Guiraud, 2013). The generated CGAs enter the cell from the bottom (Fig. 4.11(b)) and scatter laser light during the analysis process. The wavelength and diameter of the laser beam are 632.8 nm and 10 mm, respectively. At small forward angles, the scattering is predominantly resulted from diffraction and the angle of the scattered light is inversely proportional to the size of the bubbles. The detectors are equipped by a series of 36 concentric annular silicon diodes placed at the focal point of a Fourier lens, which convert the incoming rays of scattered light in to a far-field diffraction pattern (Simmons and Hanratty, 2001; Dumouchel et al., 2009). The collecting lens applied here have a focal length equal to 300 mm and the measurable diameter range is 0.5~600 µm. The volume-based diameter, $D_v(50)$, is used as the mean CGA diameter. The instrument software includes the correction for the effect of multiple scattering, allowing

measurements to be made with only 5 % transmittance of the incident laser beam; and all measurements were made at transmittance down to 25 % here.

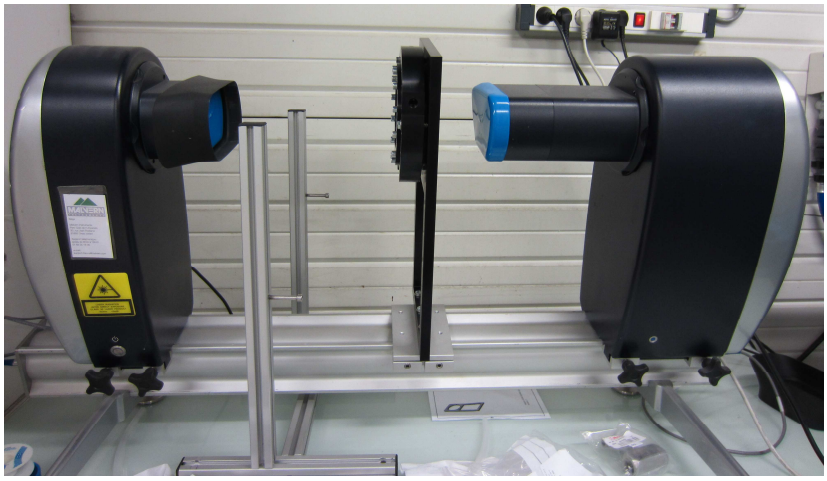

Fig. 4.10. Spraytec apparatus with measurement cell for size analysis.

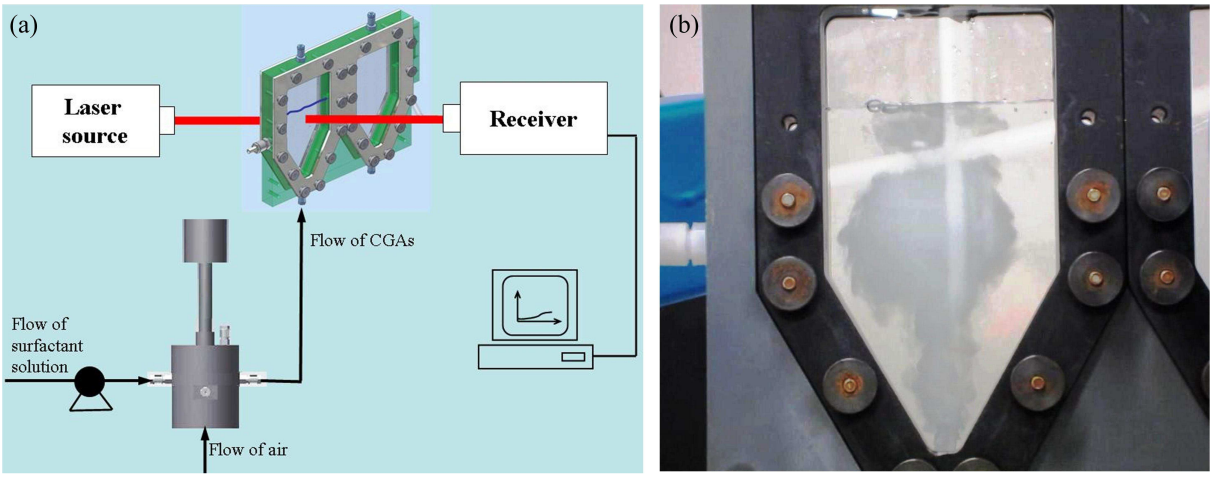

Fig. 4.11. (a) Schematic diagram of the equipment used for determining the CGA size; (b) photo of CGAs entering into the measuring chamber from the bottom.

(2) Determination of suitable measurement conditions

The difficulty of microbubble size measurement mainly comes from the determination of the appropriate bubble concentration range: a too low bubble concentration cannot provide sufficient data for a correct statistical analysis, whereas an overconcentrated bubbling sample will stop the laser beam from going it through such that the measurement is hindered owing to this multiple diffraction. The effect of concentration is visible at the transmittance lower than 5 % for Spraytec, and the results could only be attained above this value to ensure the accurate measurement. The bubble concentration changes inside the measurement chamber during the measurement process and consequently influences the transmittance. Hence, the

measurement period has to be carefully determined before examining the influence of stirring speed which is the primary parameter governing the CGA size measurement result.

- **Transmittance (CGAs produced in the batch mode)**

CGAs (C(CTAB)=0.5 mmol/L and C(SDS)=4 mmol/L, approximately half of their CMC) were produced at the stirring speed of 8000 rpm for 5 min. A volume of 50 mL CGA suspension was carefully collected and immediately transferred by 50 mL-syringe after creation to the measurement cell where 200 mL deionized water had already been pre-injected for the background measurement. The temporal evolutions of bubble size and transmittance are shown in Fig. 4.12 which was attained under the condition that the CGA suspension was added into the measurement cell at t=0 s after the measurement began. Each measurement was replicated.

As shown in Fig. 4.12, the size data could not be obtained immediately after the addition of CGA suspension (t=0 s to 20 s) due to the high light obstacle (low transmittance) of over 95 %. As the bubbles dispersed in the chamber, the bubble concentration decreased and resulted in the increase of light transmittance (higher than 5 %). The bubble size obtained kept stable and correct at t=20~50 s. Thereupon, the bubble size experienced a sharp jump possibly because the bubble concentration was too low to achieve a stable and convincing size measurement with the transmittance between 50~100 %. During the measuring duration of 20~50 s, the average size of CTAB-CGAs was determined to be 22.3±1.5 μm, and the first and second measurement results at the transmittance of 25 % were 23.2 μm and 21.9 μm, respectively; the average diameter of SDS-CGA was found to be 23.5±0.7 μm, and the two measurement data at the 25 % light transmittance were 23.0 μm and 24.0 μm, respectively. Obviously, results obtained at the transmittance of 25 % was right in the average diameter size, and hence are considered to be the representative CGA sizes in the following size measurement. CGA size distributions are shown in Fig. 4.13. The measurement exhibited the good repeatability: the CGA size kept fluctuating in the range of 20~24 μm for CTAB-CGAs and 21~26 μm for SDS-CGAs. All the monomodals indicated the uniform bubble size distribution within the stable measurement duration.

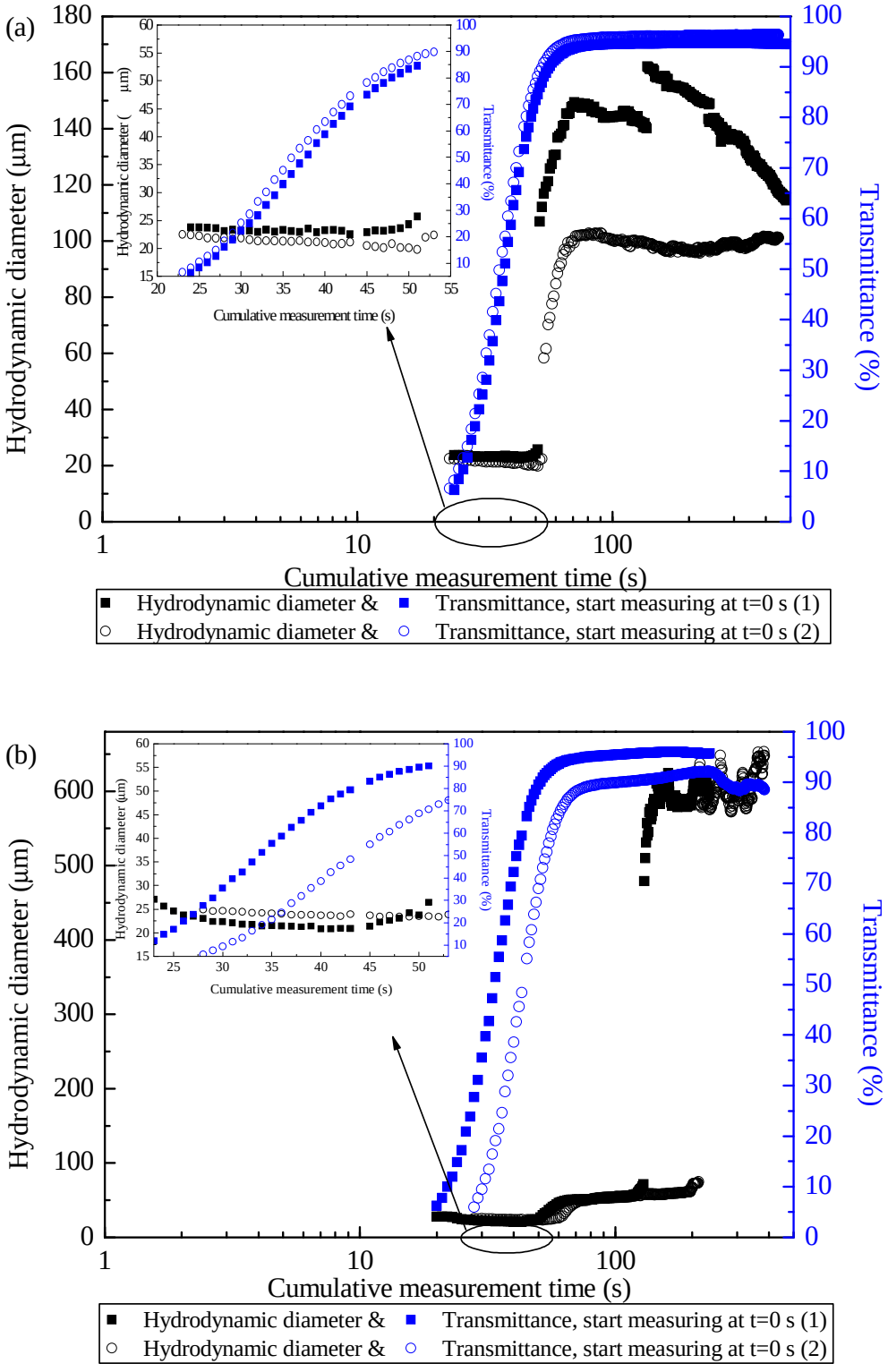

Fig. 4.12. Spraytec measurement immediately after the measurement began: (a) CTAB-CGAs; (b) SDS-CGAs. (Experiments were replicated.)

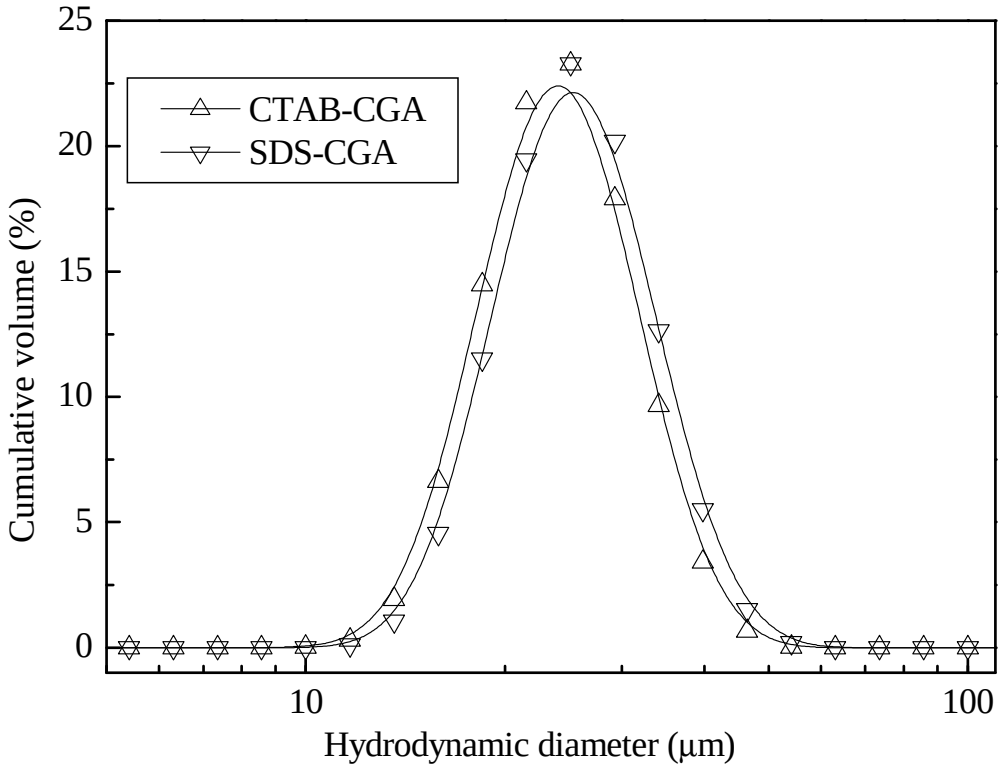

Fig. 4.13. Bubble size distribution of CGAs.

To examine and minimize the technique disturbance from the Spraytec measurement, another series of trials was also conducted by adding the CGA suspension 30 s after the Spaytec measurement started (see in Fig. 4.14). The measurement data were attained at 30~50 s after the addition of CGA suspensions. Compared with Fig. 4.12 in which the stable measurement duration was 30 s, herein the duration of CTAB-CGAs was about 26 s and that of SDS-CTAB was around 29 s, after which the bubble size measurement would increase greatly caused by the bubble crashing. By this way of measurement, the average size of CTAB-CGAs and SDS-CGAs was 23.4±0.04 μm and 26.3±0.41 μm, respectively. Given all the tests above, it was determined in this study that the CGA suspension was added immediately after the measurement began and results were obtained at the transmittance of around 25 %.

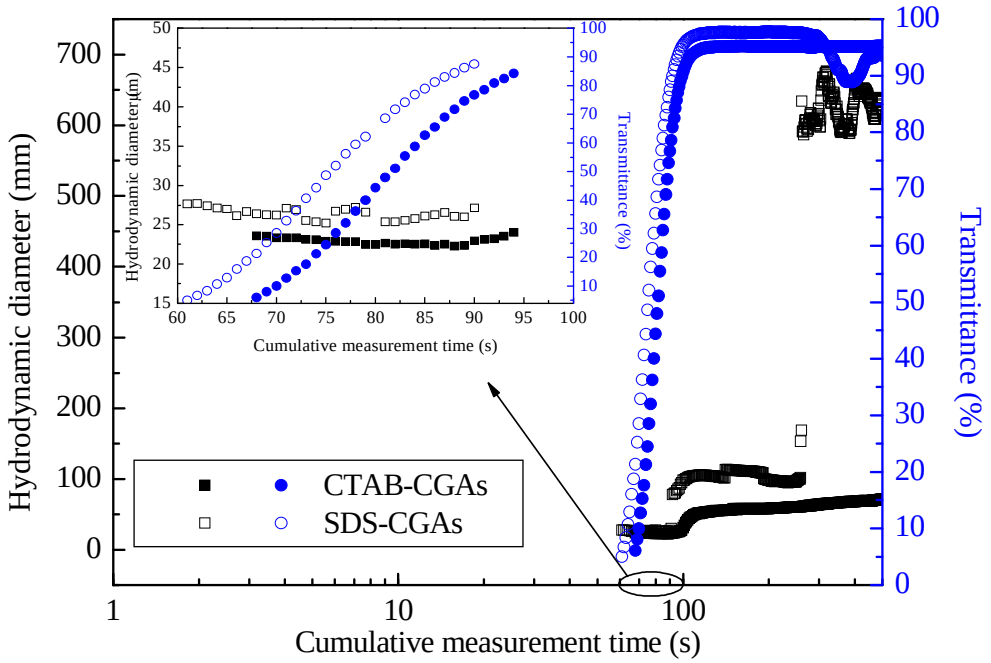

Fig. 4.14. Spraytec measurement at 30 s after the measurement began.

- **Effect of stirring speed in the continuous mode (CGAs produced in the continuous mode)**

The variation of CGA size with different stirring speeds of agitator was investigated for the determination of bubble creation condition. It was found in Fig. 4.15 and Fig. 4.16 that the CGA size reduced when the stirring speed increased from 3200 rpm to 10000 rpm: from 89.7 μm to 43.7 μm for CTAB-CGAs and from 81.5 μm to 38.4 μm for SDS-CGAs. The decrease became less and less important at the stirring speed higher than 6000 rpm. Under the tested conditions, 8000 rpm gave the narrowest CGA size distribution. Considering the great energy consumption of high stirring speed (i.e. 10000 rpm) and its limited help to further reduce the bubble size, 8000 rpm was finally used in all the following CGA generation.

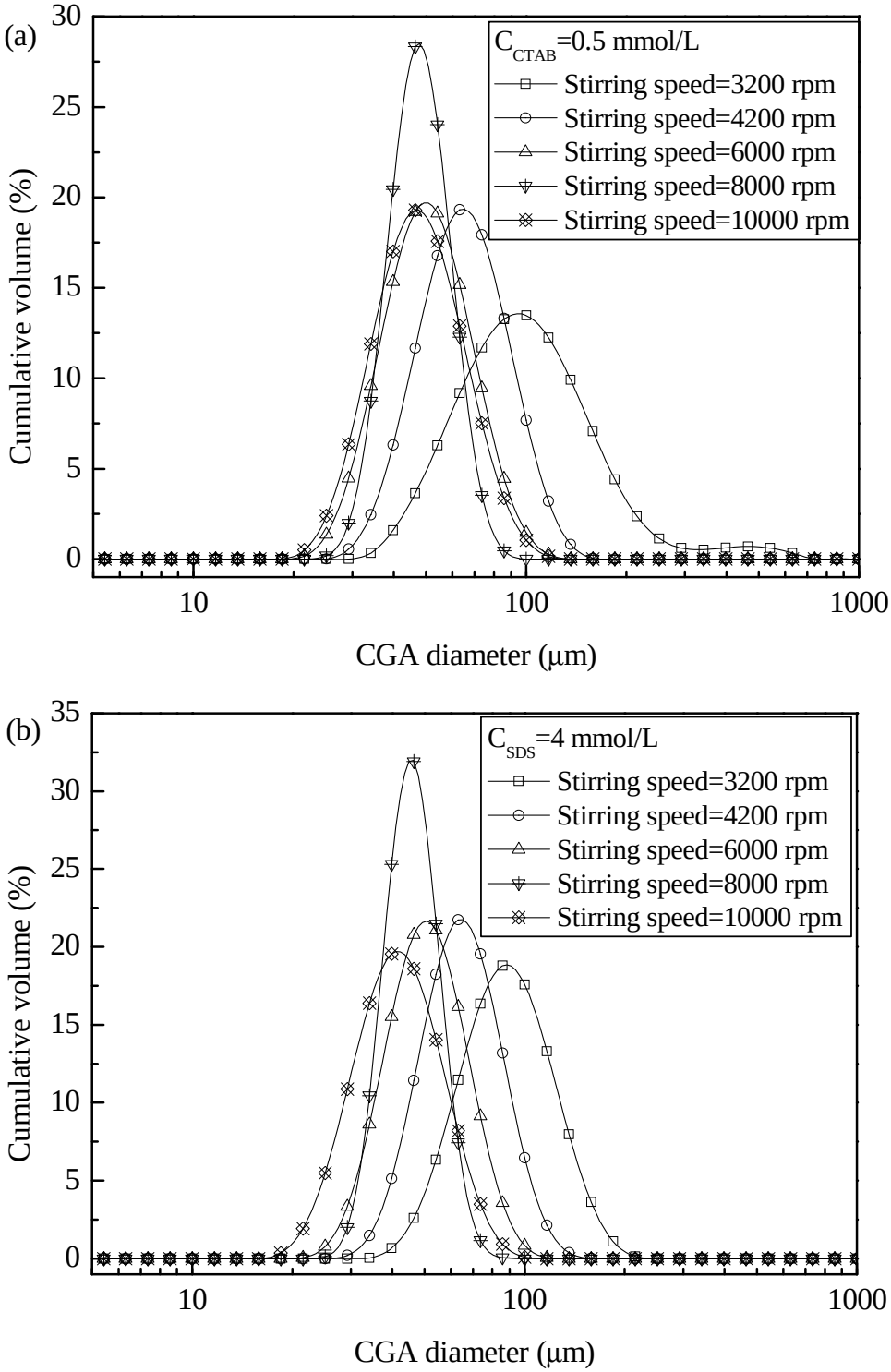

Fig. 4.15. Bubble size distribution of CGAs under different stirring speeds.

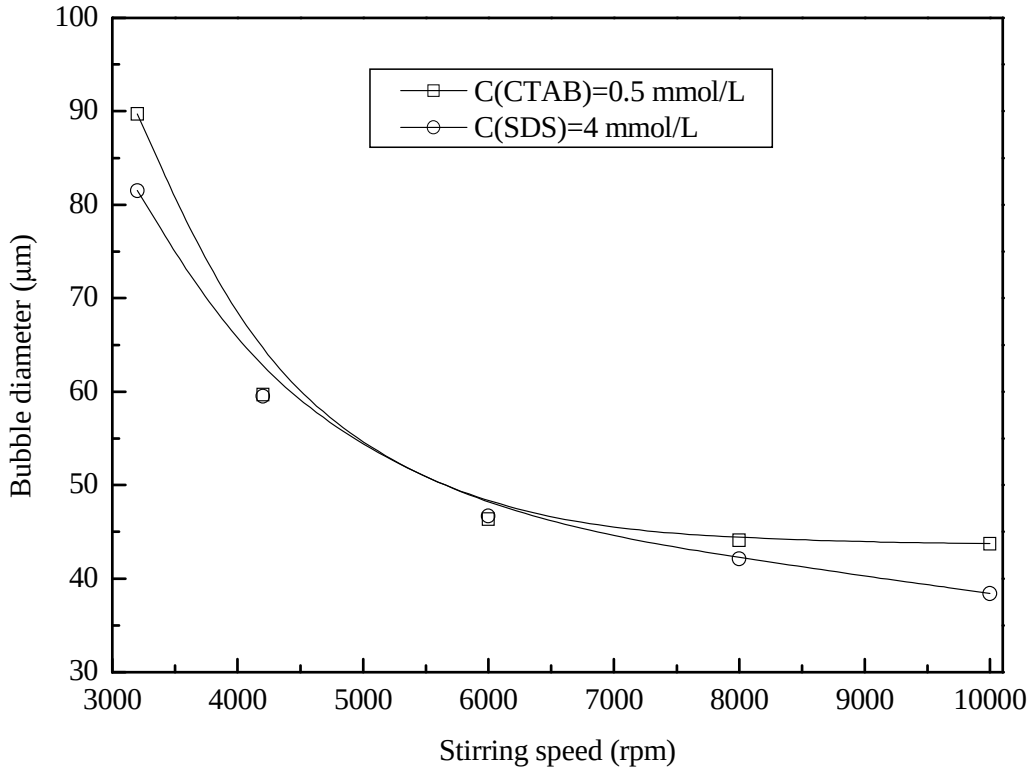

Fig. 4.16. Relationship between bubble size and stirring speed.

(3) Experimental investigation of CGA size

It is worth noting in Section 4.1.2.3(2) that the size measurement in the batch and continuous modes gave different CGA diameters: at the same surfactant concentration (0.5 CMC), the size obtained under the former condition was about 22 μm for CTAB-CGAs and 24 μm for SDS-CGAs, while results attained via the latter was around 44 μm and 42 μm, individually. Possibly this distinction of size measurement could be attributed to the following reasons:

(1) in the batch generation mode, without going through the outlet of generator and the inlet of chamber for Spraytec measurement, the careful collection of CGA suspension by syringe in the batch mode could avoid the destroy of CGAs by manipulation and kept them in small and uniform size. In the continuous mode, the transporting time of CGAs from generator to the measurement cell can be estimated as Eq. 4.5:

$$t_T = \frac{l}{\left(Q_{CGA} + Q_{air}\right) / \left(\pi \times d_{tube}^2 / 4\right)} \tag{4.5}$$

where t_T was the CGA transporting time; l, the length of the tube connecting the CGA generator and the measurement cell, equaled 1.2 m; the inner diameter of the tube d_{tube} was 10 mm. At the lowest Q_{CGA} ($=Q_{surf.}$) and Q_{air} that could be determined the peristaltic pump (8 mL/min), t_T was then calculated to be 115 s, in the same magnitude of the τ_S (80~150 s)

obtained in Section 4.1.2.2. Hence, the transportation of CGAs would not cause their instability.

(2) in the batch mode, the stirring and retention time in the generator for forming stable microbubbles was as long as 5 min; however, in the continuous mode, the contacting time $t_{contact}$ in the generator could be determined as $t_{contact} = V_{generator} / (Q_{surf} + Q_{air})$, where the $V_{generator}$ was 230 mL. For the $Q_{surf.}$ of 5~210 mL/min and Q_{air} 33.3 or 66.7 mL/min (applied in this study), the $t_{contact}$ was in the range of 0.8~6 min. For those Q_{surf} and Q_{air} values whose contacting time was in the same magnitude of that used in the batch mode (5 min), the CGAs might be of similar size.

- **Batch generation mode -- effects of concentration and pH of surfactant solution**

The surfactant concentration was thought to affect properties of CGA dispersion. Thus, CGAs were produced using CTAB and SDS at concentrations below, near and above their CMC level, and results are shown in Fig. 4.17. However, in this study, different concentrations of both CTAB and SDS solutions did not give rise to great difference in CGA size under the batch generation mode, and the average size of CTAB-CGAs was found to be approximately 24.4 μm, 24.5μm and 24.3 μm at CTAB concentrations of 0.5, 0.95 and 1.2 mmol/L, respectively, while that of SDS-CGAs was about 26.8 μm, 26.3 μm and 26.8 μm at 4, 7.5 and 10 mmol/L SDS, respectively.

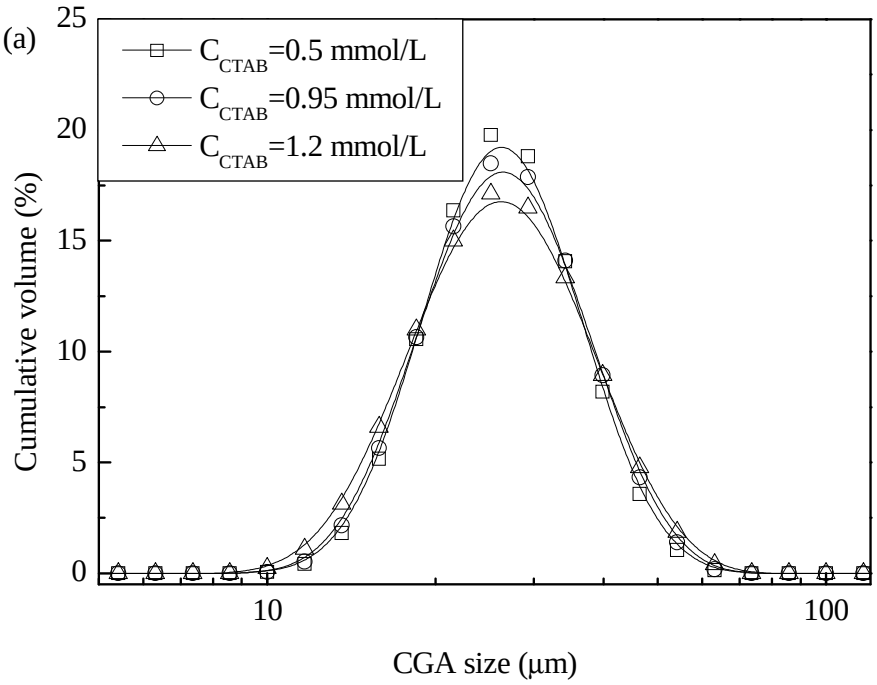

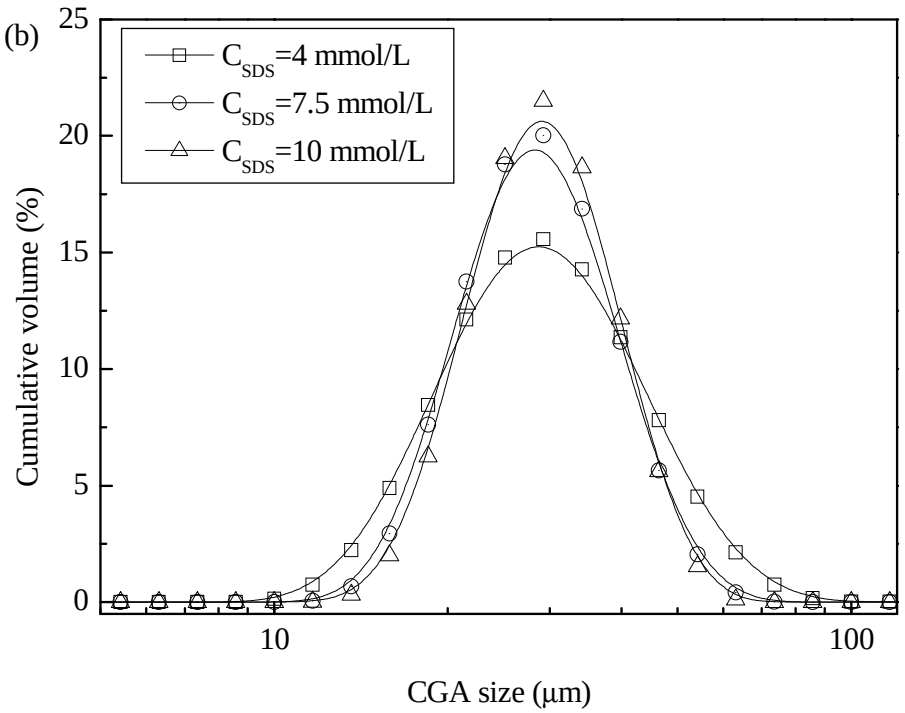

Fig. 4.17. CGA size distribution at different surfactant concentrations in the batch generation mode: (a) CTAB-CGAs and (b) SDS-CGAs.

As reported in the study of Chaphalkar (1994) (Fig. 4.18), when the surfactant concentration in the aqueous solutions is below its CMC, solute molecules will be distributed between CGAs and monomers. At concentrations above CMC, surfactant molecules will form micelles but because the CGAs are in high concentration, the solute will distribute mostly between CGAs and monomers. It is possible to achieve separation by using CGA dispersions even at CMC concentrations and above. That is quite different from what happens to normal soap bubbles generated from surfactant solutions: once the surfactant concentration reaches the CMC levels, separation efficiencies reduce dramatically because micelles have no tendency to adsorb at the air-water interface and thereby do not float with bubbles.

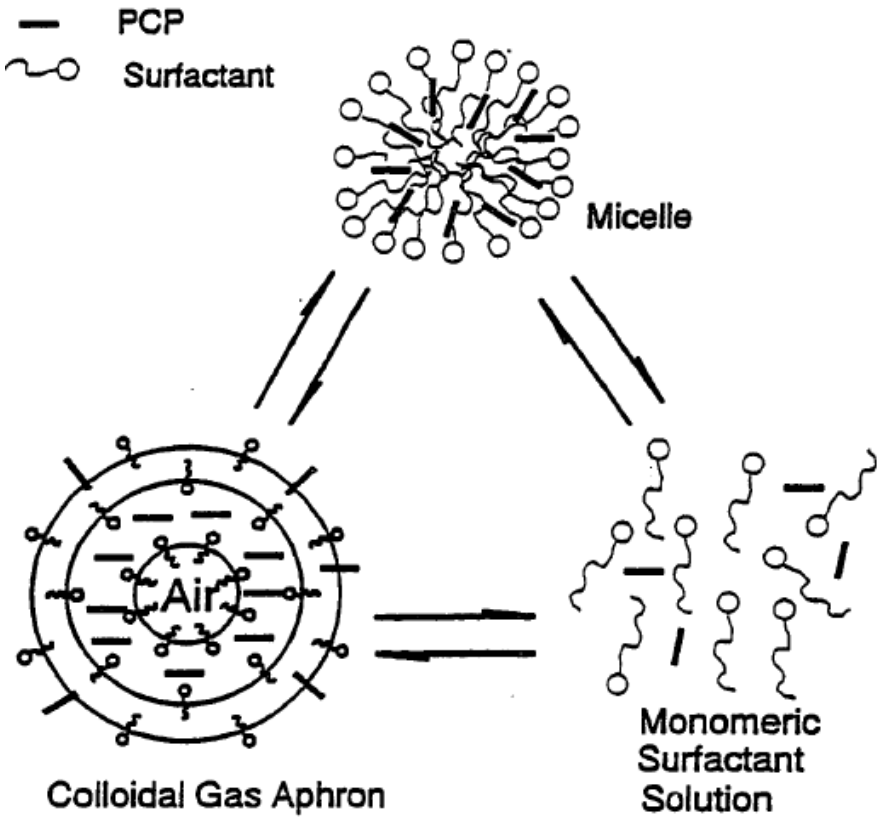

Fig. 4.18. Schematic of the solubilization process in the presence of CGAs and micelles (PCP: Pentachlorophenol, the separating target; surfactant: sodium dodecylbenzene sulfonate, hexadecyltrimethylammonium, or tergitol) (Chaphalkar, 1994).

The effect of pH value on the CGA size was also studied by testing acid, weakly acid and basic surfactant solutions in the generation process. Much the same as the concentration effect in the batch generation mode, no difference in size was found at the pH values of approximately 3, 6 and 9: the size of CTAB-CGAs kept at around 23.1±0.5 μm and that of SDS-CGAs remained at 22.6±0.3 μm (Fig. 4.19). This observation is in a good agreement with the previous report that the pH over a range of 2 to 14 has no effect on the property of CGAs that were made from sodium dodecylbenzene sulphonate (SDBS), Benzyldimethyl-*n*-hexadecylammonium chloride (BDHA) (Subramaniam et al., 1990), and cetyltrimethyl ammonium chloride (CTAC) (Save and Pangarkar, 1994).

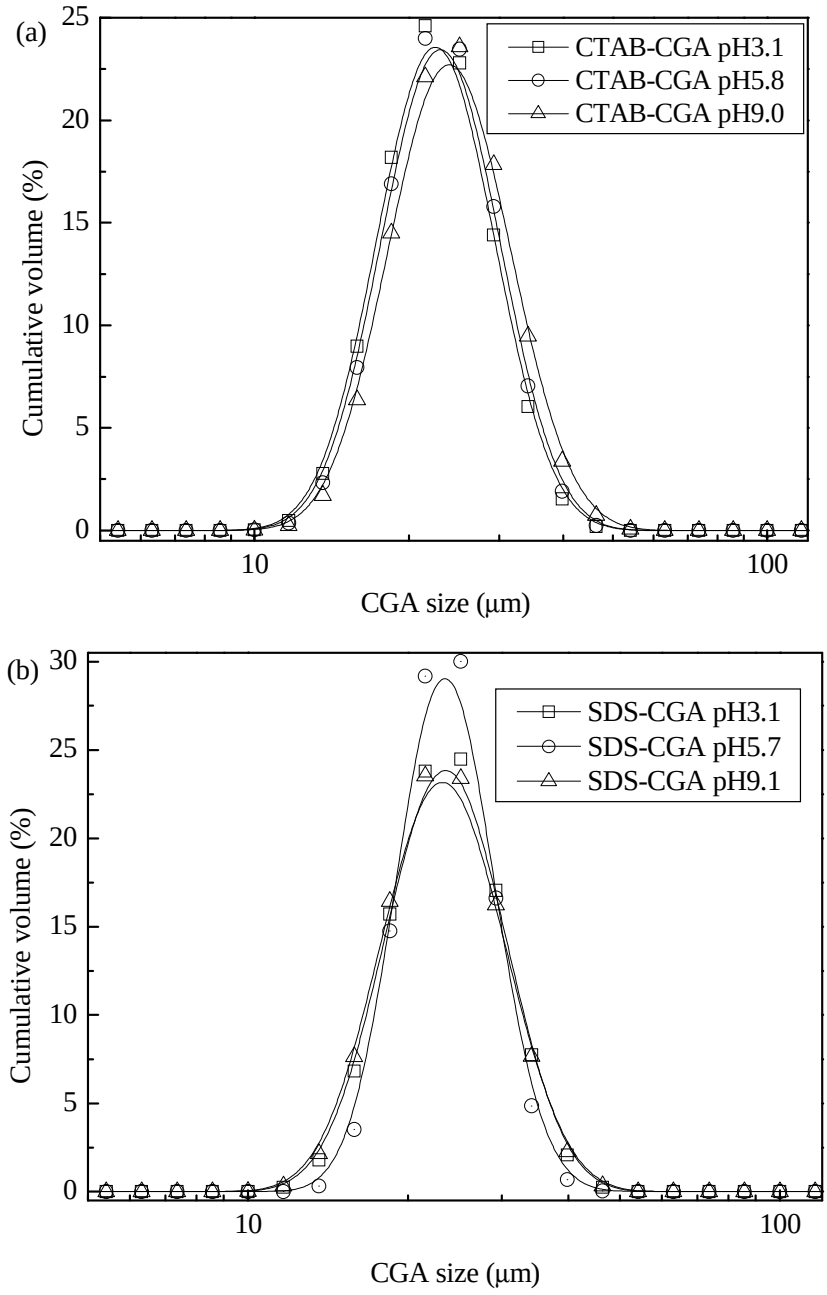

Fig. 4.19. CGA size distribution at different pH values (C_{surf} ≈0.5CMC, C_{CTAB} =0.5 mmol/L, C_{SDS} =4 mmol/L) of surfactant solutions in the batch generation mode: (a) CTAB-CGAs and (b) SDS-CGAs.

- **Continuous generation mode -- effects of air flow rate, concentration and flow rate of surfactant solution on CGA size**

Different air flow rates Q_{air} (33.3 mL/min or 66.7 mL/min), surfactant concentrations $C_{surf.}$ (C_{CTAB} or C_{SDS}) (below and above CMC levels), and flow rates of surfactant solutions $Q_{surf.}$ (18.3 mL/min or 41.6 mL/min) were tested in the generation of CTAB-CGAs and SDS-CGAs. The mean CGA diameter and size distribution obtained are presented in Table 4.3 and

Fig. 4.20, respectively: under the investigated generating conditions, the average size of CTAB-CGAs was in the range of 36~45 µm and that of SDS-CGA ranged between 40 µm and 49 µm. With the fixed $Q_{surf.}$ (18.3 mL/min), the average SDS-CGA size decreased from approximately 48.5 µm to around 46.4 µm at $C_{SDS.}$ = 0.5 mmol/L when Q_{air} increased from 33.3 mL/min to 66.7 ml/min; and it dropped from 42.1 µm to 40.5 µm at $C_{SDS.}$ = 8 mmol/L with Q_{air} increasing. As for CTAB-CGAs, with the fixed $Q_{surf.}$ (18.3 mL/min), a slight reduction in size was also found when increasing Q_{air} at the C_{CTAB} of around 2 mmol/L, whilst for the smaller C_{CTAB} of 0.5 mmol/L, the CGA size did not change much with different Q_{air}. With the same Q_{air} (33.3 mL/min) and $C_{surf.}$, when $Q_{surf.}$ increased from 18.3 mL/min to 41.6 mL/min, the CTAB-CGA size decreased from around 44.1 µm to around 39.4 µm at the concentration of 0.5 mmol/L and dropped from around 42.0 µm to around 37.0 µm at the concentration of 2 mmol/L; the average diameter of SDS-CGAs reduced by approximately 1 µm regardless of $C_{surf.}$. Fixing $Q_{surf.}$ and Q_{air}, the CGA size had a decrease of 2~3 µm when the C_{CTAB} increased from 0.5 mmol/L to 2 mmol/L; similarly, the SDS-CGA size had a drop of 6 µm. This follows the logic that an increase in the numbers of surfactant molecules beyond a certain value tends to crowd them on the microbubble surfaces, thereby reducing the interfacial tension between bubble and the bulk water. Reduction in the interfacial tension would thus reduce the bubble size (Chaphalkar et al., 1993). In general, greater air flow rate, flow rate and concentration of surfactant solution help to create smaller aphrons to some extent, but these parameters subtly impact the CGA size compared with the stirring speed that has already been confirmed in Section 4.1.2.3(2).

Table 4.3. Mean CGA size under different generating conditions.

$Q_{surf.}$ (mL/min)	Q_{air} (mL/min)	d_{CGA} (µm)			
		C_{CTAB} (mmol/L)		$C_{SDS.}$ (mmol/L)	
		0.5	2	0.5	8
41.6	33.3	39.4	37.0	47.0	41.5
18.3	33.3	44.1	42.0	48.5	42.1
18.3	66.7	44.9	36.4	46.4	40.5

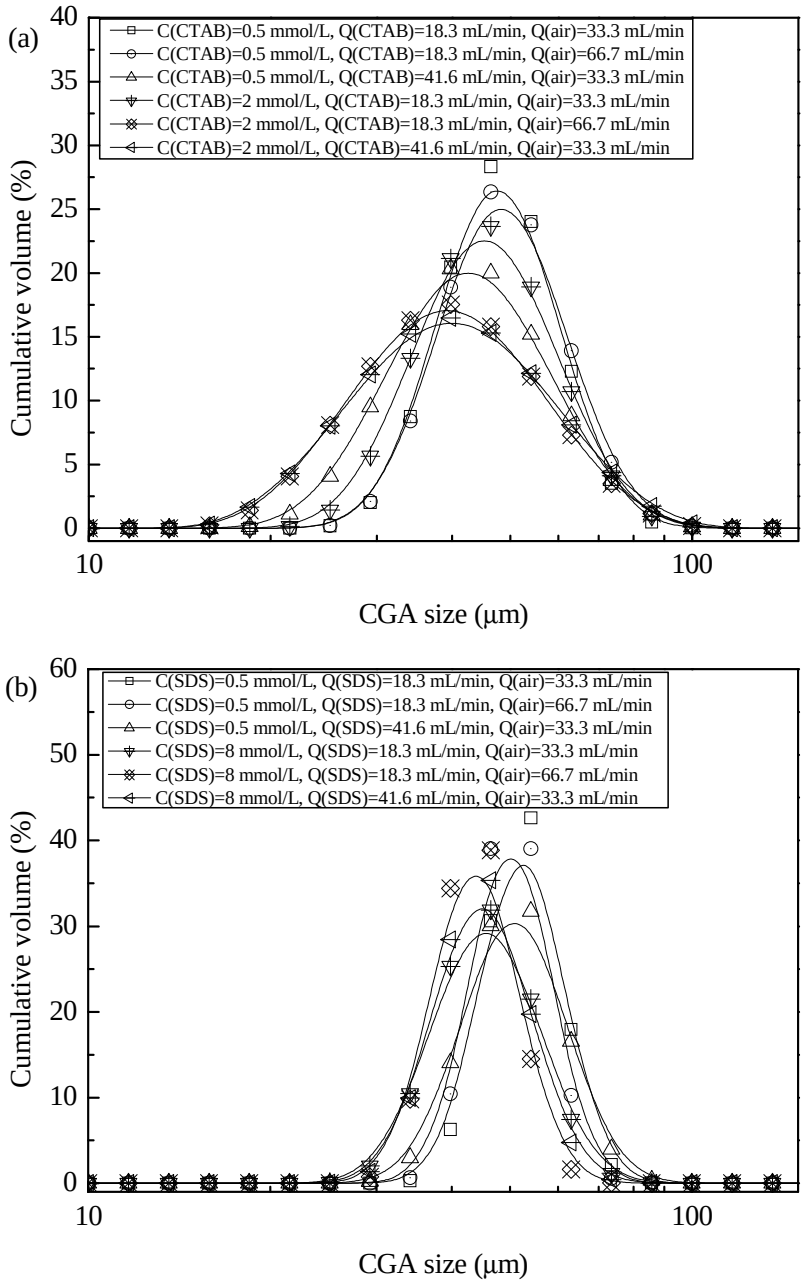

Fig. 4.20. CGA size distribution patterns under different generation conditions: (a) CTAB-CGAs; (b) SDS-CGAs.

4.1.2.4 Zeta potential

The zeta potential was measured to determine whether the surfactants altered the surface properties of bubbles. The measurement was carried out via a microelectrophoresis apparatus Zetasizer NanoZS (Malvern, UK) that has been described by Liu (2010). The CGA suspension was immediately transferred into the sample cell by syringe and analyzed after the generation of CGAs.

The zeta potential of CGAs at the air flow rate of 33.3 mL/min or 66.7 mL/min varying with different surfactant concentrations is depicted in Fig. 4.21. Samples of CGA suspension were collected by way of directly transporting the generated CGA suspension to the measurement cell of NanoZS due to the high stability of CGAs that allows them to be moved from the generation site to the place where they are used. It has been well recognized that the air bubble in pure water is of negative surface charge in the wide pH range from 2 to 12, which can be attributed to the fact that H^+ ions have a higher hydration energy than OH^- ions and thus the interface is apt to attract the latter (Yoon and Yordan, 1986; Han et al., 2004; Oliveira and Rubio, 2011). In the current study, CGAs generated from the cationic surfactant CTAB were positively surface charged with zeta potentials ranging from +34 mV to +42 mV (at the air flow rate of 33.3 mL/min) or from +15 mV to +48 mV (at the air flow rate of 66.7 mL/min) (Fig. 4.21(a)), whilst those generated using the anionic surfactant SDS were of negative surface charges with zeta potential of -15~-36 mV (at the air flow rate of 33.3 mL/min) or -22~-38 mV (at the air flow rate of 66.7 mL/min) (Fig. 4.21(b)). The results confirmed that the surface charge of CGAs could be determined by the polar group of the surfactant molecule adsorbed on the bubble surface and as well as denoted the electrostatic repulsion between CGAs which resulted in the incipient or moderate stability of CGA suspension ("Zeta potential," 2014). The magnitude of zeta potential rose along with surfactant concentration increasing because of the increased adsorption of the surfactant on the CGA surface; the trend tapered off because the surface excess should not increase above the CMC according the Gibbs equation (Kubota et al., 1983). The air flow rate does not significantly affect the surface charge of CGAs, but a slight influence could be observed.

Given that the absolute value of zeta potential was always higher than 10 mV over the investigated surfactant range and the half life τ_S could not be greatly improved at the surfactant concentration higher than CMC (Section 4.2.1.2 (2)), the CGA suspension would always remain stable at low surfactant concentrations. Thereby, it is expected to produce CGAs at surfactant concentrations lower than 0.5CMC in order to reduce the surfactant demand in the CGA applications without weakening the treatment effectiveness.

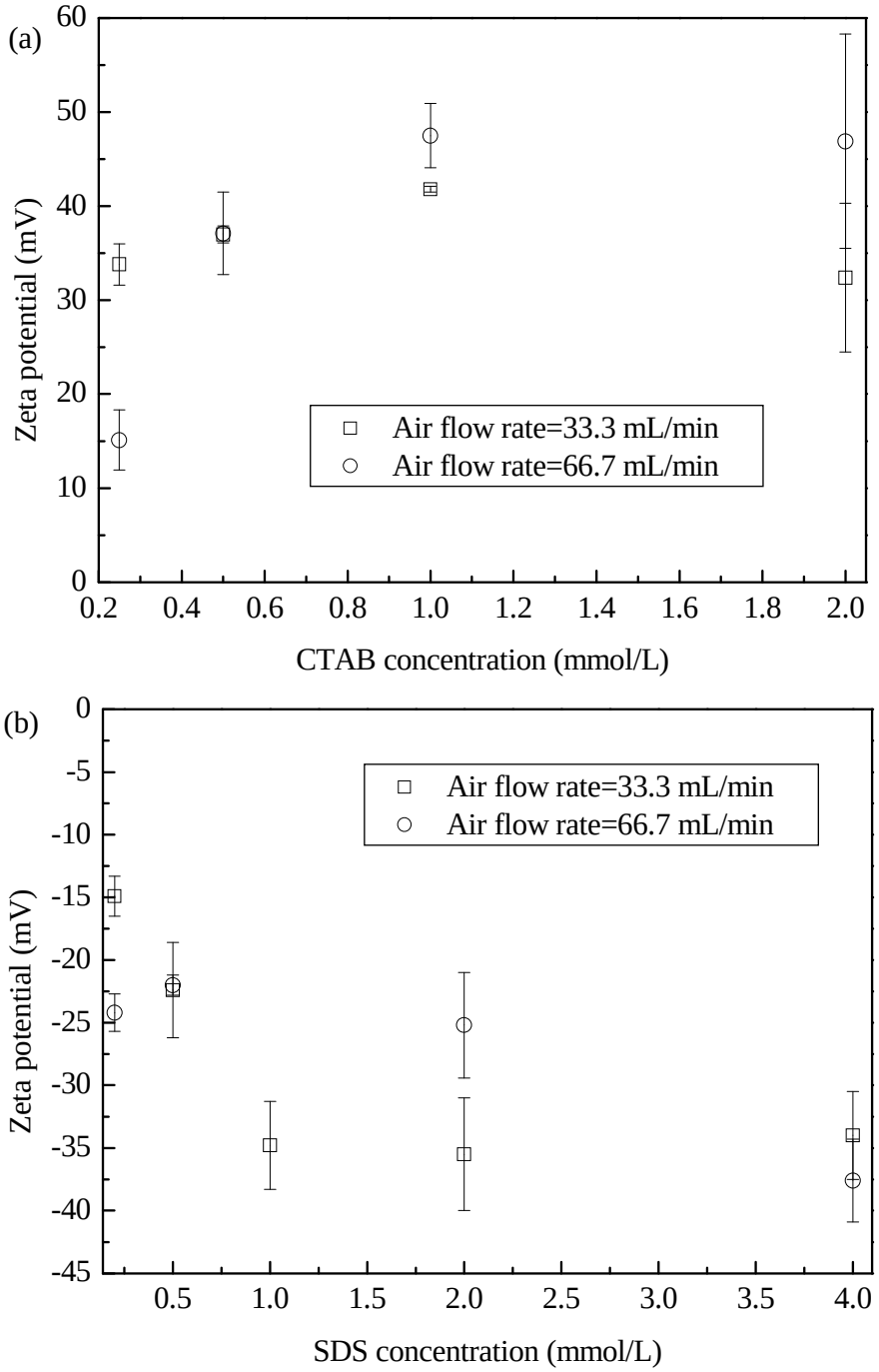

Fig. 4.21. Average CGA zeta potentials varying with the surfactant concentration at different air flow rate: (a) CTAB-CGAs;(b) SDS-CGAs.

4.2 Exploration of SNP-surfactant interaction mechanisms by adsorption-aggregation

The interaction between NPs and surfactant refers to the total depletion of the latter from the bulk suspension and herein is studied in view of both adsorption and aggregation (so is called adsorption-aggregation).

Adsorption isotherms were used to elaborate the adhesion of surfactant on the NP surface whilst particle size and fractal dimension of aggregates formed during batch adsorption tests were investigated to understand properties of NP-collector aggregate which may give an indication of NP-involved interfacial processes.

4.2.1 Experimental method

To investigate interaction mechanisms between SNPs and flotation agent (CTAB and SDS), a series of thermodynamic adsorption experiments were conducted after aggregation tests and flotation trials. The initial SNP concentration was fixed in all adsorption tests, and the agent concentration and pH varied according to experimental results of previous trials.

All batch experiments were carried out using 150 mL glass bottles with Teflon-lined screw caps to avoid the undesirable surfactant adsorption by container. 50 mL 0.03 vol.% SNP suspension was mixed with 50 mL surfactant solutions of different concentrations so as to give varying agent concentrations in the bottle. The mixed suspensions were shaken at the room temperature of approximately 25 °C (298.15 K) for 15 h at the constant rotating speed of 15 rpm. Thereafter, 30 mL supernatant was carefully withdrawn and separated by filtrating through 0.45 μm membrane filters and then centrifuging at 8000 rpm for 20 min. The adsorption duration and the way of collecting samples after adsorption tests were determined according to the experimental study of Trompette et al. (1994; 1996) and Lu Jiajuan (2009). The final sample was analyzed by TOC analyzer for surfactant concentration. Additionally, the zeta potential, the pH of suspension and the particle size of adsorbent after reaching adsorption equilibrium were also measured; and the fractal dimension was calculated. The amount of adsorbed surfactant (q_e, mg/g) at equilibrium by SNPs were obtained by the following equation:

$$q_e = \frac{(C_{0S} - C_e)V}{m} \tag{4.6}$$

where C_{0S} and C_e (mg/L) are initial and equilibrium concentrations of surfactant solution, respectively. V (mL) is the volume of the mixed suspension, m (mg) is the weight of SNPs. Since surfactant is a source of TOC, the TOC was employed as an indicator to estimate the surfactant concentration (Lissens et al., 2003; Hu et al., 2005). Fig. 4.22 and the linear regression equations illustrate the TOC variation with the surfactant concentration.

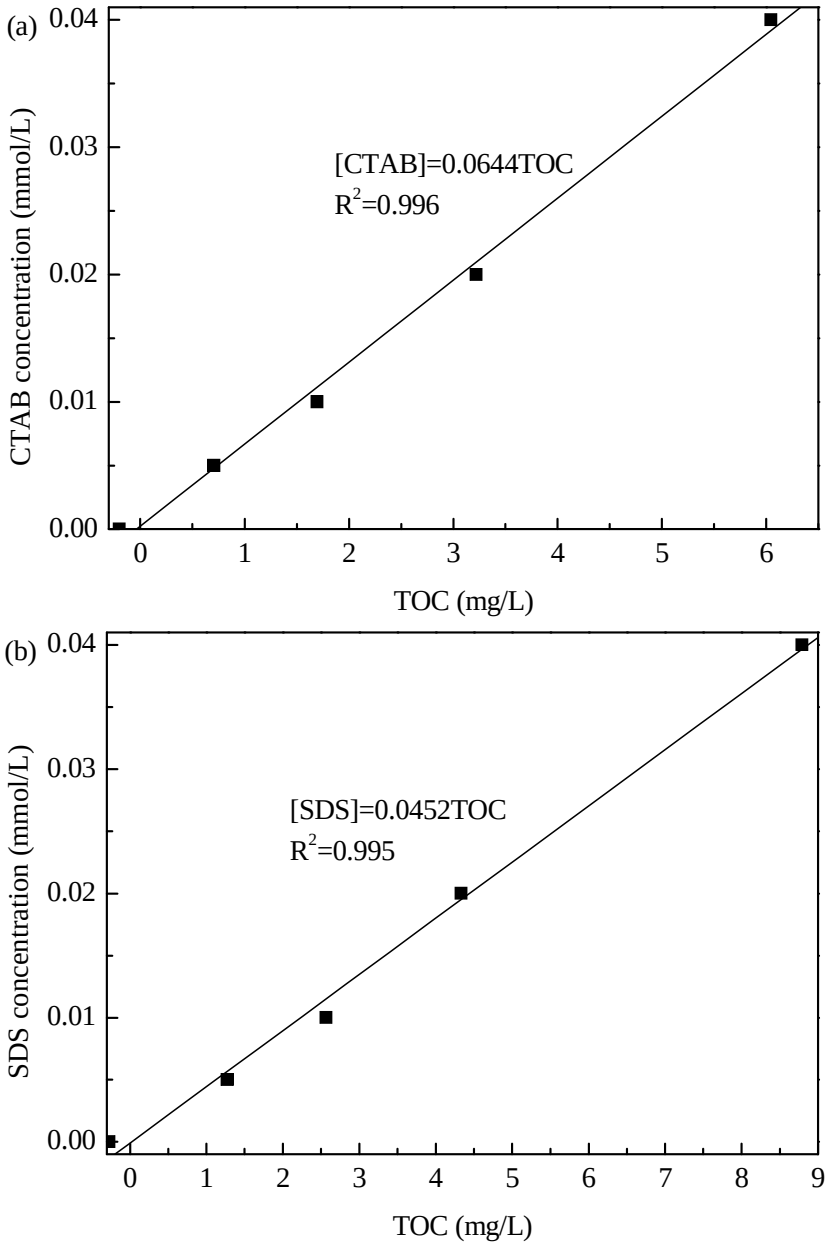

Fig. 4.22. Variation of surfactant concentration with TOC: (a) CTAB; (b) SDS.

All samples were collected and measured in the same way described above for the surfactant concentration after 72 hours of adsorption tests. The concentration kept constant and no desorption was found.

4.2.2 Adsorption isotherms

Results of surfactant adsorption onto SNPs at equilibrium was depicted in Fig. 4.23, which are evaluated using five commonly used isotherm models: Langmuir, Freundlich, Langmuir-Freundlich (L-F), Temkin, and Dubinin-Radushkevich (D-R). The extracted isotherm

information of 0.015 vol.% 30R50+CTAB, 0.015 vol.% 30R25+CTAB, and 0.015 vol.% 30CAL50+SDS is summarized in Table 4.4.

The Langmuir, Freundlich, L-F and Temkin models have been particularly described in Section 3.2 of Chapter 3. As for D-R isotherm model, the equation (Lin et al., 2011) was often used to describe adsorption on both homogeneous and heterogeneous surfaces to determine the possible sorption type (physical or chemical). The D-R isotherm equation is:

$$q_{eD-R} = q_{\max} \cdot \exp\left(-\beta \cdot \varepsilon^2\right) \tag{4.7}$$

where q_{eD-R} (mol/g) is the amount of surfactant adsorbed onto per unit dosage of SNPs and $q_{\max}$ is the theoretical monolayer sorption capacity (mol/g); β is the activity coefficient related to mean adsorption energy (mol^2/J^2), and ε is the Polanyi potential, which is equal to:

$$\varepsilon = RT \ln\left(1+1/C_e\right) \tag{4.8}$$

where T is the solution temperature (K) and R is the gas constant (8.314 J/mol/k). The mean free energy of adsorption E (kJ/mol), can be calculated from D-R parameter β as follows:

$$E = \frac{1}{\sqrt{2\beta}} \tag{4.9}$$

The E value ranging from 1 to 8 kJ/mol indicates the physical sorption and that ranging from 8 to 16 kJ/mol reveals the chemical sorption.

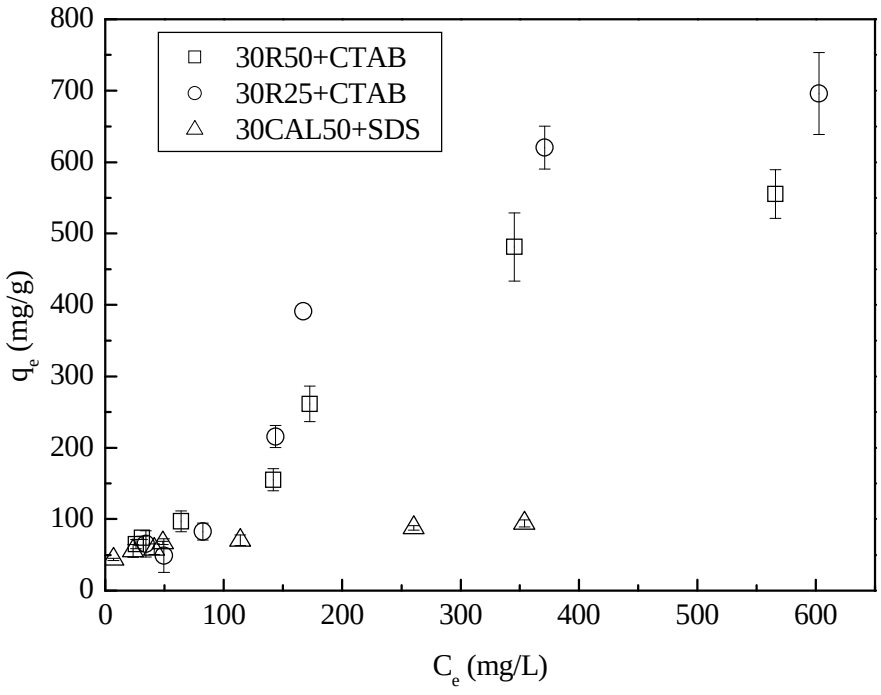

Fig. 4.23. Experimental results of SNP-surfactant adsorption-aggregation.

Table 4.4. The fitting results from different models

SNPs	Langmuir model			Freundlich model			Langmuir-Freundlich model				Temkin model				Dubinin-Radushkevich model			
	$Q_{\max L}$ (mg/g)	b_L	R^2	K_f	n_F	R^2	$Q_{\max L-F}$ (mg/g)	b_{L-F}	n_{L-F}	R^2	B	K_T	b (J/mol)	R^2	q_{eD-R} (mol/g)	β (mol^2/J^2)	E (kJ/mol)	R^2
30R50	1317.8	0.001	0.966	5.4	0.741	0.957	971.4	0.00081	1.18	0.967	160.0	0.04	61346.9	0.867	1.32E-02	8.38E-09	7.7	0.962
30R25	1622.2	0.001	0.938	5.6	0.766	0.915	731.7	3.29E-06	2.43	0.978	250.2	0.03	81795.9	0.916	1.79E-02	8.73E-09	7.6	0.930
30CAL50	86.9	0.085	0.775	29.8	0.193	0.978	388.9	0.0785	0.235	0.975	12.6	3.61	679.7	0.956	5.30E-04	1.92E-09	16.1	0.968

A comparison of R^2 was made upon adsorption isotherms and adsorptive behaviors were evaluated. As presented in Table 4.4, among the Langmuir, Freundlich and L-F models, it was evident that experimental data of CTAB-30R50 and CTAB-30R25 adsorptions agreed with the Langmuir model better than those of SDS-30CAL50 adsorption did; for the SDS adsorption on 30CAL50, the Freundlich model fitted better than Langmuir. This suggested that the adsorption of CTAB on negatively surface charged SNPs was principally controlled by the homogeneous interaction whereas that of SDS on the positively surface charged 30CAL50 was a heterogeneous process. All the three n values of the Freundlich model was lower than 1, illustrating the favorable adsorption. Comparatively, the L-F model showed the best fit among these three models with well-matching correlation coefficient, giving the good estimation of the maximum surfactant adsorption capacity of SNPs: 971.4 mg/g for 0.015 vol.% 30R50 + CTAB, 731.7 mg/g for 0.015 vol.% 30R25 + CTAB and 388.9 mg/g for 0.015 vol.% 30CAL50 + SDS, individually. The greater adsorption capacity and affinity of 30R25 and 30R50 toward the surfactant molecules were probably due to their stronger electrostatic forces of attraction involved and higher specific surface areas than 30CAL50.

Based on the R^2 value, the Temkin model gave a close fit to the SDS adsorption on 30CAL50 than to the CTAB-SNPs (30R50 or 30R25) adsorption. The adsorption heat of SDS-30CAL50 adsorption was restricted around 679.7 J/mol. D-R plots and corresponding constants demonstrated the fairly good fitting for all the three SNPs involved adsorption. The magnitudes of E are calculated to be 7.7 and 7.6 for 30R50 and 30R25, respectively. It denoted that the mechanism for the CTAB adsorption on those two negatively surface charged SNPs was dominated by the physical interaction despite of the probable tendency of chemical sorption since the values were quite close to 8 kJ/mol. The E value for SDS adsorption onto 30CAL50 was 16.1, implying a chemical sorption process. The higher ion adsorption capacities (q_{eD-R}) of 30R50 and 30R25 obtained by D-R model revealed more reactive surfaces on their surface, which were possibly resulted from the presence of high concentrations of edge/corner sites and other defects. That corresponded well with fitting results of Langmuir and L-F isotherms.

4.2.3 Properties of SNP-surfactant aggregates

4.2.3.1 Zeta potential and pH value

The analysis of the electrophoretic behavior of aggregates attained from adsorption-aggregation gives some insight into the possible mechanism. The zeta potential values of SNPs before and after interacting with surfactants are presented in Fig. 4.24. Generally, mechanisms of surface-active molecules adsorbing onto the solid substrates from aqueous solution include (i) electrostatic attraction between the charged ion or moiety of molecules and the solid surface through ion exchange or ion pairing, (ii) hydrophobic bonding, and (iii) dispersion forces in which the London-van der Waals force between adsorbate and adsorbent increases with the increasing molecular weight of the adsorbate (Paria and Khilar, 2004). In the cases of 30R50 and 30R25 involved adsorption-aggregation, the initial CTAB concentration ranged from 0 to 842 mg/L (higher than the CMC of CTAB, 357.2 mg/L or 0.98 mmol/L), and two regions in which adsorption occurred via different mechanisms could be distinguished. The first region is marked by sharp changes in the zeta potential curve. The electrophoretic mobility increased greatly with increasing initial surfactant concentrations and changed signs at molality of around 88.2 mg/L CTAB (for 30R50) and 94.4 mg/L CTAB (for 30R25), respectively, where corresponding equilibrium surfactant concentrations in the bulk suspension were about 44.5 mg/L CTAB and 71.1 mg/L CTAB, respectively. Possible explanations of this observation could be attributed to both an ion exchange between the monovalent CTA^+ ion and some other ions presented at the silica water interface as pre-adsorbed counterions and also the tendency of the hydrophobic moieties of the adsorbing surfactant to remove themselves from the aqueous environment by forming aggregates with alkyl chains of ions already adsorbed on the surface (Trompette et al., 1994). Thereafter, the excess of opposite charges resulted in further increases of absolute values of zeta potential. The surface aggregation was inferred to start at this stage. It should be noting that, at concentrations at the zeta potential of zero, the flocculation should be optimum since no charge repulsion and hydrophobic attraction between alkyl chains of molecules adsorbed on neighbor particles. In the second part of the curve, plateaus (+39.5 mV for 30R50 and +35.8 mV for 30R25, individually) appeared at surfactant concentrations higher than 360 mg/L CTAB for both 30R50 and 30R25, where the CMC of CTAB was reached. Herein, surfactant micelles formed and the additional surfactants would prefer (for thermodynamic reasons) to achieve micelles or to be incorporated in existing micelles rather than to continuing being adsorbed; hence, the adsorption process should stop and the isotherm curve was thus expected

to level off after the CMC of surfactant. As for the adsorption-aggregation test of 30CAL50+SDS, since the maximum investigated initial SDS concentration 395 mg/L was much lower than its CMC (2220.6 mg/L or 7.7 mmol/L), thereby, only the first region of adsorption being controlled by the charge neutralization between 30CAL50 and SD^- could be found. The IEP was around 76.1 mg/L SDS in accordance with the equilibrium SDS concentration of 47.6 mg/L.

As for the variation of pH in the bulk suspension after adsorption-aggregation, it indicated that the uptake of CTA^+ ions arose a release of protons, which caused the pH variation along the isotherm (from around pH6.2 to pH5.8 for 30R50, and from pH6.6 to pH5.8 for 30R25). The effect was pronounced at very low adsorption values but the absolute quantity of protons released to solution was generally very small. The pH value of the equilibrium bulk phase slightly depends on the adsorption of CTAB (Trompette et al., 1994).

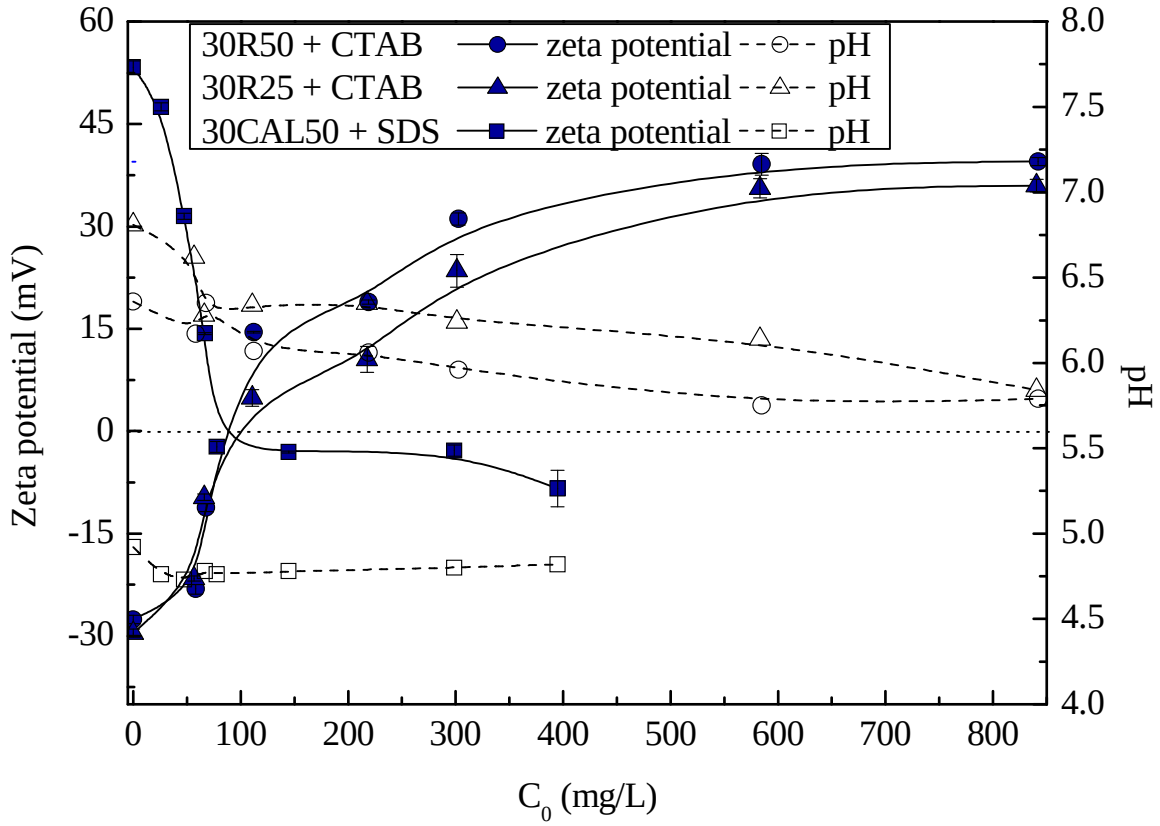

Fig. 4.24. Zeta potential and pH value of post-(adsorption-aggregation) suspension as a function of initial surfactant concentration.

4.2.3.2 Aggregate size analysis

The size measurement of surfactant-SNP aggregates is exhibited in Fig. 4.25. The size change as a function of initial surfactant concentration can be seen in Fig. 4.25(a): for 30R50 and 30R25, the aggregate size grew as the CTAB concentration increased, reached the maximum value at the CTAB concentration of 109.3 mg/L, and then decreased along with CTAB concentration; the SDS-30CAL50 aggregate had a mean diameter of more than 100 μm at the initial SDS concentration higher than about 77.9 mg/L. The formation of large aggregates was highly related to the electrostatic attraction between SNPs and surfactant with opposite charges because large aggregates were all obtained at the absolute value of zeta potential lower than 10 mV (Fig. 4.24)

In addition to the average particle size, it is necessary to take the PSD into consideration in order to completely understand the particle aggregation. As denoted in Fig. 4.25(b), the PSD was multimodal when the CTAB was slightly overdosed (302.5 mg/L). Continuing to increase the CTAB concentration would cause the re-stabilization of the SNP-surfactant suspension due to the electrostatic repulsion, and lead to the sharp drop of particle size. The re-dispersed particles exhibited uniform PSD. As for 30R25 (Fig. 4.25(d)), bimodal size distributions could be obtained at CTAB concentration below and above 218.7 mg/L. The 30CAL50-SDS aggregates were of ununiform size distribution since multi peaks were found at SDS concentrations higher than 26.0 mg/L (Fig. 4.25(e)). No re-dispersion was observed in the case of 30CAL50-SDS as expected.

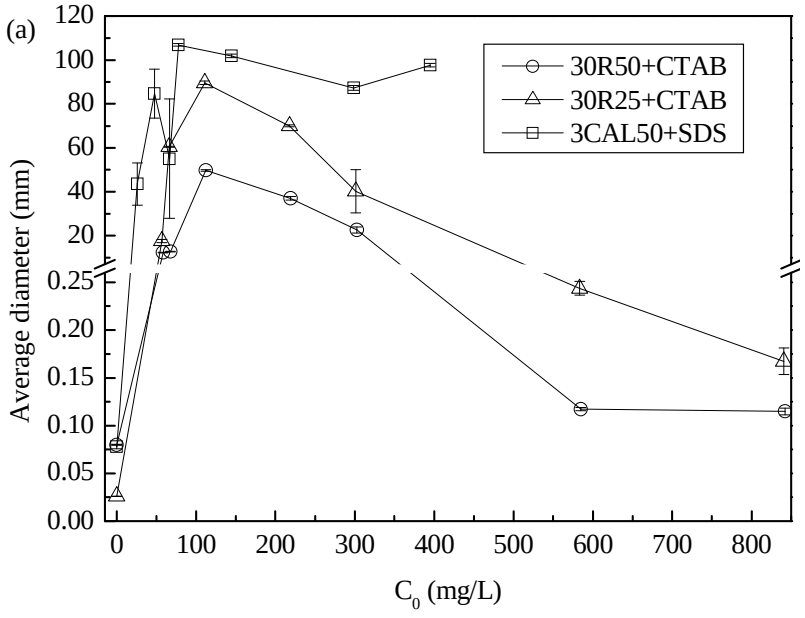

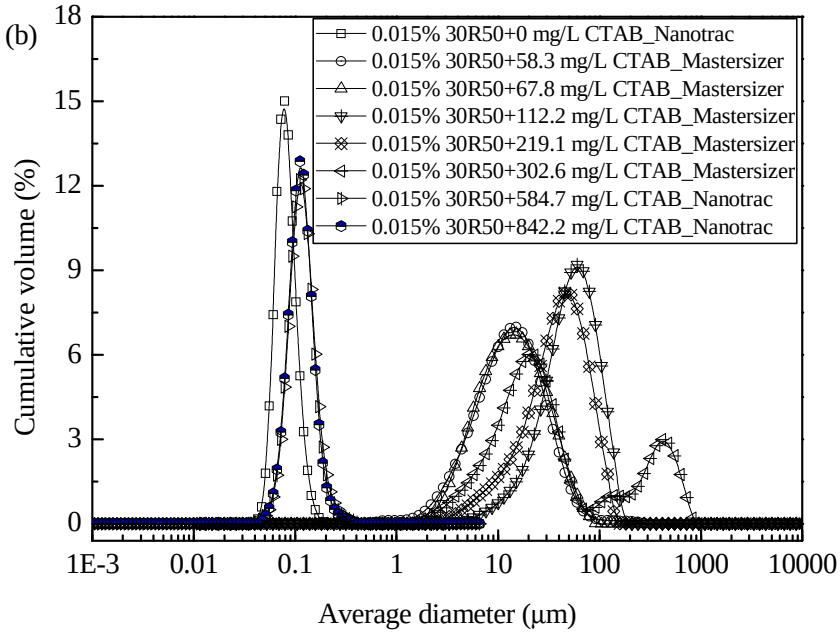
(b)
0.015% 30R50+0 mg/L CTAB_Nanotrac
0.015% 30R50+58.3 mg/L CTAB_Mastersizer
0.015% 30R50+67.8 mg/L CTAB_Mastersizer
0.015% 30R50+112.2 mg/L CTAB_Mastersizer
0.015% 30R50+219.1 mg/L CTAB_Mastersizer
0.015% 30R50+302.6 mg/L CTAB_Mastersizer
0.015% 30R50+584.7 mg/L CTAB_Nanotrac
0.015% 30R50+842.2 mg/L CTAB_Nanotrac
Cumulative volume (%)
0
3
6
9
12
15
18
1E-3
0.01
0.1
1
10
100
1000
10000
Average diameter (μm)

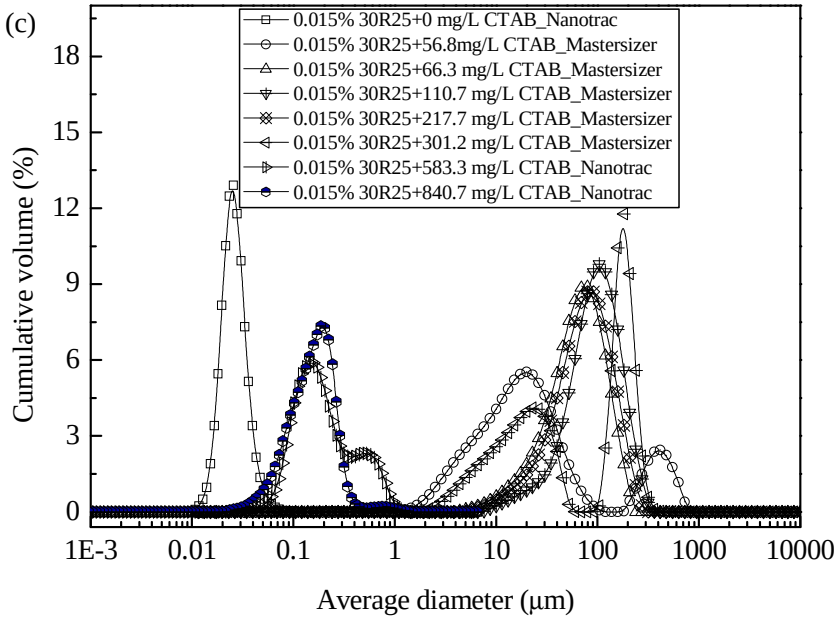
(c)
0.015% 30R25+0 mg/L CTAB_Nanotrac
0.015% 30R25+56.8mg/L CTAB_Mastersizer
0.015% 30R25+66.3 mg/L CTAB_Mastersizer
0.015% 30R25+110.7 mg/L CTAB_Mastersizer
0.015% 30R25+217.7 mg/L CTAB_Mastersizer
0.015% 30R25+301.2 mg/L CTAB_Mastersizer
0.015% 30R25+583.3 mg/L CTAB_Nanotrac
0.015% 30R25+840.7 mg/L CTAB_Nanotrac
Cumulative volume (%)
0
3
6
9
12
15
18
1E-3
0.01
0.1
1
10
100
1000
10000
Average diameter (μm)

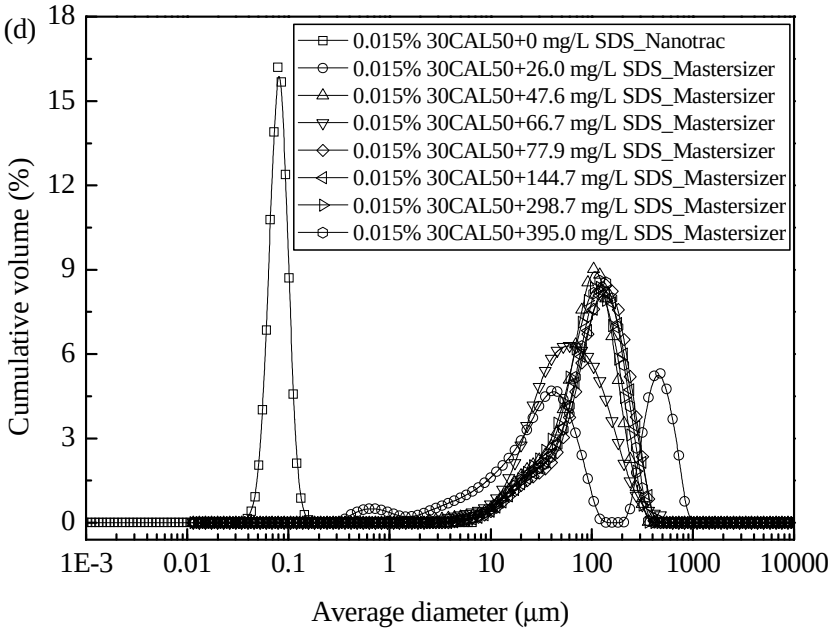

Fig. 4.25. Particle size measurement of SNP-surfactant aggregates after adsorption-aggregation: (a) variation of particle size with initial surfactant concentration; (b), (c) and (d) PSD patterns of 0.015 vol.% 30R50+CTAB, 0.015 vol.% 30R25+ CTAB; and 0.015 vol.%30CAL50+SDS, respectively.

4.2.3.3 Fractal structure

NPs provide the nuclei for the surfactant adsorption and their original surface was hence considered to be uniformly spherical with small deviations from an ideal arrangement with respect to the geometrical irregularity. However, the morphological structure of SNP-surfactant aggregates after adsorption-aggregation may differentiate due to different adsorption mechanisms. The variation of fractal structure of surfactant-SNP aggregates by SALLS along with the initial surfactant concentration is presented in Fig. 4.26. The CTAB-30R50 and CTAB-30R25 aggregates were compact and dense with respect to the morphological conformation over the investigated CTAB concentration, while the SDS-30CAL50 aggregate had loose and open fractal structure: especially, the D_f value was between 1.7~1.8 when the SDS concentration was lower than 66.3 mg/L; further increasing the SDS concentration could result in aggregates with more compact structure but still less dense, compared with the CTAB-30R50 and CTAB-30R25 aggregates. The low D_f values at low SDS contents, corresponding to the weak rising part of the isotherm in Fig. 4.23, possibly because the hydrophobic interaction between the alkyl chains of SDS molecules being adsorbed on the cationic sites of expanding polymer chains (grafted on the surface of 30CAL50) resulted in loose structure of 30CAL50-SDS flocs. When greater amount of SDS

were added, the screening of positive charges increased such that the electrostatic repulsion between particles decreased which contributed to the formation of denser aggregates.

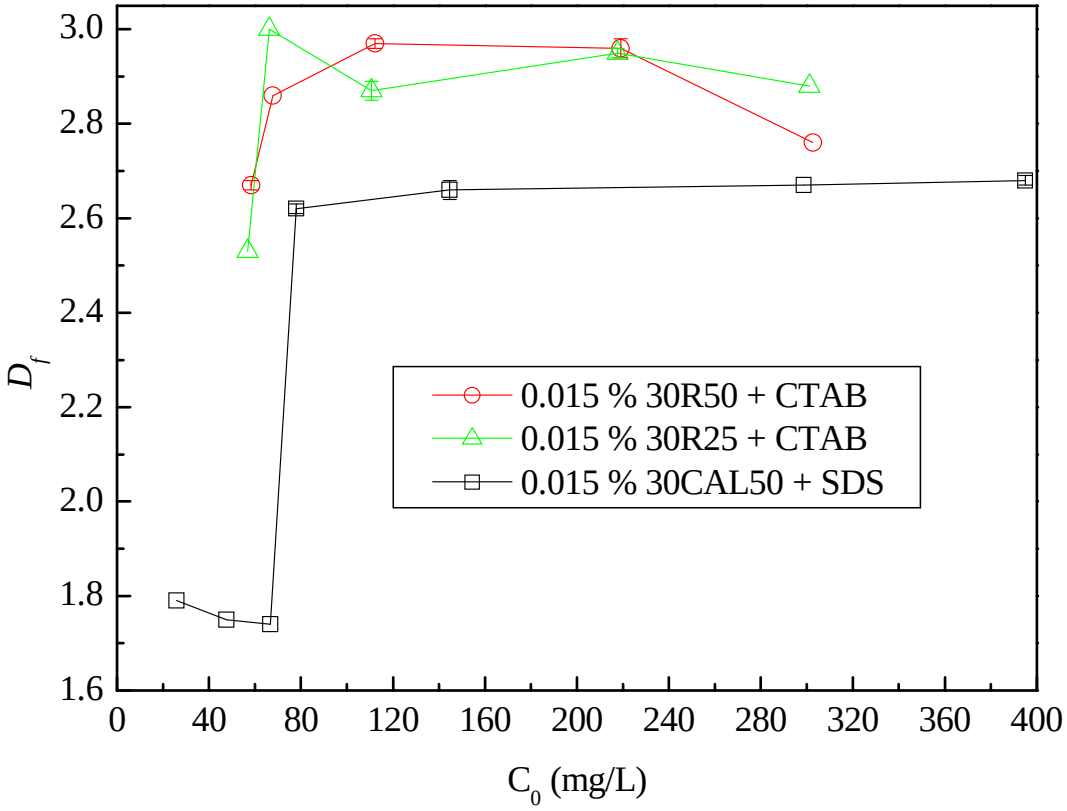

Fig. 4.26. Variation of fractal dimension with equilibrium surfactant concentration.

Combining the analysis of adsorption isotherms with the size and D_f results, the interaction between surfactants and SNPs might be interpreted that the chemical interaction process of SDS onto 30CAL50 could lead to larger and open structural aggregates whilst the physical sorption of CTAB onto SNPs would give rise to smaller and dense flocs. This information will be used to better understand the phenomena observed in the CGA-flotation of SNPs presented in the following section.

4.3 Continuous CGA-flotation separation of SNPs

4.3.1 Experimental procedure

In the present work, CGAs involved flotation trials were conducted in a continuous way, so is called “continuous CGA generation-flotation” or “CGA-flotation”. As shown in Fig. 4.1, after the pre-generation of CGAs for 1.5 min, keep pumping the surfactant solution and injecting air flow into Container A, and the generated CGA suspension would enter the contacting zone of the flotation cell from the bottom (Inlet b in Fig. 4.1) since the generator was well sealed; the liquid flow rate of CGA suspension Q_2 (or Q_{CGAs}) equals to that of the surfactant solution (Q_{surf}). Flow rates of influent (SNP aqueous suspension) Q_1 and effluent (clarified water) Q_3 are controlled for different operating conditions by peristaltic pumps, individually.

Samples of clarified water were taken after 5 min of the flotation test. The Si content in the effluent and influent was analyzed by ICP-MS for the SNP removal efficiency η; the calculation of η was explained in Chapter 3 (Section 3.3.1.5) and our previous study (Zhang and Guiraud, 2013); zeta potential and pH were also measured to characterize the water quality before and after flotation. The floats in the contacting zone were carefully collected by plastic Pasteur pipette and observed under the microscope described above for the visualization of CGA-SNP aggregates.

4.3.2 Effect of surfactant concentration in the flotation cell (C'_{surf})

Firstly, laboratory flotation trials were carried out to study the effect of surfactant dosage (C'_{surf}) on SNP removal efficiencies. CTAB-CGAs were used to treat the negatively surface charged 30R50 SNPs while SDS-CGAs were used for the positively surface charged 30CAL50 SNPs. The initial concentration of both SNPs was 0.005 vol.% and the mass concentration determined by ICP-MS could be found in Table 2.2. Q_1 was fixed to be 223.8 mL/min and Q_3 was 30 % of (Q_1 + Q_2). The surfactant dosage was controlled by changing the flow rate of CGA (Q_2, equal to the flow rate of surfactant solution) during the flotation process. Results attained are shown in Fig. 4.27.

The 30R50 removal kept higher than 75 % over the investigated CTAB dosage range (0.019~0.275 mmol/L) and meanwhile the zeta potential of flotation suspension (obtained by measuring the zeta potential of flotation effluent) increased from approximately -8 mV to +11 mV. More than 90 % 30R50 was separated at CTAB dosages above 0.114 mmol/L. The 30CAL50 removal ascended from around 23 % to almost 100 % and meanwhile the zeta potential reduced from +0.617 mV to -8.76 mV with the SDS dosage increasing from 0.047 mmol/L to 0.208 mmol/L. The turbidity could also be reduced to lower than 0.5 NTU when SNP removals were higher than 90 % (Fig. 4.27(b)). Compared with the turbidity before flotation treatment (11.0 NTU for 0.005 vol.% 30R50 and 8.08 NTU for 0.005 vol.% 30CAL50), the suspended solid in SNP suspensions was effectively removed. It is worth noting that, when optimum removal efficiencies of both SNPs were achieved (> 90 %), the magnitude of zeta potential was always around 10 mV, indicating an incipient instability of the flotation suspension ("Zeta potential," 2014). The electrostatic attraction between CGAs and SNPs with opposite surface charges played an important role in forming the SNP-CGA aggregates during flotation. The pH of flotation suspension was somewhat stable in the presence of surfactant: 5.6~6.2 for 30R50 suspensions and 5.4~5.9 for 30CAL50 (Fig. 4.27(c)). It could be inferred that the interaction between CGAs and surface charged SNPs followed the similar character as the surfactant adsorption on the silica surface proposed by Trompette et al. (1994; 1996): in the initial stage, the ionic head on the CGA surface electrostatically attracted SNPs with opposite surface charges. This stage supplied the nuclei to the later surface aggregation via forming the SNP enveloped CGA (CGA-SNPs). Thereafter, when the surfactant concentration was sufficiently high, the ion exchange could occur between stabilizer ions on the SNP surface and the ionic head of excessive free surfactants. As presented by Liu (2010), the anionic Klebosol colloidal silica (30R50 and 30R25) are stabilized with cations such as Na^+, K^+, and NH_4^+, while the stabilizer of the cationic SNP (30CAL50) is an Al derivative. Herein, the ion exchange occurred between Na^+ (or K^+, NH_4^+) and CTA^+ in the case of 30R50 or Al derivative and DS^- in the case of 30CAL50, which was followed by the hydrophobic bonding. The hydrophobic moiety might also have an influence herein because SNPs could be well removed even when the zeta potential still kept negative (for 30R50). Those mechanisms finally gave rise to the formation of (CGA-SNP)-(surfactant-SNP) aggregates whose representative photo (in the case of 30R50 with CTAB-CGAs) can be seen in Fig. 4.27. The SNPs aggregates were observed to adsorb on the CGA surface.

When the surfactant dosage was lower than 0.05 mmol/L, the removal efficiency was as high as 80 % for 0.005 vol.% 30R50 but that of 30CAL50 was lower than 25 %. Considering the adsorption performance and fractal structure analysis of Section 4.2, it possibly indicated that the physical interaction between CTAB and 30R50 was favored by flotation through forming dense aggregates, but the open structural SDS-30CAL50 aggregates formed by chemical interaction were difficult to be removed by bubble particularly if the surfactant concentration is insufficient.

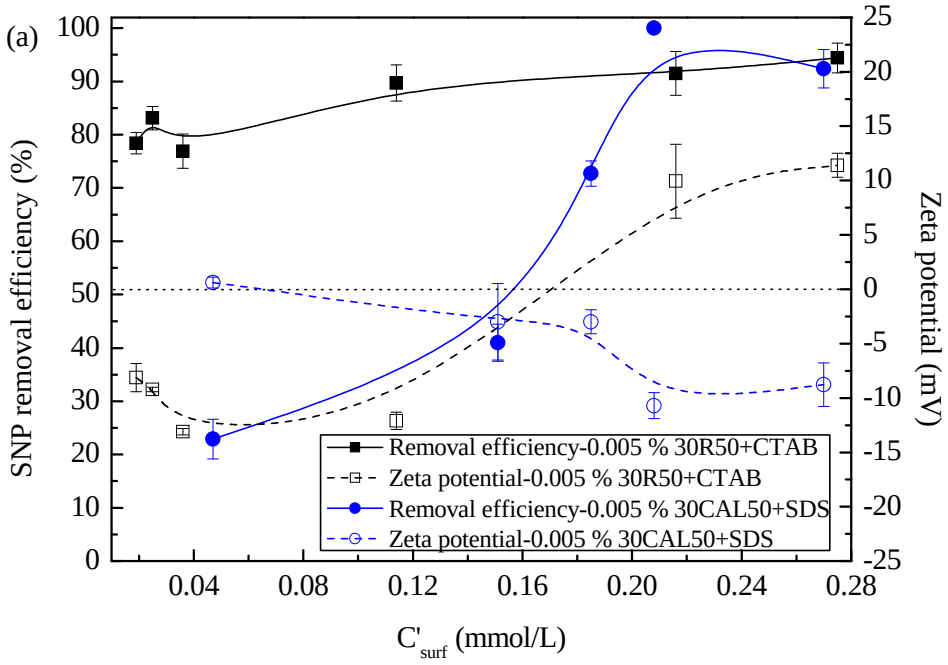

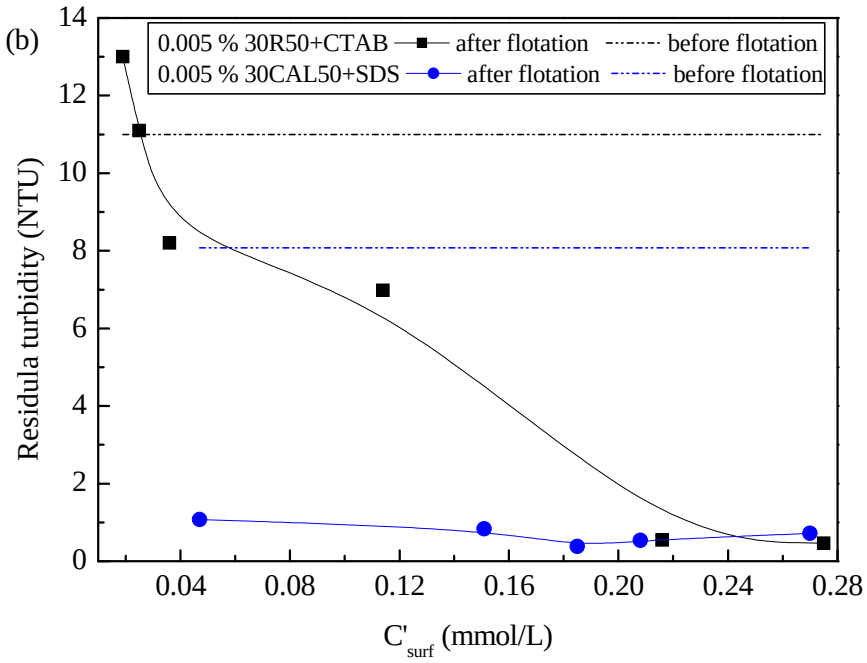

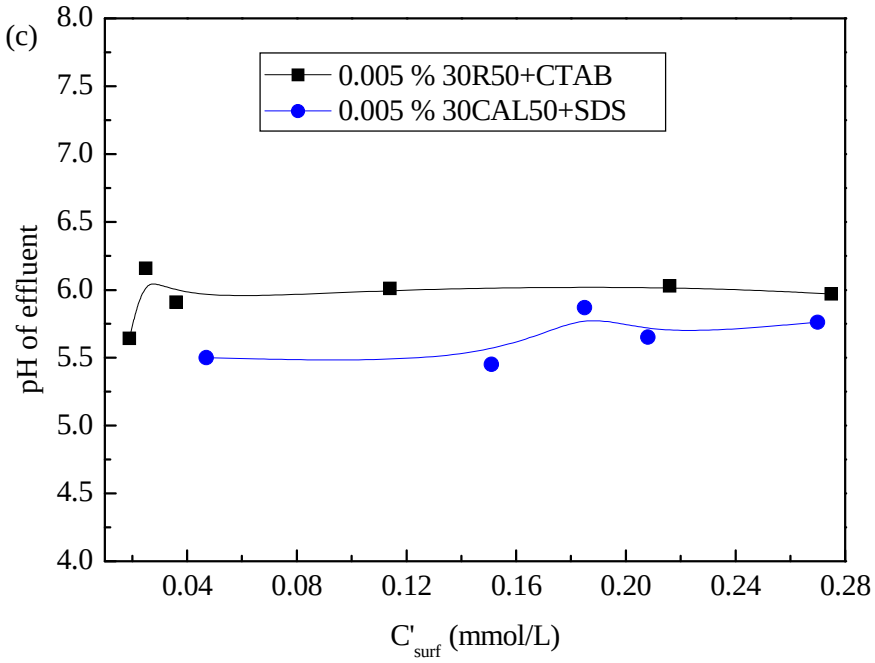

Fig. 4.27. Effect of surfactant concentration in the contacting zone of flotation cell on the performance of CGA-flotation: (a) SNP removal efficiency and zeta potential; (b) residual turbidity; (c) pH value after flotation.

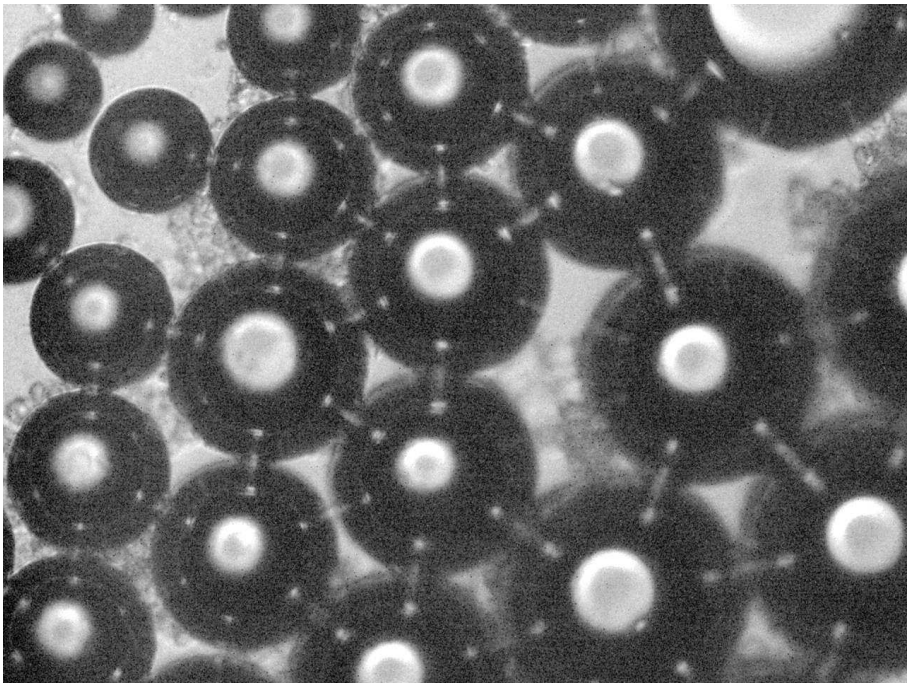

Fig. 4.28. Representative microscopic image of CGA(CTAB)-SNPs (30R50) flocs obtaining from the flotation foamate.

4.3.3 Effect of SNP size

The flotation performance of two negatively surface charged SNPs, 30R25 and 30R50, varying with C'_{surf} (C'_{CTAB}) were investigated for the influence of SNP size on the CGA-

flotation efficiency. The SNP volume concentration and flow rate Q_1 of influent were fixed to be 0.015 % and 124.4 mL/min, Q_2 changed to obtain different C'_{CTAB}, and Q_3 was 30% of (Q_1+Q_2). The CTAB concentration in the CGA generator was always 1.0 mmol/L and air flow rate for CGA creation was 66.7 mL/min. SNP removal, zeta potential of flotation suspension, residual turbidity and effluent pH were shown in Fig. 4.29. At the CTAB concentration lower than 0.09 mmol/L, the removal of 30R25 was lower compared with that of 30R50, became in the same level at the C'_{CTAB} range of 0.09~0.17 mmol/L, and turned to be greater at higher C'_{CTAB}. The zeta potential of 30R50 in the flotation suspension was reversed to positive from the lowest C'_{CTAB}; however, that of 30R25 remained negative till the C'_{CTAB} was around 0.09 mmol/L. As for the residual turbidity, in Fig. Fig. 4.29(b), that of SNP suspensions decreased from 1.41 NTU to 0.5 NTU for 30R25 involved flotation at C'_{CTAB} higher than 0.07 mmol/L; for 30R50 involved flotation, the turbidity reduced from 32.8 NTU to lower than 4 NTU at C'_{CTAB} lower than 0.2 mmol/L but sharply increased at higher CTAB dosage, possibly due to the re-stability of the suspension resulted from electrostatic repulsion between CGA-SNP flocs caused by the over CTAB addition. The pH of the flotation suspension did not fluctuate greatly according to Fig. 4.29(c).

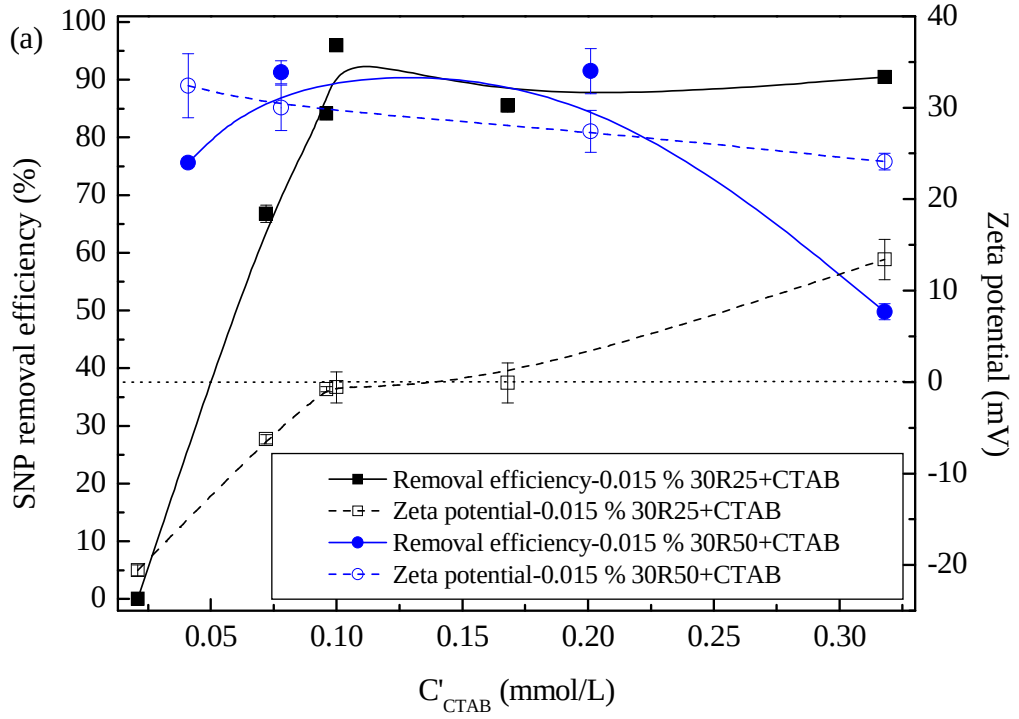

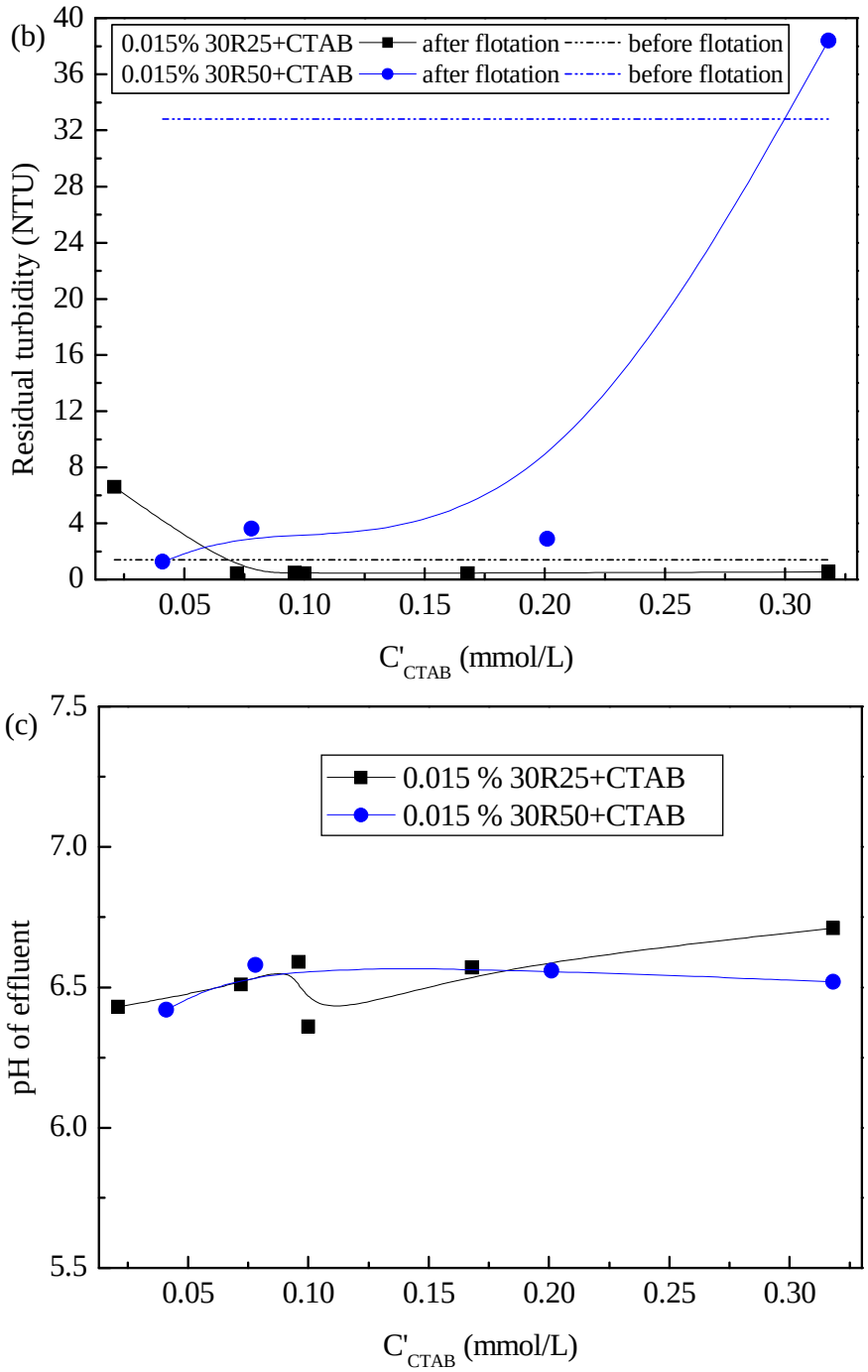

Fig. 4.29. Effect of NP size on the performance of CGA-flotation: (a) SNP removal efficiency and zeta potential; (b) residual turbidity; (c) pH value after flotation.

As already noted, the collection efficiency of NPs is mainly decided by the collision efficiency and the attachment efficiency (Mishchuk et al., 2012). The attachment efficiency takes values from 0 to 1, reaching the maximum when the energy barrier between interacting bubbles and particles is lower than the energy of thermal motion, in which case the collection efficiency will be reduced to the collision efficiency. The Brownian diffusion of particles around rising bubbles, decreasing importantly with increasing particle size, leads to the

collision of bubble-particles. The size of SNPs in the current study falls into the diffusion regime (with the diameter < 200 nm) (Reay and Ratcliff, 1973), and the time required for the spherical particle to diffuse a unit distance is directly proportional to its radius (Hiemenz and Rajagopalan, 1997). Accordingly, the smaller SNPs, 30R25, should have lead to a higher collision possibility compared with the larger SNPs, 30R50. Moreover, from the standpoint of DLVO theory, the barrier of interaction energy between 30R25 is smaller than that of 30R50, and it is more possible for the hydrophobic chains of CTAB to get close to and then interact with the 30R25 surfaces (Liu et al., 2013). Accordingly, a higher collection efficiency of 30R25 was obtained at CTAB dosages higher than 0.09 mmol/L. However, for lower C'_{CTAB}, the zeta potential of 30R25 in the flotation suspension was still negative and the electrostatic repulsion between SNPs and CTAB-CGAs might hinder the adsorption of 30R50 on bubbles, giving rise to poor SNP removals.

4.3.4 Effect of initial volume concentration of SNPs

Flotation experiments were conducted to study the influence of initial SNP volume concentrations (0.005 vol.% and 0.015 vol.%) on flotation behaviors at different C'_{surf}. Accordingly, influent suspensions of two SNPs (30R50 and 30CAL50, with opposite surface charges but similar particle size) were named as 30R50 0.005 %, 30R50 0.015 %, 30CAL50 0.005 % and 30CAL50 0.015 %, respectively. The same flow rates in the flotation process as Section 4.2.2 were used herein, and the air flow rate for CGA creation was 33.3 mL/min.

As denoted in Fig. 4.30(a), for 30R50, when adding less than 0.05 mmol/L CTAB, the removal efficiency of 30R50 0.015 % reached as high as 94.8±0.7 % whereas that of 30R50 0.005 % was lower than 80 %. The optimum removal of 30R50 0.015 % (97.6±0.5 %) was obtained at C'_{CTAB} =0.078 mmol/L, while the removal of 30R50 0.005 % achieved higher than 90 % at CTAB dosage in excess of 0.2 mmol/L. The zeta potential of 30R50 0.015 % turned to positive from the lowest CTAB dosage 0.04 mmol/L; as for 30R50 0.005 %, the zeta potential after flotation reversed only when the C'_{CTAB} was higher than 0.1 mmol/L. It is shown in Fig. 4.30(b) that, at the SDS dosage of around 0.15 mmol/L, approximately 98 % 30CAL50 0.015 % could be removed but the removal of 30CAL50 0.005% was only 41±3.5 %; with higher SDS dosages, the SNP removal increased to almost 100 % for both initial concentrations. The turbidity was reduced to below 1 NTU when optimum SNP removals

were achieved for both 30R50 and 30CAL50 of different initial SNP volume concentrations (Fig. 4.30(c)(d)). Along with the increase of surfactant addition, the pH value of flotation suspension leveled off and the fluctuation was no greater than 0.5 (Fig. 4.30(e)(f)).

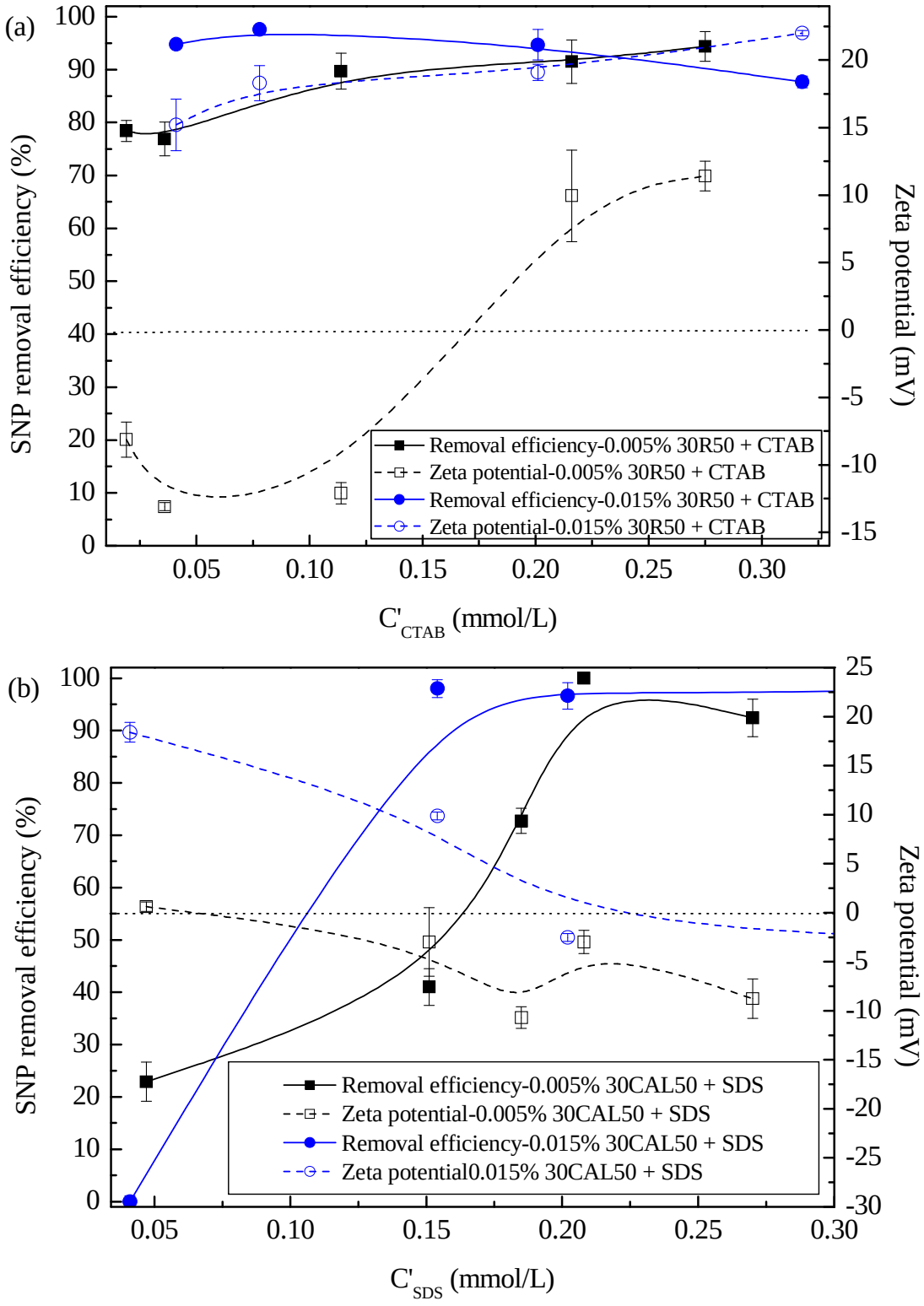

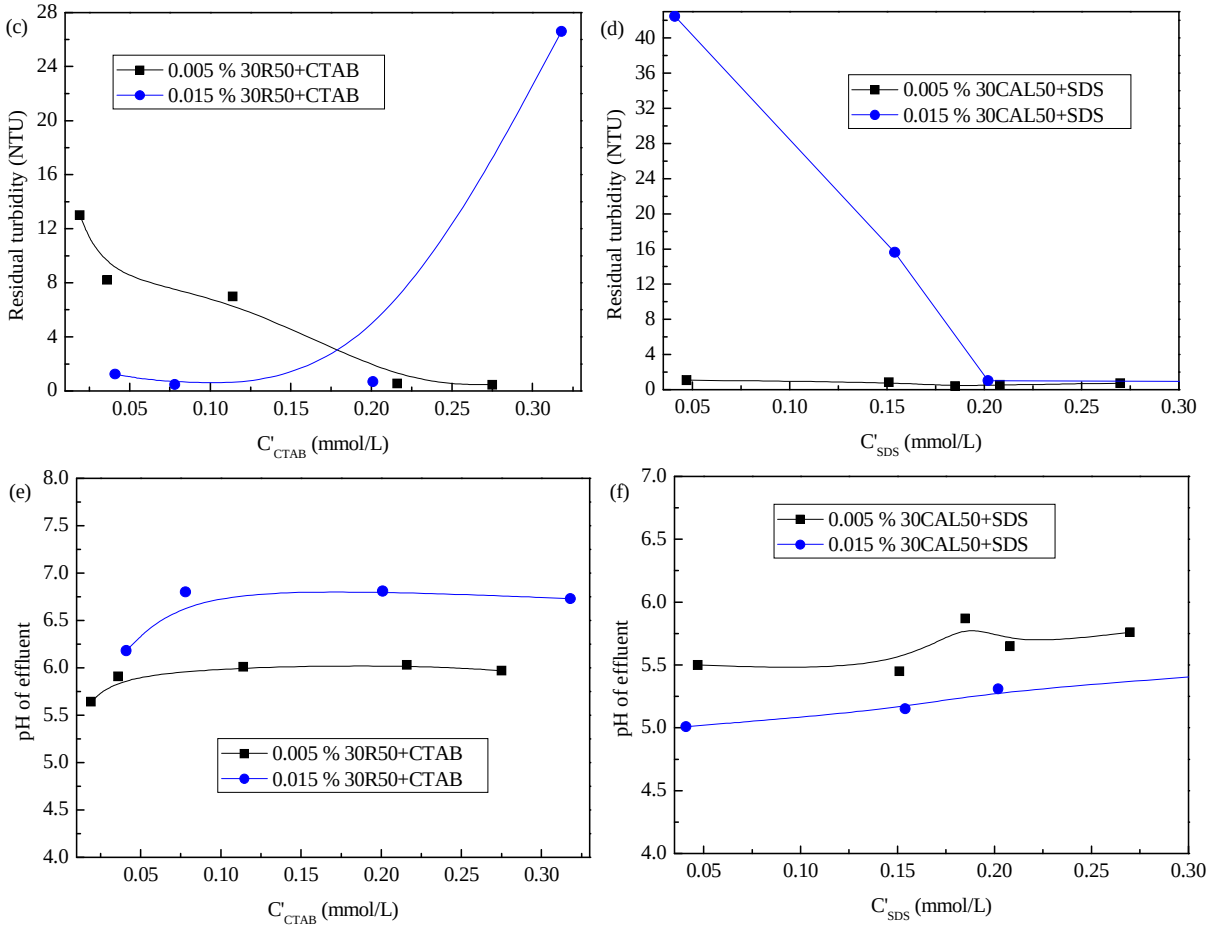

Fig. 4.30. Effect of initial SNP volume concentration on the performance of CGA-flotation: (a), (b) removal efficiency and zeta potential of 30R50 and 30CAL50, respectively; (c), (d) residual turbidity of 30R50 and 30CAL50, respectively; (e), (f) pH of 30R50 and 30CAL50, respectively.

The flotation performance of the negatively surface charged SNP, 30R50, implied that the neutralization of surface charge between CGAs and SNPs occurred more easily for 30R50 0.015 % than for 30R50 0.005 % since the zeta potential of flotation suspension was reversed to +15.2±1.9 mV at the CTAB dosage of only 0.041 mmol/L whereas the zeta potential of 30R50 0.005 % involved flotation suspension was lower than -10 mV at the same CTAB dosage. More than 90 % 30R50 (0.015 %) were removed even when the zeta potential was as high as around +30 mV. It clearly indicated that the electrostatic attraction between aphrons and SNPs was probably prone to occur at higher initial SNP volume concentrations, and subsequently the attachment of bubble-particles were strengthened by hydrophobization of the particles, which agreed well with what was reported by Waters et al. (2008). As for the positively surface charged 30CAL50 in the investigated SDS dosage range, the optimum removal (close to 100 %) could be yielded when the zeta potentials were close to zero no matter higher or lower initial SNP volume concentrations, which highlighted the role of

charge neutralization as the dominant interaction mechanism between 30CAL50 and SDS-CGAs. Moreover, George et al. (2004) found in their study that an increase in particle concentration caused a linear increase in the effective fluid viscosity. Hence the rate of drainage from the froth decreased significantly. This low rate of drainage ensured the froth remained wet with small bubble sizes and mobile interfaces accordingly, and thereby more SNPs could be captured by CGAs inside the foam.

4.3.5 Effect of initial pH of SNP suspension

Given that the pH of influent may impact chemical species involved in the flotation process and complicated reactions on the interface, it is of significance to examine the effect of initial pH of SNP suspensions on the flotation efficiency. In this investigation, pH values of SNP suspension were adjusted to acidic, neutral and basic regions, approximately 3, 6 and 9, respectively. Flotation trials were conducted at the optimum surfactant dosage for each SNP suspension (30R50, 30R25, 30CAL50) involved flotation and the same operating condition as previous experiments. Results are presented in Table 4.5.

For the negatively surface charged 30R50 and 30R25, the SNP removal efficiencies deteriorated at the initial pH around 3.4 whereas the removals were high (> 95 % for 30R50 0.015 % and > 88 % for 30R25 0.015 %) for neutral and basic SNP suspensions; the zeta potential increased gradually with pH. That was consistent with the experimental results of Lien and Liu (2006). As for the positively surface charged 30CAL50, the SNP removal stayed higher than 94 % over the investigated pH values. It is worth noting that all the pHs of effluent were acid or weak acid (around 6.3) even if the initial pH of SNP influent was adjusted to around 9, indicating that some additives in those commercial SNP products might act as buffer reagents and effectively retain these SNP suspensions in a certain pH range.

Table 4.5. Summary of flotation performance under different initial pH values of SNP suspensions.

pH of SNP suspension / Flotation performance	0.015 % 30R50 + 0.275 mmol/L CTAB			0.015 % 30R25 + 0.100 mmol/L CTAB			0.015 % 30CAL50 + 0.444 mmol/L SDS		
	3.4	6.2	9.3	3.4	6.3	9.3	3.2	6.6	8.7
SNP removal (%)	9.6	98.7	95.9	0	96	88.3	98.3	98.6	94.3
Zeta potenital (mV)	-10.6	-4.6	5.41	-7.43	-0.568	5.31	3.05	-3.33	-8.42
Residual turbidity (NTU)	30.6	0.634	0.618	2.61	0.440	0.544	0.509	0.490	0.480
pH of effluent	3.7	6.1	6.6	3.7	6.4	6.4	3.6	6.2	6.3

As shown in Fig. 2.14, in the investigated pH values (around 3, 6 and 9), all the three types of SNPs were highly surface charged (the magnitude of zeta potential was higher than 20 mV) and their suspensions were stable before flotation treatment (the IEP of 30R50 and 30R25 were around pH1~1.5 and that of 30CAL50 was approximately pH9.8). Hence, the decrease of SNP removal efficiency for 30R50 and 30R25 at acidic pH was possibly caused by the variation of CTAB species rather than the variation of SNP surface charge. CTAB is easily dissociated into cationic CTA^+ and bromide ion. Its speciation is not affected as the pH changing from 4.5 to 8.5 (Lien and Liu, 2006). The pH value around 3.4 might impede the dissociation of CTAB and further prevent the electrostatic attraction between CTA^+ and the negatively surface charged SNPs; and the adsorption density of SNPs on the positively charged CGAs could grow as the pH increased. It is worth noting that the 30CAL50 capture was always effective over the studied pH values even if the zeta potential turned to be negative, highlighting the striking capacity of the aphron surface in collecting NPs especially under unfavorable pH conditions.

4.4 Comparison between CGA-flotation and DAF

In the wastewater treatment industry, DAF is a traditionally accepted method. However, there are limitations to the existing DAF: (i) the saturator tank and air compressor used for

dissolving air into the water are inefficient due to the low mass transfer efficiency of air into the water (hence, low gas to liquid ratio), (ii) air compressors have high energy demands, and (iii) blockage of the bubble generator may result in high maintenance costs (Wen et al., 2011). The overall goal in flotation should be to maximize recovery and selectivity with a minimum cost of reagents, bubble production and time (Bai et al., 2004).

Herein, using the same flotation cells, comparative experiments between CGA-flotation and surfactant assisted DAF were carried out upon the three types of SNPs at different initial concentrations (30R50 0.005 %, 30R50 0.015 %, 30CAL50 0.005 %, 30CAL50 0.015 %, 30R25 0.015 %). Surfactant concentrations in the flotation cell ($C_{surf}^{'}$) were determined by previous results of CGA-flotation (Section 4.2): below, equal to and above the optimum concentration. The flow rate of SNP influent Q_1 kept constant in both flotation processes; flow rates of surfactant solution Q_{surf} and pressurized water Q_2 were controlled to keep the pre-determined $C_{surf}^{'}$ consistent with that in the CGA-floation; the flow rate of flotation effluent Q_3 was 30 % of the sum of Q_1 and Q_{CGA} (for CGA-flotation) or the sum of Q_1, Q_2 and Q_{surf} (for DAF). The flotation conditions are listed in Table 4.6.

Table 4.6. Experimental conditions of CGA-flotation and DAF

$C_{surf}^{'}$ (mmol/L)		Q_1 (mL/min)	C_{SNP} (vol.%)	Q_{air} (mL/min)		Q_{surf} (mL/min)		$C_{surfstock}$ (mmol/L)	Q_3 (mL/min)	
		CGAs* or DAF	CGAs* or DAF	CGAs*	DAF	CGAs*	DAF	CGAs* or DAF	CGAs*	DAF
CTAB (+30R50)	0.019	223.8	0.005	33.3	4.5	5.4	6.5	0.8	68.8	81.6
	0.275					117.4	139.1		102.4	121.4
	0.389					212.2	251.3		130.8	155.1
	0.041	124.4	0.015	66.7	8.9	5.4	8.9	1.0	64.9	65.0
	0.201					31.2	52.3		77.8	78.0
	0.318					58.0	96.9		91.2	91.4
SDS (+30CAL50)	0.047	223.8	0.005	33.3	4.5	5.4	6.4	2.0	68.8	81.6
	0.208					12.3	14.6	4.0	70.8	84.0
	0.270					10.6	12.5	6.0	70.3	83.4
	0.041	124.4	0.015	33.3	8.9	5.4	8.9	1.0	38.9	65.0
	0.444					35.5	59.3	2.0	48.0	80.1
	0.625					10.6	17.6	8.0	40.5	67.6
CTAB (+30R25)	0.072	124.4	0.015	33.3	9.7	9.7	16.7	1.0	40.2	69.7
	0.318					58.0	100.5		54.7	94.8
	0.503					126.0	218.2		75.1	130.1

*: “CGAs” stands for “CGA-flotation”.

4.4.1 Flotation performance

Results of those comparative experiments are depicted in Fig. 4.31 in terms of SNP removal efficiency and zeta potential of flotation suspension. As presented in Fig. 4.31(a) and (c), for the low initial SNP concentration as 0.005 vol.%, the NP removal of CGA-flotation was much higher than that of DAF no matter the surfactant dosage was below, equal or above the optimum value: more than 80 % 30R50 and 90 % 30CAL50 could be removed by CGAs, and at the optimum and higher $C_{SDS}^{'}$, the 30CAL50 removal reached even close to 100 %; however, the removal by DAF was always no greater than 30 %.

As for the initial SNP concentration of 0.015 vol.% (Fig. 4.31(b), (d) and (e)), CGAs removed more 30R50 than DAF at $C_{CTAB}^{'}$ below the optimum value; when the CTAB was overdosed, the DAF performed better than CGA-flotation, giving rise to around 40 % removal. DAF could remove around 32 % or 75 % 30CAL50 when SDS was less or over dosed, respectively, but CGAs showed no removal efficiency in those cases. Nevertheless, at the optimum SDS dosage, nearly all 30CAL50 were removed by CGAs whilst the separation by DAF was only around 75 %. For 0.015 vol.% 30R25, the CGA-flotation performed better than DAF over the three investigated CTAB concentrations.

Concerning the zeta potential of flotation suspension, in the CGA-flotation, both of the negatively surface charged SNPs exhibited good flotation efficiencies with the absolute zeta potential higher than 10 mV at different CTAB dosages and initial SNP concentrations. For the DAF process, the zeta potential of flotation suspension experienced from negative (below the optimum $C_{CTAB}^{'}$) to positive (equal or above the optimum $C_{CTAB}^{'}$), and the removal efficiency changed accordingly: a comparatively higher removal could be achieved when the zeta potential got close to zero. It might reveal different mechanisms between CGA-flotation and DAF in the separation process of 30R50 and 30R25: the former might depend on both the surface charge neutralization and probably also the hydrophobic attraction between aphrons and NPs whereas the latter was exclusively related to the surface charge neutralization; moreover, it could also be attributed to the greater air input in the CGA generation resulting in greater bubble amount and thus greater surface for SNP attachment or adsorption. The variation of zeta potential in the removal of positively surface charged 30CAL50 denoted that the electrostatic interaction was predominant in both flotation processes since high removals

were obtained when the zeta potential was around zero. As for the 30CAL50 0.005 vol.% involved flotation, the hydrophobic attraction of CGA-SNP might contribute to the high SNP separation (90 %) at $C_{SDS}^{'}$ above the optimum value, because the zeta potential decreased to about -10 mV in this situation and the electrostatic interaction between CGAs and SNPs turned to be repulsive.

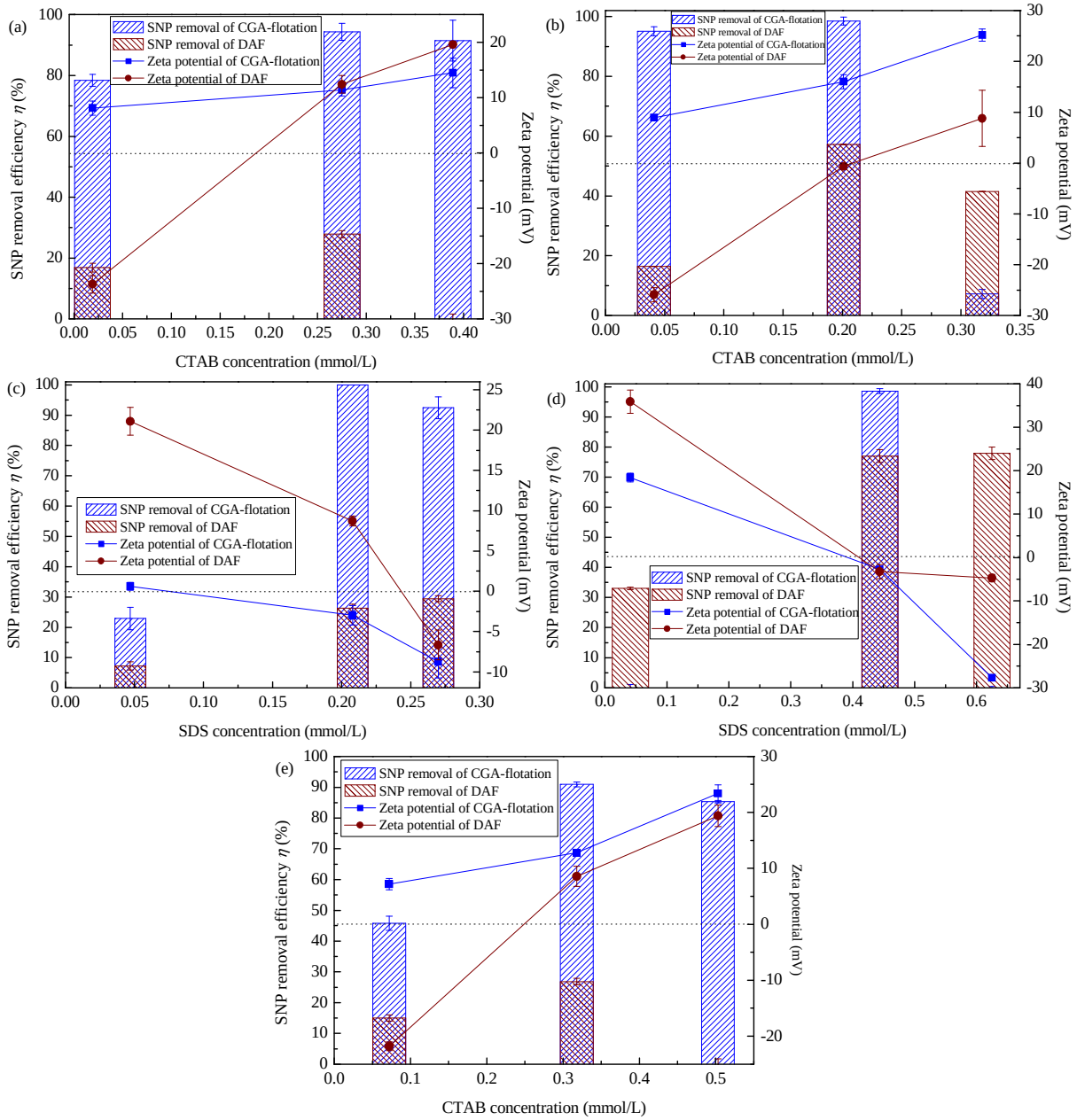

Fig. 4.31. Comparison of SNP removal efficiency and zeta potential between CGA involved flotation and surfactant assisted DAF: (a) 30R50 0.005 %; (b) 30R15 0.015 % (c) 30CAL50 0.005 %; (d) 30CAL50 0.015 %; (e) 30R25 0.015 %.

4.4.2 Reduction of surfactant addition

With the same surfactant concentration of stock solution (Table 4.6), the comparison of surfactant dosages between the two flotation processes are given in Table 4.7, and the reduction of surfactant usage was calculated as follows:

$$R_{surf} = \frac{Q_{surf\ DAF} \times C_{surf} - Q_{surf\ CGA-flotation} \times C_{surf}}{Q_{surf\ DAF} \times C_{surf}} \times 100\% = \frac{Q_{surf\ DAF} - Q_{surf\ CGA-flotation}}{Q_{surf\ DAF}} \times 100\% \quad (4.9)$$

The surfactant was added together with air bubbles in the CGA-flotation process whilst the bubble suspension and surfactant solution were input into the flotation cell separately in DAF. It is obvious in Table 4.7 that the former process demanded less surfactant than the latter. For the lower initial SNP concentration in influent (0.005 vol.% 30R50 and 30CAL50), the decrease of surfactant dosage was around 15~16 %, and for higher initial SNP concentrations as 0.015 vol.% (for 30R50, 30CAL50 and 30R25), the reduction magnitude was approximately 39~43 %. The less surfactant addition would reduce the cost of flotation treatment with respect to less reagent usage, and meanwhile make the process more environmentally friendly since surfactants were possibly the potential aqueous pollutants.

Table 4.7. Comparison of surfactant consumption between CGA-flotation and DAF.

SNP solution	Surfactant flow rate (mL/min)		Reduction (%)
	CGA-flotation	DAF	
0.005 vol.% 30R50	5.4	6.5	16.9
	117.4	139.1	15.6
	212.2	251.3	15.6
0.015 vol.% 30R50	5.4	8.9	39.3
	31.2	52.3	40.3
	58	96.9	40.1
0.005 vol.% 30CAL50	5.4	6.4	15.6
	12.3	14.6	15.8
	10.6	12.5	15.2
0.015 vol.% 30CAL50	5.4	8.9	39.3
	35.5	59.3	40.1
	10.6	17.6	39.8
0.015 vol.% 30R25	9.7	16.7	41.9
	58	100.5	42.3
	126	218.2	42.3

4.4.3 Mechanism comparison between CGA-flotation and DAF

It has been commonly accepted that the interaction between the ionic surfactants and oppositely charged surfaces are characterized by four regions (Zhang and Somasundaran, 2006): Region I – at low surfactant concentrations, the adsorption is due to electrostatic interaction between individual isolated charged monomeric species and the oppositely charged solid surface; Region II – at the onset, surfactant species begin to form surface aggregates and solloids (surface colloids) due to lateral interactions between hydrocarbon chains, the charge neutralization is still active, and the adsorption density exhibits a sharp jump in this stage; Region III – when the solid surface is electrically neutralized by the adsorbed surfactant ions, the electrostatic attraction is no longer operative and adsorption takes place because of lateral attraction alone with a reduced slope; Region IV – when the surfactant concentration reaches the CMC, the surfactant monomer activity becomes constant and any further increase in concentration contributes only to the micellization in solution and it does not change the adsorption density. In this study, the surfactant concentration was always far less than the CMC so the Region IV would not be taken into account. As for the CGAs, even at low concentrations that should have been in the Region I, due to the preformed surfactant encapsulated surface, the surfactant molecules could attach the NP surface in high density compared with the DAF process in which the surfactant was free in the flotation suspension and separated from gas bubbles. Thereby, the interaction between CGAs and SNPs probably started from Region II where both electrostatic attraction and hydrophobic lateral interaction make effect. That might be the reason why the CGA-flotation gave rise to higher SNP removal efficiency even though the surfactant dosage was low, and confirmed that, in the current work, the DAF process was mainly controlled by electrostatic interaction of SNP-surfactant-bubble while the CGA removed SNPs via both hydrophobic attraction and charge neutralization with a preference of the former.

Moreover, possible interaction mechanism schemes of CGA-flotation and DAF processes are compared in Fig. 4.32. Based on properties of CGAs and their flotation behavior, three possible configurations of CGA-SNP aggregate are proposed. Configuration 1 in Fig. 4.32(a): CGAs covered with NPs complex with each other by free surfactant molecules; Configuration 2 in Fig. 4.32(a): CGAs connect with each other directly via the NP layer on the ahpron surface; Configuration 3 in Fig. 4.32(a): NP-surfactant aggregates form and then their hydrophobic ends (provided by surfactant molecules in the aggregates) act as the bridge

between CGAs and those aggregates. It is indicative that, in the CGA-flotation, SNPs can be collected by aphrons in the absence and presence of adsorbed surfactants on the particle surface. As for DAF, the flotation aggregates can be composed by the conventional particle-surfactant aggregates adsorbing on the bubble surface (Fig. 4.32(b)). It can be assumed that air bubbles can only efficiently capture SNPs and as well as their aggregates when they are sufficiently hydrophobized by adsorbing surfactants – surfactant hydrophilic head groups interacting electrostatically with charge sites of particle surface and thus exposing their hydrophobic tails towards the bulk. But for the sake of the good adhesion onto the hydrophobic bubble surface in DAF, the presence of surfactant surface aggregates is unfavorable, which are created due to hydrophilic head groups of supplementary adsorbed surfactants. That different interaction between bubbles and SNP involved aggregates may give the proper explanation for the better flotation performance obtained by CGAs compared with dissolved air bubbles.

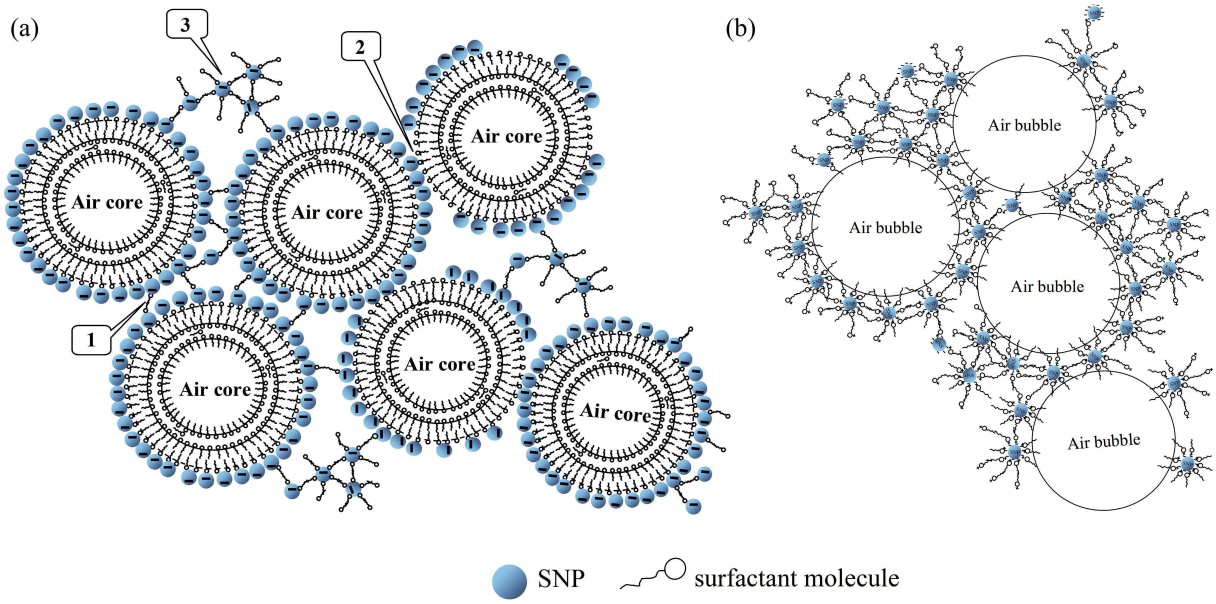

Fig. 4.32. Comparison of possible configurations between (a) CGA-SNP aggregates and (b) bubble-surfactant-SNP aggregates in flotation processes (The scheme is drawn out of proportion).

4.5 Conclusions

The main objective of this chapter is to generate the surface functionalized microbubbles, CGAs, by a laboratory designed generator based on the idea of Sebba (1985), and extend their application into the SNP separation in way of the continuous flotation process. Features of CGAs were investigated with respect to visualization, stability (τ_S), size, and surface charge

in either the batch or continuous generation mode. The mechanistic interaction between SNPs and surfactant was also studied through adsorption-aggregation experiments. The flotation removal efficiency of SNPs was then specially examined, which was followed by the comparative study between CGA-flotation and DAF. Herein, a series of conclusions can be drawn as below.

CGA generation and characteristics

- The created CGAs were observed by optic microscope, and the apparent bubble size was estimated from tens of micrometers to more than one hundred meter microns.
- The stability of CGAs was investigated at the batch generation mode. Kinetic drainage curves of CGAs were fitted well by Hill equation, and the fitting values of half life τ_S were quite close to the experimental measurement. Increasing surfactant concentration might extend τ_S but it did not help any more when the surfactant concentration was higher than CMC possibly due to the effect of CMC. Introducing air flow into the CGA production process could prolong τ_S particularly for the SDS-CGA. CGAs generated in the absence and presence of air flow both experienced the two-stage drainage process: (i) fast and linear drainage and then (ii) slow thinning of liquid film. Without air flow in generation, the drainage in Stage i had a maximum draining speed while the draining speed kept falling from the very beginning of drainage for those CGAs created with air input.
- As for the CGA size measurement by laser diffraction via Sparytec, in the batch generation mode without air flow during production, different concentrations and pH values of surfactant solution made no effects on the CGA size: average sizes of CTAB-CGAs and SDS-CGAs were around 24~25 μm and 26~27 μm, respectively, at surfactant concentrations below, equal and above CMCs. At pH values of approximately 3, 6 and 9: the size of CTAB-CGAs kept at around 23.1±0.5 μm and that of SDS-CGAs remained at 22.6±0.3 μm.

  The continuous generation mode was used in the flotation separation of NPs in this study and therefore it is necessary to measure the CGA size under this condition. Generally, the average size of CTAB-CGA was in the range of 36~45 μm and that of SDS-CGA ranged between 40 μm and 49 μm. Increasing the concentration and air flow rate of surfactant solution as well as air flow rate could help to decrease the CGA size to some extent. It is worth noting that the batch generation mode resulted in the smaller CGA size than the

continuous mode since the former (i) allowed sufficient stirring and retention time in the generator for forming stable microbubble and also (ii) avoided the destroy of CGAs by manipulation and kept them in small and uniform size via the careful collection of CGA suspension by syringe, without going through the outlet of generator and the inlet of chamber for Spraytec measurement.

- The zeta potential of CGAs could be measured by NanoZS as other particle or colloidal suspensions due to their high stability. Results clearly confirmed the charge surface modification of CGAs by anionic or cationic surfactant. The absolute zeta potential of both CTAB-CGAs and SDS-CGAs were lower than 10 mV; greater surfactant concentrations could increase the absolute zeta potential but the increasing trend tapered off at high surfactant concentrations.

Adsorption-aggregation of surfactant on SNPs

- Modeling fittings of experimental results concerning ionic surfactants adsorbing on oppositely charged surfaces denoted that the adsorption of cationic surfactant CTAB on the surface of negatively surface charged SNPs (30R50 and 30R25) was predominated by homogeneous process while the anionic surfactant SDS on the positively surface charged 30CAL50 was controlled primarily by heterogeneous interaction. The greater adsorption capacity and affinity of 30R25 and 30R50 toward the surfactant molecules were probably due to their stronger electrostatic forces of attraction involved and higher specific surface areas than those of 30CAL50. Besides, as implied by the fitting of D-R equation, there might be more reactive surfaces on the surface of 30R50 and 30R25, possibly being resulted from the presence of high concentrations of edge/corner sites and other defects.
- For the cases of 30R50+CTAB and 30R25+CTAB, the electrophoretic mobility of post-(adsorption-aggregation) suspension distinguished two regions in which adsorption occurred via different mechanisms: i) the 1st region was featured by the sharp increase of zeta potential along with the initial surfactant concentration, and the leading roles of SNP-surfactant interaction were inferred to be the charge neutralization between CTA^+ and negatively surface charged silica; ii) plateaus appeared in the 2nd region resulting from the saturated surfactant adsorption on the particle surface at the concentration higher than CMC. The aggregates of 30R50-CTAB and 30R25-CTAB were of smaller average diameter and more compact fractal structure, whilst the 30CAL50-SDS aggregates exhibited larger size and loose morphology.

Continuous CGA-flotation

- The SNP removals, in excess of 97 % for 30R50 by CTAB-CGAs, 96 % for 30R25 by CTAB-CGAs, and 98 % for 30CAL50 by SDS-CGAs, were achieved. The optimum surfactant concentration could be figured out, and for instance, the highest 30R50 0.005 % removal could be reached at 0.114 mmol/L CTAB and the highest 30CAL50 removal could be got at 0.208 mmol/L SDS. Greater initial SNP concentrations and smaller SNP size were favored for the CGA-flotation process. The neutral and basic initial SNP suspension was recommended for the CTAB involved flotation since the pH of around 3.5 could resulted in poor SNP removal. The SDS-CGAs remained high flotation efficiency over all investigated pH values.
- CGAs were effective in the flotation of NPs, possibly due to (i) its small size and stability enhancing the Brownian diffusion of SNP to the bubble surface, (ii) the strong electrostatic neutralization between the opposite surface charges of aphrons and SNPs, (iii) the hydrophobicity of aphron surface giving rise to strong non-DLVO interaction between SNP and bubbles, and (iv) the ion exchange occurring between the Na^+ and CTA^+ in the case of 30R50 (30R25), or Al derivative and DS^- in the case of 30CAL50 that favored the hydrophobic bonding mechanism, when the surfactant concentration was sufficiently high.
- The CGA-flotation performed better in the NP removal than DAF did when dosing the same amount of surfactant particularly in the case of using CTAB to remove negatively surface modified SNPs. The CGA could improve the flotation process by using less assisting reagent compared with DAF. In the CGA-flotation, SNPs could be collected by aphrons in the absence and presence of adsorbed surfactants on the particle surface. As for DAF, the flotation aggregates formed via the conventional particle-surfactant aggregates and then were adsorbed on the bubble surface. It could be assumed that air bubbles were only able to efficiently capture SNPs and their aggregates when they were sufficiently hydrophobized by adsorbing surfactants and the presence of hydrophilic surfactant surface aggregates was minimized for the sake of good adhesion onto the hydrophobic bubble surface in DAF.

Chapter 5
Conclusions and prospects

Summary

5.1 Summary of the present dissertation

The treatment of NP polluted wastewater is a serious challenge owing to extremely small particle size (< 100 nm), stable dispersion, and intricate colloidal nature. Flotation is the particle-separation process based on the attachment or adsorption of particles on the surface of bubbles passing through the particle suspension. This dissertation is devoted to improve the NP removal efficiency by flotation. It has been widely reported that the flotation of NPs is tough due to the predominant transport mechanism of NP onto the bubble surface -- Brownian diffusion. Two general methods to overcome the difficulty were taken into consideration here: (1) increasing the particle size from nanoscale to micronscale so that NPs can be floated and removed as traditionally micron aggregates; (2) decreasing bubble size and surface modifying the bubble surface in order to reinforce the Brownian motion and colloidal interaction between bubbles and NPs and thus to raise the NP capture efficiency.

Given to the consideration above, experiments were designed and divided into two parts. Firstly, attempts were made to separate NPs from aqueous suspensions by DAF. In this part, TNP was chosen as treating target, and the dissolved organic matter, HA, was selected as flotation assisting reagent. A series of agglomeration experiments were foremost carried out before flotation to understand interaction mechanisms between TNPs and HA, and also to test the feasibility of using HA in the particle separation. Results denoted that TNP-HA aggregates formed during the surface modification process and resulted in a clearest supernatants at 9.15 mg/L DOC, and the optimum HA dosage range was determined to be 7.8~9.15 mg/L. The charge neutralization between OH^- and TNPs played the leading role in inducing the real TNP agglomeration, and other anions (i.e. Cl^-, polyainons of HA molecules) with less charge density than OH^- helped to screen the particle surface charge layer. At equilibrium pH values lower than 3, the ionization of HA molecules was weak and HA colloidal precipitates were present, resulting in the insufficiently electrostatic attraction between polyanions of HA and TNPs but the aggregation between TNPs and colloidal HA. The fractal dimension analysis corroborated that aggregates of TNP-OH^--HA polyanions

attained mainly by the charge neutralization mechanism were of compact configuration whereas the interaction between TNPs and HA colloids was loose in view of morphological structure.

The HA assisted DAF and pH adjusted DAF were investigated and compared. The pH adjustment of flotation suspension could help to remove TNPs but the removal efficiency was no higher that 65 %. It was found that approximately 99 % TNPs could be removed when the pH of HA stock solution was around 4.7 and 6.2. However, when adding the basic HA stock solution, the flotation effect decreased even at the optimum HA dosage. A higher A/S value would improve the flotation performance by providing larger bubble surface for the TNP-bubble attachment. When the resulting pH of flotation suspension was higher than 4, the charge neutralization between TNPs and OH^- predominated the formation of TNP aggregate. Additionally, other interaction mechanisms might also contribute to the TNP removal: the ligand exchange, bonding effect between HA and the TNP surface, the enhanced hydrophobic attraction of TNPs possibly due to HA layer formed on the particle surface. When the pH of the TNP-HA suspension was no higher than 4, most HA molecules were not really soluble and thus uncharged, and they might aggregate themselves and form colloidal precipitates to minimize the contact with the surrounding aqueous environment by making their hydrophobic moieties outwards. The colloidal precipitate of HA could act as an extended colloidal fishnet where TNPs would be enmeshed or trapped, then leading to a greater bubble-particle attachment efficiency and stability. It is worth noting that, in either aggregation or flotation, the low residual DOC was always achieved along with the TNP separation. This revealed a sound participation of HA in the DAF process. The removal of TNPs by DAF was yielded by the formation of TNP-HA-bubble aggregates. The high removal of DOC also indicated that the release of those DAF effluents into aqueous environment would not cause an environmental problem.

The second part of this study focused on employing a system of surface modified microbubbles (CGAs) in flotation to remove NPs. CGAs were created from the cationic

surfactant CTAB and anionic surfactant SDS, individually, by the laboratory scale CGA generator which was fabricated according to the design of Felix Sebba in 1985. CGAs were observed under optical microscope for morphological visualization. The half life τ_S was used to characterize the stability of CGAs and measured to be in the range of 80~150 s under different generating conditions. A two-stage drainage behavior was found in all cases of CGA generation. The CGA size was measured by laser diffraction. The stirring speed of the agitator greatly influenced the CGA size, and 8000 rpm was selected in this study given to the consideration of energy consumption and small-sized bubble demand. Generally, the average size of CTAB-CGA was in the range of 35~45 µm and that of SDS-CTAB ranged between 40 µm and 50 µm in the continuous generation mode whilst in the batch mode, CTAB-CGAs and SDS-CTAB have a mean diameter of 20~30 µm. Increasing the concentration and the flow rate of surfactant solution and as well as the air flow rate could decrease the CGA size to very limited extent. The surface charge modification was confirmed by zeta potential measurement of CGAs. Results revealed that CGAs could be positively or negatively surface charged by using different surfactants, which might strengthen the electrostatic attraction between bubbles and particles with opposite surface charges in flotation.

Interaction mechanisms between SNPs and surfactant molecules were studied by adsorption isotherms. Compared with the Langmuir model, Freundlich and Langmuir-Freundlich models fitted the experiments data better especially the latter that could predict the maximum adsorption capacity of SNPs. Combined with the Temkin and D-R modeling fitting results, it was concluded that the interaction between CTAB and 30R50 (or 30R25) was a homogeneous process that controlled by physical sorption while the adsorption of SDS-30CAL50 was heterogeneous and mainly dominated by chemical interaction between SNPs and SDS.

Thereafter, a continuous CGA generation-flotation process was applied in the NP separation. Three types of SNPs with different particle size and surface charges were selected as treating targets. At the optimum surfactant concentration, almost 99 % SNPs could be removed.

Influences of surfactant concentration, SNP size, SNP concentration and pH value of influent on the flotation performance were investigated. Results showed that high removal efficiencies could be obtained at surfactant concentrations even less than 0.02 mmol/L. Greater initial SNP concentrations and smaller SNP size were favored for the CGA-flotation process. The neutral and basic initial SNP suspension was recommended for the CTAB involved flotation since the pH of around 3.5 could resulted in poor SNP removal. The SDS-CGAs remained high flotation efficiency over all investigated pH values. The effect of hydrophobic attraction might overweight that of electrostatic attraction for the CGAs involved flotation. The comparison between CGA-flotation and DAF was carried out under the optimum flotation condition determined by previous CGA-flotation experiments. CGAs could remove SNPs more efficiently than DAF. Compared with DAF which mainly depended on the hydrophobization of particle surface by surfactants, the CGA-flotation is distinguished in view of more effective treatment both in the absence and presence of adsorbed surfactants on the particle surface, which could result in the less surfactant demand.

5.2 Future work and prospects

Results attained in this study have presented the efficiency of HA assisted flotation and the capacity of CGAs in the NP separation. There are several areas still requiring further investigations based on the findings from this work.

- Natural organic matters such as humic substances extracted directly from water or soil sources, chitosan, and the extracellular polymeric substances (EPS) from water treatment plants, may be used to facilitate the flotation of NPs. Via the attachment or adsorption of organic matters-NPs and the following removal by bubbles, the separation of both NPs and water polluted organic matters would realized at the same time, and thereby a more environmentally friendly process can be developed;
- Polyelectrolytes (for example, polyaluminum chloride) are potential additive combined with commonly used surfactant in the CGA generation to create surface functionalized aphrons. In this case, the selective flotation removal of NPs may be done to treat the multiple NP wastewater;

- The in situ characterization of flotation aggregates in terms of size and morphology has always been a problem due to the existence of fragile bubbles inside flocs that gives rise to the instability of flocs. The dynamic study of flotation flocs needs to be further explored by applying different techniques, such as laser diffraction scattering by Spraytec or Mastersizer, or X-ray diffraction, etc. The measurement conditions should be determined and optimized;
- Using CGAs involved flotation in pilot- and plant- scale applications still remains to be developed. A capital-saving and high efficient process with CGAs needs to be worked out by improving the design of CGA generator, selecting or synthesizing functionalized surfactant, and optimizing flotation conditions.

Appendices

Appendix A

Molecular weight of HA

High performance size exclusion chromatography (HPSEC, Akta Purifer, GE Healthcare, USA) was used to measure the molecular weight (WM) of HA. Instrumentation comprised a solvent pump, a UV detector, and a rotary injector valve equipped with a 20 µL sample loop. A silica-based column was employed for this characterization, which has a general MW cutoff limit of 1000 kDa based upon the configuration of random coiled macromolecules. The column packing was selected based upon its low residual hydrophobicity and minimal ion-exchange capacity. HA was detected at wavelength of 254 nm and 280 nm. The eluent solution for the mobile phase was prepared with 25 mM Na_2SO_4 and a phosphate buffer (2.4 mM NaH_2PO_4 and 1.6 mM Na_2HPO_4 at pH 6. The flow rate of eluent passing through the column was 1.0 mL/min. The MW could be determined by calibration of retention time using known MW standard (herein, standard proteins): conalbumin (75 kDa), ovalbumin (43 kDa), carbonic anhydrase (29 kDa), ribonuclease A (13.7 kDa) and aprotinin (6.5 kDa) from GE Healthcare. Prior to HPSEC analysis, each sample was prefiltered on a 0.45 µm membrane.

The stock HA solution was diluted 500 times and filtered through the 0.45µm membrane before the HPSEC analysis. The result obtained has been presented in Fig. A(a), and the MW of HA was determined to be approximately 17.3 kDa by calibration curve in Fig. A(b).

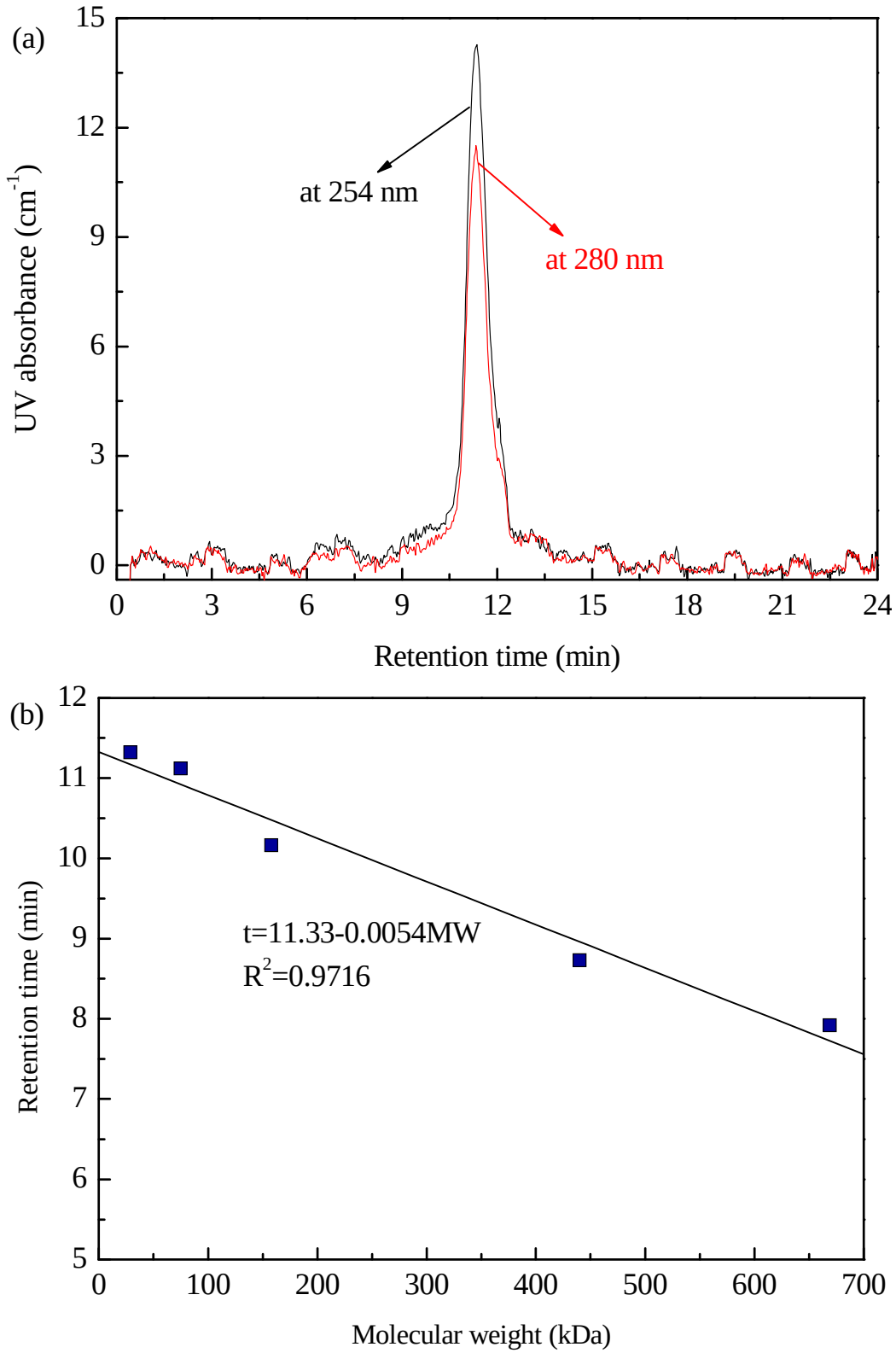

Fig. A. Determination of molecule weight by HPSEC: (a) high performance size exclusion chromatogram of HA used in this study; (b) retention time as a function of MW.

Appendix B

Adsorption-aggregation isotherm of surfactant on SNPs

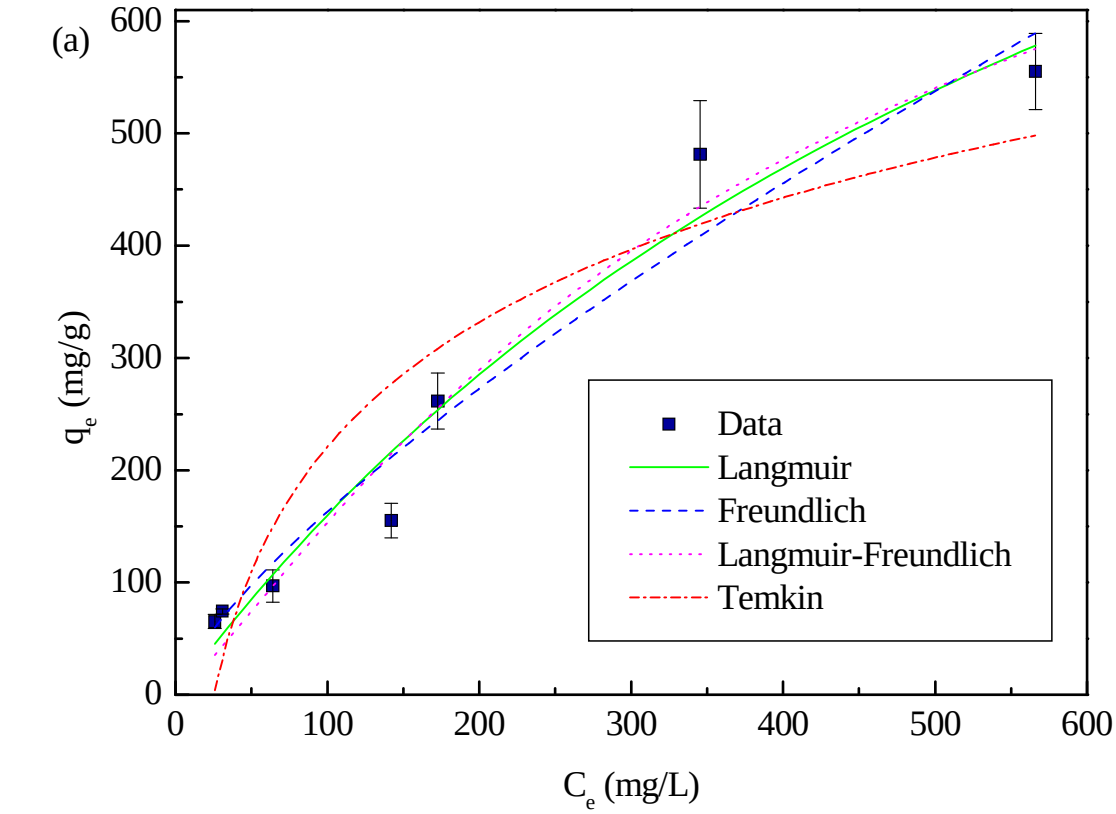
(a)
600
500
400
300
200
100
0
0
100
200
300
400
500
600
q_e (mg/g)
C_e (mg/L)
Data
Langmuir
Freundlich
Langmuir-Freundlich
Temkin

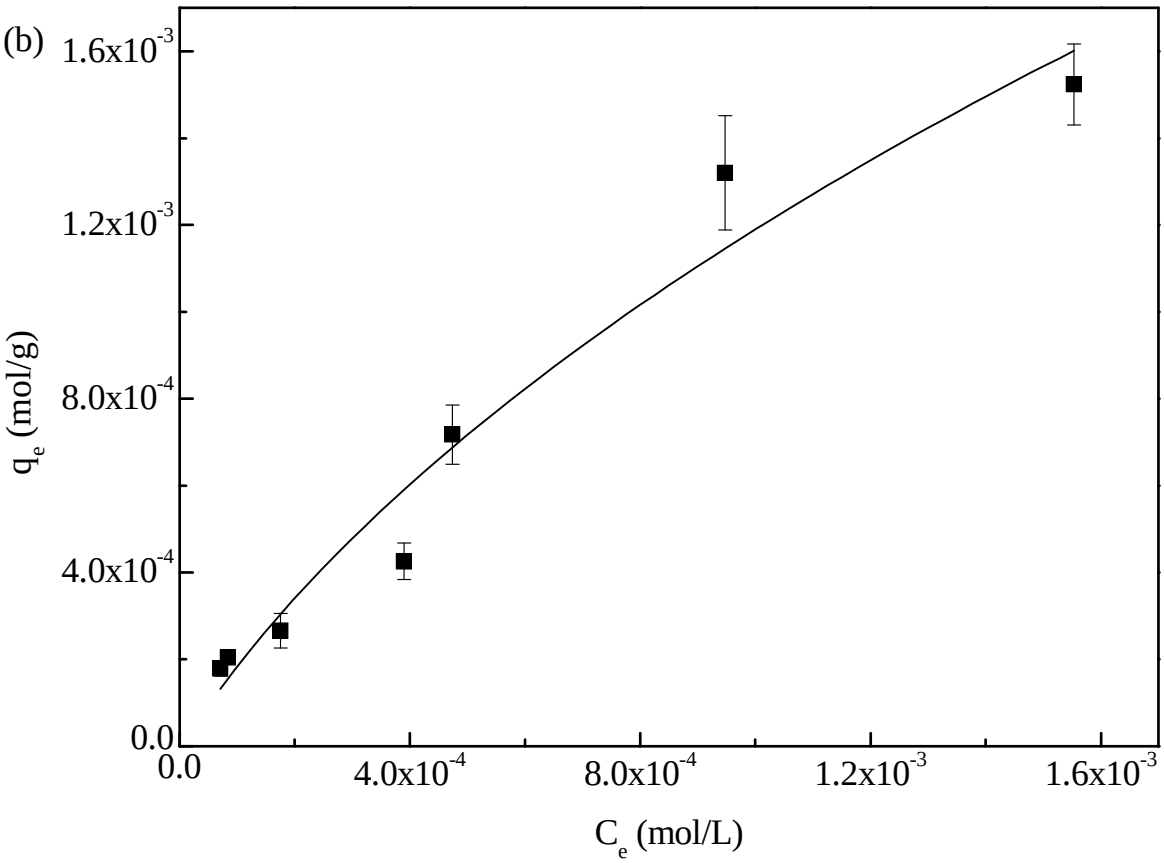
(b)
1.6x10^{-3}
1.2x10^{-3}
8.0x10^{-4}
4.0x10^{-4}
0.0
0.0
4.0x10^{-4}
8.0x10^{-4}
1.2x10^{-3}
1.6x10^{-3}
q_e (mol/g)
C_e (mol/L)

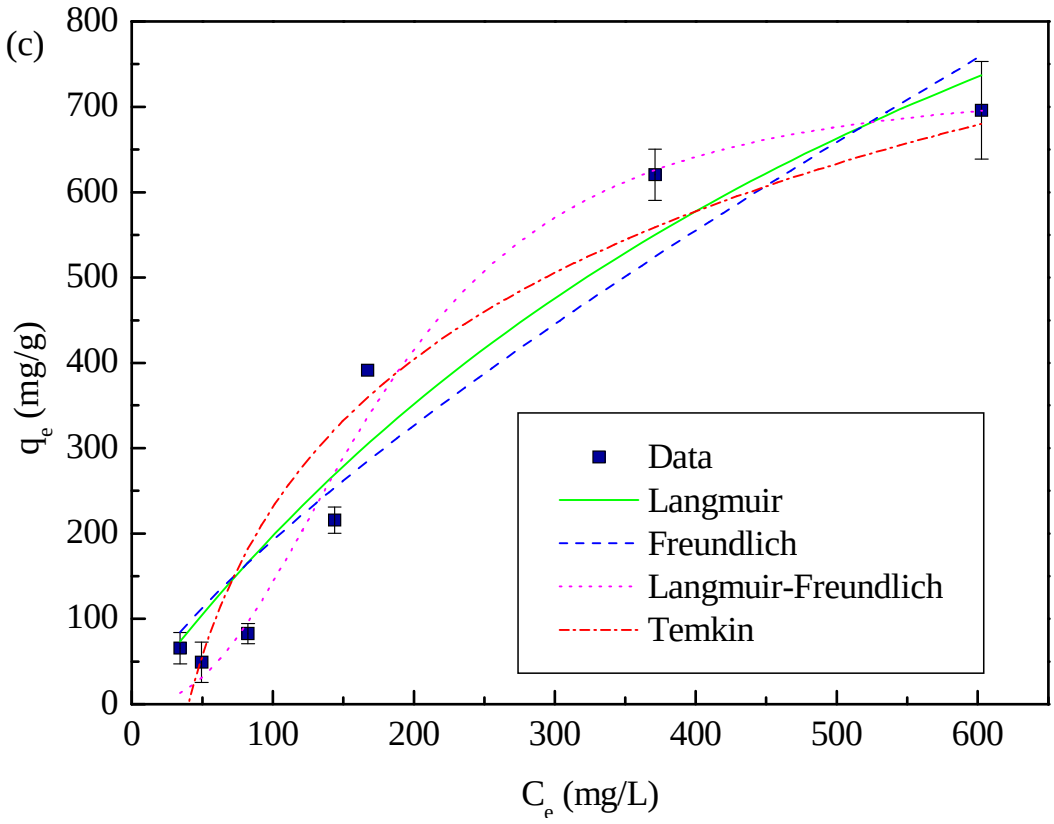
(c)
800
700
600
500
400
300
200
100
0
0
100
200
300
400
500
600
q_e (mg/g)
C_e (mg/L)
Data
Langmuir
Freundlich
Langmuir-Freundlich
Temkin

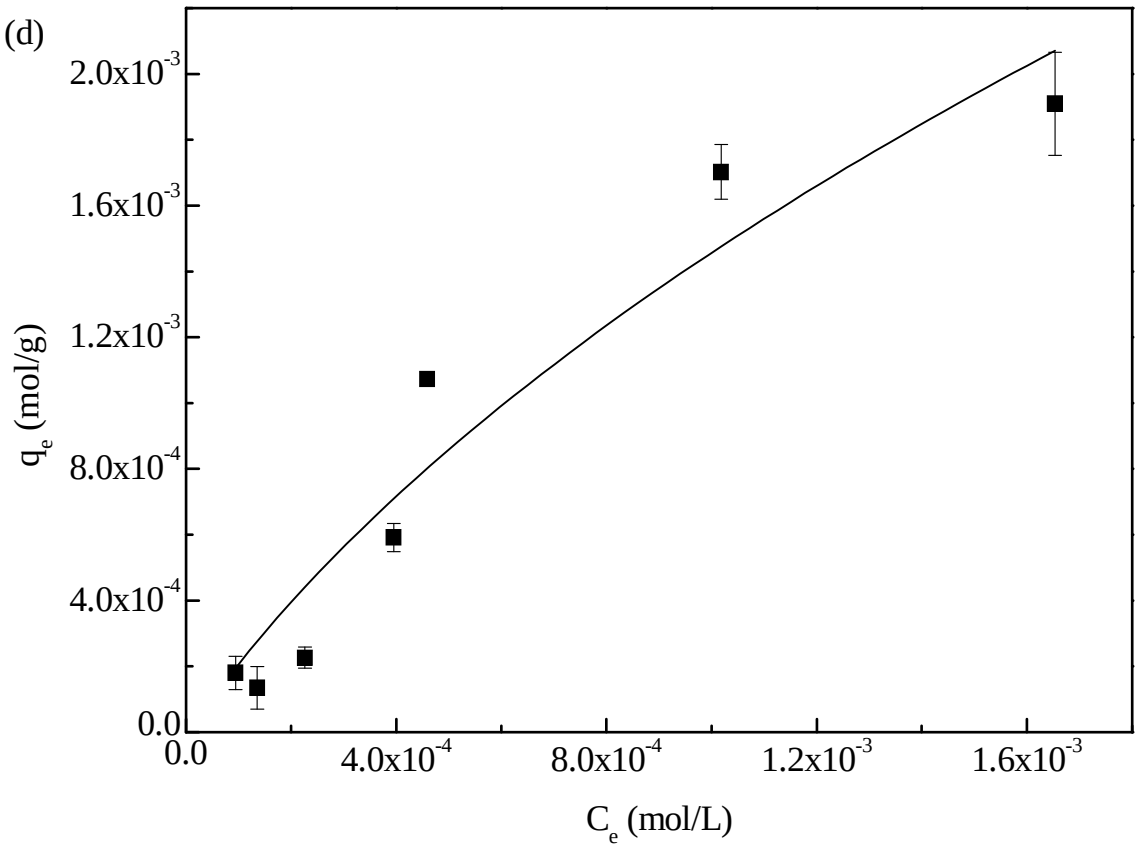
(d)
$2.0x10^{-3}$
$1.6x10^{-3}$
$1.2x10^{-3}$
$8.0x10^{-4}$
$4.0x10^{-4}$
0.0
0.0
$4.0x10^{-4}$
$8.0x10^{-4}$
$1.2x10^{-3}$
$1.6x10^{-3}$
q_e (mol/g)
C_e (mol/L)

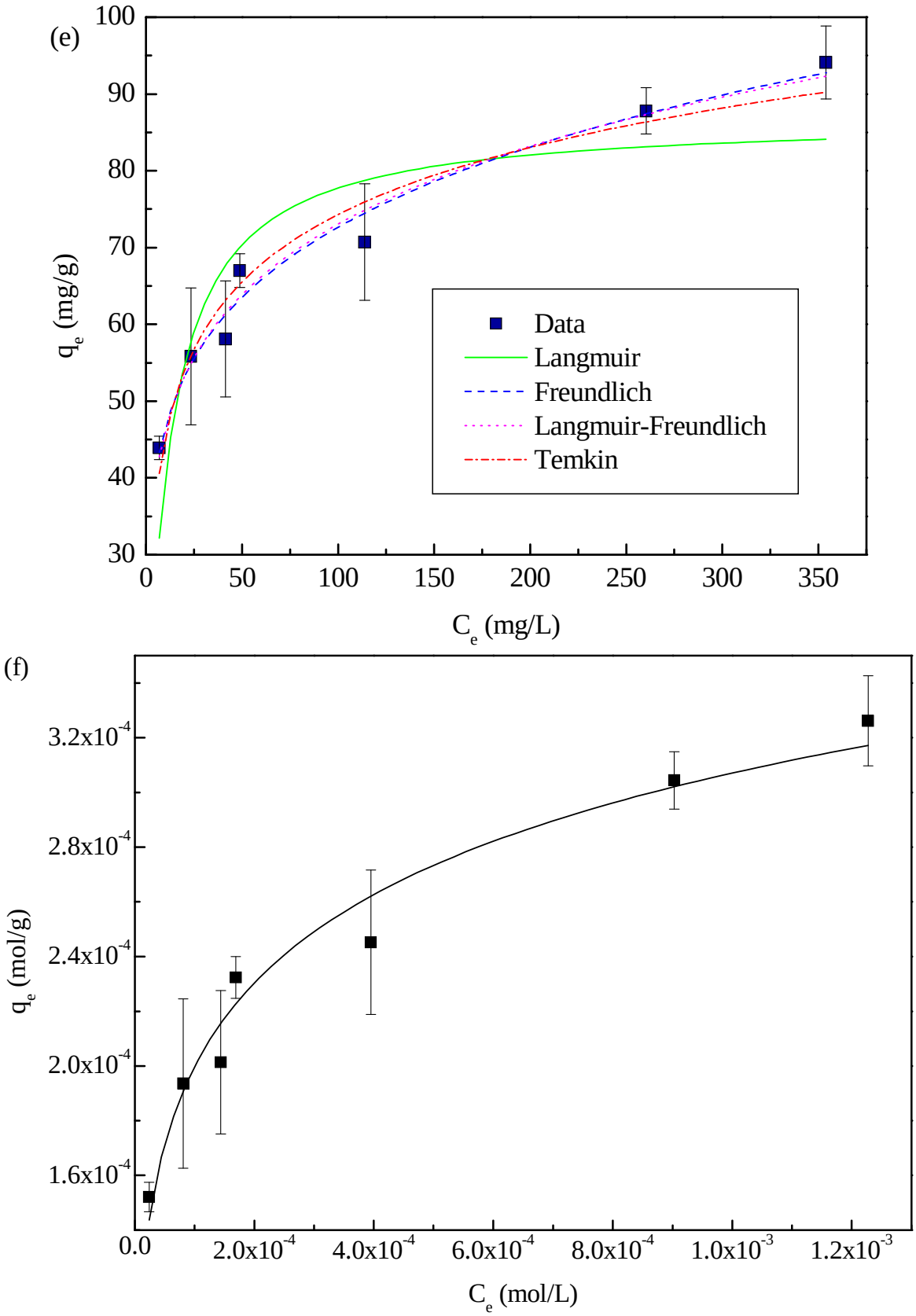

Fig. B. Adsorption results of 0.015 vol.% SNP+surfactant: (a), (c) and (e) experimental data and fitting curves of Langmuir, Freundlich, L-F and Temkin isotherms for 30R50+CTAB, 30R25+CTAB, and 30CAL50+SDS, respectively, (b), (d) and (f) experimental data and fitting curve of D-R isotherm for 30R50+CTAB, 30R25+CTAB, and 30CAL50+SDS, respectively.

Appendix C

Publication

Journal of Hazardous Materials 260 (2013) 122–130

Contents lists available at SciVerse ScienceDirect

Journal of Hazardous Materials

journal homepage: www.elsevier.com/locate/jhazmat

Elimination of TiO_2 nanoparticles with the assist of humic acid: Influence of agglomeration in the dissolved air flotation process

Ming Zhang [a,b,c], Pascal Guiraud [a,b,c,*]

[a] Université de Toulouse; INSA, UPS, INP; LISBP, 135 Avenue de Rangueil, F-31077 Toulouse, France
[b] INRA, UMR792 Ingénierie des Systèmes Biologiques et des Procédés, F-31400 Toulouse, France
[c] CNRS, UMR5504, F-31400 Toulouse, France

HIGHLIGHTS

- TiO_2 nanoparticles in the wastewater were eliminated with humic acid assisting by dissolved air flotation.
- Interaction mechanisms between TiO_2 nanoparticles and humic acid were investigated.
- Humic acid could improve the TiO_2 removal efficiency in flotation.
- Optimum operational conditions were determined.

ARTICLE INFO

Article history:
Received 26 February 2013
Received in revised form 30 April 2013
Accepted 2 May 2013
Available online xxx

Keywords:
Dissolved air flotation
TiO_2 nanoparticles elimination
Humic acid
Surface modification
Agglomeration

ABSTRACT

With recent advances in nanotechnology, environmental and health consequences of nanomaterial disposal merit close attention. In the search for environmentally-friendly reagent, this study investigates the use of humic acid (HA) as an assist of dissolved air flotation (DAF) in the TiO_2 nanoparticle (TNP) elimination. To determine mechanisms of TNPs interacting with HA, surface modification experiments were firstly carried out; thereafter, laboratory scaled DAF tests were applied to remove TNPs with HA assisting. Results of surface modification experiments showed that the zeta potential of TNP suspension system had a reversal trend due to counter ions of TNP and anions offered by the HA stock solution. The surface modified suspension was not easy to restabilize because of the close combination of TNPs and HA through sphere linkages or hydrogen-bonded surface complexes. Agglomeration took place more readily along with increasing HA concentration in the optimum dosage range (7.8-9.15 mg/L DOC). The flotation performance revealed that HA could improve the DAF efficiency in the optimum dosage range of HA. The interaction between TNPs and HA (Na^+-humate), including surface charge neutralization (electrostatic interactions), sphere linkages or hydrogen-bonded surface complexes, hydrophobic interactions, and van der Waals interactions, played dominant roles.

1. Introduction

Manufactured nanomaterials have moved well beyond laboratory settings and are now found in a variety of commercial products. Titanium dioxide (TiO_2) is one of the most widely used nanomaterials in consumer products including sunscreens, cosmetics, paints and other products. TiO_2 nanoparticles (TNPs) can be introduced into the environment from processes such as mining, TiO_2-enabled product fabrication, product use, product recycling and disposal to the aquatic environment [1]. TNPs become problematic and are viewed as an emerging pollutant due to their neurotoxicity to animals, capability of causing oxidative stress in human cells and genetic instability in mice. After being released into the environment, TNPs have the potential to be transported in the subsurface [2]. Subsequently nanoparticles may get into groundwater and enter into the food web through bioaccumulation [3,4]. Over the last decade, given the environmental and ecological risk of aqueous TNPs, the TNP elimination from wastewater has received a certain degree of attention though more exploration is still greatly in need. For instance, Shen's research results demonstrated the feasibility of separating colloidal TiO_2 (particle size 30-70 nm) from an aqueous suspension by foam flotation. It was found that coulombic interaction between TiO_2 particle surface and the ionic collectors plays a dominant role in their system [5]. A group of researchers in Arizona State University have dedicated to the nanoparticle (including TiO_2 nanoparticles) removal by biosorption in both lab-scale study [6,7]

* Corresponding author at: Université de Toulouse; INSA, UPS, INP; LISBP, 135 Avenue de Rangueil, F-31077 Toulouse, France. Tel.: +33 0 5 61 55 96 86; fax: +33 0 5 61 55 97 60.
E-mail address: pascal.guiraud@insa-toulouse.fr (P. Guiraud).

0304-3894/$ – see front matter © 2013 Elsevier B.V. All rights reserved.
http://dx.doi.org/10.1016/j.jhazmat.2013.05.002

and full-scale municipal wastewater treatment (WWT) application [8,9]. Possible mechanisms of nanoparticle sorption to active sludge were proposed, and the fate and biological effects of nanomaterials during treatment processes were explored. Their results also showed that, for 10 investigated representative WWT plants that used a range of unit processes, the effluent titanium concentration could be controlled beneath 25 μg/L.

Brown and black biopolymers associated with soil, sediment, and particles suspended in water, and consisting of material derived from the degradation of animals and plants, are referred to as humic substances. Humic acid (HA) is one of the main components of organic carbon in natural aquatic environments [10]. These substances are a mixture of weak-acid polyelectrolytes and organic macromolecules exhibiting a large range of molar-mass distribution, substances, and functionalities. The main functional groups present in a sample of HA are carboxylic acids, alcohols, phenols, carbonyls, phosphates, sulfates, amides, and sulfides, resulting in the interaction between HA and various metal ions, hydrated metal oxides, clay minerals and organic compounds [11–14].

In recent years, research on the HA assisting the flotation processes began to attract more and more attention [15–17]. However, the mechanisms involved have not been completely understood yet, particularly with reference to the phenomena observed in alkaline media [18]. Physical and chemical properties of HA endow it with a high potential value as the flotation assist, but it has not been applied in the nanoparticle elimination via dissolved air flotation (DAF). As the particle size becomes smaller, the surface-to-volume ratio increases and it becomes advantageous to use surface-dependent properties for separation. Since foam generated by adsorption of fine particles at the interfaces is the basic driving mechanism in many dynamic separation processes such as dissolved air flotation to clarify wastewater and effluents [19,20], it is interesting to deal with the nanoparticle suspension by flotation process.

This study aims at evaluating the feasibility of using HA as an assist to eliminate TNPs in wastewater. Experiments were divided into two parts: surface modification (agglomeration) experiments, and DAF tests. The former is to identify the possible interacting mechanism between TNPs and dissolved HA molecules, while the latter is to investigate the flotation performance of removing TNPs with the aid of HA.

2. Materials and methods

All chemicals used in this study were analytical reagent grade products. The water used for all experiments was produced by an AQUASOURCE system, where water was filtered for particles larger than 1 μm and de-ionized trough an ion exchange resin.

2.1. Origin and physicochemical characteristics of the TNP suspension

Nanoparticles used for these experiments are titanium dioxide (TiO_2, rutile, density 3.9 g·cm^{-3} (20 °C), 15% w/w) 5-30 nm, supplied by Nanostructured & Amorphous Materials, Inc, U.S.A. The particle size distribution was determined by dynamic light scattering (DLS, Nanotrac NPA250 from Microtrac, Malvern Instruments Ltd, U.K.). The average diameter of the 5-30 nm TNP is 41.6 nm, a little beyond its diameter range (5-30 nm) due to the slight aggregation.

Transmission electron microscopy (TEM, JEOL 100CX, Japan) was applied for the morphology observation and particle size estimation of TNPs. The TEM photograph denotes that TNPs in the suspension are round in shape with a coating layer which may result from certain additives added for the well dispersion. The TEM image also shows a particle size range from about 30 nm to 70 nm, validating the size measurement of DLS.

Table 1
Physicochemical properties of TNP suspension (0.15% w/w).

Item	Value	Item	Value
Turbidity/NTU	23.2	Si/ppm	≤0.55
Zeta potential/mV	42.0	Mg/ppm	≤0.45
pH (Temperature/°C)	2.96 (22.4)	Ca/ppm	≤0.60
Conductivity/mS/cm	0.832	Pb/ppm	≤0.002

Other physicochemical characteristics of the TNP suspension measured in the work and provided by the producer are summarized in Table 1. Turbidity was measured with a 2100N-IS Turbidimeter (Hach, U.S.A.); zeta potential was analyzed by electrophoresis with a Zetasizer 2000 (Malvern Instruments Ltd, U.K.); pH was measured at ambient temperature (around 22.4 °C) with a pH-539 pH-meter (WTW, Germany) and a SenTix 41 pH-electrode; and conductivity was measured with a LF 538 conductivity meter (WTW, Germany) and a Tetracon 325 probe. The TNP suspension in this study was set to be 0.15% w/w, and an ultrasonic bath (Branson ultrasonic) was applied for 15 min to enhance dispersion before use (prior to use).

2.2. Characteristics of HA and HA solution

A commercial sodium salt of HA (Carl ROTH, Germany) was used in this research. HA is the alkali soluble but acid insoluble fraction of humic substances [11]. The HA stock solution was prepared as follows: 1.0 g of HA powder was dissolved in 1 L of 0.1 mol/L NaOH solution, stirred for 6 h [21,22], and finally filtered through 0.45 μm membrane to remove residual non-dissolved HA powder. The amount of HA is related to its mass in general. The milligram of either its carbon content or the dried HA sample is usually used to give the concentration of HA solution in mg/L unit [21,23,24]. In this experiment, the HA concentration was determined by the TOC analyzer (Shimadzu corporation, Japan) with regard to dissolved organic carbon (DOC), mg/L DOC. This stock solution was diluted in surface modification experiments and DAF tests, and the relationship between DOC and the dilution factor is shown in Fig. 1, from which the HA concentration of the stock solution can be inferred as 391.7 mg/L DOC. An ultrasonic bath (Branson ultrasonic) was applied for 15 minutes to enhance dispersion before use.

The surfactant properties of HA have been recognized [25–27]. As a surface modifier of TNP and also flotation assist, HA may

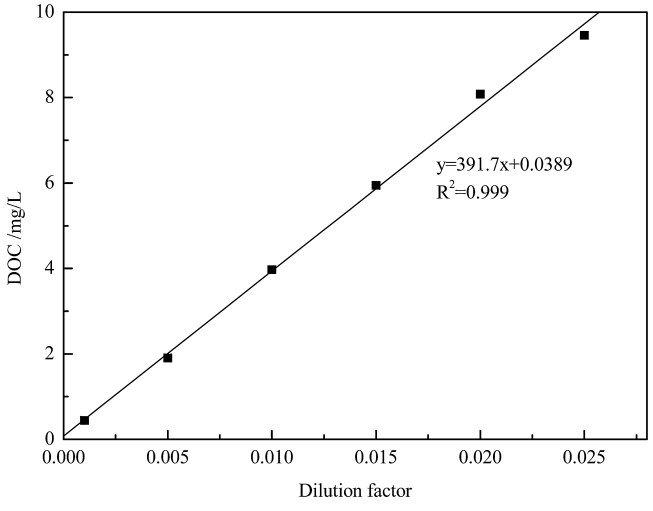

Fig. 1. DOC as a function of dilution factor of HA stock solution.

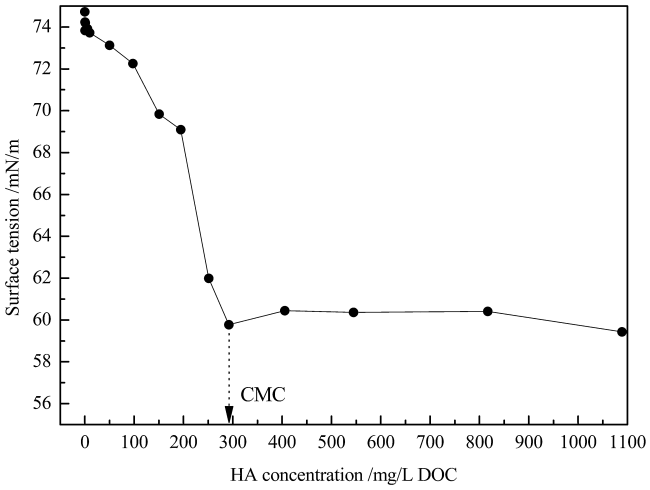

Fig. 2. CMC of HA solution.

spontaneously form micelles beyond a certain concentration and thus may not play the role we expect in agglomeration. For this reason, the critical micelle concentration (CMC) of HA is verified by measuring the surface tension (Tensiometer, GBX, France). A CMC of 290 ± 5 mg/L DOC can be observed in Fig. 2.

The particle size (determined by DLS, Nanotrac NPA250) and turbidity (determined by 2100N-IS Turbidimeter) curves at different HA concentrations are also shown in Fig. 3. In the investigated HA concentration range of this study (lower than 10 mg/L DOC), the particle size of the HA solution is only about 1 nm, and the turbidity in that range is lower than 1 NTU, which is considered to have no obvious effect on the particle size distribution of surface modified TNPs and floated TNPs with the assist of HA. When the HA concentration is higher than 10 mg/L DOC, the particle size and turbidity saw sharp increases. The averaged particle size reaches approximately 170 nm and turbidity close to 14 NTU at the CMC of HA solution.

2.3. Surface modification experiments of TNPs by HA

To study the interaction between TNPs and HA in water dispersion, TNP surface modification experiments with HA were carried out before flotation tests. The varying amount of HA stock solution was added directly into 0.15% w/w TNP suspension, and the TNP-HA suspension was then vigorously mixed on the vortex mixer (Fisher Scientific FB15024, U.K.) for 1 min. The surface charge measurement was carried out to obtain the information on the state of charge at the solid-liquid interface by Zetasizer 2000. Particle size distribution patterns of supernatant and sediments were characterized by DLS (Nanotrac) and laser diffraction (Mastersizer 2000, Malvern Instruments Ltd, U.K.), respectively, considering the different measurement precisions of the two instruments (the former is mostly used in measuring nanoscale measurement and the latter is used for microscale measurement.). The functional groups of the modified TNP surface were investigated by FT-IR performed on TENSOR 27 FT-IR Spectrometer (Bruker Optics Corporation, Germany). The infrared spectra were recorded from 4000 to 400 cm^{-1}, using a 4 cm^{-1} resolution. The samples were pressed with dried KBr pellets at a ratio of approximately 1:100 w/w. Experiments were performed to determine the amount of HA adsorbed on TNPs. The TNP-HA suspensions were kept for 24 h to allow for full adsorption, and then supernatants were analyzed for the HA adsorbed amount through TOC analyzer and for residual turbidity through 2100N-IS Turbidimeter, individually. HA adsorbed on TNPs is calculated as follows:

$$C_{\Delta} = \frac{C_{HA_0} \times V_{(TNPs+HA)} + C'_{DOC} \times V_{TNPs} - C_{HA_t} \times V_{(TNPs+HA)}}{V_{(TNPs+HA)}} \quad (1)$$

where C_{Δ} is the amount of HA adsorbed on TNPs; C_{HA_0} is the initial HA concentration after HA solution was added in the TNP suspension; C'_{DOC} is the dissolved organic matter that may exist in the original TNP suspension; C_{HA_t} is the final HA concentration in the mixed suspension after a long time until the equilibrium. Considering that the volume of HA added in the TNP suspension is ignorable, $V_{(TNPs+HA)} \approx V_{TNPs}$, therefore

$$C_{\Delta} = C_{HA_0} + C'_{DOC} - C_{HA_t} \quad (2)$$

2.4. DAF on a laboratory scale

Experiments were carried out in a continuous flotation device designed in our lab [28], shown in Fig. 4:

Before each experiment, the flotation device is totally cleaned with de-ionized water. The TNP suspension is prepared in the feed tank (1 in Fig. 4(a)) with continuous agitation in order to effectively disperse TNPs. When the DAF test starts, the TNP suspension is injected into the flotation cell with a pump, and meanwhile, the pressurized water is injected into the cell from saturation tank (3 in Fig. 4(a)) to create bubbles. The flotation cell (2 in Fig. 4(a)) is divided into two zones, one where the nanoparticle suspension is mixed with the tiny bubbles, and the other for the disengagement of the bubbles. The flotation cell has glass windows in order to visually follow the flotation process and the separation of bubbles from the clean water exit, and to perform the in situ bubble size measurement. For experiments with HA, HA is injected at the bottom of the first zone by a pump. After the first zone of the flotation cell is full, the pump controlling the flow rate of the clear water after flotation Q_3 is switched on. Bubbles capture particles in the first zone by forming "bubble-particle-HA" or "bubble-particle" aggregates. When coming to the surface, those aggregates move from first zone to the second and can be recovered by draining-off. Clear water is recovered at the bottom of the second cell (5 in Fig. 4(a)).

According to previous experimental experiences by our group of this DAF device [28], a saturation pressure of 6 bars was set in this study, and the average bubble size has been measured to be around 60 μm. During the flotation process, the flow rate of the TNP suspension Q_1 was maintained at 70 mL/min; the pressurized water flow rate Q_2 was 166.7 or 250 mL/min, and the effluent flow rate Q_3 was 100 or 200 mL/min. The flow rate of HA Q_{HA} was determined according to the result of TNP surface modification. Samples of

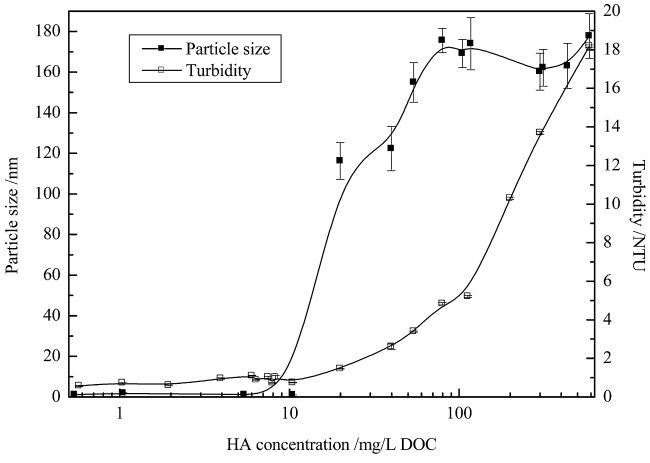

Fig. 3. Particle size and turbidity profiles of HA solution at different HA concentrations.

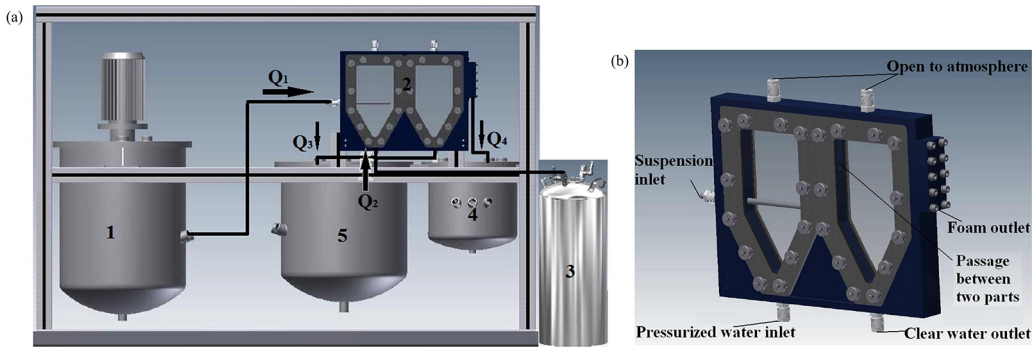

Fig. 4. Schematic representation of the laboratory scale continuous DAF device: (a) overview of the whole DAF system, (1). Feed tank (40 L), (2) Flotation cell (200 × 105 × 18 mm^3), (3) Saturation tank with pressurized water (20 L, the maximum tolerated pressure is 7 bars), (4) Tank for foam (5 L), (5) Tank for clean water (20 L); (b) archetype of the flotation cell.

clean water were taken after 5 min. The retention time of 5 min was determined by preliminary flotation experiments, which showed that the effluent could reach a steady state after 5 min. The outlet samples are analyzed by ICP-AES for the TNP removal, and zetasizer and pH to get the knowledge of their physiochemical property.

3. Results and discussion

3.1. Surface modification (agglomeration) of TNPs with HA

HA destabilized TNP suspensions for the elimination purpose from respects of surface charge, particle size distribution, bonding of functional groups, and adsorption effect.

3.1.1. Surface charge of TNP-HA aggregates

The surface charge is of great importance to understand dispersion characteristics of the TNP system. The amount of charge on the surface can dictate many ultimate uses, as nanoparticles are very reactive in aqueous suspension [29]. The effect of HA concentration on zeta potential of TNPs was investigated for the surface modification study. The adsorption of HA (0.57-9.15 mg/L DOC) modifies the TNPs from positively to negatively charged (see Fig. 5), and the zeta potential reverses near the HA concentration of approximately 7.8 mg/L DOC, which is considered to be the optimum HA dosage for the TNP agglomeration; pHs of suspensions are not higher than 6.08 (when the HA concentration is 9.15 mg/L DOC).

Since the HA solution used in this study is an alkaline solution, the effect of pH on zeta potential should also be considered in order to differentiate it from the effect of HA and clarify the surface interaction mechanism as well. The pH-dependence of zeta potential determined in the 0.15% w/w TNP suspension with and without HA can be seen in Fig. 6. It denotes that the point of zero charge (PZC) of the NaOH-adjusted curve is at pH 5.9, while that of the HA-adjusted curve is at pH 5.2, shifting to a lower pH with the presence of HA. It is worth noting that, without HA, the zeta potential value of the TNP suspension is +24.1 mV at the pH_{PZC} (5.2) of TNPS with HA; the overall particle interaction still being repulsive. In the process of TNP surface modified by HA, both the adsorbed HA and OH^- from NaOH may neutralize the positive charges on TNP surface first, and then the further adsorption of polyanions leads to the over-compensation of positive charges on the oxide surface. Due to this polyanionic coating layer on TNPs with HA addition, the measured values of zeta potential become more negative than that at the pH_{PZC} of the suspension in the absence of HA. Therefore, both the polyanions of HA and the OH^- resulting from NaOH in the HA stock solution play leading roles in the TNP agglomeration from the respect of electrostatic interaction. Similar explanation of humic substances on nanoaprticle surface charge was given in the case of HA adsorption and agglomeration of magnetite nanoparticles [23].

As presented in Fig. 7, when adjusting the pH of the HA stock solution to different values (4.64, 6.02, 8.20 and 12.65), the HA dosage for neutralizing the surface charge of TNPs greatly increased, from 7.8 mg/L DOC for pH 12.65, to 62 mg/L DOC for pH 8.20, 98 mg/L DOC for pH 6.02, and 105 mg/L DOC for pH 4.64. Quantities of studies have proven that the DOC in natural water sources may react with disinfectants to form disinfection by-products, and reduce the effectiveness of water treatment by interfering

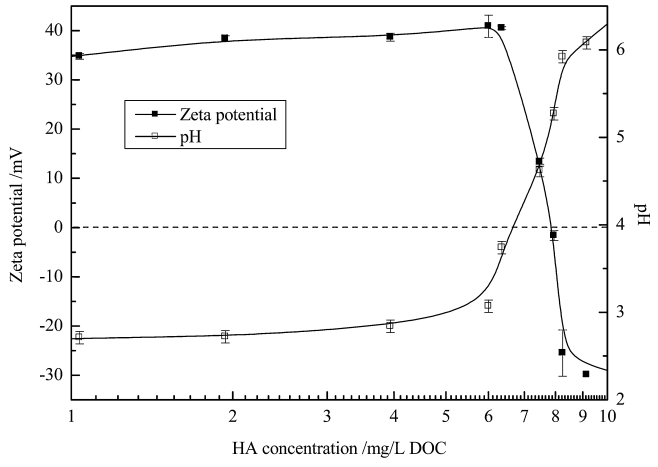

Fig. 5. Zeta potential and pH profiles of TNP suspension (0.15%) at different HA concentrations.

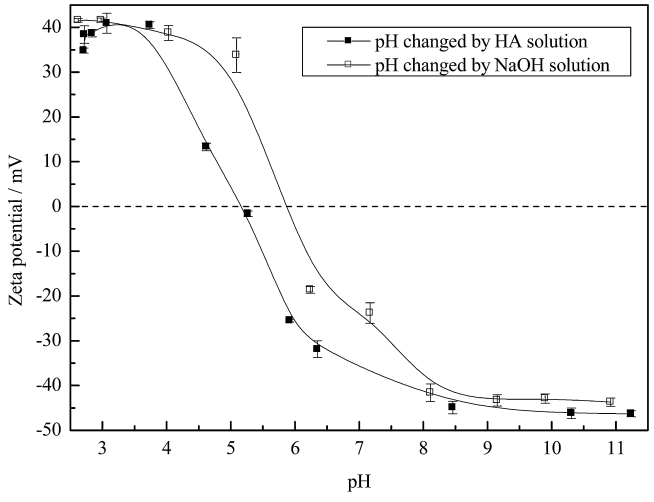

Fig. 6. Zeta potential as a function of pH in the presence and absence of HA.

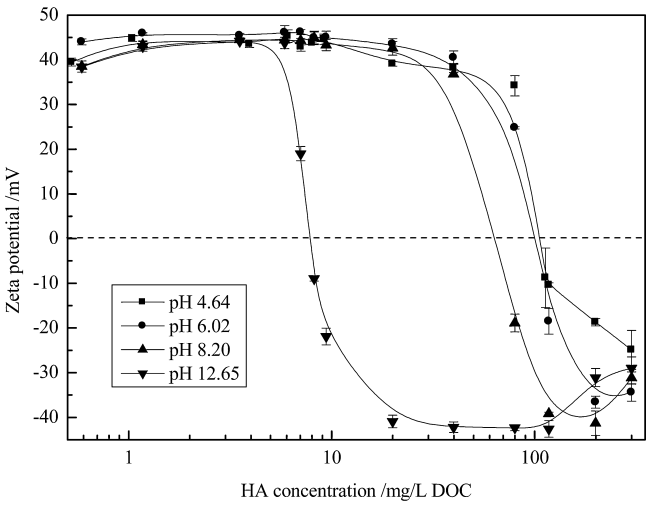

Fig. 7. Zeta potential as a function of HA concentration at different pH conditions.

with fouling membranes and adsorbents [30,31]; moreover, the dissolved HA may enhance the solubility of some organic pollutants and pesticides [32]. Therefore, the high HA concentration will not be environmentally friendly. In this study, the alkaline HA stock solution was used to control the HA dosage in a lower level.

3.1.2. Particle size distribution pattern of the TNP-HA suspension system

Four HA concentrations close to the optimum HA dosage were chosen to compare and study the particle size distribution pattern of the TNP suspension. Fig. 8 shows photographs of the HA modified TNP suspension, and size distributions of supernatants and sediments are presented in Fig. 9. In the investigated HA concentration range, the solid-liquid stratification appears, and supernatants turned from cloudy to clear, along with the increasing HA dosage. The phenomenon agrees well with what is shown in Fig. 9: In Fig 9(a), the average particle sizes with HA concentrations of 6.10 mg/L DOC to 9.15 mg/L DOC are 237.5 nm, 228.2 nm, 197.4 nm, and 0.930 nm, individually, and in Fig. 9(b), the average sizes of sediments are 8.6 μm, 19.4 μm, 26.1 μm, and 133.6 μm, respectively. The decrease of particle size in supernatants and increase of particle size in precipitants demonstrate that HA facilitates the formation of TNP-HA aggregates. By increasing the HA dosage, larger TNP-HA aggregates form and are apt to settle down. The largest aggregates are obtained at 9.15 mg/L DOC which is higher than the optimum HA dosage (7.8 mg/L DOC) resulting from the zeta potential investigation. Since both ligand exchange and electrostatic interaction have been employed to explain the natural organic matter (NOM) adsorption by nano-oxides [33,34], our result illustrates that the

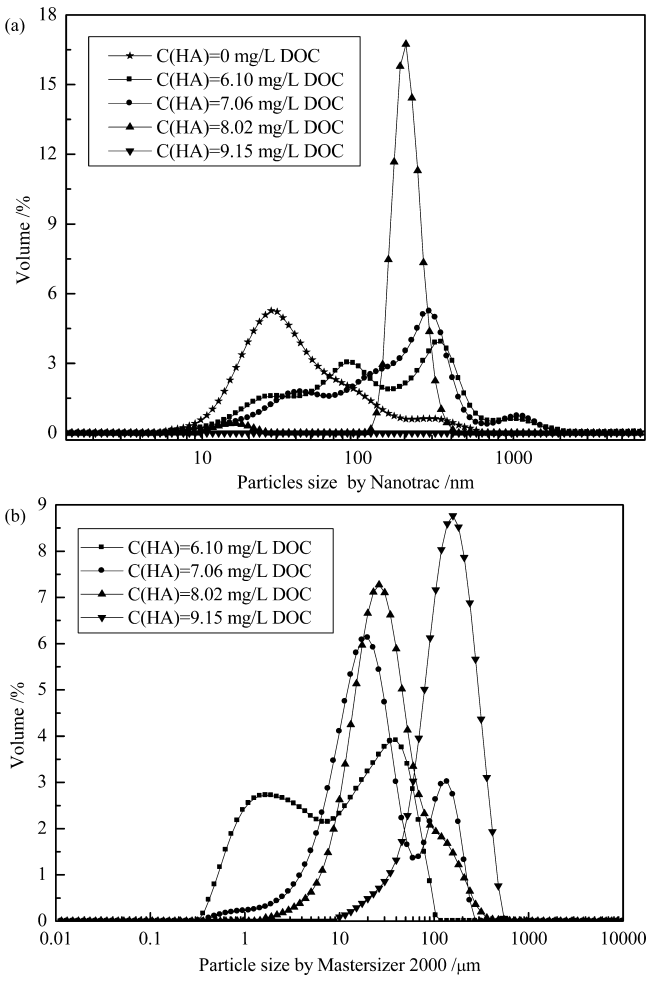

Fig. 9. Particles size distribution of surface modified TNP suspensions: (a) supernatant by Nanotrac; (b) precipitates/flocs by Mastersizer 2000.

interaction between the functional groups of HA and TNPs makes TNPs difficult to restabilize, even if zeta potential become more negative.

3.1.3. FT-IR analysis

In order to verify the interaction type between HA and TNPs, FT-IR studies were conducted on samples of TNPs conditioned with HA. Fig. 10 shows the FT-IR spectra of TNPs modified by different concentrations of HA. For HA, the broad bands at around 3400 cm^{-1} can be assigned to OH stretching of the carboxylic groups, phenolic, alcohol or bonded water; the 1773 cm^{-1} peak can be attributed to the C=O stretching of COOH groups [35]; peaks around 1600 cm^{-1} are produced by stretching of C=C linkages of

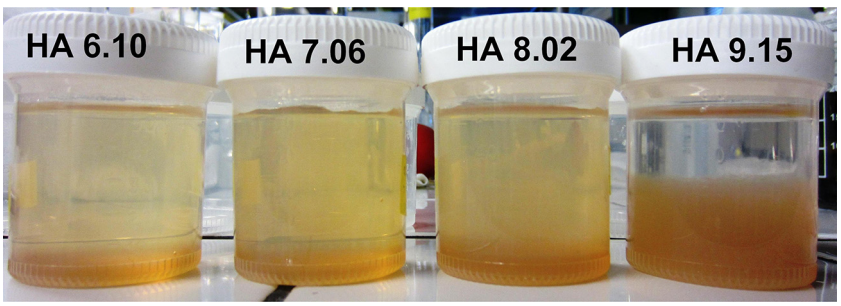

Fig. 8. Photos of surface modified TNP suspensions at different HA concentrations. (The number on the capsule represents the HA concentration (mg/L).).

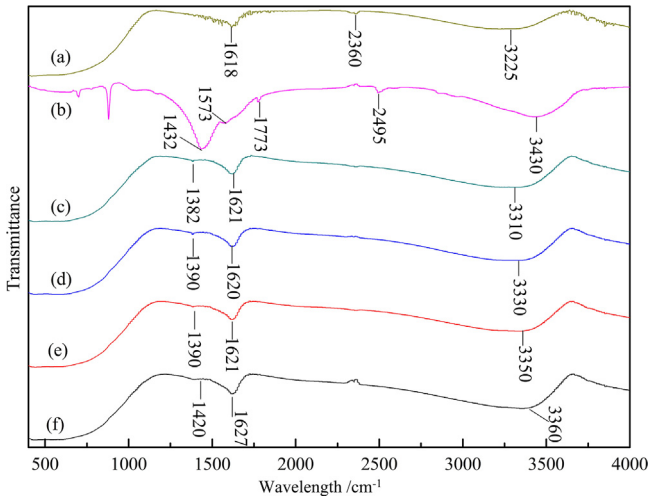

Fig. 10. FT-IR spectrum of TNPs before and after surface modification by HA with various additive contents: (a) TNPs, (b) HA, (c) TNPs + 6.10 mg/L DOC HA, (d) TNPs + 7.06 mg/L DOC HA, (e) TNPs + 8.02 mg/L DOC HA, (f) TNPs + 9.15 mg/L DOC HA.

the aromatic groups; the sharp band observed at 1432 cm^{-1} corresponds to the O—H bending vibrations of alcohols or carboxylic acids deformation of carboxyl groups [27,35]. For TNPs, the major peaks (3277 cm^{-1} and 1617 cm^{-1}) are retained but present systematic frequency shifts (red shifts) with stronger intensity, revealing the strong interaction between TNPs and HA due to adsorption of HA molecules [29,34,36]. The appearance of the peak at around 1390 cm^{-1} (the O—H bending vibration of alcohols or carboxylic acids) in the (TNP + HA) mixtures indicates the interaction of HA-OH with TNP surfaces.

3.1.4. Adsorption of HA on TNPs

The amount of HA adsorbed on TNPs and the residual turbidity of the TNP suspension after a long time (24 h) until the equilibrium were shown in Fig. 11. The HA adsorption presents a slight decrease when HA concentration is lower than 5 mg/L DOC; and thereafter, the HA adsorbed amount sharply increases along with the increasing of HA dosages, reaching the highest adsorption at the highest HA dosage of our experiment. As for the residual turbidity, it presents the worst result at the HA concentration around 6.3 mg/L DOC. That may be due to the fact that aggregated TNP-HA particles are not dense, compact and large enough to settle down. When the HA concentration is higher than 7.5 mg/L DOC, the residual turbidity in supernatants is close to 0 NTU, matching well with the zeta potential (close to 0 mV at HA concentration of 7.8 mg/L DOC). A transparent supernatant with the highest adsorbing amount of HA on TNPs can be obtained at HA concentration of 9.15 mg/L DOC. For a higher HA adsorbing amount and lower residual turbidity in the TNP suspension, an optimum HA concentration range appears at 7.8-9.15 mg/L DOC. In that HA dosage range, almost all HA can be adsorbed on TNPs (see in Fig. 8 and 9), leaving only little in the solution. Therefore, the residual HA in water will not be a threat to the environment.

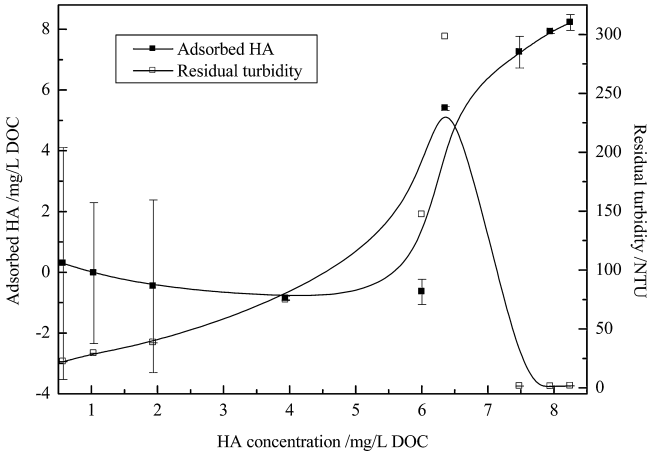

Fig. 11. Adsorbed HA and residual turbidity profiles at different HA concentrations.

The leading mechanism of controlling NOM (such as HA) adsorption on metal oxides (i.e. iron oxide) include ligand exchange, hydrophobic interactions, electrostatic interactions and van der Waals interactions [33,34,37,38]. Due to the heterogeneity and complexity of NOM and adsorbent surfaces, combinations of different adsorption mechanisms have been suggested to occur in reality. Functional groups of NOM are capable of interacting with metal species in solution or suspension. It is therefore possible that TNPs may interact with either the soluble or colloidal fraction of HA, or both [39]. On the other hand, after being alkali treated, the Me^{2+}, Me^{3+}-humates and HA become Me^{+}-humate, a water soluble substance. Due to the presence of ionogenic, the Me^{+}-humate is surface active and behaves as a colloid with properties such as coagulation, peptisation, ion exchange, and coagel formation [25]. Since the sodium hydroxide solution is usually used for dissolving the commercial HA, the surface active Na^{+}-humate is therefore easily formed in the HA alkali solution, and thereafter interacts with TNPs.

3.2. DAF tests

Results of surface modification experiments have shown that TNPs interact with HA by forming large aggregates, and the TNP suspension after surface modification is not easy to restabilize in the entire HA dosage studied. Then, to validate that this surface interaction can help to improve the efficiency of eliminating TNPs in DAF process, the DAF tests were carried out to quantify the effect of different HA concentrations on the floatability of TNPs. Considering the optimum HA dosage range obtained from surface modification experiments, four HA concentrations (4.5, 6.3, 7.9 and 9.3 mg/L DOC) were chosen to investigate the DAF process with the HA assistance.

The dilution effect cannot be neglected due to the large quantity of water introduced along with bubbles in the DAF process. In this instance, C_D is considered as the TNP concentration absolutely resulted from the dilution by the pressurized water, and it can be calculated as follows:

$$C_D = \frac{C_0 \times Q_1}{Q_1 + Q_2 + Q_{HA}} \quad (3)$$

where C_0 is the TNP concentration of 0.15% (w/w) TNPs in suspensions calculated from the result of ICP-AES, 1406.7 mg/L. Q_1 is fixed to be 70 mL/min as mentioned previously. On the basis of Eq. (3), the TNP removal efficiency η resulting from DAF is given by excluding the dilution effect:

$$\eta = \frac{C_D \times Q_3 - C_3 \times Q_3}{C_D \times Q_3} \times 100\% = \left(1 - \frac{C_3}{C_D}\right) \times 100\%$$
$$= \left[1 - \frac{C_3 \times (Q_1 + Q_2 + Q_{HA})}{C_0 \times Q_1}\right] \times 100\% \quad (4)$$

where C_3 is the TNP concentration of the clear effluent. Positive values of η demonstrate that DAF can effectively eliminate TNPs in the suspension, a higher value of η representing a higher DAF efficiency, while negative values of η denote ineffective DAF treatment. DAF experiments are performed for different flow rates of Q_{HA} (determined according to the investigating HA concentrations), Q_2 (166.7 and 250 mL/min) and Q_3 (100 and 200 mL/min).

Table 2
TNP removal by ICP-AES.

	Q_2 = 166.7 mL/min, Q_3 = 100 mL/min					Q_2 = 166.7 mL/min, Q_3 = 200 mL/min				
C_{HA}/mg/L DOC	0.0	4.5	6.3	7.9	9.3	0.0	4.5	6.3	7.9	9.3
C_3/mg/L	443.3	300.0	363.3	203.3	33.3	373.3	/	310.0	216.7	263.3
C_D/mg/L	416.0	402.8	397.2	391.7	386.4	416.0	402.8	397.2	391.7	386.4
η/%	–	25.5	8.5	48.1	91.4	10.3	/	21.9	44.7	31.8
	Q_2 = 250 mL/min, Q_3 = 100 mL/min					Q_2 = 250 mL/min, Q_3 = 200 mL/min				
C_{HA}/mg/L DOC	0.0	4.5	6.3	7.9	9.3	0.0	4.5	6.3	7.9	9.3
C_3/mg/L	353.3	336.7	210.0	86.7	166.7	326.7	316.7	326.7	40	176.7
C_D/mg/L	307.7	300.4	297.3	294.2	291.2	307.7	300.4	297.3	294.2	291.2
η/%	–	–	29.4	70.5	42.8	–	–	–	86.4	39.3

/: Ti (TNPs) concentration that was not detected by ICP-AES;
–: The negative η value.

Table 2 and Fig. 12 present the TNP removal of DAF tests by ICP-AES. It can be found that, without the HA addition, DAF was poorly effective in the investigating Q_2 and Q_3 ranges. For low pressurized water flow rate Q_2 = 166.7 mL/min, higher HA dosages (≥7.9 mg/L DOC) could better improve the TNP removal, and the maximum removal efficiency of 91.4% was achieved when C_{HA} = 9.3 mg/L DOC. For high pressurized water flow rate Q_2 = 250 mL/min, the DAF failed to have any treating effect when HA concentration was lower than 6.3 mg/L DOC; but for the HA concentration of 7.9 mg/L DOC, better TNPs elimination efficiency of higher than 70% were obtained. Fig. 12 denotes that high efficiencies of 91.4% and 86.4% are obtained at points of HA dosages 7.9 and 9.3 mg/L DOC, whereas their pressurized water flow rates and effluent flow rates are quite different, indicating that the effect of HA outweighs that of bubbles (Q_2) and also effluent flow velocity (Q_3). Therefore, higher TNP removal efficiencies can be obtained by applying higher dosages of HA (increasing Q_{HA}). From the respect of higher TNP removal and lower dilution effect, the optimum operational condition for TNPs elimination for DAF process in this study is determined to be (C_{HA} = 7.9–9.3 mg/L DOC, Q_2 = 166.7 mL/min and Q_3 = 100 mL/min).

Zeta potential of the effluent was also measured to get a complete comprehension of the effect of HA on TNP removal efficiency (see in Fig. 13). It denotes that the zeta potential of the flotation suspension keeps highly positive when HA dosage is lower than around 6.3 mg/L DOC. With the increasing of HA concentration (>6.3 mg/L DOC), this stability is undermined, and the TNP removal correspondingly increases. In Fig. 12, the removal show a trend of deceasing when the HA dosage is higher than 7.9 mg/L DOC (for (Q_2 = 166.7 mL/min, Q_3 = 200 mL/min), (Q_2 = 250 mL/min, Q_3 = 100 mL/min), (Q_2 = 250 mL/min, Q_3 = 200 mL/min)), which may result from particles re-stabilize due to the formation of negatively charged small flocs.

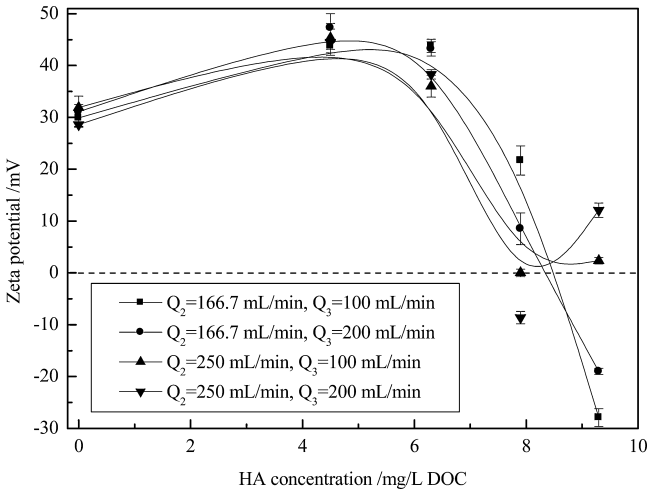

Fig. 13. Effect of HA concentration on Zeta potential of treated TNP suspensions.

Based on data of Table 2 and the measurement of the treated suspension, the flotation performance is also expressed as Fig. 14. It is indicative that TNP removals remain high (>60%) even when

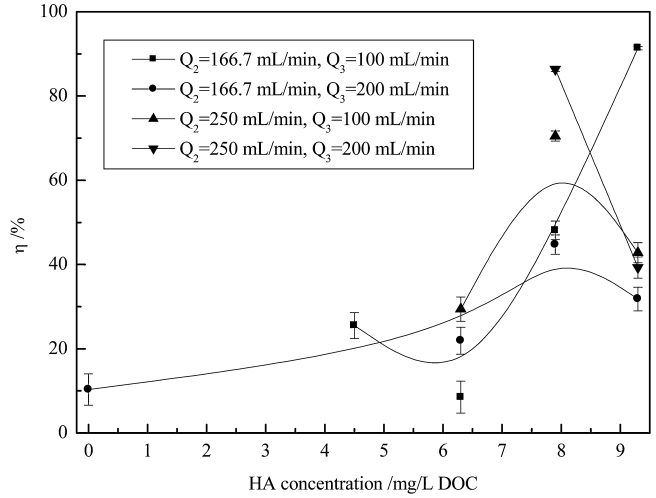

Fig. 12. Effect of HA concentration on TNP removal efficiency. (Negative efficiencies are omitted.).

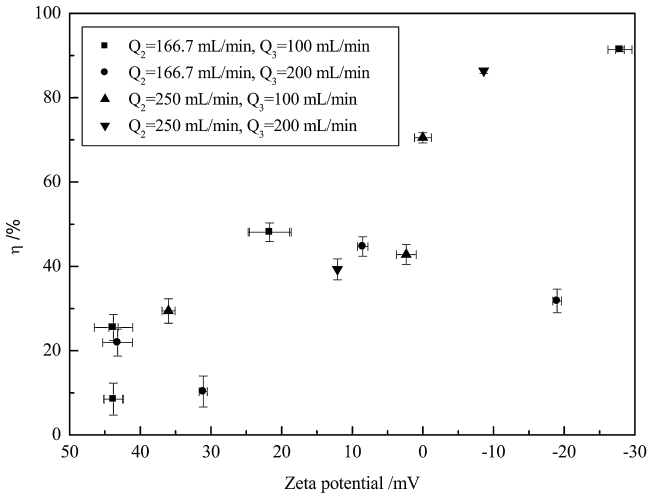

Fig. 14. Relationship between TNP removal efficiency and zeta potential of the flotation suspension. (Negative efficiencies are omitted.).

zeta potentials are negative. This is because TNP removal efficiency is achieved due to not only the electrostatic attraction between negative HA, bubbles and surface positive TNPs, but also the hydrophobic interaction between TNPs and HA. The assistance of HA to TNP removal efficiencies in the DAF process can be understood from the physiochemical interaction among TNPs, HA and bubbles. According to the discussion in Section 3.1, TNPs and HA are able to form flocs because of charge neutralization, ligand exchange, hydrophobic interaction, and van der Waals interactions when they contact each other. In the DAF process, air bubbles with negative surface charges and smaller size (approximately 60 μm) are introduced [40,41], and subsequently, bubble-TNP-HA or bubble-TNP aggregates are generated due to the collision of bubbles, TNPs and HA.

4. Conclusions

This work focuses on the elimination of TNPs with the assist of HA in water resources, and the commercial rutile TNP dispersion was chosen as representative. TNP properties have been characterized. Its high positive surface charge (42 mV) ensures the dispersing stability of TNPs in suspension, and their nanoscale size poses difficulties to their separation. In this study, surface modification of TNPs with HA was firstly conducted to investigate the mechanism of TNP-HA interaction and also as an exploratory study for the DAF separation; thereafter, DAF experiments were done to test the TNP removal efficiency in flotation process.

Both the polyanions of HA and the OH^- resulting from NaOH in the HA stock solution contribute to electrostatic attraction in the TNP aggregation. The alkaline HA stock solution was used to control the HA dosage in a lower level. Ligand exchange, bonding effect, hydrophobic interaction and van der Waals interaction also induced the HA adsorption in addition to the charge neutralization. TNP-HA aggregates formed during the surface modification process and resulted in a clearest supernatants at 9.15 mg/L DOC, and the optimum HA dosage range was determined to be 7.8-9.15 mg/L DOC by the surface modification (agglomeration) experiments.

The surface modification study provided a possibility of applying flotation treatment in removing TNPs with the assist of HA. DAF tests reveal that, compared with the DAF without HA and dilution effect caused by water, the TNPs elimination efficiency of DAF tests was improved to 91.4% when the HA dosages were in the optimum dosage range. The optimum HA dosage range determined by the DAF test differs only slightly from that found in the surface modification experiments, but quite close to. The optimum operational DAF condition in eliminating TNPs in this study is C_{HA} = 7.9–9.3 mg/L DOC, Q_2 = 166.7 mL/min and Q_3 = 100 mL/min.

Base on results of this research, further study of TNPs elimination by DAF with HA are proposed: 1) since HA commonly exists in natural water bodies, it is quite possible and promising to use natural water containing HA to treat TNP wastewaters; 2) the large amount of water introduced along with the inputting of gas bubbles results in a considerably dilution effect. Further work is required to reduce the dilution effect resulting from Q_2 by changing the way of producing bubbles and thereby further increasing the TNP removal efficiency.

Acknowledgements

We are very grateful to Marie-Line de Solan Bethmale and Mallorie Tourbin in Laboratoire de Génie Chimique (LGC) of Toulouse University for the ICP-AES measurement. We acknowledge China Scholarship Council (CSC) for the scholarship.

References

[1] C.O. Robichaud, A.E. Uyar, M.R. Darby, L.G. Zucker, M.R. Wiesner, Estimates of upper bounds and trends in nano-TiO_2 production as a basis for exposure assessment, Environ. Sci. Technol. 43 (2009) 4227–4233.
[2] J. Labille, J. Feng, C. Botta, D. Borschneck, M. Sammut, M. Cabie, M. Auffan, J. Rose, J.-Y. Bottero, Aging of TiO_2 nanocomposites used in sunscreen. Dispersion and fate of the degradation products in aqueous environment, Environ. Pollut. 158 (2010) 3482–3489.
[3] M. Fouqueray, B. Dufils, B. Vollat, P. Chaurand, C. Botta, K. Abacci, J. Labille, J. Rose, J. Garric, Effects of aged TiO_2 nanomaterial from sunscreen on *Daphnia magna* exposed by dietary route, Environ. Pollut. 163 (2012) 55–61.
[4] D.A. Navarro, S.W. Depner, D.F. Watson, D.S. Aga, S. Banerjee, Partitioning behavior and stabilization of hydrophobically coated HfO_2, ZrO_2 and $Hf_xZr_{1-x}O_2$ nanoparticles with natural organic matter reveal differences dependent on crystal structure, J. Hazard. Mater. 196 (2011) 302–310.
[5] Y.-H. Shen, Colloidal titanium dioxide separation from water by foam flotation, Sep. Sci. Technol. 33 (1998) 2623–2635.
[6] M.A. Kiser, H. Ryu, H. Jang, K. Hristovski, P. Westerhoff, Biosorption of nanoparticles to heterotrophic wastewater biomass, Water Res. 44 (2010) 4105–4114.
[7] Y. Wang, P. Westerhoff, K.D. Hristovski, Fate and biological effects of silver titanium dioxide, and C_{60} (fullerene) nanomaterials during simulated wastewater treatment processes, J. Hazard. Mater. 201-202 (2012) 16–22.
[8] M.A. Kiser, P. Westerhoff, T. Benn, Y. Wang, J. Peĭrez-Rivera, K. Hristovski, Titanium nanomaterial removal and release from wastewater treatment plants, Environ. Sci. Technol. 43 (2009) 6757–6763.
[9] P. Westerhoff, G. Song, K. Hristovski, M.A. Kiser, Occurrence and removal of titanium at full scale wastewater treatment plants: implications for TiO_2 nanomaterials, J. Environ. Monit. 13 (2011) 1195–1203.
[10] J.W. Parsons, Humus chemistry-genesis composition, reactions, Soil Sci. 135 (1983) 129–130.
[11] M. Hiraide, T. Shima, H. Kawaguchi, Concentration of humic and fulvic acids in large aqueous samples by continuous-flow coprecipitation-flotation, Fresenius J. Anal. Chem. 345 (1993) 780–783.
[12] R.F. Christman, E.T. Gjessing, Aquatic and Terrestrial Humic Materials, Ann Arbor Science, Michigan, 1983.
[13] K. Li, Y. Chen, Effect of natural organic matter on the aggregation kinetics of CeO_2 nanoparticles in KCl and $CaCl_2$ solutions: measurements and modeling, J. Hazard. Mater. 209–210 (2012) 264–270.
[14] D. Wang, S.A. Bradford, R.W. Harvey, X. Hao, D. Zhou, Transport of ARS-labeled hydroxyapatite nanoparticles in saturated granular media is influenced by surface charge variability even in the presence of humic acid, J. Hazard. Mater. 229–230 (2012) 170–176.
[15] I.D. dos Santos, J.F. Oliveira, Utilization of humic acid as a depressant for hematite in the reverse flotation of iron ore, Miner. Eng. 20 (2007) 1003–1007.
[16] L. Reyes-Bozo, R. Herrera-Urbina, M. Escudey, A. Godoy-Faúndez, C. Sáez-Navarrete, M. Herrera, R. Ginocchio, Role of biosolids on hydrophobic properties of sulfide ores, Int. J. Miner. Process. 100 (2011) 124–129.
[17] L. Reyes-Bozo, R. Herrera-Urbina, C. Sáez-Navarrete, A.F. Otero, A. Godoy-Faúndez, R. Ginocchio, Rougher flotation of copper sulphide ore using biosolids and humic acids, Miner. Eng. 24 (2011) 1603–1608.
[18] S. Kumpulainen, F. von der Kammer, T. Hofmann, Humic acid adsorption and surface charge effects on schwertmannite and goethite in acid sulphate waters, Water Res. 42 (2008) 2051–2060.
[19] R.J. Pugh, Foaming in chemical surfactant free aqueous dispersions of anatase (titanium dioxide) particles, Langmuir 23 (2007) 7972–7980.
[20] P. George, A.V. Nguyen, G.J. Jameson, Assessment of true flotation and entrainment in the flotation of submicron particles by fine bubbles, Miner. Eng. 17 (2004) 847–853.
[21] M. Rebhun, S. Meir, Y. Laor, Using dissolved humic acid to remove hydrophobic contaminants from water by complexation-flocculation process, Environ. Sci. Technol. 32 (1998) 981–986.
[22] H. Liu, C. Hu, H. Zhao, J. Qu, Coagulation of humic acid by PACl with high content of Al_{13}: the role of aluminum speciation, Sep. Purif. Technol. 70 (2009) 225–230.
[23] E. Illés, E. Tombácz, The effect of humic acid adsorption on pH-dependent surface charging and aggregation of magnetite nanoparticles, J. Colloid Interface Sci. 295 (2006) 115–123.
[24] R. Kretzschmar, H. Holthoff, H. Sticher, Influence of pH and humic acid on coagulation kinetics of kaolinite: a dynamic light scattering study, J. Colloid Interface Sci. 202 (1998) 95–103.
[25] M. Tschapek, C. Wasowski, R. Sánchez, Humic acid as a colloidal surfactant, Plant Soil 63 (1981) 261–271.
[26] T.F. Guetzloff, J.A. Rice, Does humic acid form a micelle? Sci. Total Environ. 152 (1994) 31–35.
[27] S. Agarwal, K. Anwer, R. Khanna, A. Ali, Y. Sultana, Humic acid from shilajit: a physico-chemical and spectroscopic characterization, J. Serb. Chem. Soc. 75 (2010) 413–422.
[28] Y. Liu, Elimination de Nanoparticules D'effluents Liquides, INSA de Toulouse, Toulouse, 2010.
[29] B.P. Singh, S. Nayak, S. Samal, S. Bhattacharjee, L. Besra, The role of poly(methacrylic acid) conformation on dispersion behavior of nano TiO_2 powder, Appl. Surf. Sci. 258 (2012) 3524–3531.
[30] M. Kitis, J.E. Kilduff, T. Karanfil, Isolation of dissolved organic matter (DOM) from surface waters using reverse osmosis and its impact on the reactivity of DOM to formation and speciation of disinfection by-products, Water Res. 35 (2001) 2225–2234.

[31] H. Huang, Q.-Y. Wu, H.-Y. Hu, W.A. Mitch, Dichloroacetonitrile and dichloroacetamide can form independently during chlorination and chloramination of drinking waters model organic matters, and wastewater effluents, Environ. Sci. Technol. 46 (2012) 10624–10631.
[32] C.T. Chiou, R.L. Malcolm, T.I. Brinton, D.E. Kile, Water solubility enhancement of some organic pollutants and pesticides by dissolved humic and fulvic acids, Environ. Sci. Technol. 20 (1986) 502–508.
[33] B. Gu, J. Schmitt, Z. Chen, L. Liang, J.F. McCarthy, Adsorption and desorption of natural organic matter on iron oxide: mechanisms and models, Environ. Sci. Technol. 28 (1994) 38–46.
[34] K. Yang, D. Lin, B. Xing, Interactions of humic acid with nanosized inorganic oxides, Langmuir 25 (2009) 3571–3576.
[35] S.L. de Moraes, M.O.O. Rezende, Behavior of humic acid as a micellar phase in micellar electrokinetic chromatography (MEKC), Microchim. Acta 151 (2005) 115–122.
[36] M. Iijima, M. Kobayakawa, H. Kamiya, Tuning the stability of TiO_2 nanoparticles in various solvents by mixed silane alkoxides, J. Colloid Interface Sci. 337 (2009) 61–65.
[37] T.S. Arnarson, R.G. Keil, Mechanisms of pore water organic matter adsorption to montmorillonite, Mar. Chem. 71 (2000) 309–320.
[38] C. Ding, C. Shang, Mechanisms controlling adsorption of natural organic matter on surfactant-modified iron oxide-coated sand, Water Res. 44 (2010) 3651–3658.
[39] K. Baek, J.-W. Yang, Humic-substance-enhanced ultrafiltration for removal of heavy metals, Sep. Sci. Technol. 40 (2005) 699–708.
[40] J.K. Edzwald, Developments of high rate dissolved air flotation for drinking water treatment, J. Water Supply Res. Technol.-Aqua 56 (2007) 399–409.
[41] C. Oliveira, J. Rubio, Zeta potential of single and polymer-coated microbubbles using an adapted microelectrophoresis technique, Int. J. Miner. Process. 98 (2011) 118–123.

References

Abraham, P.M., Barnikol, S., Baumann, T., Kuehn, M., Ivleva, N.P., Schaumann, G.E., 2013. Sorption of Silver Nanoparticles to Environmental and Model Surfaces. *Environ. Sci. Technol.* 47, 5083–5091.

Agarwal, S., Anwer, K., Khanna, R., Ali, A., Sultana, Y., 2010. Humic acid from Shilajit: A physico-chemical and spectroscopic characterization. *J. Serbian Chem. Soc.* 75, 413–422.

Agarwal, A., Ng, W.J., Liu, Y., 2011. Principle and applications of microbubble and nanobubble technology for water treatment. *Chemosphere* 84, 1175–1180.

Ahmed, N., Jameson, G.J., 1985. The effect of bubble size on the rate of flotation of fine particles. *Int. J. Miner. Process.* 14, 195–215.

Arnarson, T.S., Keil, R.G., 2000. Mechanisms of pore water organic matter adsorption to montmorillonite. *Mar. Chem.* 71, 309–320.

Baek, K., Yang, J., 2005. Humic-substance-enhanced ultrafiltration for removal of heavy metals. *Sep. Sci. Technol.* 40, 699–708.

Bai, B.F., Hankins, N.P., Hey, M.J., Kingman, S.W., 2004. In situ mechanistic study of SDS adsorption on hematite for optimized froth flotation. *Ind. Eng. Chem. Res.* 43, 5326–5338.

Bakker, M.I., 2012. Development of an inventory of consumer products containing nanomaterials (Formation/ information about nanotechnology, Ne3ls analyse, Reports, Strategic intelligence). *Centre for Substances and Integrated Risk Assessment*.

Benn, T.M., Westerhoff, P., 2008. Nanoparticle silver released into water from commercially available sock fabrics. *Environ. Sci. Technol.* 42, 7025–7026.

Blazy, P., Jdid, E.A., 2000. Flottation: Aspects pratiques. *Tech. Ing. Génie Procédés* J3, J3360.1–J3360.22.

Brown, D.M., Wilson, M.R., MacNee, W., Stone, V., Donaldson, K., 2001. Size-dependent proinflammatory effects of ultrafine polystyrene particles: a role for surface area and oxidative stress in the enhanced activity of ultrafines. *Toxicol. Appl. Pharmacol.* 175, 191–199.

Brum, M.C., Oliveira, J.F., 2007. Removal of humic acid from water by precipitate flotation using cationic surfactants. *Miner. Eng.* 20, 945–949.

Bushell, G.C., Yan, Y.D., Woodfield, D., Raper, J., Amal, R., 2002. On techniques for the measurement of the mass fractal dimension of aggregates. *Adv. Colloid Interface Sci.* 95, 1–50

Chalew, T.E.A., Ajmani, G.S., Huang, H., Schwab, K.J., 2013. Evaluating nanoparticle breakthrough during drinking water treatment. *Environ. Health Perspect.* 121, 1161–1166.

Chang, M.R., Lee, D.J., Lai, J.Y., 2007. Nanoparticles in wastewater from a science-based industrial park — Coagulation using polyaluminum chloride. *J. Environ. Manage.* 85, 1009–1014.

Chaphalkar, P.G., 1994. *Characterization and application of colloidal gas aphrons for groundwater remediation*. Louisiana State University, Baton Rouge.

Chaphalkar, P.G., Valsaraj, K.T., Roy, D., 1993. A Study of the size distribution and stability of colloidal gas aphrons using a particle size analyzer. *Sep. Sci. Technol.* 28, 1287–1302.

Chaphalkar, P., Valsaraj, K., Roy, D., 1994. Flotation using microgas dispersions for the removal of pentachlorophenol from aqueous-solutions. *Sep. Sci. Technol.* 29, 907–921.

Chau, K.W., 2004. Investigation on effects of aggregate structure in water and wastewater treatment. *Water Sci. Technol.* 50, 119–124.

Chen, G., 2004. Electrochemical technologies in wastewater treatment. *Sep. Purif. Technol.* 38, 11–41.

Chen, X., Chen, G., Yue, P.L., 2002. Novel electrode system for electroflotation of wastewater. *Env. Sci. Technol.* 36, 778–783.

Chin, C.-J.M., Chen, P.-W., Wang, L.-J., 2006. Removal of nanoparticles from CMP wastewater by magnetic seeding aggregation. *Chemosphere* 63, 1809–1813.

Chiou, C.T., Malcolm, R.L., Brinton, T.I., Kile, D.E., 1986. Water solubility enhancement of some organic pollutants and pesticides by dissolved humic and fulvic acids. *Environ. Sci. Technol.* 20, 502–508.

Cho, S.-H., Kim, J.-Y., Chun, J.-H., Kim, J.-D., 2005. Ultrasonic formation of nanobubbles and their zeta-potentials in aqueous electrolyte and surfactant solutions. *Colloids Surf. Physicochem. Eng. Asp.* 269, 28–34.

Chungchamroenkit, P., Chavadej, S., Yanatatsaneejit, U., Kitiyanan, B., 2008. Residue catalyst support removal and purification of carbon nanotubes by NaOH leaching and froth flotation. *Sep. Purif. Technol.* 60, 206–214.

Conte, P., Piccolo, A., 2002. *Effect of concentration on the self-assembling of dissolved humic substances*, in: A. Violante, P.M.H. (Ed.), Developments in Soil Science. Elsevier, pp. 409–417.

Dai, Y., Deng, T., 2003. Stabilization and characterization of colloidal gas aphron dispersions. *J. Colloid Interface Sci.* 261, 360–365.

De Moraes, S.L., Rezende, M.O.O., 2005. Behavior of Humic Acid as a Micellar Phase in Micellar Electrokinetic Chromatography (MEKC). *Microchim. Acta* 151, 115–122.

Ding, C., Shang, C., 2010. Mechanisms controlling adsorption of natural organic matter on surfactant-modified iron oxide-coated sand. *Water Res.* 44, 3651–3658.

Ding, C., Yang, X., Liu, W., Chang, Y., Shang, C., 2010. Removal of natural organic matter using surfactant-modified iron oxide-coated sand. *J. Hazard. Mater.* 174, 567–572.

Dos Santos, I.D., Oliveira, J.F., 2007. Utilization of humic acid as a depressant for hematite in the reverse flotation of iron ore. *Miner. Eng.* 20, 1003–1007.

Duan, J., Fornasiero, D., Ralston, J., 2003. Calculation of the flotation rate constant of chalcopyrite particles in an ore. *Int. J. Miner. Process.* 72, 227–237.

Dumouchel, C., Yongyingsakthavorn, P., Cousin, J., 2009. Light multiple scattering correction of laser-diffraction spray drop-size distribution measurements. *Int. J. Multiph. Flow* 35, 277–287.

Edzwald, J.K., 1995. Principles and applications of dissolved air flotation. *Water Sci. Technol.* 31, 1–23.

Edzwald, J.K., 2007. Developments of high rate dissolved air flotation for drinking water treatment. *J. Water Supply Res. Technol.-Aqua* 56, 399–409.

Edzwald, J.K., 2010. Dissolved air flotation and me. *Water Res.* 44, 2077–2106.

Fan, M., Tao, D., Honaker, R., Luo, Z., 2010. Nanobubble generation and its application in froth flotation (part I): nanobubble generation and its effects on properties of microbubble and millimeter scale bubble solutions. *Min. Sci. Technol. China* 20, 1–19.

Foss Hansen, S., Larsen, B.H., Olsen, S.I., Baun, A., 2007. Categorization framework to aid hazard identification of nanomaterials. *Nanotoxicology* 1, 243–250.

French, R.A., Jacobson, A.R., Kim, B., Isley, S.L., Penn, R.L., Baveye, P.C., 2009. Influence of ionic strength, pH, and cation valence on aggregation kinetics of titanium dioxide nanoparticles. *Environ. Sci. Technol.* 43, 1354–1359.

Fuguet, E., Ràfols, C., Rosés, M., Bosch, E., 2005. Critical micelle concentration of surfactants in aqueous buffered and unbuffered systems. *Anal. Chim. Acta* 548, 95–100.

Gai, K., Shi, B., Yan, X., Wang, D., 2011. Effect of dispersion on adsorption of atrazine by aqueous suspensions of fullerenes. *Environ. Sci. Technol.* 45, 5959–5965.

George, P., Nguyen, A.V., Jameson, G.J., 2004. Assessment of true flotation and entrainment in the flotation of submicron particles by fine bubbles. *Miner. Eng.* 17, 847–853.

Gochin, R.J., Solari, J., 1983. The role of hydrophobicity in dissolved air flotation. *Water Res.* 17, 651–657.

Gregory, J., O'Melia, C.R., 1989. Fundamentals of flocculation. *Crit. Rev. Environ. Control* 19, 185–230.

Groso, A., Petri-Fink, A., Magrez, A., Riediker, M., Meyercorresponding author, T., 2010. Management of nanomaterials safety in research environment. *Part. FIBRE Toxicol.* 7, 1–8.

Guan, J., Waite, T.D., Amal, R., 1998. Rapid structure characterization of bacterial aggregates. *Environ. Sci. Technol.* 32, 3735–3742.

Guetzloff, T.F., Rice, J.A., 1994. Does humic acid form a micelle? *Org. Subst. Soil Water* 152, 31–35.Hallock, M.F., Greenley, P., DiBerardinis, L., Kallin, D., 2009. Potential risks of nanomaterials and how to safely handle materials of uncertain toxicity. *J. Chem. Health Saf.* 16, 16–23.

Gu, B., Schmitt, J., Chen, Z., Liang, L., McCarthy, J.F., 1994. Adsorption and desorption of natural organic matter on iron oxide: mechanisms and models. *Env. Sci. Technol.* 28, 38–46.

Guzman, K.A.D., Finnegan, M.P., Banfield, J.F., 2006. Influence of surface potential on aggregation and transport of titania nanoparticles. *Environ. Sci. Technol.* 40, 7688–7693.

Hanotu, J., Bandulasena, H.C.H., Zimmerman, W.B., 2012. Microflotation performance for algal separation. *Biotechnol. Bioeng.* 109, 1663–1673.

Han, M., Dockko, S., 1998. Zeta potential measurement of bubbles in DAF process and its effect on the removal efficiency. *KSCE J. Civ. Eng.* 2, 461–466.

Han, M.Y., Ahn, H.J., Shin, M.S., Kim, S.R., 2004. The effect of divalent metal ions on the zeta potential of bubbles. *Water Sci. Technol.* 50, 49–56.

Hashim, M.A., Gupta, B.S., 1998. The application of colloidal gas aphrons in the recovery of fine cellulose fibres from paper mill wastewater. *Bioresour. Technol.* 64, 199–204.

Hashim, M.A., Mukhopadhyay, S., Gupta, B.S., Sahu, J.N., 2012. Application of colloidal gas aphrons for pollution remediation. *J. Chem. Technol. Biotechnol.* 87, 305–324.

Henderson, R.K., Parsons, S.A., Jefferson, B., 2010. Polymers as bubble surface modifiers in the flotation of algae. *Environ. Technol.* 31, 781–790.

Hiemenz, P.C., Rajagopalan, R., 1997. *Principles of colloid and surface chemistry.* Marcel Dekker, New York.

Hiraide, M., Shima, T., Kawaguchi, H., 1993. Concentration of humic and fulvic acids in large aqueous samples by continuous-flow coprecipitation-flotation. *Fresenius J. Anal. Chem.* 345, 780–783.

Hofmeyr, J.-H.S., Cornish-Bowden, H., 1997. The reversible Hill equation: how to incorporate cooperative enzymes into metabolic models. *Comput. Appl. Biosci. CABIOS* 13, 377–385.

Ho, Y.S., Porter, J.F., Mckay, G., 2002. Equilibrium isotherm studies for the sorption of divalent metal ions onto peat: Copper, nickel and lead single component systems. *Water. Air. Soil Pollut.* 141, 1–33.

Huang, H., Wu, Q.-Y., Hu, H.-Y., Mitch, W.A., 2012. Dichloroacetonitrile and dichloroacetamide can form independently during chlorination and chloramination of drinking waters, model organic matters, and wastewater effluents. *Environ. Sci. Technol.* 46, 10624–10631.

Huang, Z., Legendre, D., Guiraud, P., 2011. A new experimental method for determining particle capture efficiency in flotation. *Chem. Eng. Sci.* 66, 982–997.

Huang, Z., Legendre, D., Guiraud, P., 2012. Effect of interface contamination on particle–bubble collision. *Chem. Eng.* Sci. 68, 1–18。

Hu, C.Y., Lo, S.L., Li, C.M., Kuan, W.H., 2005. Treating chemical mechanical polishing (CMP) wastewater by electro-coagulation-flotation process with surfactant. *J. Hazard. Mater.* 120, 15–20.

Hwang, S., Martinez, D., Perez, P., Rinaldi, C., 2011. Effect of surfactant-coated iron oxide nanoparticles on the effluent water quality from a simulated sequencing batch reactor treating domestic wastewater. *Environ. Pollut.* 159, 3411–3415.

Iijima, M., Kobayakawa, M., Kamiya, H., 2009. Tuning the stability of TiO_2 nanoparticles in various solvents by mixed silane alkoxides. *J. Colloid Interface Sci.* 337, 61–65.

Illés, E., Tombácz, E., 2006. The effect of humic acid adsorption on pH-dependent surface charging and aggregation of magnetite nanoparticles. *J. Colloid Interface Sci.* 295, 115–123.

Jarvie, H.P., Al-Obaidi, H., King, S.M., Bowes, M.J., Lawrence, M.J., Drake, A.F., Green, M.A., Dobson, P.J., 2009. Fate of silica nanoparticles in simulated primary wastewater treatment. *Environ. Sci. Technol.* 43, 8622–8628.

Jarvis, P., Jefferson, B., Parsons, S.A., 2005. Breakage, regrowth, and fractal nature of natural organic matter flocs. *Environ. Sci. Technol.* 39, 2307–2314.

Jassby, D., Chae, S.-R., Hendren, Z., Wiesner, M., 2010. Membrane filtration of fullerene nanoparticle suspensions: Effects of derivatization, pressure, electrolyte species and concentration. *J. Colloid Interface Sci.* 346, 296–302.

Jauregi, P., Mitchell, G.R., Varley, J., 2000. Colloidal gas aphrons (CGA): Dispersion and structural features. *AIChE J.* 46, 24–36.

Jiang, W., Pelaez, M., Dionysiou, D.D., Entezari, M.H., Tsoutsou, D., O'Shea, K., 2013. Chromium(VI) removal by maghemite nanoparticles. *Chem. Eng. J.* 222, 527–533.

Johnson, D., Hilal, N., Waters, K., Hadler, K., Cilliers, J., 2009. Measurements of interactions between particles and charged microbubbles using a combined micro- and macroscopic strategy. *Langmuir* 25, 4880–4885.

Ju-Nam, Y., Lead, J.R., 2008. Manufactured nanoparticles: An overview of their chemistry, interactions and potential environmental implications. *Sci. Total Environ.* 400, 396–414.

Keller, A.A., Wang, H., Zhou, D., Lenihan, H.S., Cherr, G., Cardinale, B.J., Miller, R., Ji, Z., 2010. Stability and aggregation of metal oxide nanoparticles in natural aqueous matrices. *Environ. Sci. Technol.* 44, 1962–1967.

Ketkar, D.R., Mallikarjunan, R., Venkatachalam, S., 1991. Electroflotation of quartz fines. *Int. J. Miner. Process.* 31, 127–138.

Kile, D.E., Chiou, C.T., 1989. Water solubility enhancements of DDT and trichlorobenzene by some surfactants below and above the critical micelle concentration. *Environ. Sci. Technol.* 23, 832–838.Kiser, M.A., Ryu, H., Jang, H., Hristovski, K., Westerhoff, P., 2010. Biosorption of nanoparticles to heterotrophic wastewater biomass. *Water Res.* 44, 4105–4114.

Kim, J., Shan, W., Davies, S.H.R., Baumann, M.J., Masten, S.J., Tarabara, V.V., 2009. Interactions of aqueous NOM with nanoscale TiO_2: Implications for ceramic membrane filtration-ozonation hybrid process. *Environ. Sci. Technol.* 43, 5488–5494.

Kitis, M., Kilduff, J.E., Karanfil, T., 2001. Isolation of dissolved organic matter (dom) from surface waters using reverse osmosis and its impact on the reactivity of dom to formation and speciation of disinfection by-products. *Water Res.* 35, 2225–2234.

Kommalapati, R.R., Roy, D., Valsaraj, K.T., Constant, W.D., 1996. Characterization of colloidal gas aphron suspensions generated from plant-based natural surfactant solutions. *Sep. Sci. Technol.* 31, 2317–2333.

Kretzschmar, R., Holthoff, H., Sticher, H., 1998. Influence of pH and Humic Acid on Coagulation Kinetics of Kaolinite: A Dynamic Light Scattering Study. *J. Colloid Interface Sci.* 202, 95–103.

Kubota, K., Hayashi, S., Inaoka, M., 1983. A convenient experimental method for measurement of zeta-potentials generating on the bubble suspended in aqueous surfactant solutions. *J. Colloid Interface Sci.* 95, 362–369.

Kumpulainen, S., von der Kammer, F., Hofmann, T., 2008. Humic acid adsorption and surface charge effects on schwertmannite and goethite in acid sulphate waters. *Water Res.* 42, 2051–2060.

Labille, J., Feng, J., Botta, C., Borschneck, D., Sammut, M., Cabie, M., Auffan, M., Rose, J., Bottero, J.-Y., 2010. Aging of TiO_2 nanocomposites used in sunscreen. Dispersion and fate of the degradation products in aqueous environment. *Environ. Pollut.* 158, 3482–3489.

Lai, C.L., Lin, S.H., 2003. Electrocoagulation of chemical mechanical polishing (CMP) wastewater from semiconductor fabrication. *Chem. Eng. J.* 95, 205–211.

Legendre, D., Sarrot, V., Guiraud, P., 2009. On the particle inertia-free collision with a partially contaminated spherical bubble. *Int. J. Multiph. Flow* 35, 163–170.

Li, C., Somasundaran, P., 1991. Reversal of bubble charge in multivalent inorganic salt solutions — effect of magnesium. *J. Colloid Interface Sci.* 146, 215–218.

Li, C., Somasundaran, P., 1992. Reversal of bubble charge in multivalent inorganic salt solutions — effect of aluminum. *J. Colloid Interface Sci.* 148, 587–591.

Li, C., Somasundaran, P., 1993. Reversal of bubble charge in multivalent inorganic salt solutions — effect of lanthanum. *Colloids Surf. Physicochem. Eng. Asp.* 81, 13–15.

Lien, C.Y., Liu, J.C., 2006. Treatment of polishing wastewater from semiconductor manufacturer by dispersed air flotation. *J. Environ. Eng.* 132, 51–57.

Limbach, L.K., Bereiter, R., Müller, E., Krebs, R., Gälli, R., Stark, W.J., 2008. Removal of oxide nanoparticles in a model wastewater treatment plant: influence of agglomeration and surfactants on clearing efficiency. *Environ. Sci. Technol.* 42, 5828–5833.

Lin, J., Zhan, Y., Zhu, Z., 2011. Adsorption characteristics of copper (II) ions from aqueous solution onto humic acid-immobilized surfactant-modified zeolite. *Colloids Surf. Physicochem. Eng. Asp.* 384, 9–16.

Lissens, G., Pieters, J., Verhaege, M., Pinoy, L., Verstraete, W., 2003. Electrochemical degradation of surfactants by intermediates of water discharge at carbon-based electrodes. *Electrochimica Acta* 48, 1655–1663.

Liu, Y., 2010. *Elimination de Nanoparticules d'Effluents Liquides*. Institut national des sciences appliquées (Toulouse), France.

Liu, Y., Tourbin, M., Lachaize, S., Guiraud, P., 2012. Flotation separation of SiO_2 nanoparticles from water, in: *IWA Conference (Flotation 2012)*, Columbia University, New York, USA.

Liu, Y., Tourbin, M., Lachaize, S., Guiraud, P., 2012. Silica nanoparticle separation from water by aggregation with $AlCl_3$. *Ind. Eng. Chem. Res.* 51, 1853–1863.

Liu, Y., Tourbin, M., Lachaize, S., Guiraud, P., 2013. Silica nanoparticles separation from water: Aggregation by cetyltrimethylammonium bromide (CTAB). *Chemosphere* 92, 681–687.

Lu J.J., 2009. *Sorption of atrazine by nanoparticles and their complexes with humic acids*. Chinese Academy of Sciences (Beijing), China.

Lye, G.J., Stuckey, D.C., 1998. Structure and stability of colloidal liquid aphrons. *Colloids Surf. Physicochem. Eng. Asp.* 131, 119–136.

Lynch, I., Dawson, K.A., 2008. Protein-nanoparticle interactions. *Nanotoday* 3, 40–48.

Mansur, E.H.A., Wang, Y., Dai, Y., 2006. Removal of suspensions of fine particles from water by colloidal gas aphrons (CGAs). *Sep. Purif. Technol.* 48, 71–77.

Maynard, A.D., n.d. PEN 3 - Nanotechnology: A Research Strategy for Addressing Risk. http://www.wilsoncenter.org/publication/nanotechnology-research-strategy-for-addressing-risk-0.

Miettinen, T., Ralston, J., Fornasiero, D., 2010. The limits of fine particle flotation. *Miner. Eng.* 23, 420–437.

Mishchuk, N., Ralston, J., Fornasiero, D., 2012. The analytical model of nanoparticle recovery by microflotation. *Adv. Colloid Interface Sci.* 179–182, 114–122.

Molaei, A., Waters, K.E., 2015. Aphron Applications – A review of recent and current research. *Adv. Colloid Interface Sci.* 216, 35-54.

Moore, M.N., 2006. Do nanoparticles present ecotoxicological risks for the health of the aquatic environment? *Environ. Int.* 32, 967–976.

Musee, N., 2011. Nanowastes and the environment: Potential new waste management paradigm. *Environ. Int.* 37, 112–128.

Najafi, A.S., Drelich, J., Yeung, A., Xu, Z., Masliyah, J., 2007. A novel method of measuring electrophoretic mobility of gas bubbles. *J. Colloid Interface Sci.* 308, 344–350.

Nguyen, A.V., George, P., Jameson, G.J., 2006. Demonstration of a minimum in the recovery of nanoparticles by flotation: Theory and experiment. *Chem. Eng. Sci.* 61, 2494–2509.

Oberdörster, G., Ferin, J., Lehnert, B.E., 1994. Correlation between Particle Size, In Vivo Particle Persistence, and Lung Injury. *Environ. Health Perspect.* 102, 173–179.

Oeffinger, B.E., Wheatley, M.A., 2004. Development and characterization of a nano-scale contrast agent. *Ultrasonics* 42, 343–347.

Ohgaki, K., Khanh, N.Q., Joden, Y., Tsuji, A., Nakagawa, T., 2010. Physicochemical approach to nanobubblesolutions. *Chem. Eng. Sci.* 65, 1296–1300.

Oliveira, C., Rubio, J., 2011. Zeta potential of single and polymer-coated microbubbles using an adapted microelectrophoresis technique. *Int. J. Miner. Process.* 98, 118–123.

Painmanakul, P., Sastaravet, P., Lersjintanakarn, S., Khaodhiar, S., 2010. Effect of bubble hydrodynamic and chemical dosage on treatment of oily wastewater by Induced Air Flotation (IAF) process. *Chem. Eng. Res. Des.* 88, 693–702.

Paria, S., Khilar, K.C., 2004. A review on experimental studies of surfactant adsorption at the hydrophilic solid–water interface. *Adv. Colloid Interface Sci.* 110, 75–95.

Paulson, O., Pugh, R.J., 1996. Flotation of inherently hydrophobic particles in aqueous solutions of inorganic electrolytes. *Langmuir* 12, 4808–4813.

Peralta-Videa, J.R., Zhao, L., Lopez-Moreno, M.L., de la Rosa, G., Hong, J., Gardea-Torresdey, J.L., 2011. Nanomaterials and the environment: A review for the biennium 2008–2010. *J. Hazard. Mater.* 186, 1–15.

Pettibone, J.M., Cwiertny, D.M., Scherer, M., Grassian, V.H., 2008. Adsorption of organic acids on TiO_2 nanoparticles: effects of pH, nanoparticle size, and nanoparticle aggregation. *Langmuir* 24, 6659–6667.

Platz, G., 1989. *Foams and biliquid foams—aphrons*. By F. Sebba. Wiley, Chichester 1987. vii, 236 pp., ISBN 0- 47 1-9 1685-4. Adv. Mater. 1, 94–95.

Pyke, B., Fornasiero, D., Ralston, J., 2003. Bubble particle heterocoagulation under turbulent conditions. *J. Colloid Interface Sci.* 265, 141–151.

Qian, J.-H., Zhu, L.-W., Guo, R., 2005. Effect of Sodium Barbital on the Physico-chemical Properties of Surfactants with Different Charges. *J. Chin. Chem. Soc.* 52, 1245–1252.

Ramirez, J.A., Zinchenko, A., Loewenberg, M., Davis, R.H., 1999. The flotation rates of fine spherical particles under Brownian and convective motion. *Chem. Eng. Sci.* 54, 149–157.

Rao, G.V., 1997. Spherical agglomeration of scheelite fines with amphoteric collector. *Met. Mater. Process.* 9, 57–63.

Reay, D., Ratcliff, G.A., 1973. Removal of fine particles from water by dispersed air flotation: Effects of bubble size and particle size on collection efficiency. *Can. J. Chem. Eng.* 51, 178–185.

Rebhun, M., Meir, S., Laor, Y., 1998. Using dissolved humic acid to remove hydrophobic contaminants from water by complexation−flocculation process. *Environ. Sci. Technol.* 32, 981–986.

Reyes-Bozo, L., Herrera-Urbina, R., Escudey, M., Godoy-Faúndez, A., Sáez-Navarrete, C., Herrera, M., Ginocchio, R., 2011. Role of biosolids on hydrophobic properties of sulfide ores. *Int. J. Miner. Process.* 100, 124–129.

Reyes-Bozo, L., Herrera-Urbina, R., Sáez-Navarrete, C., Otero, A.F., Godoy-Faúndez, A., Ginocchio, R., 2011. Rougher flotation of copper sulphide ore using biosolids and humic acids. *Miner. Eng.* 24, 1603–1608.

Rico, I., Lattes, A., 1986. Formamide, a water substitute. 12. Krafft temperature and micelle formation of ionic surfactants in formamide. *J. Phys. Chem.* 90, 5870–5872.

Rita K. Henderson, S.A.P., 2009. The potential for using bubble modification chemicals in dissolved air flotation for algae removal. *Sep. Sci. Technol.* 44, 1923–1940.

R K L Yap, M.W., 2014. Hydrophobically-associating cationic polymers as micro-bubble surface modifiers in dissolved air flotation for cyanobacteria cell separation. *Water Res.* 61C, 253–262.

Rubio, J., Souza, M., Smith, R., 2002. Overview of flotation as a wastewater treatment technique. *Miner. Eng.* 15, 139–155.

Saleh, N., Kim, H.-J., Phenrat, T., Matyjaszewski, K., Tilton, R.D., Lowry, G.V., 2008. Ionic strength and composition affect the mobility of surface-modified Fe_0 nanoparticles in water-saturated sand columns. *Environ. Sci. Technol.* 42, 3349–3355.

Sarrot, V., Guiraud, P., Legendre, D., 2005. Determination of the collision frequency between bubbles and particles in flotation. *Chem. Eng. Sci.* 60, 6107–6117.

Sarrot, V., Huang, Z., Legendre, D., Guiraud, P., 2007. Experimental determination of particles capture efficiency in flotation. *Chem. Eng. Sci.* 62, 7359–7369.

Save, S.V., Pangarkar, V.G., 1994. Characterisation of Colloidal Gas Aphrons. *Chem. Eng. Commun.* 127, 35–54.

Schwarz, S., Grano, S., 2005. Effect of particle hydrophobicity on particle and water transport across a flotation froth. *Colloids Surf. Physicochem. Eng. Asp.* 256, 157–164.

Sebba, F., 1982. *Investigations of the Contaminant Capture in CGA (MGD) Foams* (Report to US. Department of the Interior No. OWRT/RU-82/10), Office of Water Resources and Technology. USA.

Sebba, F., 1985. An improved generator for micron-sized bubbles. *Chem. Ind.* 91–92.

Shen, Y.-H., 1998. Colloidal titanium dioxide separation from water by foam flotation. *Sep. Sci. Technol.* 33, 2623–2635.

Simate, G.S., Iyuke, S.E., Ndlovu, S., Heydenrych, M., 2012. The heterogeneous coagulation and flocculation of brewery wastewater using carbon nanotubes. *Water Res.* 46, 1185–1197.

Simmons, M.J.H., Hanratty, T.J., 2001. Droplet size measurements in horizontal annular gas–liquid flow. *Int. J. Multiph. Flow* 27, 861–883.

Singh, B.P., Nayak, S., Samal, S., Bhattacharjee, S., Besra, L., 2012. The role of poly(methacrylic acid) conformation on dispersion behavior of nano TiO_2 powder. *Appl. Surf. Sci.* 258, 3524–3531.

Spielman, L.A., Goren, S.L., 1970. Capture of small particles by London forces from low-speed liquid flows. *Env. Sci Technol.* 4, 135–140.

Spigno, G., Amendola, D., Dahmoune, F., Jauregi, P., 2014. Colloidal gas aphrons based separation process for the purification and fractionation of natural phenolic extracts. *Food Bioprod. Process.* in press.

Springer, F., Laborie, S., Guigui, C., 2013. Removal of SiO_2 nanoparticles from industry wastewaters and subsurface waters by ultrafiltration: Investigation of process efficiency, deposit properties and fouling mechanism. *Sep. Purif. Technol.* 108, 6–14.

Subrahmanyam, T.V., Forssberg, K.S.E., 1990. Fine particles processing: shear-flocculation and carrier flotation — a review. *Int. J. Miner. Process.* 30, 265–286.

Subramaniam, M.B., Blakebrough, N., Hashim, M.A., 1990. Clarification of suspensions by colloidal gas aphrons. *J. Chem. Technol. Biotechnol.* 48, 41–60.

Sung, M., Huang, C.P., Weng, Y.-H., Lin, Y.-T., Li, K.-C., 2007. Enhancing the separation of nano-sized particles in low-salt suspensions by electrically assisted cross-flow filtration. *Sep. Purif. Technol.* 54, 170–177.

Terasaka, K., Hirabayashi, A., Nishino, T., Fujioka, S., Kobayashi, D., 2011. Development of microbubble aerator for waste water treatment using aerobic activated sludge. *Chem. Eng. Sci.* 66, 3172–3179.

The true colours of fizzy drinks: Stunning pictures taken using a powerful microscope reveal vibrant crystals in a multitude of different patterns [WWW Document], n.d. Mail

Online.http://www.dailymail.co.uk/news/article-2193885/The-true-colours-fizzy-drinks-Stunning-pictures-taken-using-powerful-microscope-reveal-vibrant-crystals-multitude-different-patterns.html.

Tourbin, M., 2006. *Caractérisation et comportement de suspensions concentrées de nanoparticules sous écoulement : Application aux processus d'agrégation et de rupture* (PhD Thesis), Toulouse, France.

Tourbin, M., Frances, C., 2007. A survey of complementary methods for the characterization of dense colloidal silica. *Part. Part. Syst. Charact.* 24, 411–423.

Trompette, J., Zajac, J., Keh, E., Partyka, S., 1994. Scanning of the cationic surfactant adsorption on a hydrophilic silica surface at low surface coverages. *Langmuir* 10, 812–818.

Tsai, J.C., Kumar, M., Chen, S.Y., Lin, J.G., 2007. Nano-bubble flotation technology with coagulation process for the cost-effective treatment of chemical mechanical polishing wastewater. *Sep. Purif. Technol.* 58, 61–67.

Tschapek, M., Wasowski, C., Sánchez, R., 1981. Humic acid as a colloidal surfactant. *Plant Soil* 63, 261–271.

Vermeer, A.W.P., Koopal, L.K., 1998. Adsorption of humic acids to mineral particles. 2. Polydispersity effects with polyelectrolyte adsorption. *Langmuir* 14, 4210–4216.

Vermeer, A.W.P., van Riemsdijk, W.H., Koopal, L.K., 1998. Adsorption of humic acid to mineral particles. 1. Specific and electrostatic interactions. *Langmuir* 14, 2810–2819.

Wandruszka, R. von, 2000. Humic acids: Their detergent qualities and potential uses in pollution remediation. *Geochem. Trans.* 1, 10–15.

Wang, L., Fahey, E., Wu, Z., 2005. Dissolved Air Flotation, in: Wang, L., Hung, Y.-T., Shammas, N. (Eds.), *Physicochemical Treatment Processes, Handbook of Environmental Engineering*. Humana Press, pp. 431–500.

Warheit, D.B., Sayes, C.M., Reed, K.L., Swain, K.A., 2008. Health effects related to nanoparticle exposures: Environmental, health and safety considerations for assessing hazards and risks. *Pharmacol. Ther.* 120, 35–42.

Waters, K.E., Hadler, K., Cilliers, J.J., 2008. The flotation of fine particles using charged microbubbles. *Miner. Eng.* 21, 918–923.

Wen, L., Bin Ismail, A., Menon, P.M., Saththasivam, J., Thu, K., Choon, N., 2011. Case studies of microbubbles in wastewater treatment.

Westerhoff, P.K., Kiser, A., Hristovski, K., 2013. Nanomaterial Removal and Transformation During Biological Wastewater Treatment. *Environ. Eng. Sci.* 30, 109–117.

Westerhoff, P., Song, G., Hristovski, K., Kiser, M.A., 2011. Occurrence and removal of titanium at full scale wastewater treatment plants: implications for TiO2 nanomaterials. *J. Environ. Monit.* 13, 1195–1203.

What Is the pH of Water? [WWW Document], n.d. URL http://chemistry.about.com/od/ph/f/What-Is-The-Ph-Of-Water.htm.

Wiesner, M.R., Bottero, J.Y., 2007. *Environmental nanotechnology□: applications and impacts of nanomaterials*. McGraw-Hill.

Xu, R., 2000. *Particle Characterization: Light Scattering Methods*. Kluwer Academic Publishers.

Xu, Q., Nakajima, M., Ichikawa, S., Nakamura, N., Shiina, T., 2008. A comparative study of microbubble generation by mechanical agitation and sonication. *Innov. Food Sci. Emerg. Technol.* 9, 489–494.

Yan, Y., Qu, C., Zhang, N., Yang, Z., Liu, L., 2005. A study on the kinetics of liquid drainage from colloidal gas aphrons (CGAs). *Colloids Surf. Physicochem. Eng. Asp.* 259, 167–172.

Yang, J., Alemany, L.B., Driver, J., Hartgerink, J.D., Barron, A.R., 2007. Fullerene-derivatized amino acids: synthesis, characterization, antioxidant properties, and solid-phase peptide synthesis. *Chem. Eur. J.* 13, 2530–2545.

Yang, K., Lin, D., Xing, B., 2009. Interactions of humic acid with nanosized inorganic oxides. *Langmuir* 25, 3571–3576.

Yang, X.Y., Edelmann, R.E., Oris, J.T., 2010. Suspended C_{60} nanoparticles protect against short-term UV and fluoranthene photo-induced toxicity, but cause long-term cellular damage in daphnia magna. *Aquat. Toxicol.* 100, 202–210.

Yoon, R.-H., Yordan, J.L., 1986. Zeta-potential measurements on microbubbles generated using various surfactants. *J. Colloid Interface Sci.* 113, 430–438.

Yotsumoto, H., Yoon, R.-H., 1993. Application of extended DLVO theory: II. Stability of silica suspensions. *J. Colloid Interface Sci.* 157, 434–441.

Zajac, J., Trompette, J.L., Partyka, S., 1996. Adsorption of cationic surfactants on a hydrophilic silica surface at low surface coverages: Effects of the surfactant alkyl chain and exchangeable sodium cations at the silica surface. *Langmuir* 12, 1357–1367.

Zeta potential, 2014. *Wikipedia Free Encycl.*

Zhang, M., Guiraud, P., 2013. Elimination of TiO_2 nanoparticles with the assist of humic acid: Influence of agglomeration in the dissolved air flotation process. *J. Hazard. Mater.* 260, 122–130.

Zhang, R., Somasundaran, P., 2006. Advances in adsorption of surfactants and their mixtures at solid/solution interfaces. *Adv. Colloid Interface Sci.*, Special Issue in Honor of Dr. K. L. Mittal 123–126, 213–229.

Zhao, J., Milanova, M., Warmoeskerken, M.M.C.G., Dutschk, V., 2012. Surface modification of TiO_2 nanoparticles with silane coupling agents. *25th Meet. Eur. Colloid Interface Soc. 25th Meet. Eur. Colloid Interface Soc.* 413, 273–279.

Zhou, Z.A., Xu, Z., Finch, J.A., Masliyah, J.H., Chow, R.S., 2009. On the role of cavitation in particle collection in flotation – A critical review. II. *Miner. Eng.* 22, 419–433.

Zimmerman, W.B., Tesař, V., Bandulasena, H.C.H., 2011. Towards energy efficient nanobubble generation with fluidic oscillation. Curr. Opin. *Colloid Interface Sci.* 16, 350–356.

Zouboulis, A.I., Jun, W., Katsoyiannis, I.A., 2003. Removal of humic acids by flotation. *Colloids Surf. Physicochem. Eng. Asp.* 231, 181–193.